Universitätsklinikum Hamburg-Eppendorf

Institut für Osteologie und Biomechanik

Prof. Dr. Björn Busse

Bone matrix characterization and analysis of AGE accumulation in diabetic bone

Dissertation

zur Erlangung des Doktorgrads Ph.D.

an der Medizinischen Fakultät der Universität Hamburg

präsentiert von:

Sofie Dragoun Kolibová

Hamburg, Februar 2024

(wird von der Medizinischen Fakultät ausgefüllt)

Angenommen von der

Medizinischen Fakultät der Universität Hamburg am: **30.04.2024**

Veröffentlicht mit Genehmigung der

Medizinischen Fakultät der Universität Hamburg.

Prüfungsausschuss, der/die Vorsitzende: **Prof. Dr. Björn Busse**

Prüfungsausschuss, zweite/r Gutachter/in: **Prof. Dr. Benjamin Ondruschka**

Table of Contents

1. Introduction

1.1. Diabetes mellitus

Diabetes mellitus (DM) is a chronic metabolic disease associated with abnormally high levels of glucose circulating in the blood. With currently 537 million adults living with diabetes, it is one of the fastest growing health challenges of our century, and its prevalence is still increasing, reaching almost eight hundred million by 2045[1,2]. The alterations in glucose metabolism in diabetes are caused by the changes in insulin synthesis and production or its utilization. Insulin is a pivotal hormone secreted by the pancreas, and, together with glucagon, insulin regulates the glucose levels in the blood. With increasing glucose levels in the blood, the pancreatic β-cells release insulin into the circulation, leading to increased cellular glucose intake, resulting in lower serum glucose levels. On the other side, the low glucose concentration stimulates the pancreatic α-cells to release glucagon, allowing stored glycogen to be converted into glucose. This mechanism balances the circulating blood glucose concentrations at normal levels. Impaired insulin sensing causes glucose accumulation in the blood, resulting in hyperglycemia—the defining feature of diabetes. Reduced ability of individual patients to regulate glucose concentration effectively, leading to several diabetic complications. We recognize different mechanisms for DM development together with diverse manifestations and impact of the disease, and therefore, DM is classified mainly into type 1 diabetes and type 2 diabetes [3].

Type 1 diabetes mellitus (T1DM) accounts for 10% of all diabetes cases worldwide and is juvenile-onset or in early adulthood. The etiology of T1DM is caused by autoimmune destruction of the pancreatic β-cells leading to insulin deficiency [4,5]. Type 2 diabetes mellitus (T2DM) stands for approximately 90% of all affected individuals worldwide and is usually diagnosed later in a patient's lifetime. In contrast to T1DM, in T2DM, the pancreas still produces insulin, but either the quality is poor or the cellular receptors do not respond to insulin, causing insulin resistance [6,7].

Hyperglycemia in DM can lead to an increase in oxidative stress, which contributes to the progression of diabetes and its complications [8–10]. DM is associated with alterations in cellular homeostasis, causing increased vascular permeability and apoptosis of specific vascular cells, contributing to an increased risk of developing vascular complications affecting both large (macrovascular) and small (microvascular) blood vessels [11] **(Figure 1)**. Macrovascular complications lead to a higher stroke incidence, coronary heart disease (CHO), and peripheral vascular disease. Microvascular complications contribute to diabetic neuropathy (nerve damage), nephropathy (kidney disease), and retinopathy (eye disease). Damaged nerves and vascularity can lead to ulceration, gangrene, and, in extreme cases, limb amputations [3,12,13]. Recently, fragility fractures were identified as an important complication

linked to both T1DM and T2DM. Fracture risk is often underdiagnosed in DM individuals and is associated with excess morbidity, mortality, and decreased life quality of patients [14].

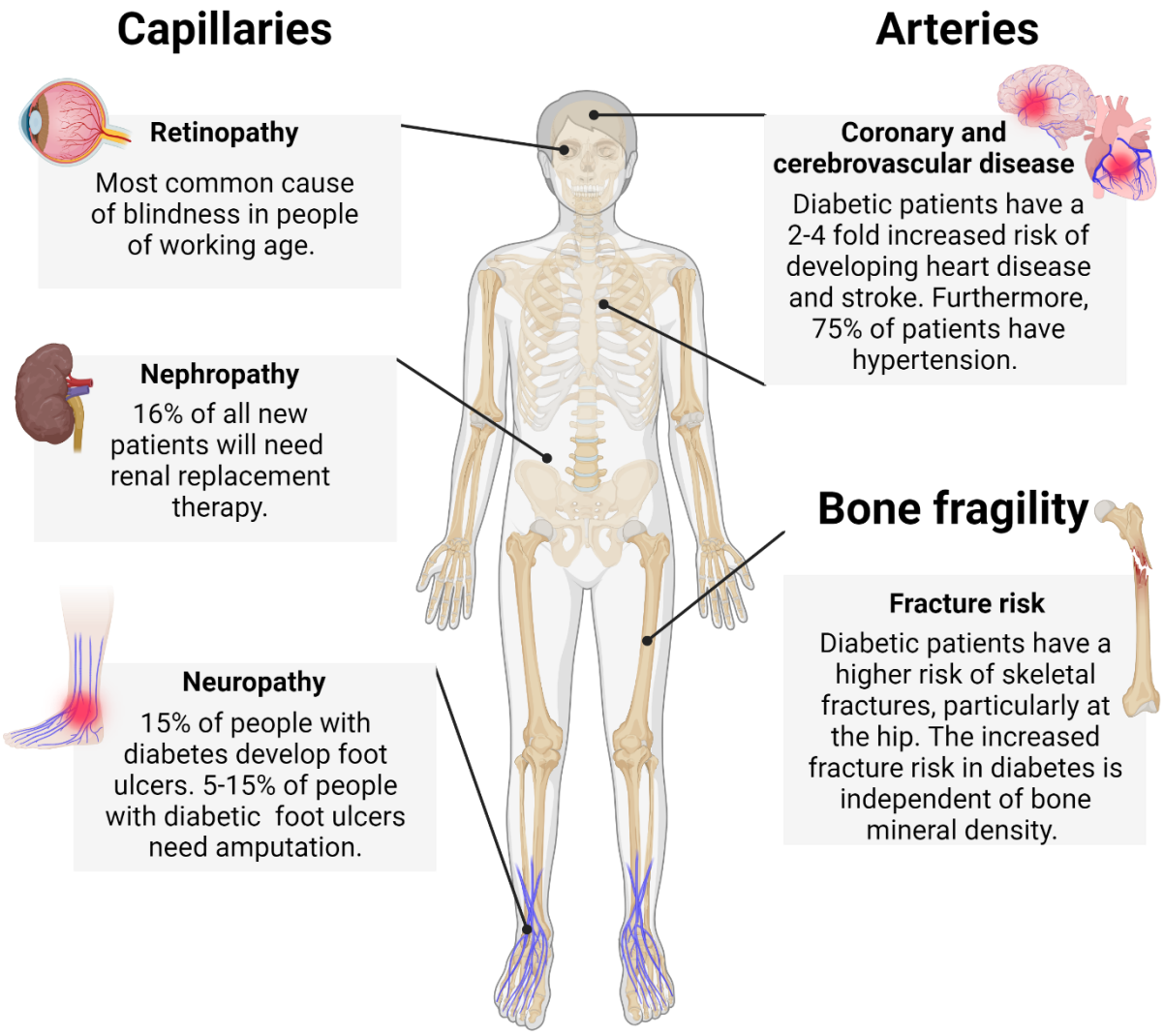

Figure 1. Effects of microvascular and macrovascular complications in diabetes mellitus. Chronic hyperglycemia in diabetic patients is associated with the development of microvascular complications affecting the capillaries and leads to the development of retinopathy, nephropathy, and neuropathy. Furthermore, diabetes is also associated with macrovascular complications causing damage to the arteries, leading to coronary and cerebrovascular disease. Recent research also identified bone fragility as a diabetes-related complication. Diabetic complications greatly influence the rate of mortality and morbidity of the disease and affect the life quality of diabetic individuals. Modified from Shamim, Diabetes An Old Disease, a New Insight, 2019.

1.2. Hierarchical structure and bone quality

Human bone is a complex biological material with many irreplaceable bodily functions. The primary function of the skeleton is to provide a structural scaffold that supports and allows for movement [15,16]. Furthermore, bone tissue serves as a reservoir for essential minerals (such as calcium, phosphorus, and magnesium), takes part in hematopoiesis (production of blood cells), and provides a shield for vital organs. The bone consists of an extracellular matrix and living cells. The extracellular matrix of the bone tissue contributes to its mechanical properties. At the same time, the living cells facilitate the exchange of nutrients, hormones, and other regulatory factors between the bone and other tissues [17,18]. Also, bone is a dynamic tissue that undergoes continuous bone remodeling, ensuring the maintenance of strength and mineral balance that influences an individual's overall health and well-being [19].

One of the main indicators of bone health is the density of the bone tissue or bone mineral density (BMD). BMD provides information on the mineral content, which is predominantly determined by calcium and is measured radiographically. Dual-energy X-ray absorptiometry (DXA) is a diagnostic method that measures BMD, and it is used to diagnose bone loss (e.g., osteoporosis) and to assess fracture risk [20]. A decrease in BMD often signals compromised bone strength and an increased susceptibility to fractures. However, the fracture resistance of a bone is not only determined by its quantity but also by the quality of the bone tissue. Therefore, it is crucial to consider additionally the cellular, structural, compositional, and mechanical parameters, generally referred to as bone quality parameters [21]. Recognizing the importance of bone quality can be essential for predicting fracture risks and developing effective strategies for osteoporosis management and other bone-related disorders. The bone quality parameters vary across different length scales, ranging from macro to nanoscale, due to the hierarchical organization of human bone [19] **(Figure 2).**

The unique combination of strength, flexibility, and resistance of bone has its foundation in the hierarchical structure. The bone matrix is structurally arranged into dense cortical and trabecular (cancellous or spongy) bone. The trabecular bone is composed of numerous trabeculae that make up the internal framework of the bone and are enclosed by the bone marrow, which plays a crucial role in the production of blood cells, thus serving as a metabolically active bone compartment [22,23]. The dense bone compartment, cortical bone, is composed of micrometer-sized building blocks called osteons. Osteons contain centrally located Haversian canals carrying blood vessels and nerves that provide nutrients and signaling molecules [24]. The Haversian canal is surrounded by concentric lamellae comprising of layers of collagen fibers. These lamellae are organized in alternating patterns

of twisted plywood structure. Each lamellar layer comprises mineralized collagen fibrils formed of hydroxyapatite nanocrystals placed within the collagen molecules [22,25,26].

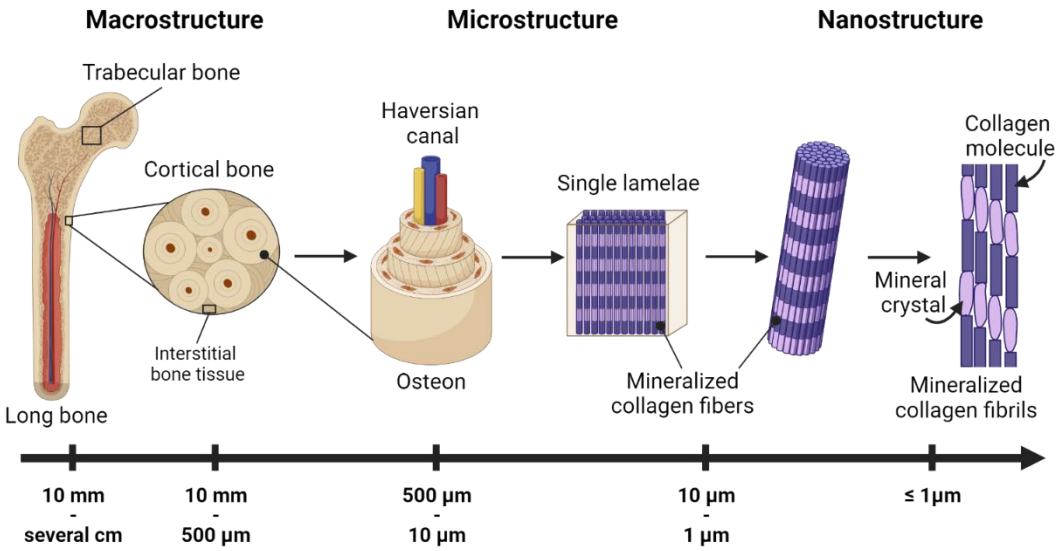

Figure 2. Hierarchical structure of human bone. Long bones have two main bone compartments: spongy trabecular and compact cortical bone. The main building block of cortical bone is an osteon containing blood vessels and nerves in the central part named the Haversian canal. Each osteon consists of several layers of concentric lamellae, and each lamella consists of assembled collagen fibers. In bone, the mineralized collagen fibril serves as the tiniest structural unit. It is composed of collagen molecules that are arranged periodically with embedded mineral crystals in between.

During the initial bone formation stages, the organic matrix is produced by osteoblasts (bone-forming cells). This young, unmineralized bone matrix is called osteoid and becomes slowly harder due to subsequent nucleation of mineral particles within the collagen fibrils, increasing bone hardness [27,28]. Because the formation of a single osteon occurs at different time points, each osteon has a unique arrangement of collagen fibrils and mineralization levels and, therefore, a different tissue age. A recently formed osteon is considered a younger tissue compared to older and more mineralized regions of osteonal fragments called interstitial bone [29,30]. The stability of the bone matrix further improves as the tissue age increases. This is achieved in the organic phase by the controlled formation of enzymatic and non-enzymatic cross-links between collagen molecules and in the inorganic phase via the transformation of an amorphous mineral particle to a more structurally ordered crystal [31]. An increased risk of fractures can occur under pathological conditions when there are changes in bone quality parameters at any length scale. In osteoporosis, the reduced trabecular thickness and increased cortical porosity contribute to higher fracture risk [32]. Moreover, secondary osteoporosis, with

underlying conditions e. g., diabetes mellitus, medication, or even immobilization, also leads to alterations in bone quality, resulting in increased bone fragility [14,33–35].

1.3. Bone quality in diabetes mellitus

Diabetes has a significant impact on bone health, leading to alterations in bone mineral density, composition, and strength. These changes increase the likelihood of fractures and musculoskeletal complications, which are frequently disregarded in diabetes management. Diabetes is recognized as a risk factor for increased bone fragility and a risk of osteoporosis-associated fractures [14,36].

Commonly used measurements for fracture risk using DXA based on BMD underestimate the fracture risk for patients with both T1DM and T2DM. Additionally, past studies have drawn a relationship between T1DM and reduced BMD due to a chronic lack of anabolic actions of insulin, whereas T2DM patients usually present with normal or even increased BMD **(Figure 3)**. Nevertheless, both types of DM patients are at increased fracture risk [37,38]. These findings indicate that diabetes not only affects bone quantity but also negatively affects bone quality.

Diabetes can lead to an increased likelihood of falls and injury due to several associated risk factors. These risk factors include poor vision, reduced balance, peripheral neuropathy, stroke, and physical disability. Additionally, poor bone quality in diabetes, when combined with frequent falls, increases the chances of experiencing fractures [39]. While both type 1 and type 2 DM have been linked to higher chances of bone fractures, the reasons behind diabetic bone fragility can differ between the two types [40,41].

Fracture risk is significantly higher in T1DM patients compared to T2DM patients. This is reflected in a recent meta-analysis where it is reported that T1DM increases hip fracture risk by a relative risk (RR) of 4.93, whereas in T2DM, the hip fracture risk is increased by an RR of 1.33 [42]. Differences in BMD do not solely cause diabetic bone fragility. Changes in bone microstructure and the intrinsic properties of the bone material itself may also influence diabetic bone quality. A study of postmenopausal T2DM women revealed increased cortical porosity in the radius and increased pore volume in the tibia among T2DM women compared to controls [43]. Furthermore, DM is characterized by a low bone turnover status, increased levels of sclerostin (inhibits osteoblast-induced bone formation), and osteoprotegerin (inhibits osteoclast-induced bone resorption) [44]. The decrease in bone turnover markers in diabetic patients is associated with chronic hyperglycemia [44,45].

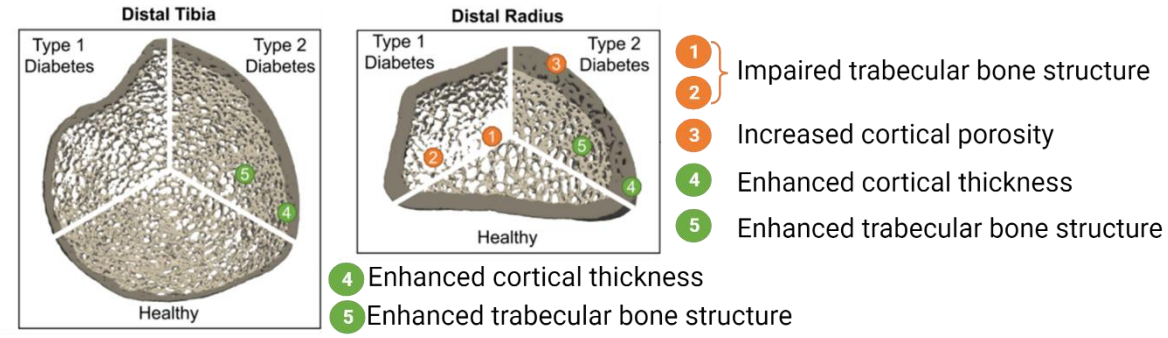

Figure 3. Bone microarchitecture in type 1 (T1DM) and type 2 diabetes mellitus (T2DM). High-resolution peripheral quantitative computed tomography images of distal tibia and radius in T1DM and T2DM patients compared to healthy controls. Annotations 1–2 show impaired bone microarchitecture characteristics in T1DM and the catabolic effect of insulin shortage is demonstrated by the reduced volume of trabecular bone at the distal radius. Annotation 3 demonstrates the increased cortical porosity in T2DM. Annotations 4–5 show enhanced bone microarchitecture characteristics associated with T2DM. Modified from Walle et al., 2022.

Altered glucose metabolism in diabetes leads to prolonged exposure to hyperglycemia, causing the accumulation of advanced glycation end-products (AGEs). AGEs are a heterogeneous group of compounds originating from the Maillard reaction between the protein amino group and carbonyl group from a reducing sugar [46]. Due to high heterogeneity, some AGES are fluorescent, cross-link forming, or both [47] **(Figure 4)**. Type I collagen is a major component of the bone matrix and, therefore, a crucial determinant of bone strength. Collagen is a protein with a long half-life, and chronic hyperglycemic conditions allow more side-chain glycation [45], resulting in increased AGEs accumulation among diabetic patients compared to healthy populations [48]. AGEs accumulation in bone tissue introduces physical changes to the collagenous matrix negatively associated with bone mechanical properties [49] compared to stabilizing enzymatic cross-linking arising during the collagen maturation processes [31].

Pentosidine is a fluorescent cross-linking forming type of AGE. It is often used as a marker of total fluorescent AGEs content in bone. In T2DM individuals is, increased urine pentosidine levels associated with a higher incidence of clinical and vertebral fractures compared to non-diabetic individuals [50]. Similarly, elevated serum pentosidine levels were associated with more prevalent fractures in T1DM patients [51]. In addition, a higher pentosidine content was also found in trabecular bone from T1DM patients with fracture history compared to healthy controls [52]. Carboxymethyllysine (CML) is another type of AGE that is highly abundant in bone. Compared to pentosidine, CML is a non-fluorescent and non-cross-linking type of AGE, and it is considered a biomarker for aging and oxidative stress in tissue [47]. Our previous work showed an increased CML content in the femoral cortical bone of T2M individuals compared to the healthy control group [53].

AGEs interact with the receptor for AGEs (RAGE). Activation of RAGE signaling includes upregulation of inflammation, induction of oxidative injury, and reactive oxygen species (ROS) production [54,55]. Elevated levels of oxidative stress in cells driven by RAGE signaling pathways lead to substantial changes in cellular function [55–57].These can cause alterations to bone cells [58,59], dysregulating bone turnover and contributing to the further development of diabetic bone disease **(Figure 4)**. A range of complex factors, including hyperglycemia, oxidative stress, and the accumulation of AGEs, contribute to bone fragility in DM. These factors can compromise collagen properties, release inflammatory factors, and potentially affect the function of regulatory bone cells.

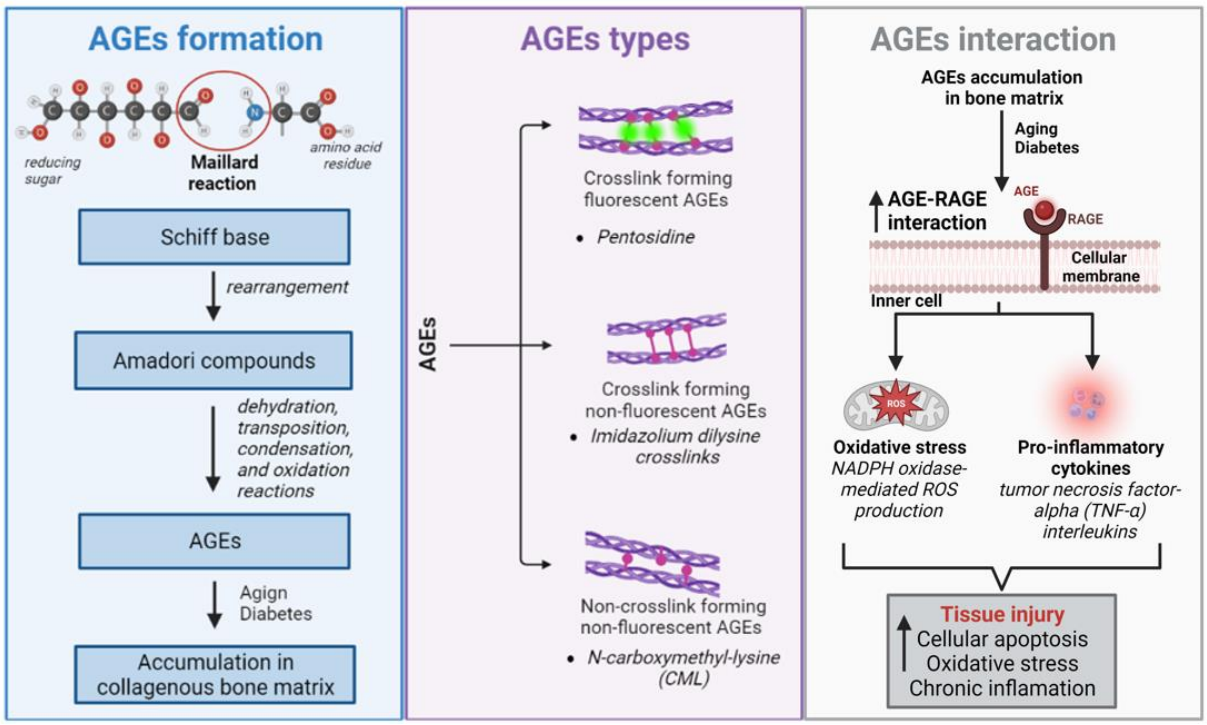

Figure 4. Graphical summary of formation, classification, and interaction of advanced glycation end-products (AGEs). AGEs are a heterogeneous group of chemical compounds formed during the Maillard reaction. This chemical reaction between amino acids and reducing sugars creates an unstable Schiff base, which is rearranged into Amadori compounds. Amadori compounds then undergo various chemical modifications, resulting in the formation of AGEs. Accumulation of AGEs in tissues, especially with long half-lives like collagen, is increasing with advancing age or during diabetes. AGEs introduce chemical modification to collagen, which can be divided into three main groups based on fluorescent and cross-linking properties. RAGE is a transmembrane receptor which serves as a primary receptor for AGEs. Accumulation of AGEs in collagen overstimulates AGE-RAGE interactions, leading to increased oxidative stress and release of inflammatory cytokines and causing tissue damage.

1.4. Osteocytes as the mechanosensors of bone

Bone is made of a complex bone matrix consisting of living cells, collagen fibers, and inorganic minerals, which exhibit the ideal balance of strength and flexibility crucial to its physiological function. Mechanosensitivity of the bone allows for maintaining this balance due to high adaptability to environmental changes and external factors [17–19].

Osteocytes are the major bone cells living inside lacunae – a small cavity embedded within the mineralized bone matrix. A key feature of osteocytes is to facilitate mechanosensitivity at the cellular level. These cells recognize mechanical stimuli and convert them into biochemical signals to modulate the actions of osteoblasts (bone-forming cells) and osteoclasts (bone-resorbing cells) in a process called bone remodeling, ensuring a dynamic balance between bone deposition and resorption to maintain bone homeostasis [61–63]. The position of osteocytes within the mineralized matrix led to the creation of nano-channels (canaliculi), through which the osteocytes are connected by long cytoplasmic dendrites, resulting in a communication network called a lacuno canalicular network (LCN). Fluid flow distributes nutrients, oxygen, signal molecules, and waste products [64,65]. The integrity of LCN is a critical determinant of osteocyte viability and influences bone homeostasis [62,66] **(Figure 5)**.

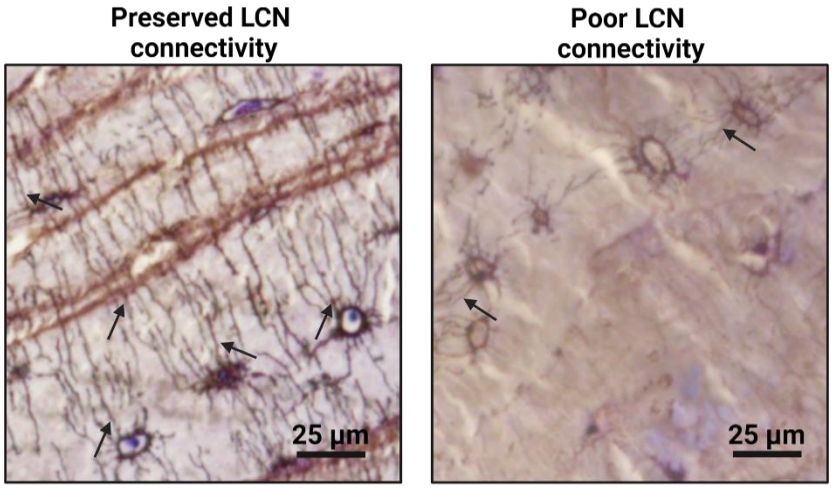

Figure 5. Osteocyte connectivity. Osteocyte communication is mediated by the lacuno-canalicular network (LCN), an extensive network of nano-canals called canaliculi through which cytoplasmic extensions interconnect individual osteocytes. Representative images of human cortical bone stain with Ploton silver staining visualizing LCN marked with black arrows between the embedded osteocytes. In the first image, the LCN is preserved, maintaining bone mechanosensitivity. The second image represents a significantly reduced LCN that poses possible alteration in mechanosensitivity and microdamage detection.

Osteocytes are postmitotic and can live up to 50 years thereby they are thought to be the long-lived cell type in human bone. The end of the osteocyte lifetime can result in one of the three major cell death mechanisms, including cellular apoptosis, autophagy, and necrosis [67,68]. Osteocyte apoptosis is vital in signaling and initiating bone-repairing mechanisms. The resorption of the damaged bone is initiated by apoptotic osteocytes secreting RANKL (receptor activator of nuclear factor-kappa B ligand), attracting the osteoclasts to the damage site. Therefore, osteocyte apoptosis is a crucial signaling mechanism that induces bone repair and prevents microdamage accumulation in the bone matrix [69,70]. With increasing age, osteocyte cell death is more frequently detected in bone tissue disorders such as postmenopausal osteoporosis, glucocorticoid-induced osteoporosis, and immobilization. These conditions are associated with a higher risk of fractures [35,71,72].

Viable osteocytes produce crystallization inhibitors like pyrophosphate or osteopontin to keep their lacunar cavity unmineralized [73,74]. When osteocyte die, osteoclasts are responsible for removing the affected bone area. However, if bone resorption is not locally activated, the dying osteocytes remain buried within the mineralized bone tissue, inaccessible to macrophages. This enables a unique micro-mineralization process of osteocyte lacunae or so-called micropetrosis. The process of micropetrosis involves the slow filling of the lacunar space with mineral occlusions until the lacuna becomes entirely sealed with the mineral content [65,75–77] **(Figure 6)**.

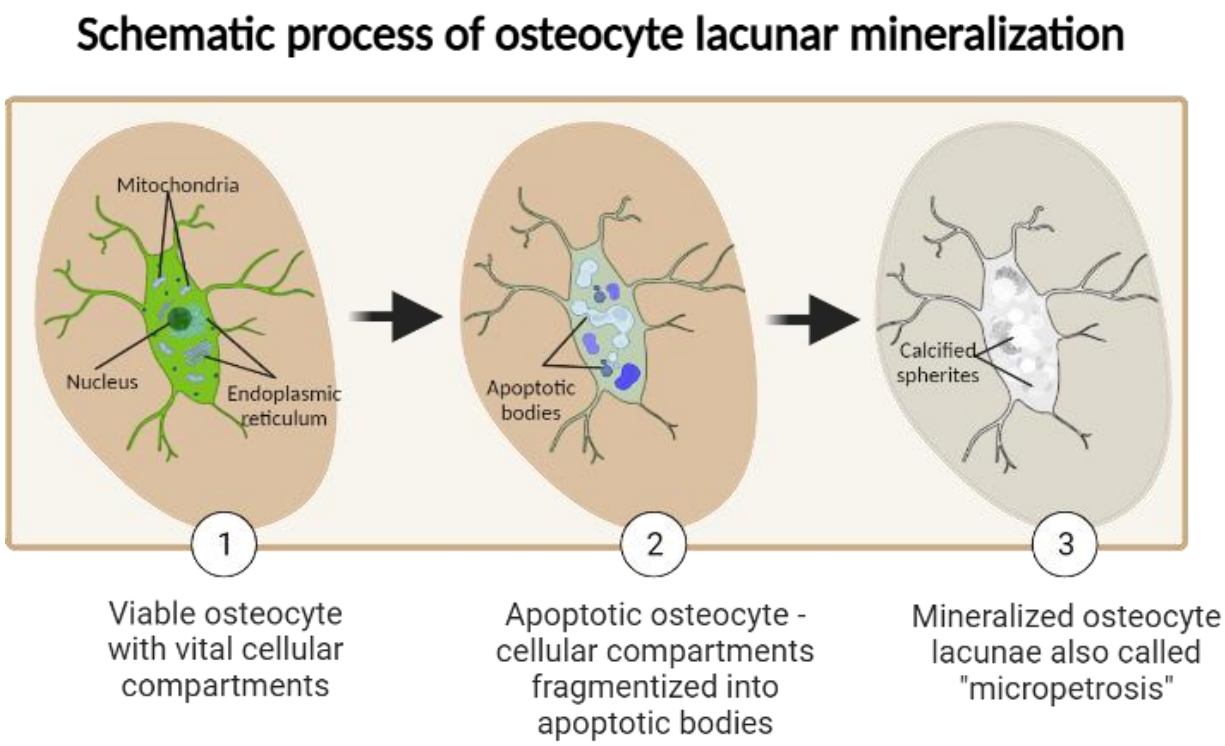

Figure 6. Osteocyte lacunar mineralization follows cellular apoptosis. Osteocyte cell death increases with aging or during bone pathologies (e.g., osteoporosis or diabetes mellitus). An increased pool of dying osteocytes provides more opportunities for osteocyte lacunar mineralization (micropetrosis). 1) To keep the lacunar cavity

unmineralized, functional osteocytes generate mineralization inhibitors (pyrophosphates) that prevent crystallization. 2) As the osteocyte undergoes apoptosis, it initiates the formation of lacunar mineralization by breaking down its cellular compartments and releasing matrix vesicles and apoptotic bodies. These cellular components may act as nuclei for independent mineralization processes, resulting in the development of calcified spherites. 3) Finally, lacunar mineralization reaches the stage where the individual mineral spherites fuse together and thus completely seal the lacunar cavity with minerals. Modified from Dragoun Kolibová et al., 2022.

The presence of cellular and apoptotic organelles inside the osteocyte lacunae potentially serves as nuclei for spontaneous mineralization processes. Magnesium is an essential intracellular ion increasing in the beginning phases of apoptosis, and mineralized lacunae are enriched with magnesium content, which further supports the theory that micropetrosis follows osteocyte apoptosis [78,79]. Therefore, it is generally accepted that osteocyte cell death precedes lacunar mineralization. Aging or pathologies like osteoporosis can increase the micropetrosis levels in bone tissue and reflect the decreasing number of osteocytes. Accumulation of mineralized lacunae within the bone matrix locally increases bone brittleness and promotes microcracking. Furthermore, mineralized lacunae block fluid flow within the LCN, which is essential for maintaining signal transduction and can contribute to compromised bone integrity in aged or diseased individuals [65,75,77]. Investigating the lacunar mineralization during pathological conditions could yield valuable insights into the origins of bone fragility. This knowledge is essential for developing effective preventive and curative measures to address the complications arising from high bone fragility.

1.5. Objectives of this thesis

The underlying mechanisms of poor bone strength in T1DM and T2DM are complex and multifactorial and have not yet been completely elucidated. This thesis aims to contribute fundamental knowledge of multiscale characteristics of the human bone matrix affected by diabetic bone disease, with the goal of identifying a potential novel biomarker for impaired bone matrix in individuals with DM.

Objective 1: Multiscale characterization of bone matrix and osteocyte pathology in T1DM *(publication 1:* ***Dragoun Kolibová, S.*** *et al., Acta Biomaterialia 2023)*

Increased fracture risk associated with T1DM can lead to significant patient morbidity. Osteocytes, which construct a mechanosensitive network within the mineralized bone matrix, are vital in regulating bone remodeling. Therefore, maintaining osteocyte viability is essential for ensuring proper bone

function. It has been demonstrated that diabetic hyperglycemia has an adverse impact on osteocyte viability. Additionally, the T1D-rat model has revealed an increased microdamage accumulation when subjected to fatigue loading. Validation of current findings in the literature on T1D-bone disease requires human bone material, and data on such specimens are scarce. Therefore, this project aims to characterize the effect of T1DM on human femoral cortical bone using an interdisciplinary approach. Applying novel imaging techniques for detecting and quantifying osteocyte viability, bone mineralization, and microdamage accumulation in the human femoral cortical bone will provide valuable insight into underlying mechanisms driving bone fragility in T1DM.

Objective 2: Investigation of osteocyte lacunar mineralization under metabolic disorders

*(publication 2: **Dragoun Kolibová, S.** et al., Osteologie 2022)*

Reduced bone mineral density and increased fracture risk are the main characteristics of osteoporosis, which is a systemic disease that primarily affects postmenopausal women and the elderly through primary osteoporosis and is associated with underlying conditions like diabetes mellitus through secondary osteoporosis. One of the factors contributing to osteoporotic bone loss and low bone turnover in diabetes is an increase in osteocyte cell death. Mineralization of osteocyte-lacunae after osteocyte death is called micropetrosis. The level of micropetrosis increases with advancing age, however, the frequency of micropetrosis has not yet been characterized in metabolic bone diseases. This project aims to investigate the occurrence of micropetrosis in metabolic bone diseases and evaluate its relevance as a potential novel biomarker of altered bone quality.

Objective 3: Clinical and laboratory-based assessment of bone quality indices in T2DM tibial bone

*(publication 3: Wölfel, E. M., Fiedler, I. A. K., **Dragoun Kolibová, S.** et al., Bone 2022)*

Assessing fracture risk through the peripheral tibia is a preferred option in clinical settings. This is done by combining high-resolution peripheral quantitative computed tomography (HR-pQCT) with measurements of areal bone mineral density (aBMD) in the spine or hip using DXA. However, increased fracture risk in T2DM is challenging to identify with standard clinical methods since T2DM patients often have normal or high bone mineral density. The increased fracture risk despite normal or high BMD in T2DM patients points towards impaired bone material quality, possibly influenced by AGE accumulation. Pentosidine, a fluorescent type of AGE creating cross-links in collagen, has been suggested as a possible factor contributing to bone fragility in T2D-bone disease. This project aims to investigate the influence of compositional changes on the bone matrix, including the accumulation of fluorescent AGEs and their influence on biomechanical properties in T2DM cortical tibial bone.

Objective 4: Evaluation of fracture resistance in T2DM cortical bone

*(publication 4: Wölfel, E. M., Bartsch, B., Koldehoff, J., Fiedler, I. A. K**., Dragoun Kolibová, S.** et al., JBMR Plus 2023)*

Aged or diseased bones tend to have reduced fracture toughness properties. In the case of individuals with T2DM, bone fracture toughness is primarily determined in the trabecular bone, and data on cortical bone toughness in T2DM are scarce. Therefore, this project aims to utilize a multiscale assessment approach to evaluate microstructure and bone material quality indices of cortical bone tissue affected by T2DM and concurrently determine the fracture toughness of the same tissue.

2. Material and methods

2.1. Collection and preparation of human bone tissue for bone quality evaluation

We evaluated the influence of diabetes mellitus on bone microarchitecture, matrix quality, and cellular parameters of cortical bone. We collected femoral and tibial bone specimens from human donors of both sexes for cortical bone quality analysis. The specimens were obtained in collaboration with the Institute of Legal Medicine at the University Medical Center Hamburg-Eppendorf (ethical approval: WT037/15). According to medical records, donors were divided into two study groups, including a group of donors diagnosed with diabetes mellitus (T1DM and T2DM groups) during their lifetime and a group of age-matched healthy donors (control group) with normal sugar metabolism. For each donor, we collected deidentified patient data (age, BMI). Donors in this study did not suffer from any form of bone disease (i.e., osteogenesis imperfecta, Paget's disease, fibrous dysplasia, or malignancy).

Part of the collected bone material was frozen as unfixed fresh material to assess fluorescent advanced glycation end-products (fAGEs). The remaining cortical bone specimens were fixed in 4% paraformaldehyde (Sigma–Aldrich, Darmstadt, Germany) for seven days. Several 4-mm-thick sections were cut out from the fixed specimens using a diamond belt saw (EXAKT Advanced Technologies GmbH, Norderstedt, Germany), followed by imaging the whole cross-sections in a cabinet X-ray system. The anterior quadrant was extracted from each cross-section and additionally fixed in 4% paraformaldehyde (Sigma–Aldrich, Darmstadt, Germany) overnight before embedding in methyl methacrylate (MMA). The anterior quadrant from another cross-section was cut and decalcified for six weeks in a 20% ethylenediaminetetraacetic (EDTA) solution before paraffin embedding for immunohistochemistry (IHC).

2.2. Multiscale analysis of human bone tissue

2.2.1. Assessment of bone microstructure with microcomputed tomography

The skeletal microstructure of the femoral anterior quadrant was assessed using microcomputed tomography (µCT 40, Scanco Medical AG, Switzerland) at a spatial resolution of 10 µm. In order to maintain tissue integrity, bone specimens were first fixed in 4 % formaldehyde. The X-ray settings were standardized to 55 kV and 145 µA with an integration time of 200 ms. A threshold of 550 mg HA/cm^3 was applied to assess cortical porosity (Ct. Po) and tissue mineral density (TMD) using Scanco image

processing software. Cortical thickness (Ct. Th) was calculated from the contact radiography images within the whole cross-section of the femoral diaphysis using ImageJ/Fiji software (NIH, USA).

2.2.2. Static cellular histomorphometry

Static histomorphometry was performed on the femoral cortical bone with and without T1DM. The fixed samples were dehydrated using increasing ethanol concentrations and embedded in MMA. We cut five µm-thick-sections from the embedded specimens on a microtome (Leica Microsystems, Wetzlar, Germany) and stained the sections with toluidine blue dye to visualize the cellular structures. We evaluated the cellular presence in the endocortical and periosteal regions of the femoral anterior quadrant using Osteomeasure software (Osteometrix, Atlanta, USA). Assessed histomorphometric indices were following the ASBMR nomenclature guidelines [80]. We evaluated following histomorphometric indices: Bone formation indices: number of osteoblasts per unit bone perimeter (N.Ob/B.Pm; #/mm); osteoblast surface (Ob.S/BS): percent of bone surface occupied by osteoblasts; osteoid volume (OV/BV; %): percent of a given volume of bone tissue that consists of unmineralized bone (osteoid); osteoid surface (OS/BS; %): percent of bone surface covered in osteoid; osteoid thickness (O.Th): mean thickness, provided in micrometers for osteoid bone. Bone resorption indices: number of osteoclasts per unit bone perimeter (N.Oc/B.Pm; #/mm); osteoclast surface (Oc.S/BS): percent of bone surface occupied by osteoclasts; eroded surface (ES/BS; %): percent of bone surface occupied by resorption cavities with or without osteoclasts.

2.2.3. Analysis of the bone mineral density distribution using quantitative backscattered electron imaging

The bone mineral density distribution (BMDD) and 2D morphological analysis of the osteocyte lacunae were evaluated via quantitative backscattered electron imaging (qBEI) based on previously established protocols (Roschger et al. 1998). Coplanar and polished MMA-embedded specimens were carbon-coated before imaging to prevent charging effects under vacuum. A scanning electron microscope (Crossbeam 340, GeminiSEM, Zeiss AG, Oberkochen, Germany) was operated at backscattered electron mode at 20 keV with a constant working distance of 20 mm. We used a Faraday cup to monitor the current beam, and grayscale values were calibrated using pure aluminum and carbon standards. All parameters were monitored during imaging and kept at a constant level. We calculated calcium wt% from the backscattered electron images using a custom-made MATLAB code (MATLAB, Natick, Massachusetts) and assessed following parameters: the average calcium concentration (CaMean, wt%), the most frequently occurring calcium concentration (CaPeak, wt%), the heterogeneity of the

mineral distribution (CaWidth, wt%), and the percentage of bone area with low (CaLow, % bone area) and high (CaHigh, % bone area) mineralized bone [81].

2.2.4. Quantification of the osteocyte apoptosis using immunohistochemistry (IHC) and TUNEL assay

Terminal deoxynucleotidyl transferase dUTP nick end labeling or TUNEL assay detects and visualizes DNA breaks during the final phase of cell death when the DNA fragments occur. The embedding medium was washed out from the undecalcified MMA sections using xylene, and the sections were rehydrated by a descending ethanol series (absolute, 90%, 80%, and distilled water). We performed enzymatic antigen unmasking by incubation with proteinase K for 20 minutes at room temperature (RT), followed by incubation with 20% EDTA for 30 minutes at 37 °C. The pretreated sections were stained using fluorescein from an In Situ Cell Death Detection Kit (Roche, Basel, Switzerland) overnight at 37 °C. After staining, the sections were washed with phosphate-buffered saline (PBS) solution and treated with a permeabilization solution with 0.1% Triton X-100 and 0.1% sodium citrate for 8 minutes at RT. The samples were then mounted using a mounting medium with DAPI stain. We determined the number of apoptotic cells per bone area in ImageJ/Fiji software.

One of the key proteins in signaling cellular apoptosis is caspase-3. In order to identify and measure apoptosis in tissue sections, we employed immunohistochemistry staining for the caspase-3 protein. Decalcified paraffin sections were deparaffinized using xylene and rehydrated by a descending ethanol series (absolute, 90%, 80%, and distilled water). The enzymatic antigen unmasking consists of 20 min of incubation at RT with Proteinase K and subsequent treatment with 20% EDTA for 30 min at 37 °C. For staining, we used a SignalStain® Apoptosis Cleaved Caspase-3 Detection Kit (Cell Signaling Technology, Danvers, MA, United States). The pretreated sections were then stained in accordance with the manufacturer's recommendation overnight at 4°C. Following the incubation, the sections were washed, and apoptotic cells were detected by the 3,3-diaminobenzidine (DAB) chromogen (DAKO, Carpinteria, CA, USA). Lastly, the slides were counterstained in hematoxylin, washed in distilled water, dehydrated, and mounted. The slides were imaged using a PANNORAMIC MIDI Digital Slide Scanner (Sysmex Corporation, Kobe, Hyogo, Japan). The apoptotic cells were counted manually using an object-counting tool in Olympus cellSens software (Shinjuku City, Tokyo, Japan), and we quantified the total number of apoptotic osteocytes per bone area (B.Ar; #/mm2).

2.2.5. Microdamage accumulation assessment with laser scanning confocal microscopy (LSCM)

Bone specimens are infiltrated with fluorescent dye rhodamine-6G before MMA embedding to visualize microdamage in the bone matrix. This approach enables the visualization of only the pre-existing microcracks in the bone matrix and eliminates embedding artifacts. Laser scanning confocal microscopy is then used to examine the specimens. This technique is adapted from the Fuchsin microcrack protocol [82]. From the fixed femoral cross-sections, we cut out a 10 mm bone piece from the region next to the anterior quadrant using a diamond belt saw (EXAKT Advanced Technologies GmbH, Norderstedt, Germany). After dehydration, the bone specimens were infiltrated with 0.002 % WT rhodamine-6G for ten days before being embedded in MMA. With a confocal laser scanning microscope (Leica SP5, Leica Microsystems, Wetzlar, Germany), we imaged microcracks with a 561 nm laser excitation wavelength. We quantified the following parameters in ImageJ/Fiji software to assess linear microdamage accumulation: total number of linear microcracks per mineralized bone area (B.Ar; #/mm2) and total length of linear microcracks per mineralized bone area (B.Ar; µm/mm2). Microcracks derived from the main branch were counted as microcrack branching.

2.2.6. Evaluation of the total fluorescent advanced glycation end-products (fAGEs)

Fluorescent AGEs (fAGEs) content was measured using fluorescence spectroscopy and then normalized to collagen content determined by colorimetric assay. Fresh frozen tibial bone samples from the anterior-medial section of the mid-diaphyseal tibia were first washed and defatted by soaking them in 70% ethanol and saline for 15 minutes each. Following a lyophilization period of 18 hours, these samples underwent hydrolysis in 6 M HCl (10 µl of HCl for every mg of bone) at a temperature of 110 °C over a duration of 16 hours. Bone hydrolysates were diluted in deionized water to a final concentration of 0.5 mg bone/ml and centrifuged at 13,000 rpm at four °C. The obtained supernatant was used for the rest of the assay.

For fluorescence measurements, we serially diluted both quinine standards (with a stock solution of 10 µg quinine in 0.1 N H_2SO_4 per ml) and bone hydrolysates. The resulting solutions were measured in a dark 96-well plate using the multi-mode microplate reader at an excitation of 360 nm and emission of 460 nm.

The total collagen content in the bone lysate was determined with a colorimetric assay using hydroxyproline standards (stock concentration: 2 mg/ml hydroxyproline in 0.001 N HCl). In the first step, chloramine-T (0.06 M chloramine-T, deionized water, 2- metoxyethanol, and hydroxyproline

buffer in a proportion of 2:3:5) was mixed with bone hydrolysates and standards in a 1:2 ratio. This mixture was then incubated in darkness at RT for 20 minutes to oxidize the hydroxyproline. The oxidation was terminated by adding 4.5 M perchloric acid and incubating for another 5 minutes in the dark. Subsequently, p-dimethylaminobenzaldehyde (200 mg/ml in 2-metoxyethanol) was added to the mixture, followed by an incubation period at 60 °C for 20 minutes, forming a chromophore. Following the incubation, the samples cooled for 5 minutes at room temperature. The absorbance of bone hydrolysates and hydroxyproline standards was measured at 570 nm using a multi-mode microplate reader (Inifinite® 200, Tecan Group Ltd., Männedorf, CH). The total fAGEs are depicted in units of ng quinine fluorescence per mg of collagen. The collagen content is derived from previous research indicating that collagen is composed of 14% hydroxyproline. The total fAGEs are presented in ng quinine fluorescence/mg collagen content.

3. Results

3.1. Multiscale bone quality of cortical bone in T1DM bone disease

We evaluated the bone quality in the human cortical bone, comparing the T1DM group to the age-matched healthy control group in a multiscale manner to better understand the underlying mechanisms of skeletal fragility in T1DM. We analyzed the microstructure of human cortical bone at the femoral mid-diaphysis with micro-computed tomography **(Figure 7A, B)** and found no significant differences between the control and T1DM groups in terms of cortical thickness (p = 0.297; **Figure 7C**), cortical porosity (p = 0.776; **Figure 7D**), and tissue mineral density (p = 0.145; **Figure 7E**).

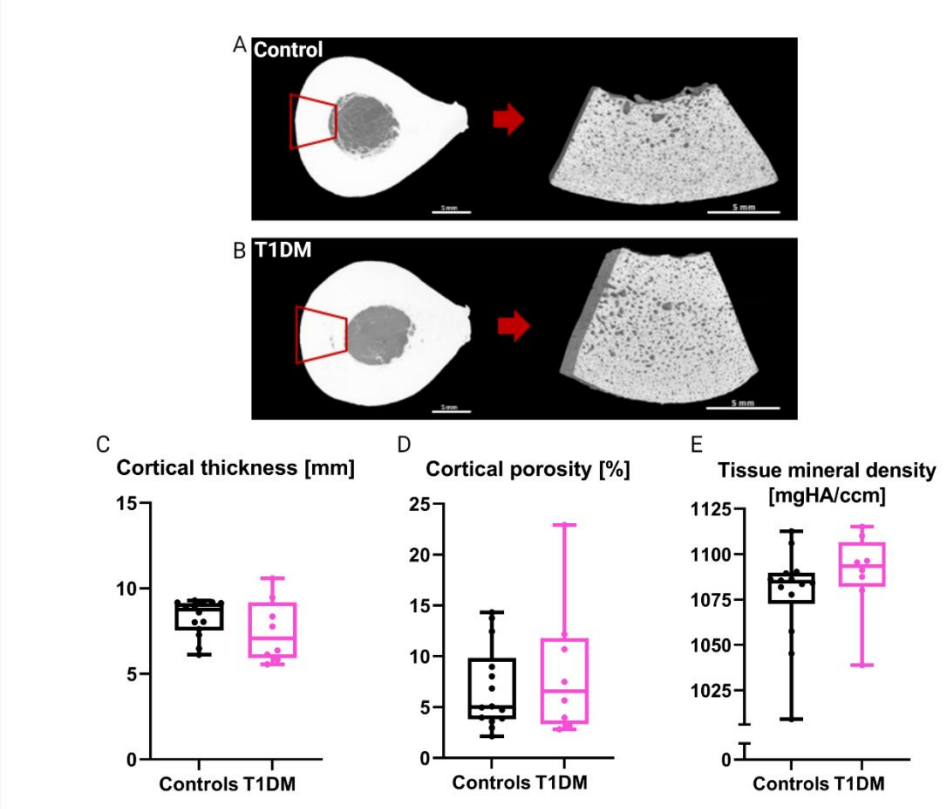

Figure 7: Unchanged microstructure in femoral cortical bone of T1DM individuals. The images denote the whole femoral cross-section imaged with contact radiography and matching 3D scan from microcomputed tomography of the anterior quadrant for the **(A)** control group and **(B)** T1DM group. Parameters derived from microcomputed tomography did not show any differences between the control and T1DM group in **(C)** cortical thickness (p = 0.297), **(D)** cortical porosity (p = 0.776), or **(E)** tissue mineral density (p = 0.145). Cohort details: 22 femoral samples of the mid-diaphysis, eight individuals with diagnosed T1DM, both sexes. Adapted from Dragoun Kolibová et al., 2023.

The activity of bone cells was assessed in toluidine blue–stained sections at the endocortical and periosteal regions using static cellular histomorphometry. The overall cellular activity was low in both groups. We observed osteoblasts in 28.5% of controls and in 25% of the T1DM samples in the endocortical region. In the periosteal region, we observed active osteoblasts in 35.7% of controls and 25% of T1DM specimens. Osteoclasts were present in 21.4% of control samples and in 12.5% of T1DM samples in the endocortical area. In the periosteal region, we found active osteoclasts in only 21.4% of controls, whereas 37.5% of T1DM cases showed osteoclast activity.

Osteocytes are the main mechanosensors and bone-regulating cells. Therefore, we further investigated their viability in cortical bone specimens. We used the TUNEL assay to visualize DNA breakage in the human cortical bone to identify apoptotic osteocytes. We normalized the number of apoptotic osteocytes per analyzed bone area. The results of TUNEL staining showed a comparable number of apoptotic osteocytes per bone area between the control and T1DM group in the endocortical ($p = 0.322$; **Figure 8E**) and periosteal regions ($p = 0.239$; **Figure 8G**). Caspase-3 IHC staining is a more sensitive technique and can determine earlier stages of apoptosis; therefore, it was used as a complementary method to quantify osteocyte apoptosis. In the T1DM group, we found a significantly higher occurrence of apoptotic osteocytes per bone area in the endocortical region ($p = 0.035$; **Figure 8D**) and periosteal region ($p = 0.013$; **Figure 8H**) compared to the healthy control group.

The last morphological state of osteocytes undergoing cell death is the mineralization of the osteocyte lacunae (micropetrosis). We visualized and quantified osteocyte lacunar mineralization using high-resolution qBEI. We determined the number of fully mineralized and partially mineralized lacunae (**Figure 9C-F**) to demonstrate the longitudinal process of micropetrosis. The total number of micropetrotic lacunae did not differ between controls and T1DM in the endocortical ($p = 0.704$) and periosteal regions ($p = 0.263$). In the periosteal region, T1DM showed a significantly higher number of fully mineralized lacunae than controls ($p = 0.043$). Furthermore, we found a comparable level of micropetrosis in the interstitial bone between controls and T1DM in the endocortical ($p = 0.906$) and the periosteal regions ($p = 0.522$). In osteonal bone, the number of micropetrotic osteocytes was not different in the endocortical region ($p = 0.183$). In contrast, it was higher within osteons of the periosteal region in T1DM compared to controls ($p= 0.049$).

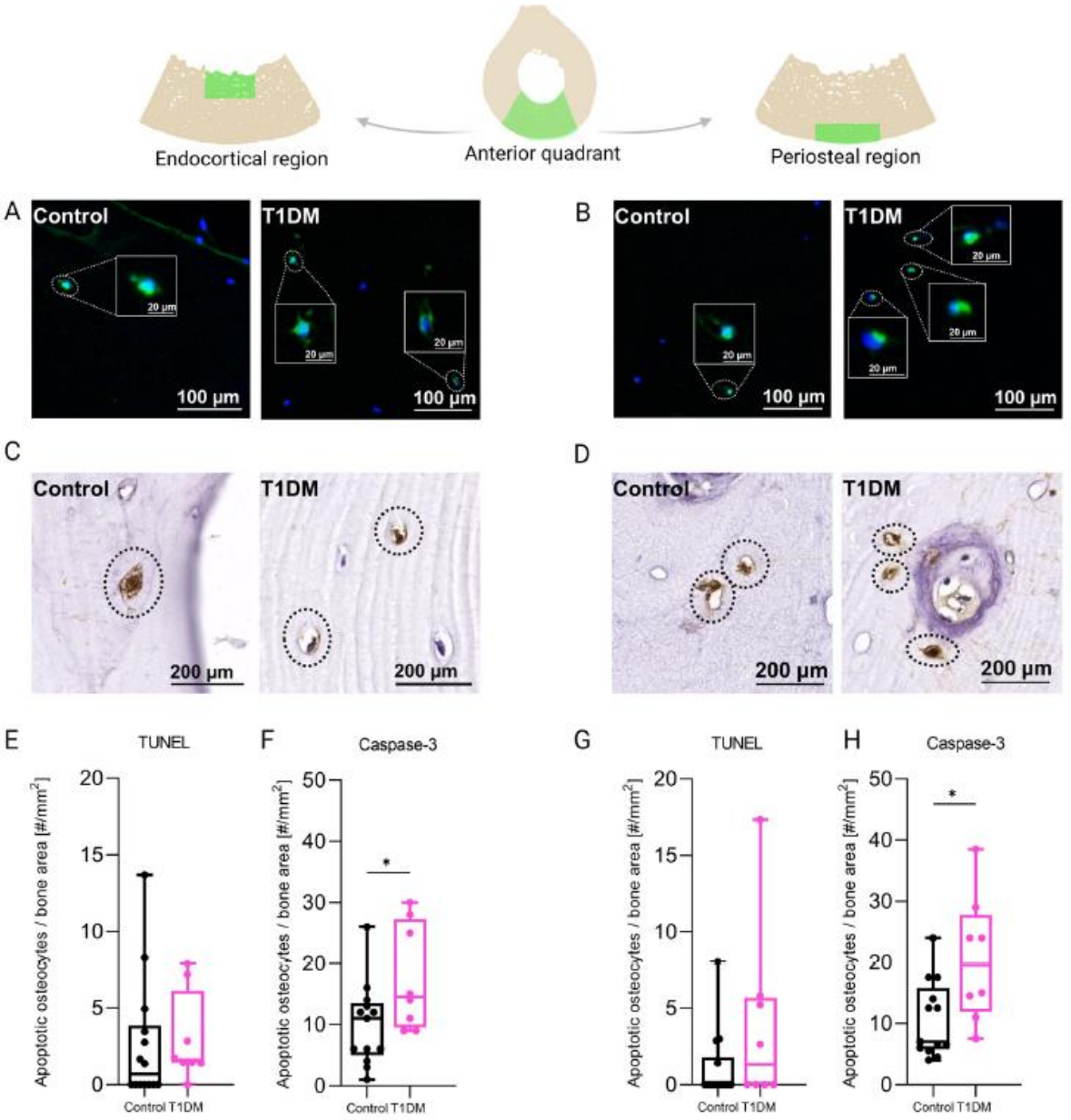

Figure 8. Increased osteocyte apoptosis in the T1D cortical bone. Illustrative images from TUNEL assay **(A)** endocortical and **(B)** periosteal regions of the control and T1DM groups. Illustrative images of apoptotic osteocyte marked in black stained with caspase-3 IHC assay from **(C)** endocortical and **(D)** periosteal regions of the control and T1DM groups. (**E, G)** A comparable level of apoptotic osteocyte from TUNEL assay. **(F, H)** A significantly increased number of apoptotic osteocytes in T1DM was detected with caspase-3 IHC (endocortical: $p = 0.035$ and periosteal: $p = 0.013$ regions). Cohort details: 22 femoral samples of the mid-diaphysis, eight individuals with diagnosed T1DM, both sexes. Adapted from Dragoun Kolibová et al., 2023.

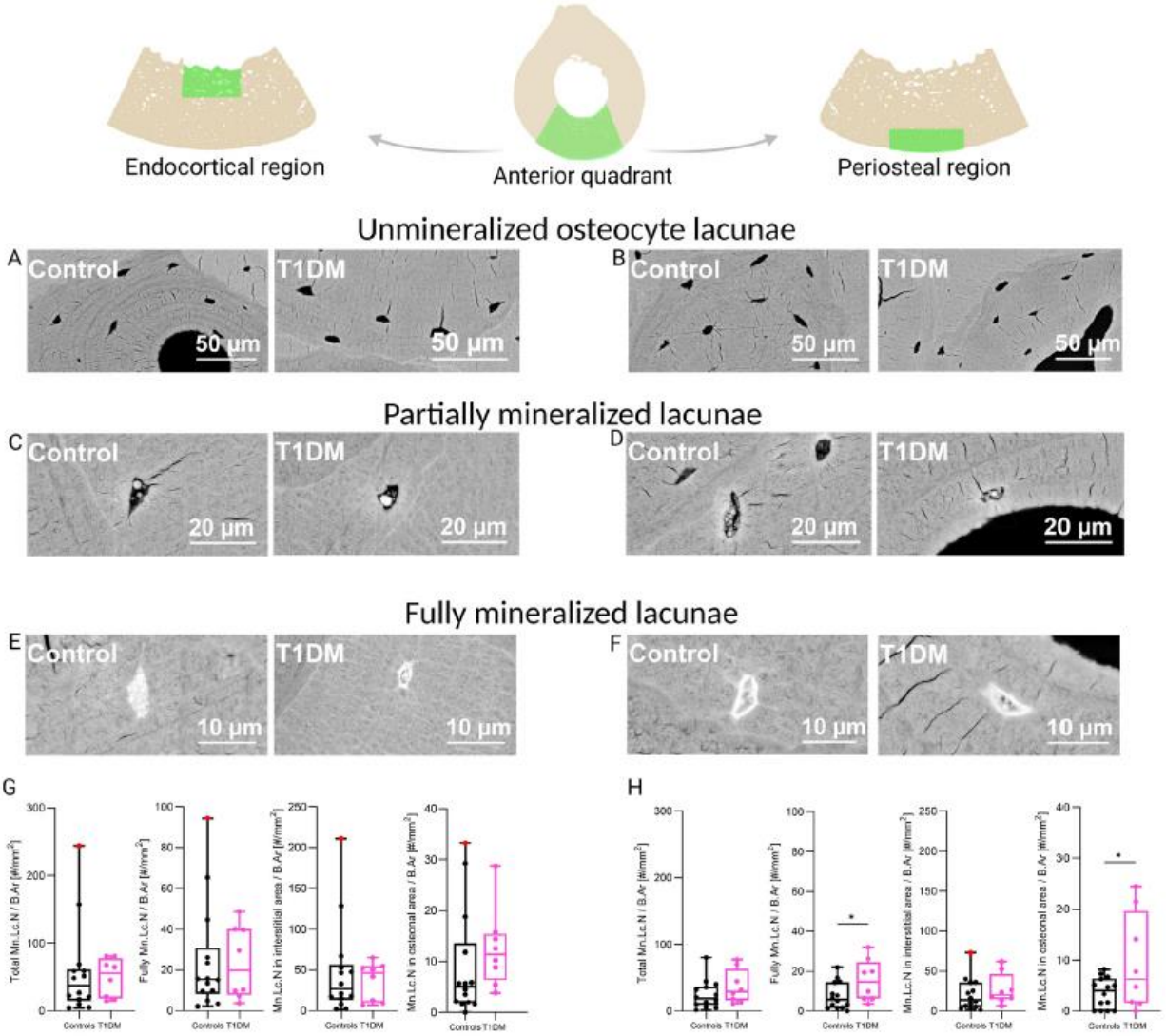

Figure 9: The periosteal region of the T1DM group exhibits altered osteocyte viability. Illustrative images of unmineralized osteocyte lacunae in the **(A)** endocortical and **(B)** periosteal regions of the control and T1DM groups. Osteocyte lacunar mineralization (micropetrosis) is a gradual mineralization process. In the beginning phases, the osteocyte lacunae are partially filled with calcified nanospherites or by a white layer around the lacunar edges. Partially filled lacunae are shown from **(C)** endocortical and **(D)** periosteal regions for the control and T1DM groups. Completely mineralized lacunae are the last stage of the micropetrotic events. These fully mineralized lacunae are shown from the **(E)** endocortical and **(F)** periosteal regions for the control and T1DM groups. **(G)** In the endocortical region, the number of micropetic lacunae showed comparable values between the control and T1DM group in the following parameters: total number of mineralized lacunae per bone area (Total Mn.Lc.N/B.At; partially and fully mineralized lacunae; p = 0.570); number of fully mineralized lacunae per bone area (Fully Mn.Lc.N/B.At; p = 0.868); number of mineralized lacunae per interstitial bone area (Mn.Lc.N/B.At in interstitial area; p = 0.920); number of mineralized lacunae per osteonal bone area (Mn.Lc.N/B.At in osteonal area; p = 0.145). **(H)** In the periosteal region was found a significantly higher number of Fully Mn.Lc.N/B.At (p = 0.046) and Mn.Lc.N/B.At in osteonal area (p = 0.041) in the T1DM group compared to control specimens. Total Mn.Lc.N/B.At (p = 0.212) and Mn.Lc.N/B.At in interstitial area (p = 0.297) was unchanged in the control and T1DM groups. Cohort details: 22 femoral samples of the mid-diaphysis, eight individuals with diagnosed T1DM, both sexes. Adapted from Dragoun Kolibová et al., 2023.

qBEI also allowed us to obtain bone mineral density distribution (BMDD) from the endocortical (**Figure 10A**) and periosteal regions (**Figure 10B**) in both the control and T1DM groups. There was no difference in BMDD between controls and the T1DM group in either the endocortical region ($p = 0.412$) or the periosteal region ($p = 0.551$). We further subdivided the analyzed bone into the osteonal and interstitial bone areas, and we did not observe any differences in calcium weight percentage between the control and T1DM groups in either the endocortical ($F(1,13) = 0.494$; $p = 0.495$, **Figure 10C**) or the periosteal region ($F(1,13) = 0.099$; $p = 0.757$, **Figure 10D**). However, among both studied groups, the osteonal bone area showed a lower degree of mineralization (lower calcium content) than interstitial bone for both the endocortical ($F(1,13) = 159.3$; $p = <0.0001$, **Figure 10E**) and periosteal ($F(1,13) = 65,24$; $p = <0.0001$, **Figure 10F**) regions, pointing to the fact that the tissue age of the osteonal area is younger compared to the more mineralized interstitial area.

Microdamage accumulation in the bone matrix can have a harmful impact on bone quality. The presence of a greater number of microcracks leads to a deterioration in the structural integrity of the bone, thereby increasing the fracture risk. Fluorescent dye rhodamine-6G was used to infiltrate cortical bone specimens, allowing visualization of the microcracks with confocal microscopy. To assess microdamage accumulation, we quantified the number and length of microcracks and normalized them to the mineralized bone area in the endocortical (**Figure 11A**) and periosteal regions (**Figure 11B**). In the endocortical region, we did not observe any changes in the number, length, or branching of microcracks between the control and T1DM groups (**Figure 11C-E**). In contrast, a statistically significant increase in the number ($p = 0.048$; **Figure 11F**) and length ($p = 0.015$; **Figure 11G**) of microcracks was observed in the periosteal region. Microcracks originating from the main crack branch are indicated as microcrack branching. The degree of branching was more prominent in the T1DM group compared to the control group, although the difference was not statistically significant ($p = 0.059$; **Figure 11H).**

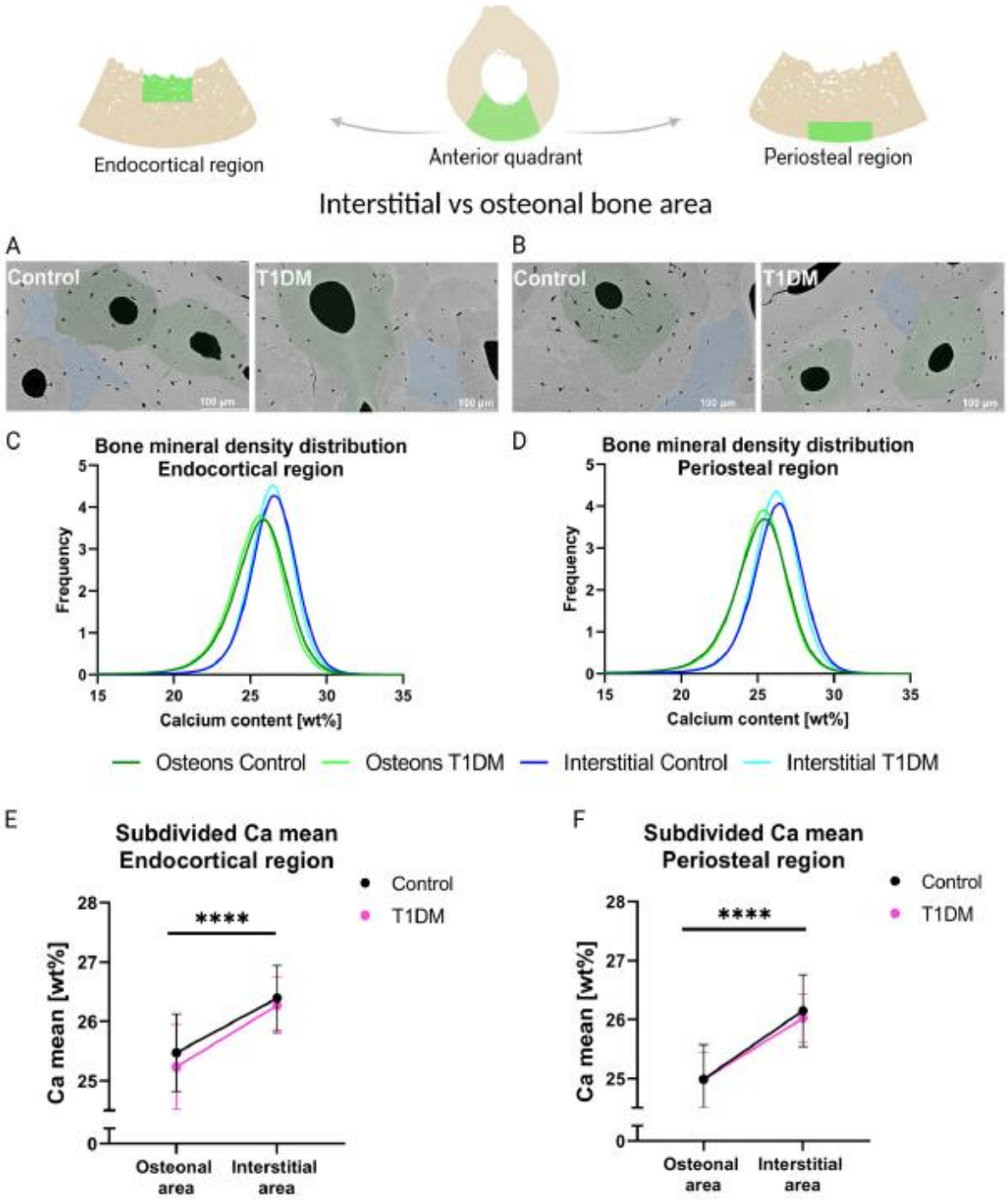

Figure 10: Unchanged BMDD in T1DM cortical bone. Representative qBEI images from the control and T1DM groups in the **(A)** endocortical and **(B)** periosteal regions, with highlighted examples of the osteonal area in blue and the interstitial area in green. Frequency distribution graphs illustrate that the mineral distribution is comparable between the control and T1DM groups. The interstitial area contained higher calcium content than the osteonal bone area in the control and T1DM groups in the **(C)** endocortical and **(D)** periosteal regions. The mean calcium weight percentage (Ca mean, wt%) in the osteonal bone area consistently showed a significantly lower Ca mean than the interstitial area in both the **(E)** endocortical and **(F)** periosteal regions in the control and T1DM groups. Cohort details: 22 femoral samples of the mid-diaphysis, eight individuals with diagnosed T1DM, both sexes. Adapted from Dragoun Kolibová et al., 2023.

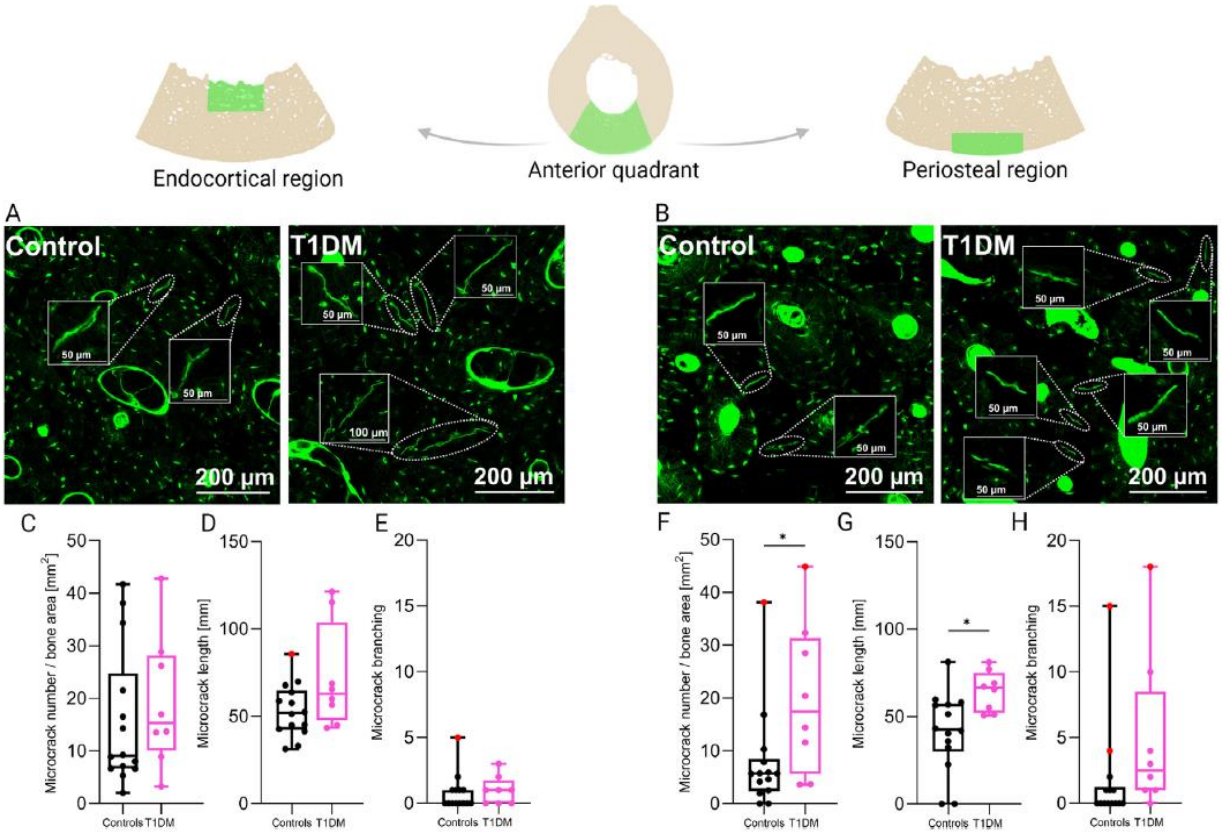

Figure 11: The T1DM group exhibits greater microcrack accumulation and total microcrack length in the periosteal cortex. Representative images of linear microcracking in (A) endocortical and (B) periosteal regions of the control and T1DM groups. Quantification of microdamage accumulation, including the (C, F) number of linear microcracks per bone area (endocortical: p = 0.365 and periosteal: p = 0.048), (D, G) microcrack length per bone area (endocortical: p = 0.165 and periosteal: 0.015), and (E, H) microcrack branching as microcracks derived from the main branch (endocortical: p = 0.720 and periosteal: p = 0.059). Cohort details: 22 femoral samples of the mid-diaphysis, eight individuals with diagnosed T1DM, both sexes. Adapted from Dragoun Kolibová et al., 2023.

3.2. Mineralization of osteocyte lacunae in diabetic bone disease

Micropetrosis is a process of gradual mineralization of the osteocyte lacune, and it is increasing in the elderly population or during pathological conditions. The living stages of the osteocyte and consequent lacunar mineralization are depicted in **Figure 12**. Our study on T1DM cortical bone revealed an increasing number of micropetrosis in the younger periosteal region of T1DM individuals (**publication 1**). However, only a few studies investigate lacunar mineralization under metabolic diseases such as osteoporosis or diabetes. Therefore, we evaluated the current knowledge on micropetrosis in clinically relevant bone pathologies. Our finding consistently indicates that micropetrosis is an independent mineralization process that significantly differs from a standard bone matrix mineralization, and individuals with increased lacunar mineralization do not have a difference in bone mineralization level. Apart from increased lacunar mineralization in T1DM, there is evidence of higher lacunar mineralization in osteoporosis and osteoarthritis [83]. Furthermore, some medications can also affect lacunar mineralization [72,84,85]. Denosomab inhibits osteoclast formation and decreases bone remodeling by reducing bone resorption, leading to higher levels of micropetrosis in the cortical bone of denosomab-treated patients [84]. Taken together with our recent results from T1DM cortical bone, these findings indicate the relevance of lacunar mineralization in metabolic bone pathologies.

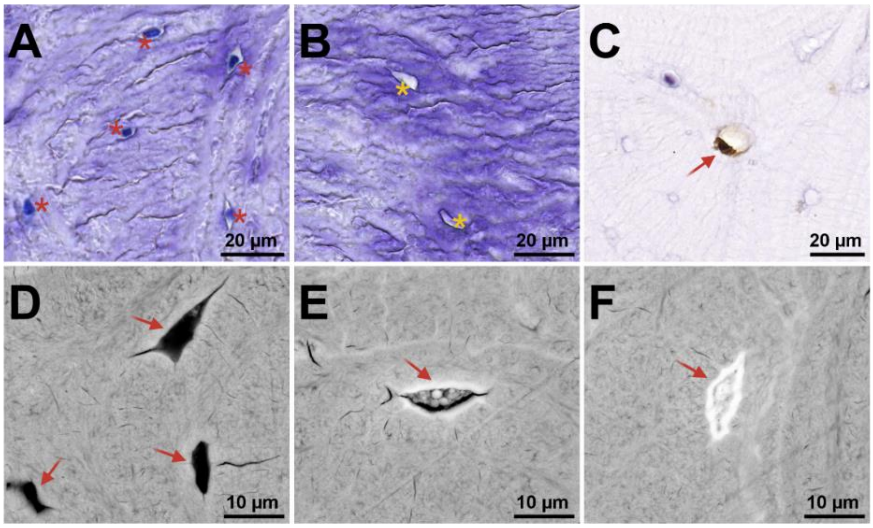

Figure 12: Individual life stages of the osteocyte. (A) The histological image of toluidine blue stained human cortical bone with living osteocyte cells highlighted by red asterisks. **(B)** Toluidine blue stained human cortical bone demonstrating empty osteocyte lacune highlighted by yellow asterisks. **(C)** Apoptotic osteocyte stained with caspase-3 antibody highlighted by the red arrow. After osteocyte cell death, its lacuna gradually fills with mineral in several stages detectable by electron microscopy. **(D)** Red arrows highlight non-mineralized osteocyte lacunae. **(E)** Osteocyte lacunae undergoing mineralization with visible individual calcified spherites. **(F)** Completely mineralized osteocyte lacunae, the red arrow highlights a fully mineralized lacuna. Adapted from Dragoun Kolibová et. al, Osteologie 2022

3.3. Comparable fAGE levels in T2DM tibial bone

We used clinical and laboratory measures to assess the impact of T2DM on structural and compositional factors in human cortical bone. We analyzed thirty tibial samples from both sexes, divided into a healthy control group (n=15) and a T2DM group (n=15). Micro-CT evaluation identified a subgroup of individuals with high cortical porosity in the T2DM group, annotated as T2DMwHP. The T2DM high cortical porosity subgroup was presented with a higher cortical pore diameter measured with HR-pQCT compared to the T2DM group ($p = 0.03$). The mechanical behavior of the cortical bone was tested via in situ impact indentation (BMSi: bone material strength index, which can be assessed in vivo) and reference point indentation (RPI: cyclic measurement technique evaluating the material's behavior during several loading cycles). Although there were no significant differences in clinical in situ BMSi, the experimental RPI measurement revealed altered cyclic indentation properties in the T2DMwHP group. BMDD was comparable between the control and T2DM groups, and further evaluation of composition with Raman spectroscopy found a significant change in the carbonate-to-amide I ratio in the endocortical region of the T2DMwHP group compared to the control ($p = 0.047$) and T2DM ($p = 0.029$) groups. The assessment consisted of fluorescent and colorimetric assays to obtain relative fluorescence per collagen content **(Figure 13A).** Our results did not show any differences between the studied groups. However, in the T2DMwHP group, we observed the highest mean value of 402.2 ± 149.6 ng quinine/mg collagen compared to the control group with 321.9 ± 121.2 ng quinine/mg collagen and the T2DM group with the lowest mean value of 305.7 ± 89.28 ng quinine/mg collagen **(Figure 13B).**

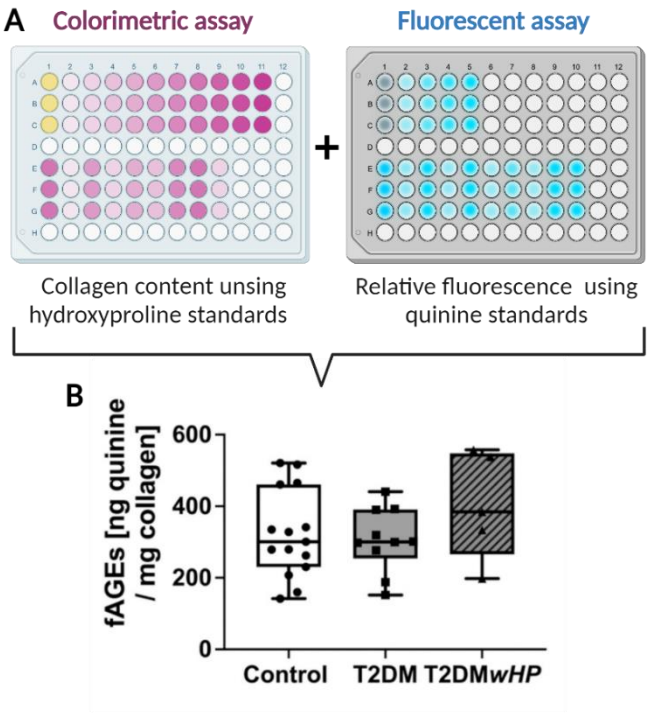

Figure 13: Assessment of total fluorescent AGEs in diabetic bone. (A) Schematic illustrations of the fluorescent and colorimetric assay used to evaluate total fAGEs in the analyzed bone tissue. **(B)** Analysis of fAGEs did not show any significant differences between all three groups despite the highest fAGE levels in the T2DMwHP group. Data in box plots represented individual data points for each group. One-way ANOVA was applied for normally distributed data to determine p values. $p < 0.05$ is regarded as statistically significant. T2DM: type 2 diabetes mellitus; T2DMwHP: type 2 diabetes mellitus with high cortical porosity. Cohort details: 30 tibial samples of the mid-diaphysis, 15 individuals with diagnosed T2M, both sexes. Adapted from Wölfel, E. M., Fiedler, I. A. K., **Dragoun Kolibová, S.**, et al., 2022.

3.4. Unchanged cortical matrix composition and fracture properties in T2DM

Fracture toughness was evaluated on notched tibial cortical bone samples obtained from twenty-nine male donors, divided into a healthy control group (n=18) and a T2DM group (n=11). Both groups have comparable microstructure determined with micro-CT. Further investigation of bone quality indices revealed no changes in bone matrix composition assessed with Raman spectroscopy. Notched samples were used for biomechanical testing with a 3-point bending test showing unchanged properties between the control and T2DM groups. Following the 3-point bending test, we determined the mineralization degree at a tissue level around the crack path with qBEI. The average calcium content (Ca Mean) was 25.54 ± 0.45 and 25.79 ± 0.57 calcium weight percentage for control and T2DM groups, respectively **(Figure 14A)**. The highest calcium weight percentage (Ca peak) was 25.84 ± 0.51 and 26.01 ± 0.6 calcium weight %, for control and T2DM groups, respectively **(Figure 14B, C)**. Furthermore, to assess bone nanoscale biomechanical properties, nanoindentation was performed around the crack region on a smaller sample set **(Figure 14D)**. We observed a similar Young's modulus (control: 19.26 ± 0.5 GPa and T2DM: 20.26 ± 1.74 GPa) and hardness (control: 0.78 ± 0.02 GPa and T2DM: 0.82 ± 0.08 Gpa; **Figure 14E, F**). Data from nanoindentation experiments reflected the unchanged mineralization parameters, indicating similar bone matrix composition in both the control and T2DM groups.

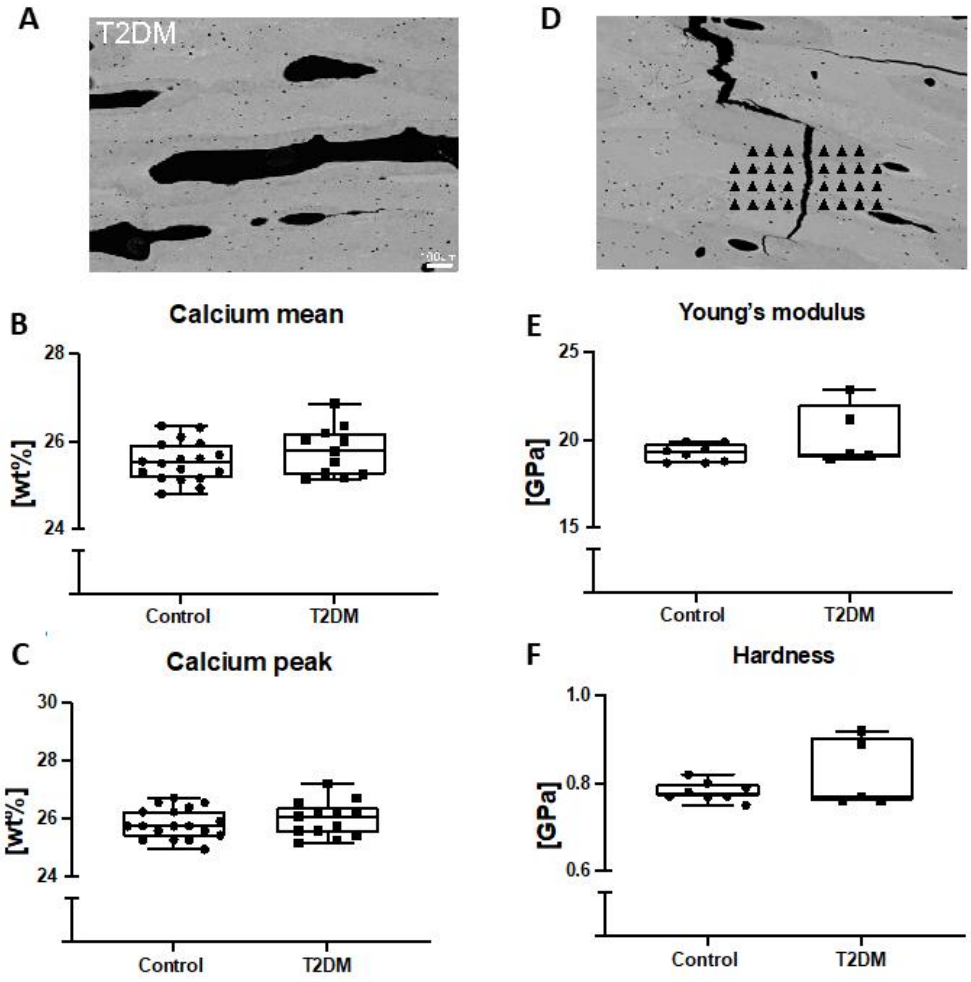

Figure 14: Comparable bone mineralization and nano-biomechanical properties in T2DM cortical bone. (A) Representative image acquired in BSE imaging mode. **(C)** Average calcium weight percentage and **(C)** highest calcium weight percentage are comparable in control and T2DM groups around the crack path. **(D)** Nanoindentation was performed around the crack path. **(E)** Young's modulus and **(F)** hardness show analogous values for a subset of samples from both groups. Cohort details: 29 tibial samples of the mid-diaphysis, 11 individuals with diagnosed T2M, males. Adapted from Wölfel, E. M., Bartsch, B., Koldehoff, J., Fiedler, I. A. K., **Dragoun Kolibová, S.** et al., 2023.

4. Discussion

Diabetes mellitus is identified as a novel risk factor for fragility fractures and represents a significant burden from diabetes-induced osteoporosis, which is on the rise globally with the aging population. Fractures related to diabetes are a contributing factor to the increase in morbidity, mortality, and healthcare expenses. This thesis identified novel predictors of fracture risk in diabetic patients that may contribute to future development and research of possible biomarkers characterizing the impaired bone matrix. Thereby, this thesis provides novel insights into biological mechanisms that contribute to altered bone quality parameters in human cortical bone affected by diabetes. The following discussion summarizes information from the attached original manuscripts (**Dragoun Kolibová** et al., 2023; **Dragoun Kolibová** et al., 2022; Wölfel, Fiedler, **Dragoun Kolibová** et al., 2022; Wölfel, Bartsch, Koldehoff, Fiedler, **Dragoun Kolibová** et al., 2023).

4.1. Osteocyte apoptosis and microdamage accumulation in T1DM

Osteocytes are responsible for constructing a mechanosensitive network within the mineralized bone matrix and play a crucial role in regulating bone remodeling. As a result, it is pivotal to maintain the viability of osteocytes to ensure proper bone homeostasis. Research has shown that osteocyte viability is negatively impacted by diabetic hyperglycemia [86,87]. We analyzed femoral cortical bone samples, focusing on two regions of interest: endocortical and periosteal bone areas. To address objective 1, we employed a multiscale imaging approach, combining high-resolution microcomputed tomography, quantitative backscattered electron imaging, confocal laser scanning microscopy, and immunohistochemistry to comprehensively evaluate the effect of T1DM on bone quality in human cortical bone, with the main focus on osteocyte viability, mineralization, and microdamage accumulation.

Clinical research indicates reduced BMD in T1DM individuals. However, DXA data in our study did not show differences in vertebral BMD, which is consistent with a previous study [88]. Similarly, there were no differences in microarchitecture between T1DM and the control group, which was in line with unchanged cortical geometric indices in the T1DM group compared to the control groups. Microarchitectural changes in T1DM bone seem to be more pronounced in individuals with diabetic complications, which might explain the observed discrepancies [89] and further emphasize the need to explore beyond traditional BMD assessments.

While it is commonly expected that individuals with T1DM would have low bone turnover [90], the rate of bone turnover and the number of bone cells are already low in the cortical bone compared to the trabecular bone [91]. As a result, it becomes difficult to identify any significant differences between the T1DM and control groups. In order to obtain a more comprehensive understanding of the remodeling capability of diabetic bone, we conducted a study on osteocyte viability parameters in the cortical bone rather than the metabolically active trabecular bone.

Earlier investigations have shown that fatigue microcracking and subsequent osteocyte apoptosis can initiate new resorption centers in bone tissue [92]. Various studies involving animals and *in vitro* experiments have suggested that high glucose levels or diabetes may induce osteocyte apoptosis [86,87].

While the TUNEL data did not reveal any significant differences between the groups, it did hint at a possible increase in osteocyte apoptosis in the T1DM group. A complementary method was required to obtain accurate measurements of apoptosis. The TUNEL assay detects DNA fragmentation, which can also occur in cells undergoing DNA repair and not necessarily in apoptotic cells. On the other hand, the caspase-3 assay detects earlier stages of apoptosis, and the DAB detection utilized in the caspase-3 assay amplifies the signal, further enhancing its sensitivity [93,94]. By leveraging the caspase-3 assay, we were able to determine a significantly increased level of osteocyte apoptosis in the T1DM group compared to the healthy control group. *In vitro* studies on osteocyte-like MLO-Y4 cells confirm our findings. Tanaka and colleagues found that MLO-Y4 cells undergo apoptosis in response to high glucose levels and AGEs [95]. The potential mechanism behind AGE-induced osteocyte apoptosis involves the upregulation of RAGE, proapoptotic genes such as p53, and transcriptional factors like FOXO1 [96]. This leads to the activation of caspase-3 signaling [96], which ultimately results in cellular apoptosis.

Our previous research demonstrated that the mineralization of osteocyte lacunae with mineral occlusions, known as micropetrosis, is more prominent in aged human bone and may lead to reduced bone mechanical competence [65,76]. We examined partially and fully mineralized osteocyte lacunae. The partially mineralized lacunae may not reach complete mineralization as they can be removed during remodeling compared to fully mineralized osteocyte lacunae, the endpoint of micropetrosis. As we showed in our previous study, the accumulation of mineralized lacunae occurs more frequently in the endocortical region with aging compared to the periosteal region [65]. This is because the periosteal region is younger due to the apposition of the newly formed bone matrix during lifespan [21]. Interestingly, geometric cross-section indices were similar in the T1DM and age-matched control groups, indicating that T1DM does not impact the periosteal apposition process. However, we found a significantly higher number of fully mineralized lacunae in the periosteal region of the T1DM group,

which is counterintuitive given the younger bone tissue of the periosteal bone. An increase in osteocyte apoptosis causes a reduction in the viable osteocyte cell pool and provides more opportunities for micropetrotic events, which in turn can negatively impact bone mechanical properties. Specifically, a higher density of micropetrotic lacunae can make the bone matrix more brittle [97,98], resulting in a higher susceptibility to microcracking.

Prolonged low-bone turnover in diabetes can lead to defects in microdamage repair, which can cause an increase in microcrack accumulation. This is supported by a study conducted on the streptozotocin-induced rat model of T1DM, which showed a significantly higher density of both linear and diffuse microdamage in diabetic ulnae when compared to non-diabetic ulnae after ulnar loading [99]. The accumulated microdamage in diabetic rat bones caused a severe disruption of the LCN and reduced osteoclast activation, resulting in a reduction in bone resorption [99]. Our data were consistent with the findings in the T1DM rat model, as they showed an increased number and length of linear microcracks per bone area in the periosteal region in the T1DM group when compared to the control group. Increased osteocyte apoptosis in the diabetic group suggests that T1DM induces early osteocyte cell death, causing malfunction of the osteocyte network, which reduces the ability of bone to repair microdamage, resulting in higher microcrack accumulation in the cortical bone of the T1DM group.

Furthermore, we evaluated the mineralization degree of bone regions with different tissue ages in the osteonal and interstitial bone areas. The younger osteonal bone area is less mineralized than the older and more mineralized interstitial bone area [29,100], and there were no differences in mineralization profiles between osteonal and interstitial bone in either T1DM or the control group. However, we observed variations in micropetrosis levels within the osteonal and interstitial bone area in the periosteal region of the T1DM group. Notably, T1DM patients had a significantly higher number of micropetrotic lacunae in the osteonal bone area compared to the control group. This observation is surprising given that the interstitial bone area is characterized by higher mineralization and a reduced number of osteocytes with a limited supply of nutrients, making the interstitial bone area a preferential site for micropetrosis [65,101]. Nevertheless, we determined an increased number of micropetrotic lacunae within the osteonal bone area in the periosteal region of the T1DM group. Presented data suggest that individuals with T1DM may experience accelerated cellular aging, which could lead to the premature death of osteocytes and pronounced lacunar mineralization, as seen in the osteonal bone of the periosteal region in the T1DM group.

The study suggests that osteocyte apoptosis is a potential cause of cortical T1DM pathology. Osteocyte apoptosis was found to be more common in both endocortical and periosteal regions in T1DM patients. The study also found that T1DM impairs bone quality. Specifically, we found increased microcrack

accumulation and micropetrosis levels in the periosteal region of T1DM cortical bone. These findings suggest that T1DM accelerates the aging effects in the bone matrix and leads to the premature death of osteocytes, which is summarized in Figure 15.

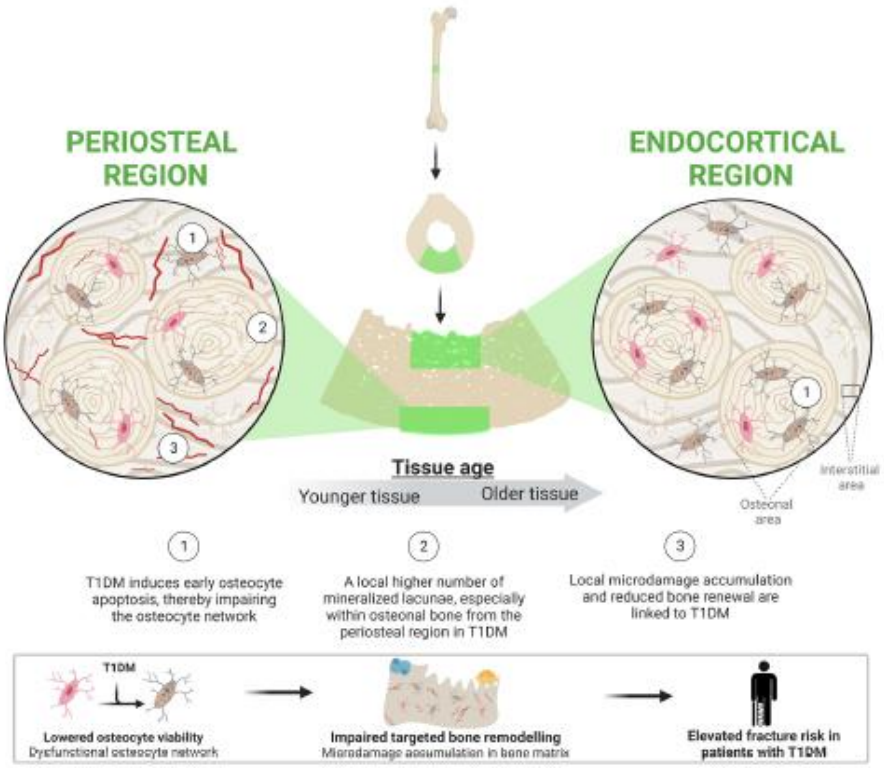

Figure 15: Impact of T1DM on human cortical bone. T1DM negatively impacts bone mechanical competence as it leads to an increase in osteocyte cell death followed by a higher level of lacunar mineralization, which results in a decreased ability to detect and repair microdamage. This, in turn, leads to failure, delay, or prevention of the remodeling process in the diabetic cortical bone. Adapted from Dragoun Kolibová et al., 2023.

4.2. Impact of metabolic disorders on osteocyte-lacunar mineralization

Micropetrosis is a gradual process of filling osteocyte lacunar space with mineral occlusions and is an end state of the osteocyte lifespan. The elliptical shape of osteocyte lacunar cavities contributes to bone toughening mechanisms by attracting or deflecting cracks, preventing crack propagation, and dissipating energy [102,103]. Therefore, the investigation of the lacunar fate after osteocyte cell death is an intriguing area of study due to the potential negative impact of mineralized lacunae on the mechanical behavior of bone because hypermineralized spots in the bone matrix do not contribute to the toughening mechanism and can increase bone brittleness [97,98]. The level of micropetrosis naturally increases in the aged bone matrix [65,76]. However, not many studies investigated the implication of lacunar mineralization under pathological conditions.

Metabolic diseases such as diabetes mellitus cause chronic hyperglycemia and osteocyte dysfunction [14,104]. Hyperglycemia harms bones by forming AGEs and stimulating their receptor RAGE, causing an increase in oxidative stress. This alteration in the bone matrix increases cytokine production, which

negatively affects the survival of osteoblasts and osteocytes [104–106]. Furthermore, insulin plays a critical role in facilitating mineral accretion, which refers to the process of mineral deposition and growth [107,108]. Therefore, the combination of high blood sugar and high insulin levels in T2DM can potentially lead to increased lacunar mineralization [104]. Additionally, T2DM is associated with a reduced bone remodeling rate and thereby a decreased replacement of bone matrix [109,110], which may contribute to the accumulation of micropetrotic lacunae in the bone matrix. The impact of long-term glycemic control on fracture risk varies between patients with T1DM and T2DM [111]. Maintaining a healthy metabolism requires consistent monitoring of glycemia. The functionality of osteocytes is directly impacted by the level of glucose in the blood. As a result, any blood glucose fluctuations can harm osteocytes and ultimately reduce their survival ability [13, 77, 78]. Because glycemic control influences more T1DM patients [112], it can be assumed that the effect of poor glycemic control on lacunar mineralization in T1DM would be more significant compared to that in T2DM. In T1DM cortical bone, we determined an increased number of micropetrotic lacunae within the periosteal osteons **(Publication 1)**, which is counterintuitive with the younger bone tissue being present in osteonal bone, suggesting the effect of T1DM on osteocyte viability and consequent lacunar mineralization.

Osteoporosis and osteoarthritis are two distinct bone pathologies that are commonly found in the elderly population. Carpentier and colectiv conducted a study to analyze lacunar mineralization in trabecular bone biopsies of individuals with osteoporosis (OP) and osteoarthritis (OA) compared to healthy individuals. The study found a significantly higher incidence of lacunar mineralization in the bone specimens of OP and OA patients [83]. Moreover, the level of bone mineralization was comparable between the OP, OA, and control groups [83]. Our investigation of cortical bone in T1DM **(Publication 1)** revealed results consistent with those found in OP and OA bone specimens. Specifically, we observed no differences in bone mineralization between the healthy and diseased groups. The data suggests that the total amount of calcium does not influence the mineralization of lacunae in the bone matrix **(Publication 1)** [83].

Denosumab is a monoclonal antibody used to treat bone loss in osteoporosis. It targets the RANKL protein, which prevents the activation of the RANK receptor on osteoclasts and their precursors. As a result, it inhibits the formation of osteoclasts and reduces bone remodeling by decreasing bone resorption [113]. We have previously analyzed bone biopsies of patients on denosumab treatment, patients who had discontinued their denosumab treatment without further osteoporosis treatment, and a treatment-naive group [84]. We found that osteocyte viability remained consistently low after treatment discontinuation, in the absence of follow-up osteoporosis medication, and without any increase in osteocyte apoptosis. Additionally, we found an increased number of mineralized lacunae

in the cortical bone of patients who received denosumab treatment, emphasizing the importance of removing old bone matrix and highlighting the significance of bone remodeling status[84]. Bisphosphonates, another bone-loss treatment, not only inhibit bone resorption but also prevent osteocyte cell death and promote their survival. Moreover, bisphosphonates act as analogs to pyrophosphates (mineralization inhibitors) and help prevent excessive lacunar mineralization and maintain the fluid flow within the osteocyte network, positively affecting the regulation of bone turnover [85].

Micropetrosis or osteocyte lacunar mineralization is a unique process that significantly differs from normal bone matrix mineralization. Chronic bone-related diseases, such as osteoporosis or diabetic bone disease, are prevalent among millions of individuals and significantly affect the welfare of patients. The higher incidence of micropetrosis in OP, OA, and diabetic patients highlights lacunar mineralization as a novel feature of pathological changes in diseased bone. The current treatments for bone loss mainly target the regulation of osteoblasts or osteoclasts. However, shifting the focus to osteocytes as a pharmacological target may offer potential benefits in treating bone loss.

4.3. Clinical and experimental parameters of bone quality in cortical bone of individuals with T2DM

Higher fracture risk in diabetic patients is challenging to detect with common clinical fracture risk assessment due to normal or high BMD in T2DM. The observed higher fracture risk despite normal to high BMD in T2DM patients points towards impaired bone material quality. Here, we analyze tibial bone from individuals with type 2 diabetes mellitus using a multiscale approach, which includes clinical and laboratory-based bone quality measures to investigate how structural and compositional factors affect bone mechanical properties in healthy and T2DM cortical bone.

The T2DMwHP subgroup was presented with a higher cortical pore diameter measured with HR-pQCT compared to the T2DM group. While cortical porosity alone does not fully explain the increased risk of fractures observed in T2DM patients [36,110], it has been reported by other researchers as a common feature of T2DM [42,111].

Although the in situ BMSi measurements did not show any differences between all groups, the altered cyclic indentation properties in the T2DMwHP group suggest lower bone toughness in the T2DMwHP group but not in the T2DM group. This is supported by results from a study on the diabetic ZDF rat model showing increased indentation distance in diabetic animals, which was negatively associated with bone toughness determined with 3-point bending in rat femurs and lumbar vertebrae [112].

Bone mineralization reflected as calcium density distribution was comparable between control and T2DM groups. Further compositional changes analyzed with Raman spectroscopy revealed a higher carbonate-to-amide I ratio in the T2DMwHP group, which can result from either a higher carbonate content or a lower collagenous amide I content. Based on similar mineralization across all groups, it can be assumed that the carbonate content remains unaffected and points towards lower amide I content.

Diabetic hyperglycemia contributes to the increased accumulation of AGEs in the bone matrix, which changes collagen properties. In this study, we measured the content of fluorescent AGEs normalized to hydroxyproline content. We observed an increase of 25% higher values in the T2DMwHP group compared to the T2DM and control groups. Nevertheless, this difference was not statistically significant. However, it is consistent with other studies that have reported similar results. For instance, a study reported comparable values from the cortical mid-diaphysis of T2DM individuals [52].

Similarly, another study on the trabecular bone from the femoral head obtained during total hip arthroplasty found comparable levels of fAGEs [114]. In addition, our findings have been further supported by a study that observed only a rise in the prevalence of fAGES content in cortical bone from the femoral neck [115]. Another study with a similar sample size reported a 1.5-fold higher fAGE level in trabecular bone from T2DM postmenopausal women with osteoarthritis who underwent total hip replacement [116]. It is worth noting that fAGEs assay cannot detect all bone-relevant AGEs. A recent study revealed that non-fluorescent AGE, such as CML, is more abundant in cortical bone than pentosidine [117]. In our previous study, we showed increased CML content in femoral cortical bone from T2DM individuals [52], nonetheless, we can only assume that CML might be higher in the presented T2DM cohort, and further investigation is needed to verify this assumption.

Our research combines in vivo and laboratory techniques to gain insight into translating experimental results into clinically relevant information. Our study uncovered new data on bone material quality parameters in the tibial mid-diaphysis. By merging these data sets, we found that the T2DMwHP group displayed greater cortical pore diameter than the T2DM group measured with HR-pQCT.

4.4. Fracture resistance in male T2DM cortical bone

Bone toughness is not solely determined by bone mass but also by bone material quality parameters such as mineralization or compositional changes. T2DM affects these parameters and may result in a higher fracture risk in diabetic patients. However, there is limited data on the fracture toughness in human diabetic cortical bone. Thus, in this case-control study, we examined fracture resistance in

T2DM cortical bone from male individuals in combination with a multiscale approach to assess bone material quality parameters.

Although we did not detect any changes in bone material quality indices in terms of mineralization, compositional, and mechanical properties in this cohort, previous research has demonstrated that individuals with T2DM exhibit differences in bone matrix characteristics. Increased cortical porosity is a feature reported in some but not all postmenopausal women with T2DM [42,110]. This is accompanied by changes in composition, as found in our previous studies on cohorts of male and female individuals with T2DM [52,111](Publication 3). Compositional changes in the collagenous bone matrix can alter the integrity of the collagen network, which might provide a more robust explanation for discrepancies in fracture toughness among T2DM individuals [113,114]. Furthermore, studies on human bone tissue often bring a significant level of variation. In the context of T2DM bone disease, this complexity poses a challenge in identifying the underlying mechanisms contributing to diabetic bone fragility at the tissue level.

The duration of diabetes significantly impacts the susceptibility of bones to fractures. Findings from a Swedish cohort study suggest that T2DM alone may not necessarily increase fracture risk. However, certain risk factors, such as the duration of diabetes, can considerably elevate the risk of fractures in T2DM patients [115]. The authors of the study estimate that around 21 million people are affected by a risk factor profile that contributes to an increased risk of fractures in T2DM [115]. Longer diabetes duration leads to prolonged high glucose levels in the body, adversely affecting bone cellular activity and decreasing bone turnover in T2DM. Furthermore, prolonged high glucose levels lead to the formation of AGEs, which can impair the properties of collagen within the bone tissue.

To summarize, our research indicates that the cortical bone of individuals with T2DM displays no differences in microstructure or bone material quality compared to healthy, age-matched controls. Similarly, the fracture toughness was unchanged in this cohort. These findings are consistent with recent research that suggests that some subgroups of patients with T2DM may be at a higher risk of fractures, but not all patients share this risk profile.

5. Conclusion and Outlook

Diabetes mellitus (DM) is a chronic metabolic disease that causes high blood glucose levels. Considering the escalating prevalence of diabetes, addressing associated complications, notably bone fragility, is crucial but often underdiagnosed among diabetic patients. This thesis aims to contribute fundamental knowledge of the multiscale characteristics of the human bone matrix affected by T1DM and T2DM.

Investigating the influence of T1DM on cortical bone quality revealed evidence for accelerated aging in terms of increased osteocyte apoptosis and microdamage accumulation. To better understand the mechanisms leading to osteocyte apoptosis in T1DM, future research should investigate how aspects such as oxidative stress and AGE-RAGE interaction contribute to this cellular signaling. Additionally, potential drug screening targets should be identified to improve osteocyte survival. Identifying osteocyte apoptosis as a potential determinant of cortical T1DM pathology proposes a shift from current treatments for bone loss that primarily concentrate on the activities of osteoblasts and osteoclasts while neglecting the potential advantages that could be derived from targeting pharmacological targets towards osteocytes.

More prevalent osteocyte cell death in T1DM leads to excessive lacunar mineralization in the bone matrix. The long-lasting nature of the mineralized lacune might serve as a novel biomarker for assessing bone quality in metabolic and other bone pathologies, providing a promising direction for further exploration. More basic and clinical research is necessary to understand better the structural consequences of lacunar mineralization following osteocyte apoptosis during various pathological conditions. This would create new opportunities for innovative treatments.

Our findings indicate that the risk of fractures is not elevated in all T2DM patients. Rather, it suggests that certain subgroups of T2DM patients have compromised bone mechanical competence. The multiscale approach combining clinical and experimental bone quality assessments identified a subgroup of T2DM individuals with high porosity and altered bone biomechanical properties. While certain subsets of individuals with T2DM may have a greater likelihood of developing fractures, not all T2DM patients exhibit the same risk profile. This heterogeneity within the T2DM population requires the implementation of customized approaches to evaluate and manage fracture risk in those with diabetes mellitus.

6. List of Abbreviations

2D / 3D	two-dimensional/three-dimensional
aBMD	areal bone mineral density
AGEs	advanced glycation end-products
BMD	BMD
BMDD	bone mineral density distribution
BS	bone surface
BV	bone volume
CaHigh	amount of highly mineralized bone tissue above the 95th percentile
CaLow	amount of low mineralized bone tissue below the 5th percentile
CaMean	mean calcium concentration
CaPeak	most frequently occurring calcium concentration
CaWidth	heterogeneity of the mineral distribution
CML	carboxymethyllysine
Ct. Th	cortical thickness
Ct.Po	cortical porosity
DAB	3,3-diaminobenzidine
DM	diabetes mellitus
DXA	dual-energy X-ray absorptiometry
EDTA	ethylenediaminetetraacetic
ES/BS	eroded surface per bone surface
fAGEs	fluorescent advanced glycation end-products
HR-pQCT	high-resolution peripheral quantitative computed tomography
CHO	coronary heart disease
IHC	immunohistochemistry
LCN	lacunar canalicular network
LSCM	laser scanning confocal microscopy
MMA	methyl methacrylate
N.Ob/B.Pm; #/mm	number of osteoblasts per unit bone perimeter
N.Oc/B.Pm; #/mm	number of osteoclasts per unit bone perimeter
O.Th	osteoid thickness
Ob.S/BS	osteoblast surface per bone surface
Oc.S/BS	osteoclast surface per bone surface
OS/BS	osteoid surface per bone surface
OV/BV	osteoid volume per bone volume
PBS	phosphate-buffered saline
qBEI	quantitative backscattered electron imaging
RAGE	receptor for AGEs
RANKL	receptor activator of nuclear factor-kappa B ligand
ROS	reactive oxygen species
RR	relative risk
RT	room temperature
T1DM	type 1 diabetes mellitus
T2DM	type 2 diabetes mellitus
TMD	tissue mineral density
TUNEL	terminal deoxynucleotidyl transferase dUTP nick end labeling

7. List of Figures

8. References

[1] International Diabetes Federation. IDF Diabetes Atlas, 10th edn. Brussels, Belgium: International Diabetes Federation, 2021, 2021.

[2] H. Sun, P. Saeedi, S. Karuranga, M. Pinkepank, K. Ogurtsova, B.B. Duncan, C. Stein, A. Basit, J.C.N. Chan, J.C. Mbanya, M.E. Pavkov, A. Ramachandaran, S.H. Wild, S. James, W.H. Herman, P. Zhang, C. Bommer, S. Kuo, E.J. Boyko, D.J. Magliano, IDF Diabetes Atlas: Global, regional and country-level diabetes prevalence estimates for 2021 and projections for 2045, Diabetes Res Clin Pract 183 (2022). https://doi.org/10.1016/j.diabres.2021.109119.

[3] I. Shamim, Diabetes An Old Disease, a New Insight, 2019.

[4] L.A. DiMeglio, C. Evans-Molina, R.A. Oram, Type 1 diabetes, Lancet 391 (2018) 2449–2462. https://doi.org/10.1016/S0140-6736(18)31320-5.

[5] M. Mobasseri, M. Shirmohammadi, T. Amiri, N. Vahed, H. Hosseini Fard, M. Ghojazadeh, Prevalence and incidence of type 1 diabetes in the world: a systematic review and meta-analysis, Health Promot Perspect 10 (2020) 98–115. https://doi.org/10.34172/hpp.2020.18.

[6] M. Roden, G.I. Shulman, The integrative biology of type 2 diabetes, Nature 576 (2019). https://doi.org/10.1038/s41586-019-1797-8.

[7] M. Stumvoll, B.J. Goldstein, T.W. Van Haeften, Type 2 diabetes: Principles of pathogenesis and therapy, in: Lancet, 2005. https://doi.org/10.1016/S0140-6736(05)61032-X.

[8] A. Ceriello, Oxidative stress and glycemic regulation, in: Metabolism, 2000. https://doi.org/10.1016/S0026-0495(00)80082-7.

[9] A. Ceriello, Glucose Variability and Diabetic Complications: Is It Time to Treat?, Diabetes Care 43 (2020) 1169–1171. https://doi.org/10.2337/dci20-0012.

[10] J.W. Baynes, S.R. Thorpe, The role of oxidative stress in diabetic complications, Curr Opin Endocrinol Diabetes 3 (1996). https://doi.org/10.1097/00060793-199608000-00001.

[11] C. Rask-Madsen, G.L. King, Vascular Complications of Diabetes: Mechanisms of Injury and Protective Factors, Cell Metab 17 (2013) 20–33. https://doi.org/10.1016/J.CMET.2012.11.012.

[12] A. Ceriello, Hyperglycaemia: The bridge between non-enzymatic glycation and oxidative stress in the pathogenesis of diabetic complications, (1999).

[13] A.C. Maritim, R.A. Sanders, J.B. Watkins, Diabetes, oxidative stress, and antioxidants: A review, J Biochem Mol Toxicol 17 (2003). https://doi.org/10.1002/jbt.10058.

[14] N. Napoli, M. Chandran, D.D. Pierroz, B. Abrahamsen, A. V Schwartz, S.L. Ferrari, Mechanisms of diabetes mellitus-induced bone fragility, (2017). https://doi.org/10.1038/nrendo.2016.153.

[15] H.M. Frost, Wolff's Law and bone's structural adaptations to mechanical usage: an overview for clinicians., Angle Orthodontist 64 (1994). https://doi.org/10.1043/0003-3219(1994)064<0175:WLABSA>2.0.CO;2.

[16] K.D. Cashman, Diet, nutrition, and bone health, in: Journal of Nutrition, 2007. https://doi.org/10.1093/jn/137.11.2507s.

[17] G. Karsenty, M. Ferron, The contribution of bone to whole-organism physiology, Nature 481 (2012). https://doi.org/10.1038/nature10763.

[18] A. Wawrzyniak, K. Balawender, Structural and Metabolic Changes in Bone, Animals 12 (2022). https://doi.org/10.3390/ani12151946.

[19] E.A. Zimmermann, B. Busse, R.O. Ritchie, The fracture mechanics of human bone: influence of disease and treatment, Bonekey Rep 4 (2015). https://doi.org/10.1038/bonekey.2015.112.

[20] G.M. Blake, I. Fogelman, The role of DXA bone density scans in the diagnosis and treatment of osteoporosis, Postgrad Med J 83 (2007). https://doi.org/10.1136/pgmj.2007.057505.

[21] E. Seeman, P.D. Delmas, Bone Quality — The Material and Structural Basis of Bone Strength and Fragility, New England Journal of Medicine 354 (2006). https://doi.org/10.1056/nejmra053077.

[22] S. Tadano, B. Giri, X-ray diffraction as a promising tool to characterize bone nanocomposites, Sci Technol Adv Mater 12 (2011). https://doi.org/10.1088/1468-6996/12/6/064708.

[23] R.J. Valderrábano, J.Y. Wu, Bone and blood interactions in human health and disease, Bone 119 (2019). https://doi.org/10.1016/j.bone.2018.02.019.

[24] I. Jäger, P. Fratzl, Mineralized Collagen Fibrils: A Mechanical Model with a Staggered Arrangement of Mineral Particles, Biophys J 79 (2000) 1737–1746. https://doi.org/10.1016/S0006-3495(00)76426-5.

[25] K.E. Stockhausen, M. Qwamizadeh, E.M. Wölfel, H. Hemmatian, I.A.K. Fiedler, S. Flenner, E. Longo, M. Amling, I. Greving, R.O. Ritchie, F.N. Schmidt, B. Busse, Collagen Fiber Orientation Is Coupled with Specific Nano-Compositional Patterns in Dark and Bright Osteons Modulating Their Biomechanical Properties, ACS Nano 15 (2021) 455–467. https://doi.org/10.1021/acsnano.0c04786.

[26] M. Murshed, Mechanism of Bone Mineralization, Cold Spring Harb Perspect Med 8 (2018) a031229. https://doi.org/10.1101/cshperspect.a031229.

[27] H. Clarke Anderson, Matrix Vesicles and Calcification, Curr Rheumatol Rep 5 (2003) 222–226.

[28] H.C. Blair, Q.C. Larrouture, Y. Li, H. Lin, D. Beer-Stoltz, L. Liu, R.S. Tuan, L.J. Robinson, P.H. Schlesinger, D.J. Nelson, Osteoblast Differentiation and Bone Matrix Formation In Vivo and In Vitro, (n.d.). https://doi.org/10.1089/ten.teb.2016.0454.

[29] C. Bergot, Y. Wu, E. Jolivet, L.Q. Zhou, J.D. Laredo, V. Bousson, The degree and distribution of cortical bone mineralization in the human femoral shaft change with age and sex in a microradiographic study, Bone 45 (2009). https://doi.org/10.1016/j.bone.2009.05.025.

[30] S.L. Dallas, L.F. Bonewald, Dynamics of the transition from osteoblast to osteocyte, in: Ann N Y Acad Sci, 2010. https://doi.org/10.1111/j.1749-6632.2009.05246.x.

[31] N.C. Avery, A.J. Bailey, Enzymic and non-enzymic cross-linking mechanisms in relation to turnover of collagen: Relevance to aging and exercise, in: Scand J Med Sci Sports, 2005. https://doi.org/10.1111/j.1600-0838.2005.00464.x.

[32] A.L. Boskey, L. Imbert, Bone quality changes associated with aging and disease: a review, Ann N Y Acad Sci 1410 (2017). https://doi.org/10.1111/nyas.13572.

[33] Z.A. Cole, E.M. Dennison, C. Cooper, Osteoporosis epidemiology update, Curr Rheumatol Rep 10 (2008). https://doi.org/10.1007/s11926-008-0017-6.

[34] N.C. Harvey, E.M. Curtis, E.M. Dennison, C. Cooper, The epidemiology of osteoporotic fractures, in: Primer on the Metabolic Bone Diseases and Disorders of Mineral Metabolism, 2018. https://doi.org/10.1002/9781119266594.ch50.

[35] T. Rolvien, P. Milovanovic, † Felix, N. Schmidt, S. Von Kroge, E.M. Wölfel, M. Krause, B. Wulff, K. Püschel, R.O. Ritchie, M. Amling, B. Busse, Long-Term Immobilization in Elderly Females Causes a Specific Pattern of Cortical Bone and Osteocyte Deterioration Different From Postmenopausal Osteoporosis, (2020). https://doi.org/10.1002/jbmr.3970.

[36] S. Kurra, E. Siris, Diabetes and bone health: The relationship between diabetes and osteoporosis-associated fractures, Diabetes Metab Res Rev 27 (2011). https://doi.org/10.1002/dmrr.1197.

[37] P. Vestergaard, Discrepancies in bone mineral density and fracture risk in patients with type 1 and type 2 diabetes--a meta-analysis, Osteoporos Int 18 (2007) 427–444. https://doi.org/10.1007/s00198-006-0253-4.

[38] K.M. Thrailkill, C.K. Lumpkin, R.C. Bunn, S.F. Kemp, J.L. Fowlkes, Is insulin an anabolic agent in bone? Dissecting the diabetic bone for clues, (2005). https://doi.org/10.1152/ajpendo.00159.2005.

[39] A. V. Schwartz, D.E. Sellmeyer, Diabetes, fracture, and bone fragility, Curr Osteoporos Rep 5 (2007). https://doi.org/10.1007/s11914-007-0025-x.

[40] C. Romero-Díaz, D. Duarte-Montero, S.A. Gutiérrez-Romero, C.O. Mendivil, Diabetes and Bone Fragility, Diabetes Therapy 12 (2021) 71–86. https://doi.org/10.1007/s13300-020-00964-1.

[41] M. Walle, D.E. Whittier, M. Frost, R. Müller, C.J. Collins, Meta-analysis of Diabetes Mellitus-Associated Differences in Bone Structure Assessed by High-Resolution Peripheral Quantitative Computed Tomography, Curr Osteoporos Rep 20 (2022). https://doi.org/10.1007/s11914-022-00755-6.

[42] T. Vilaca, M. Schini, S. Harnan, A. Sutton, E. Poku, I.E. Allen, S.R. Cummings, R. Eastell, The risk of hip and non-vertebral fractures in type 1 and type 2 diabetes: A systematic review and meta-analysis update, Bone 137 (2020) 115457. https://doi.org/10.1016/j.bone.2020.115457.

[43] A.J. Burghardt, A.S. Issever, A. V. Schwartz, K.A. Davis, U. Masharani, S. Majumdar, T.M. Link, High-resolution peripheral quantitative computed tomographic imaging of cortical and trabecular bone microarchitecture in patients with type 2 diabetes mellitus, Journal of Clinical Endocrinology and Metabolism 95 (2010). https://doi.org/10.1210/jc.2010-0226.

[44] K. Hygum, J. Starup-Linde, T. Harsløf, P. Vestergaard, B.L. Langdahl, MECHANISMS IN ENDOCRINOLOGY: Diabetes mellitus, a state of low bone turnover – a systematic review and meta-analysis, Eur J Endocrinol 176 (2017) R137–R157. https://doi.org/10.1530/eje-16-0652.

[45] K. Hygum, J. Starup-Linde, B.L. Langdahl, Diabetes and bone, Osteoporos Sarcopenia 5 (2019) 29–37. https://doi.org/10.1016/J.AFOS.2019.05.001.

[46] M. Yamamoto, T. Sugimoto, Advanced Glycation End Products, Diabetes, and Bone Strength, Curr Osteoporos Rep 14 (2016) 320–326. https://doi.org/10.1007/s11914-016-0332-1.

[47] C. Delgado-Andrade, Carboxymethyl-lysine: Thirty years of investigation in the field of AGE formation, Food Funct 7 (2016). https://doi.org/10.1039/c5fo00918a.

[48] R. Bucala, H. Vlassara, Advanced glycosylation end products in diabetic renal and vascular disease, American Journal of Kidney Diseases 26 (1995). https://doi.org/10.1016/0272-6386(95)90051-9.

[49] M. Unal, A. Creecy, J.S. Nyman, The Role of Matrix Composition in the Mechanical Behavior of Bone, Curr Osteoporos Rep 16 (2018). https://doi.org/10.1007/s11914-018-0433-0.

[50] A. V. Schwartz, P. Garnero, T.A. Hillier, D.E. Sellmeyer, E.S. Strotmeyer, K.R. Feingold, H.E. Resnick, F.A. Tylavsky, D.M. Black, S.R. Cummings, T.B. Harris, D.C. Bauer, Pentosidine and increased fracture risk in older adults with type 2 diabetes, Journal of Clinical Endocrinology and Metabolism 94 (2009). https://doi.org/10.1210/jc.2008-2498.

[51] T. Neumann, S. Lodes, B. Kästner, S. Franke, M. Kiehntopf, T. Lehmann, U.A. Müller, G. Wolf, A. Sämann, High serum pentosidine but not esRAGE is associated with prevalent fractures in type 1 diabetes independent of bone mineral density and glycaemic control, Osteoporosis International 25 (2014) 1527–1533. https://doi.org/10.1007/s00198-014-2631-7.

[52] D. Farlay, L.A. Armas, E. Gineyts, M.P. Akhter, R.R. Recker, G. Boivin, Nonenzymatic Glycation and Degree of Mineralization Are Higher in Bone From Fractured Patients With Type 1 Diabetes Mellitus, Journal of Bone and Mineral Research 31 (2016) 190–195. https://doi.org/10.1002/jbmr.2607.

[53] E.M. Wolfel, K. Jahn-Rickert, F.N. Schmidt, B. Wulff, H. Mushumba, G.E. Sroga, K. Puschel, P. Milovanovic, M. Amling, G.M. Campbell, D. Vashishth, B. Busse, Individuals with type 2 diabetes mellitus show dimorphic and heterogeneous patterns of loss in femoral bone quality, Bone 140 (2020) 115556. https://doi.org/10.1016/j.bone.2020.115556.

[54] J. V. Gefter, A.L. Shaufl, M.P. Fink, R.L. Delude, Comparison of distinct protein isoforms of the receptor for advanced glycation end-products expressed in murine tissues and cell lines, Cell Tissue Res 337 (2009). https://doi.org/10.1007/s00441-009-0791-0.

[55] R. Ramasamy, S.F. Yan, A.M. Schmidt, Advanced glycation endproducts: From precursors to RAGE: Round and round we go, Amino Acids 42 (2012). https://doi.org/10.1007/s00726-010-0773-2.

[56] K. Asadipooya, E.M. Uy, Advanced Glycation End Products (AGEs), Receptor for AGEs, Diabetes, and Bone: Review of the Literature, J Endocr Soc 3 (2019) 1799–1818. https://doi.org/10.1210/js.2019-00160.

[57] E.M.S. Litwinoff, C. Hurtado Del Pozo, R. Ramasamy, A.M. Schmidt, Emerging targets for therapeutic development in diabetes and its complications: The RAGE signaling pathway, Clin Pharmacol Ther 98 (2015). https://doi.org/10.1002/cpt.148.

[58] M.P. Wautier, P.J. Guillausseau, J.L. Wautier, Activation of the receptor for advanced glycation end products and consequences on health, Diabetes and Metabolic Syndrome: Clinical Research and Reviews 11 (2017). https://doi.org/10.1016/j.dsx.2016.09.009.

[59] J. Liu, J. Mao, Y. Jiang, L. Xia, L. Mao, Y. Wu, P. Ma, B. Fang, AGEs Induce Apoptosis in Rat Osteoblast Cells by Activating the Caspase-3 Signaling Pathway Under a High-Glucose Environment In Vitro, Appl Biochem Biotechnol 178 (2016). https://doi.org/10.1007/s12010-015-1925-3.

[60] X. Yang, C. Gandhi, M.D.M. Rahman, M. Appleford, L.W. Sun, X. Wang, Age-Related Effects of Advanced Glycation End Products (Ages) in Bone Matrix on Osteoclastic Resorption, Calcif Tissue Int 97 (2015). https://doi.org/10.1007/s00223-015-0042-1.

[61] M.C.M. Li, S.K.H. Chow, R.M.Y. Wong, L. Qin, W.H. Cheung, The role of osteocytes-specific molecular mechanism in regulation of mechanotransduction – A systematic review, J Orthop Translat 29 (2021) 1–9. https://doi.org/10.1016/J.JOT.2021.04.005.

[62] M.L. Knothe Tate, “Whither flows the fluid in bone?” An osteocyte’s perspective, J Biomech 36 (2003) 1409–1424. https://doi.org/10.1016/S0021-9290(03)00123-4.

[63] L.F. Bonewald, The amazing osteocyte, Journal of Bone and Mineral Research 26 (2011) 229–238. https://doi.org/10.1002/jbmr.320.

[64] P.R. Buenzli, N.A. Sims, Quantifying the osteocyte network in the human skeleton, Bone 75 (2015) 144–150. https://doi.org/10.1016/J.BONE.2015.02.016.

[65] B. Busse, D. Djonic, P. Milovanovic, M. Hahn, K. Püschel, R.O. Ritchie, M. Djuric, M. Amling, Decrease in the osteocyte lacunar density accompanied by hypermineralized lacunar occlusion reveals failure and delay of remodeling in aged human bone, Aging Cell 9 (2010) 1065–1075. https://doi.org/10.1111/j.1474-9726.2010.00633.x.

[66] A. Vom Scheidt, B. Busse, Characteristics of the osteocyte network in healthy and diseased human bone, Osteologie 25 (2016). https://doi.org/10.1055/s-0037-1619006.

[67] S.L. Fink, B.T. Cookson, Apoptosis, pyroptosis, and necrosis: Mechanistic description of dead and dying eukaryotic cells, Infect Immun 73 (2005). https://doi.org/10.1128/IAI.73.4.1907-1916.2005.

[68] E. Farber, Programmed cell death: necrosis versus apoptosis., Mod Pathol 7 (1994).

[69] L.I. Plotkin, SKELETAL BIOLOGY AND REGULATION (MR FORWOOD AND A ROBLING, SECTION EDITORS) Apoptotic Osteocytes and the Control of Targeted Bone Resorption, (n.d.). https://doi.org/10.1007/s11914-014-0194-3.

[70] J.-Y. Ru, Y.-F. Wang, Osteocyte apoptosis: the roles and key molecular mechanisms in resorption-related bone diseases, (n.d.). https://doi.org/10.1038/s41419-020-03059-8.

[71] R.S. Weinstein, R.W. Nicholas, S.C. Manolagas, Apoptosis of Osteocytes in Glucocorticoid-Induced Osteonecrosis of the Hip 1 , J Clin Endocrinol Metab 85 (2000). https://doi.org/10.1210/jcem.85.8.6714.

[72] C.C. Kennedy, A. Papaioannou, J.D. Adachi, A. for correspondence, Glucocorticoid-induced osteoporosis, Women’s Health 2 (2006) 65–74. https://doi.org/10.2217/17455057.2.1.65.

[73] W.R. Thompson, S. Modla, B.J. Grindel, K.J. Czymmek, C.B. Kirn-Safran, L. Wang, R.L. Duncan, M.C. Farach-Carson, Perlecan/Hspg2 Deficiency Alters the Pericellular Space of the Lacunocanalicular System Surrounding Osteocytic Processes in Cortical Bone, (n.d.). https://doi.org/10.1002/jbmr.236.

[74] L.S. Bell, M. Kayser, C. Jones, The mineralized osteocyte: A living fossil, Am J Phys Anthropol 137 (2008). https://doi.org/10.1002/ajpa.20886.

[75] P. Milovanovic, B. Busse, Phenomenon of osteocyte lacunar mineralization: Indicator of former osteocyte death and a novel marker of impaired bone quality?, BioScientifica, 2020. https://doi.org/10.1530/EC-19-0531.

[76] H.M. Frost, Micropetrosis, J Bone Joint Surg Am 42-A (1960) 144–150. https://www.ncbi.nlm.nih.gov/pubmed/13849862.

[77] P. Milovanovic, E.A. Zimmermann, A. Vom Scheidt, B. Hoffmann, G. Sarau, T. Yorgan, M. Schweizer, M. Amling, S. Christiansen, B. Busse, The Formation of Calcified Nanospherites during Micropetrosis Represents a Unique Mineralization Mechanism in Aged Human Bone, Small 13 (2017) 1602215. https://doi.org/10.1002/smll.201602215.

[78] J.L. Reynolds, A.J. Joannides, J.N. Skepper, R. Mcnair, L.J. Schurgers, D. Proudfoot, W. Jahnen-Dechent, P.L. Weissberg, C.M. Shanahan, Human Vascular Smooth Muscle Cells Undergo Vesicle-Mediated Calcification in Response to Changes in Extracellular Calcium and Phosphate Concentrations: A Potential Mechanism for Accelerated Vascular Calcification in ESRD, (2004). https://doi.org/10.1097/01.ASN.0000141960.01035.28.

[79] F.A. Shah, B.E.J. Lee, J. Tedesco, C. Larsson Wexell, C. Persson, P. Thomsen, K. Grandfield, A. Palmquist, Micrometer-Sized Magnesium Whitlockite Crystals in Micropetrosis of Bisphosphonate-Exposed Human Alveolar Bone, Nano Lett 17 (2017). https://doi.org/10.1021/acs.nanolett.7b02888.

[80] D.W. Dempster, J.E. Compston, M.K. Drezner, F.H. Glorieux, J.A. Kanis, H. Malluche, P.J. Meunier, S.M. Ott, R.R. Recker, A.M. Parfitt, Standardized nomenclature, symbols, and units for bone histomorphometry: A 2012 update of the report of the ASBMR Histomorphometry Nomenclature Committee, Journal of Bone and Mineral Research 28 (2013) 2–17. https://doi.org/10.1002/jbmr.1805.

[81] P. Milovanovic, A. Vom Scheidt, K. Mletzko, G. Sarau, K. Puschel, M. Djuric, M. Amling, S. Christiansen, B. Busse, Bone tissue aging affects mineralization of cement lines, Bone 110 (2018) 187–193. https://doi.org/10.1016/j.bone.2018.02.004.

[82] D.B. Burr, M. Hooser, Alterations to the en bloc basic fuchsin staining protocol for the demonstration of microdamage produced in vivo, Bone 17 (1995) 431–433. https://doi.org/10.1016/S8756-3282(95)00241-3.

[83] V.T. Carpentier, J. Wong, Y. Yeap, C. Gan, P. Sutton-Smith, A. Badiei, N.L. Fazzalari, J.S. Kuliwaba, Increased proportion of hypermineralized osteocyte lacunae in osteoporotic and osteoarthritic human trabecular bone: Implications for bone remodeling, Bone 50 (2012). https://doi.org/10.1016/j.bone.2011.11.021.

[84] K. Jahn-Rickert, E.M. Wolfel, B. Jobke, C. Riedel, M. Hellmich, M. Werner, M.M. McDonald, B. Busse, Elevated Bone Hardness Under Denosumab Treatment, With Persisting Lower Osteocyte Viability During Discontinuation, Front Endocrinol (Lausanne) 11 (2020) 250. https://doi.org/10.3389/fendo.2020.00250.

[85] T. Bellido, L.I. Plotkin, Novel actions of bisphosphonates in bone: Preservation of osteoblast and osteocyte viability, Bone 49 (2011) 50–55. https://doi.org/10.1016/j.bone.2010.08.008.

[86] M. Maycas, K.A. McAndrews, A.Y. Sato, G.G. Pellegrini, D.M. Brown, M.R. Allen, L.I. Plotkin, A.R. Gortazar, P. Esbrit, T. Bellido, PTHrP-Derived Peptides Restore Bone Mass and Strength in Diabetic Mice: Additive Effect of Mechanical Loading, J Bone Miner Res 32 (2017) 486–497. https://doi.org/10.1002/jbmr.3007.

[87] S. Portal-Núñez, D. Lozano, L. Fernández De Castro, A.R. De Gortázar, X. Nogués, P. Esbrit, Alterations of the Wnt/b-catenin pathway and its target genesfor the N- and C-terminal domains of parathyroid hormone-related proteinin bone from diabetic mice, FEBS Lett 584 (2010) 3095–3100. https://doi.org/10.1016/j.febslet.2010.05.047.

[88] T. Miazgowski, S. Pynka, M. Noworyta-Zietara, B. Kryzanowska-Świniarska, R. Pikul, Bone mineral density and hip structural analysis in type 1 diabetic men, Eur J Endocrinol 156 (2007). https://doi.org/10.1530/eje.1.02309.

[89] V. V. Shanbhogue, S. Hansen, M. Frost, N.R. Jørgensen, A.P. Hermann, J.E. Henriksen, K. Brixen, Bone Geometry, Volumetric Density, Microarchitecture, and Estimated Bone Strength Assessed by HR-

pQCT in Adult Patients with Type 1 Diabetes Mellitus, Journal of Bone and Mineral Research 30 (2015). https://doi.org/10.1002/jbmr.2573.

[90] L.J. Raggatt, N.C. Partridge, Cellular and Molecular Mechanisms of Bone Remodeling, Journal of Biological Chemistry 285 (2010) 25103–25108. https://doi.org/10.1074/jbc.r109.041087.

[91] J. Compston, L. Skingle, D.W. Dempster, Bone Histomorphometry, Vitamin D: Fourth Edition 1 (2018) 959–973. https://doi.org/10.1016/B978-0-12-809965-0.00053-7.

[92] L. Cardoso, B.C. Herman, O. Verborgt, D. Laudier, R.J. Majeska, M.B. Schaffler, Osteocyte Apoptosis Controls Activation of Intracortical Resorption in Response to Bone Fatigue, JOURNAL OF BONE AND MINERAL RESEARCH 24 (2009) 597–605. https://doi.org/10.1359/JBMR.081210.

[93] D.T. Loo, In Situ Detection of Apoptosis by the TUNEL Assay: An Overview of Techniques, in: 2011: pp. 3–13. https://doi.org/10.1007/978-1-60327-409-8_1.

[94] W.R. Duan, D.S. Garner, S.D. Williams, C.L. Funckes-Shippy, I.S. Spath, E.A. Blomme, R. Duan, D.S. Garner, S.D. Williams, C.L. Funckes-Shippy, I.S. Spath, E.A. Blomme, Comparison of immunohistochemistry for activated caspase-3 and cleaved cytokeratin 18 with the TUNEL method for quantification of apoptosis in histological sections of PC-3 subcutaneous xenografts, 199 (2003) 221–228. https://doi.org/10.1002/path.1289.

[95] K.I. Tanaka, T. Yamaguchi, I. Kanazawa, T. Sugimoto, Effects of high glucose and advanced glycation end products on the expressions of sclerostin and RANKL as well as apoptosis in osteocyte-like MLO-Y4-A2 cells, Biochem Biophys Res Commun 461 (2015) 193–199. https://doi.org/10.1016/J.BBRC.2015.02.091.

[96] C. Zhang, W. Wei, M. Chi, Y. Wan, X. Li, M. Qi, Y. Zhou, Research Article FOXO1 Mediates Advanced Glycation End Products Induced Mouse Osteocyte-Like MLO-Y4 Cell Apoptosis and Dysfunctions, 2019.

[97] W.S.S. Jee, Integrated bone tissue physiology: Anatomy and physiology, in: Bone Mechanics Handbook, Second Edition, 2001.

[98] T.M. Boyce, R.D. Bloebaum, Cortical aging differences and fracture implications for the human femoral neck, Bone 14 (1993). https://doi.org/10.1016/8756-3282(93)90209-S.

[99] X. Liu, W. Li, J. Cai, Z. Yan, X. Shao, K. Xie, X.E. Guo, E. Luo, D. Jing, Spatiotemporal characterization of microdamage accumulation and its targeted remodeling mechanisms in diabetic fatigued bone, The FASEB Journal 34 (2020) 2579–2594. https://doi.org/10.1096/fj.201902011rr.

[100] Y. Wu, C. Bergot, E. Jolivet, L.Q. Zhou, J.D. Laredo, V. Bousson, Cortical bone mineralization differences between hip-fractured females and controls. A microradiographic study, Bone 45 (2009). https://doi.org/10.1016/j.bone.2009.04.202.

[101] P. Milovanovic, E.A. Zimmermann, C. Riedel, A. vom Scheidt, L. Herzog, M. Krause, D. Djonic, M. Djuric, K. Püschel, M. Amling, R.O. Ritchie, B. Busse, Multi-level characterization of human femoral cortices and their underlying osteocyte network reveal trends in quality of young, aged, osteoporotic and antiresorptive-treated bone, Biomaterials (2015). https://doi.org/10.1016/j.biomaterials.2014.12.024.

[102] E.A. Zimmermann, E. Schaible, H. Bale, H.D. Barth, S.Y. Tang, P. Reichert, B. Busse, T. Alliston, J.W. Ager, R.O. Ritchie, Age-related changes in the plasticity and toughness of human cortical bone at

multiple length scales, Proc Natl Acad Sci U S A 108 (2011). https://doi.org/10.1073/pnas.1107966108.

[103] D. Yin, B. Chen, S. Lin, Finite element analysis on multi-toughening mechanism of microstructure of osteon, J Mech Behav Biomed Mater 117 (2021). https://doi.org/10.1016/j.jmbbm.2021.104408.

[104] I.D. Cooper, K.H. Brookler, C.A.P. Crofts, Rethinking fragility fractures in type 2 diabetes: The link between hyperinsulinaemia and osteofragilitas, Biomedicines 9 (2021). https://doi.org/10.3390/biomedicines9091165.

[105] G.L. King, M.R. Loeken, Hyperglycemia-induced oxidative stress in diabetic complications, Histochem Cell Biol 122 (2004). https://doi.org/10.1007/s00418-004-0678-9.

[106] F. Giacco, M. Brownlee, Oxidative Stress and Diabetic Complications, Circ Res 107 (2010) 1058–1070. https://doi.org/10.1161/CIRCRESAHA.110.223545.

[107] A.D. Sonagra, Normal Pregnancy- A State of Insulin Resistance, JOURNAL OF CLINICAL AND DIAGNOSTIC RESEARCH (2014). https://doi.org/10.7860/jcdr/2014/10068.5081.

[108] M.I. Goran, B.A. Gower, Longitudinal Study on Pubertal Insulin Resistance, Diabetes 50 (2001). https://doi.org/10.2337/diabetes.50.11.2444.

[109] A. Gaudio, F. Privitera, K. Battaglia, V. Torrisi, M.H. Sidoti, I. Pulvirenti, E. Canzonieri, G. Tringali, C.E. Fiore, Sclerostin levels associated with inhibition of the Wnt/β-catenin signaling and reduced bone turnover in type 2 diabetes mellitus, Journal of Clinical Endocrinology and Metabolism 97 (2012). https://doi.org/10.1210/jc.2012-1901.

[110] F. Sassi, I. Buondonno, C. Luppi, E. Spertino, E. Stratta, M. Di Stefano, M. Ravazzoli, G. Isaia, M. Trento, P. Passera, M. Porta, G.C. Isaia, P. D'Amelio, Type 2 diabetes affects bone cells precursors and bone turnover, BMC Endocr Disord 18 (2018). https://doi.org/10.1186/s12902-018-0283-x.

[111] J. Vavanikunnel, S. Charlier, C. Becker, C. Schneider, S.S. Jick, C.R. Meier, C. Meier, Association between glycemic control and risk of fracture in diabetic patients: A nested case-control study, Journal of Clinical Endocrinology and Metabolism 104 (2019). https://doi.org/10.1210/jc.2018-01879.

[112] G. Leanza, E. Maddaloni, D. Pitocco, C. Conte, A. Palermo, A.R. Maurizi, A.L. Pantano, C. Suraci, M. Altomare, R. Strollo, S. Manfrini, P. Pozzilli, A. V Schwartz, N. Napoli, Risk factors for fragility fractures in type 1 diabetes, Bone 125 (2019) 194–199. https://doi.org/10.1016/j.bone.2019.04.017.

[113] I.R. Reid, P.D. Miller, J.P. Brown, D.L. Kendler, A. Fahrleitner-Pammer, I. Valter, K. Maasalu, M.A. Bolognese, G. Woodson, H. Bone, B. Ding, R.B. Wagman, J. San Martin, M.S. Ominsky, D.W. Dempster, Effects of denosumab on bone histomorphometry: The FREEDOM and STAND studies, Journal of Bone and Mineral Research 25 (2010). https://doi.org/10.1002/jbmr.149.

9. Published Articles

9.1. Publication 1: Osteocyte apoptosis and cellular micropetrosis signify skeletal aging in type 1 diabetes

Acta Biomaterialia 162 (2023) 254–265

Contents lists available at ScienceDirect

Acta Biomaterialia

journal homepage: www.elsevier.com/locate/actbio

Full length article

Osteocyte apoptosis and cellular micropetrosis signify skeletal aging in type 1 diabetes

Sofie Dragoun Kolibová[a], Eva Maria Wölfel[a,b], Haniyeh Hemmatian[a], Petar Milovanovic[a,c], Herbert Mushumba[d], Birgit Wulff[d], Maximilian Neidhardt[e,b], Klaus Püschel[d], Antonio Virgilio Failla[f], Annegreet Vlug[g], Alexander Schlaefer[e,b], Benjamin Ondruschka[d], Michael Amling[a], Lorenz C. Hofbauer[h], Martina Rauner[h], Björn Busse[a,b,*], Katharina Jähn-Rickert[a,i]

[a] Department of Osteology and Biomechanics, University Medical Center Hamburg Eppendorf, Hamburg, Germany
[b] Interdisciplinary Competence Center for Interface Research, University Medical Center Hamburg Eppendorf, Hamburg, Germany
[c] University of Belgrade, Faculty of Medicine, Center of Bone Biology, Institute of Anatomy, Belgrade, Serbia
[d] University Medical Center Hamburg Eppendorf, Institute of Legal Medicine, Hamburg, Germany
[e] Institute of Medical Technology and Intelligent Systems, Hamburg University of Technology, Am-Schwarzenberg-Campus 3, Hamburg 21073, Germany
[f] University Medical Center Hamburg Eppendorf, UKE microscopy Imaging facility, Hamburg, Germany
[g] Leiden University Medical Center (LUMC), Centre for Bone Quality, Leiden, the Netherlands
[h] Division of Endocrinology, Department of Medicine III, Technische Universität Dresden Medical Center, Diabetes, and Metabolic Bone Diseases, Dresden, Germany
[i] Mildred Scheel Cancer Career Center Hamburg, University Cancer Center Hamburg, University Medical Center Hamburg-Eppendorf, Hamburg 20251, Germany

ARTICLE INFO

Article history:
Received 12 October 2022
Revised 3 February 2023
Accepted 27 February 2023
Available online 4 March 2023

Keywords:
Type 1 diabetes mellitus
Micropetrosis
Osteocyte apoptosis
Cell death
Microdamage accumulation
Skeletal aging

ABSTRACT

Bone fragility is a profound complication of type 1 diabetes mellitus (T1DM), increasing patient morbidity. Within the mineralized bone matrix, osteocytes build a mechanosensitive network that orchestrates bone remodeling; thus, osteocyte viability is crucial for maintaining bone homeostasis. In human cortical bone specimens from individuals with T1DM, we found signs of accelerated osteocyte apoptosis and local mineralization of osteocyte lacunae (micropetrosis) compared with samples from age-matched controls. Such morphological changes were seen in the relatively young osteonal bone matrix on the periosteal side, and micropetrosis coincided with microdamage accumulation, implying that T1DM drives local skeletal aging and thereby impairs the biomechanical competence of the bone tissue. The consequent dysfunction of the osteocyte network hampers bone remodeling and decreases bone repair mechanisms, potentially contributing to the enhanced fracture risk seen in individuals with T1DM.

Statement of significance

Type 1 diabetes mellitus (T1DM) is a chronic autoimmune disease that causes hyperglycemia. Increased bone fragility is one of the complications associated with T1DM. Our latest study on T1DM-affected human cortical bone identified the viability of osteocytes, the primary bone cells, as a potentially critical factor in T1DM-bone disease. We linked T1DM with increased osteocyte apoptosis and local accumulation of mineralized lacunar spaces and microdamage. Such structural changes in bone tissue suggest that T1DM speeds up the adverse effects of aging, leading to the premature death of osteocytes and potentially contributing to diabetes-related bone fragility.

1. Introduction

Diabetes mellitus (DM) represents a significant public health concern, with approximately 537 million adults currently living

* Corresponding author at: Department of Osteology and Biomechanics, University Medical Center Hamburg-Eppendorf, Lottestr. 55A, Hamburg 22529, Germany.
E-mail address: b.busse@uke.de (B. Busse).

https://doi.org/10.1016/j.actbio.2023.02.037

with diabetes, and its global prevalence is rising [1]. DM is a chronic metabolic disorder characterized by high blood glucose levels. In type 1 DM (T1DM), accounting for 10% of all diabetes cases worldwide, hyperglycemia is caused by a lack of insulin due to autoimmune-induced damage to pancreatic beta cells [2,3]. The long-term effects of T1DM are tissue and organ damage, including impaired skeletal health involving a significant increase in fracture risk; the relative risk of hip fracture is reported to be as high as 6.94 for individuals with T1DM [4–8]. Bone mineral density (BMD), the general predictor of bone fragility, is reduced in T1DM [9–12]. However, the reported increase in fracture risk cannot be explained solely by the reduction in BMD; thus, there is a need to identify novel markers of reduced mechanical competence of bone.

It is thought that decreased bone turnover contributes to diabetic bone disease [13]. Bone turnover is accomplished through the bone remodeling process, in which the central regulatory cells, osteocytes, orchestrate bone-resorbing osteoclasts and bone-forming osteoblasts in response to mechanical loading. The cellular processes of bone remodeling are coupled in a spatiotemporal sequence by a functional osteocyte network to maintain bone tissue homeostasis or adapt to changing mechanical or hormonal environments [14].

Osteocytes are the most abundant bone cells, forming a mechanosensory and force-translating network within the mineralized bone matrix [15]. Each osteocyte forms approximately 90 dendrites [16], long cytoplasmic extensions that run through nanoscale canals (canaliculi) and enable the connection of osteocytes to each other and to other cells at the periosteum or in the bone marrow cavity, resulting in an extensive communication system called a lacunar (harboring the cell body)-canalicular network (LCN). As postmitotic cells, osteocyte viability [17] is crucial for the maintenance of bone homeostasis. Through a functional fluid-filled LCN, nutrients and waste products are transported to preserve osteocyte viability and maintain their mechanosensory function.

The lifespan of osteocytes is thought to be between 1 and 50 years, starting from a subpopulation of osteoblasts that become embedded into their newly formed bone matrix and differentiate into dendritic osteocytes, ultimately ending in one of the known cell death mechanisms. Osteocyte cell death becomes more prominent with aging [18] but is also associated with multiple bone pathologies, i.e., postmenopausal osteoporosis, glucocorticoid-induced osteoporosis [19,20], or immobilization [21]· which are all characterized by elevated bone fragility and therefore higher fracture risk. The fragility is likely caused by a decreased ability to sense and repair microdamage in the bone matrix. In a physiological state, osteocyte apoptosis induces local bone resorption, resulting in the removal of damaged bone matrix, and coupled bone formation ensures the renewal of the bone matrix and the osteocyte cell pool [22,23]. The phenomenon of osteocyte lacunar mineralization, also known as micropetrosis, reflects the decreased number of osteocytes due to cell death and lack of newly embedded osteocytes during bone formation seen with bone pathologies [24]. Micropetrosis negatively affects the mechanical properties of bone tissue, lowering energy absorption and dissipation capacities and thereby causing the bone matrix to become more susceptible to fragility fractures [17,25–27]. An impaired osteocyte network in the form of lower numbers of viable interconnected osteocytes leads to a reduced recognition of microdamage within the bone matrix [28].

Microdamage removal requires communication between apoptotic osteocytes at the site of damage and adjacent nonapoptotic osteocytes, which subsequently activate the osteoclastogenic signaling response for local bone remodeling [29]. The accumulation of microdamage, such as microcracks, creates morphological changes in the LCN, which induce osteocyte apoptosis [30,31]. These effects induce osteoclast-dependent resorption of the damaged bone matrix as a part of functional bone homeostasis. However, when the rate of osteocyte apoptosis exceeds osteocyte viability or when bone resorption is lowered or less targeted (i.e., due to reduced activation by osteocytes), bone resistance to fracture decreases. In a streptozotocin-induced rat model of T1DM, the accumulation of microdamage after ulnar loading led to a severe disruption of the LCN and reduced osteoclast activation, causing a reduction in bone resorption [32]. Because studies with human bone specimens are rare, it is yet unknown whether and to what extent there is microdamage accumulation in the bone matrix of human individuals with T1DM and if it characterizes diabetic bone pathology.

We investigated the effect of T1DM on human femoral cortical bone using an interdisciplinary approach, applying clinical imaging (e.g., microcomputed tomography) and standardized bone histological methods (e.g., bone histomorphometry), material-based techniques (e.g., quantitative backscattered electron microscopy), and novel imaging approaches to detect and quantify microdamage accumulation. We hypothesized that T1DM would promote osteocyte apoptosis, which would affect the integrity of the LCN and result in the accumulation of microcracks in T1DM-induced bone disease.

2. Materials and methods

2.1. Study design

We evaluated the influence of T1DM on bone microarchitecture, matrix quality, and cellular parameters of cortical bone. We collected approximately 1.5-cm-thick bone specimens from the femoral mid-diaphysis of 22 human donors of both sexes for cortical bone quality analysis. The specimens were obtained in collaboration with the Institute of Legal Medicine at University Medical Center Hamburg-Eppendorf (ethics approval: WT037/15). According to medical records, donors were divided into two study groups, including a group of eight donors diagnosed with T1DM (T1DM group: 55.0 ± 10.6 years) during their lifetime and a group of 14 age-matched healthy donors (control group: 53.1 ± 9.5 years) with normal sugar metabolism. For each donor, we collected deidentified patient data (age, BMI) and BMD measured via *ex vivo* DXA measurement of the 12th thoracic vertebra (Table 1). Donors in this study did not suffer from any form of bone disease (i.e., trauma, osteogenesis imperfecta, Paget's disease, fibrous dysplasia, or malignancy).

Femoral bone specimens were fixed in 4% paraformaldehyde (Sigma–Aldrich, Darmstadt, Germany) for 7 days. From the fixed specimens, several 4-mm-thick sections were cut out using a diamond belt saw (EXAKT Advanced Technologies GmbH, Norderstedt, Germany) followed by imaging the whole cross-sections in a cabinet X-ray system. The anterior quadrant was extracted from each cross-section and additionally fixed in 4% paraformaldehyde (Sigma–Aldrich, Darmstadt, Germany) overnight before embedding in methyl methacrylate (MMA). The anterior quadrant from another cross-section was cut and decalcified for six weeks in a 20% ethylenediaminetetraacetic (EDTA) solution prior to paraffin embedding for immunohistochemistry (IHC). The methodology of the study is summarized in Supplemental Fig. 9. All analyses were performed in a blinded manner.

2.2. Microcomputed tomography

The microstructure of the anterior quadrant was assessed using microcomputed tomography (µCT 40, Scanco Medical AG, Switzerland) at a spatial resolution of 10 μm. The X-ray settings were standardized to 55 kV and 145 µA with an integration time of 200 ms. A threshold of 550 mg HA/cm^3 was applied to assess cortical porosity (Ct. Po) and tissue mineral density (TMD) using Scanco

Table 1
Cohort characteristics.

	Control $n = 14$	T1DM $n = 8$	p value
Age (years)	51 ± 34[b]	52 ± 31[b]	0.603
Sex (m/f)	12/2	6/2	0.602
BMI (kg/m^2)	29 ± 14[b]	22 ± 38[b]	0.127
Ex vivo BMD of 12th thoracic vertebra (g/cm^2)	AP: 0.9 ± 0.2[a] LAT: 0.7 ± 0.1[a]	AP: 0.8 ± 0.1[a] LAT: 0.6 ± 0.2[a]	0.191 0.390

Notes: The table summarizes the information on age, sex, BMI, and ex vivo BMD of the 12th thoracic vertebra (T12) for the control and T1DM groups. Data are presented as the mean ± standard deviation for normally distributed data (marked with a superscript "a"), and nonnormally distributed data are presented as the median ± interquartile range (marked with a superscript "b"). A t test was applied for normally distributed data to determine p values, and the Mann–Whitney test was used for nonnormally distributed data. Fisher's exact test was applied to determine the p value for sex distribution. BMI: body mass index, BMD: bone mineral density, AP: anterior–posterior, LAT: lateral.

image processing software. Cortical thickness (Ct. Th) was calculated from the contact radiography images within the whole cross-section of the femoral diaphysis using ImageJ/Fiji software (NIH, USA).

2.3. Geometric analysis

Biomechanical properties, such as diaphyseal strength and rigidity, depend upon geometric indices of the femoral diaphysis. To evaluate bone geometry indices, the whole cross-sectional area of the midshaft femur was visualized by contact radiography (Faxitron MX-20, Faxitron, Arizona, USA). The images were analyzed using the EPJ macro [33] in ImageJ/Fiji. The EPJ macro derives periosteal and endosteal contours from images and computes the following cross-sectional properties: total cross-sectional area (TA, mm^2), which reflects resistance to compression; cortical area (CA, mm^2), which indicates compressive/tensile strength; medullary cavity area (MA, mm^2); percent cortical area (%CA, %), which is determined as (CA/TA) x 100; second moment of area, which indicates bending rigidity in the medial–lateral axis (Ix, mm^4) and anterior–posterior axis (Iy, mm^4); maximum and minimum second moment of area, which indicate maximum bending rigidity (Imax, mm^4) and minimum bending rigidity (Imin, mm^4), respectively; section modulus, which indicates resistance to bending along the medial–lateral axis (Zx, mm^3) and anterior–posterior axis (Zy, mm^3); and buckling ratio (BR), which indicates resistance to buckling.

2.4. Cellular histomorphometry

For cellular histomorphometry, we cut 5 μm-thick sections from MMA blocks on a microtome (Leica Microsystems, Wetzlar, Germany) and stained the sections with toluidine blue. A total bone area of 1.875 mm^2 in the endocortical region and a total bone area of 0.625 mm^2 in the periosteal region were analyzed using Osteomeasure software (Osteometrix, Atlanta, USA). Histomorphometric variables are derived from primary measurements such as bone area or perimeter. These parameters are presented as the source (the structure on which the measurement is made), the measurement, and the referent (source-measurement/referent), in accordance with the ASBMR nomenclature guidelines [34]. The histomorphometric variables were as follows. Bone formation indices: number of osteoblasts per unit bone perimeter (N.Ob/B.Pm; #/mm); osteoblast surface (Ob.S/BS): percent of bone surface occupied by osteoblasts; osteoid volume (OV/BV; %): percent of a given volume of bone tissue that consists of unmineralized bone (osteoid); osteoid surface (OS/BS; %): percent of bone surface covered in osteoid; osteoid thickness (O.Th): mean thickness, provided in micrometers for osteoid bone. Bone resorption indices: number of osteoclasts per unit bone perimeter (N.Oc/B.Pm; #/mm); osteoclast surface (Oc.S/BS): percent of bone surface occupied by osteoclasts; eroded surface (ES/BS; %): percent of bone surface occupied by resorption cavities with or without osteoclasts.

2.5. Bone mineral density distribution

To evaluate the bone mineral density distribution (BMDD) and 2D morphological analysis of the osteocyte lacunae, we performed quantitative backscattered electron imaging. The PMMA-embedded specimens were subjected to coplanar grinding and subsequently polished and carbon-coated before imaging. A scanning electron microscope (Crossbeam 340, GeminiSEM, Zeiss AG, Oberkochen, Germany) in backscattered electron mode was operated at 20 keV with a constant working distance of 20 mm. A Faraday cup was used to control the current beam, and grayscale values were calibrated using an aluminum–carbon standard. All parameters were monitored during imaging and kept at a constant level. The magnification used for acquiring images was 250x, corresponding to 1 µm/pixel. Two images per region were taken for BMDD and osteocyte lacunae morphology analysis. The total mean calcium content of the BMDD (CaMean, wt%) was assessed from the backscattered electron images using a custom-made MATLAB code (MATLAB, Natick, Massachusetts). We evaluated BMDD in the endocortical and periosteal regions separately. Additionally, we manually created masks in ImageJ/Fiji to separate the osteonal and interstitial areas, and we assessed BMDD for these two areas separately. For this purpose, osteonal bone was defined as a circular region of bone matrix surrounding a Haversian canal; interstitial bone was defined as bone matrix between the circular osteonal structures. Cement lines were used as visual borders for the measurement of bone matrix area.

2.6. Supervised deep learning to detect osteocyte lacunae

To analyze the occurrence of mineralized osteocyte lacunae (Mn.Lc. N), we used images acquired for BMDD on a scanning electron microscope (Crossbeam 340, GeminiSEM, Zeiss AG, Oberkochen, Germany). We trained a deep convolutional neural network (CNN) to detect and classify lacunae as nonmineralized, partially mineralized, or fully mineralized using a pretrained YOLOv5 [35] model as a single-stage object detection algorithm. The model was adapted for the detection of lacunae by training in an end-to-end fashion on lacunae in 50 expert-labeled images. Overall, 8716 nonmineralized, 314 partially mineralized, and 394 fully mineralized lacunae were labeled. We used 10-fold cross-validation to train and validate the model's performance. For each iteration, we split our data into 40 images for training (80%), 5 images for validation (10%), and 5 excluded images (10%) for testing. To leverage the data set, we performed random horizontal and vertical flipping and rotation followed y random cropping into patches of 256 × 256 pixels, which resulted in a total data set of 7500 patches. We trained the model using stochastic gradient descent with a learning rate of 0.01, a batch size of 324, and 200 epochs;

we report the mean average precision (mAP) metric for all 10 iterations with an intersection over the union threshold of 50%. The network performance was evaluated exclusively on the test set. For further statistical evaluations, we used all available images. Detected artifacts were cleared from the output image data, and we distinguished the locations of micropetrotic lacunae within the osteonal and interstitial areas in the endocortical and periosteal regions. We normalized the number of partially mineralized and fully mineralized lacunae and the total number of mineralized osteocyte lacunae to the mineralized bone area (B.Ar; #/mm2) for evaluation.

2.7. Osteocyte apoptosis

For osteocyte apoptosis detection, a TUNEL assay, allowing visualization of DNA breaks, was used. The plastic embedding medium was washed out from the undecalcified MMA sections using xylene, and the sections were rehydrated by a descending ethanol series (absolute, 90%, 80%, and distilled water). Following 20 minutes at room temperature (RT) of incubation with proteinase K, the sections were treated with 20% EDTA for 30 minutes at 37 °C. The pretreated sections were then stained using fluorescein from an *In Situ* Cell Death Detection Kit (Roche, Basel, Switzerland) overnight at 37 °C. After staining, the sections were washed with phosphate-buffered saline (PBS) solution and treated with a permeabilization solution with 0.1% Triton X-100 and 0.1% sodium citrate for 8 minutes at RT. The samples were then mounted using mounting medium with DAPI stain. The excitation wavelength for visualization was between 450 nm and 500 nm, while detection was between 515 nm and 568 nm. We acquired five images in the periosteal and endosteal regions in the blue and green channels. For evaluation, ImageJ software was used to merge both fluorescent images, and only cells where the signal from both channels was firmly overlapping were counted as apoptotic. We counted viable and apoptotic osteocytes per bone area (B.Ar; #/mm^2) in the endocortical and periosteal regions.

Caspase-3 is one of the main "executioners" in cell apoptosis. Therefore, IHC staining for caspase-3 is recommended to detect and quantify apoptosis in tissue sections [36,37]. Decalcified sections were deparaffinized using xylene and rehydrated by a descending ethanol series (absolute, 90%, 80%, and distilled water). We performed enzymatic antigen unmasking by 20 min of incubation at RT with Proteinase K and subsequent treatment with 20% EDTA for 30 min at 37 °C. For staining, we used a SignalStain® Apoptosis Cleaved Caspase-3 Detection Kit (Cell Signaling Technology, Danvers, MA, United States). The pretreated sections were then stained in accordance with the manufacturer's recommendation overnight at 4°C. After incubation, the sections were washed, and apoptotic cells were detected by the 3,3-diaminobenzidine (DAB) chromogen (DAKO, Carpinteria, CA, USA) for approximately 8 min. Finally, the slides were counterstained in hematoxylin for 1 s, washed in distilled water, dehydrated, and mounted. The slides were imaged using a PANNORAMIC MIDI Digital Slide Scanner (Sysmex Corporation, Kobe, Hyogo, Japan) at a 60 × objective magnification. We analyzed a total bone area of 1 mm^2 for the endosteal region and 2 mm^2 for the periosteal region. The apoptotic cells were counted manually using an object-counting tool in Olympus cellSens software (Shinjuku City, Tokyo, Japan). We quantified the total number of apoptotic osteocytes per bone area (B.Ar; #/mm^2) in the endocortical and periosteal regions.

2.8. Microcrack accumulation

To investigate microcrack accumulation, we used infiltration with rhodamine-6G and confocal laser scanning microscopy [38]. The advantage of this approach is infiltration with rhodamine-6G before embedding, meaning that only the existing cracks are labeled, and no artifacts created during the embedding process are stained. From the fixed femoral cross-sections, we cut out the region next to the anterior quadrant in a lateral direction using a diamond belt saw (EXAKT Advanced Technologies GmbH, Norderstedt, Germany) to obtain a 10 mm bone piece. The specimens were dehydrated by an ascending ethanol series and infiltrated for 10 days with 0.002% WT rhodamine-6G before being embedded in MMA. The embedded specimens were then ground to 1 cm to fit into the imaging chamber with a glass bottom. Using a confocal laser scanning microscope (Leica SP5, Leica Microsystems, Wetzlar, Germany), we imaged microcracks with a 561 nm laser excitation wavelength at a 20 × objective magnification. For each periosteal and endosteal region, two Z-stacks of fifty images were acquired with a 1 μm distance between images. We quantified the following parameters in ImageJ/Fiji to assess linear microdamage accumulation: total number of linear microcracks per mineralized bone area (B.Ar; #/mm^2) and total length of linear microcracks per mineralized bone area (B.Ar; μm/mm^2). Microcracks derived from the main branch were counted as microcrack branching.

2.9. Statistical analysis

All analyses were performed using Prism 9 software (GraphPad, San Diego, California). The Shapiro–Wilk test assessed the normality of the data. To analyze whether the studied bone parameters differed between the two groups (control and T1DM), we used an unpaired two-tailed t test for normally distributed data or a nonparametric Mann–Whitney test for nonnormally distributed data, and we analyzed the endocortical and periosteal regions separately. For the evaluation of BMDD parameters, we used ANOVA for repeated measures to evaluate the effect of the group (between-subject factor: control vs. T1DM) and area (within-subject factor: osteonal vs. interstitial bone), as well as their interaction. To compare endocortical and periosteal regions, we used a two-sided paired t test for normally distributed data and a Wilcoxon test for nonnormally distributed data, followed by a Bonferroni correction. Data from the comparison between the endocortical and periosteal regions are shown in the supplemental material. Simple linear regression was used to evaluate the relationship between calcium content and the number of mineralized lacunae per bone area. We used the ROUT method to identify potential outliers with Q = 1%. A two-tailed alpha level below 0.05 was set to identify statistically significant results ($^*p < 0.05$).

3. Results

3.1. Caspase-3 immunostaining reveals an elevated number of apoptotic osteocytes in cortical bone from individuals with T1DM

Within our T1DM cohort (Table 1), we did not observe any effect of T1DM on the geometric properties of the midshaft femoral cortical bone compared to the control, including neither elevated cortical porosity nor cortical thickness (Supplemental Table 1 and Supplemental Fig. 1). In addition, bone histomorphometry reflected the low bone remodeling rate that is generally seen in cortical bone and did not show any group-specific differences (Supplemental Table 2 and Supplemental Fig. 2). Histomorphometric analysis of osteocytes (Supplemental Fig. 2H) and empty lacunae (Supplemental Fig. 2I) showed similar results for both groups in both regions (Supplemental Table 2). We noted that 40%-50% of the osteocyte lacunae were already empty in both study groups and both of the analyzed bone regions, possibly decreasing the detection of apoptotic osteocytes.

We assessed signs of osteocyte apoptosis as a means of determining osteocyte viability (Fig. 1A, B). With the terminal deoxynu-

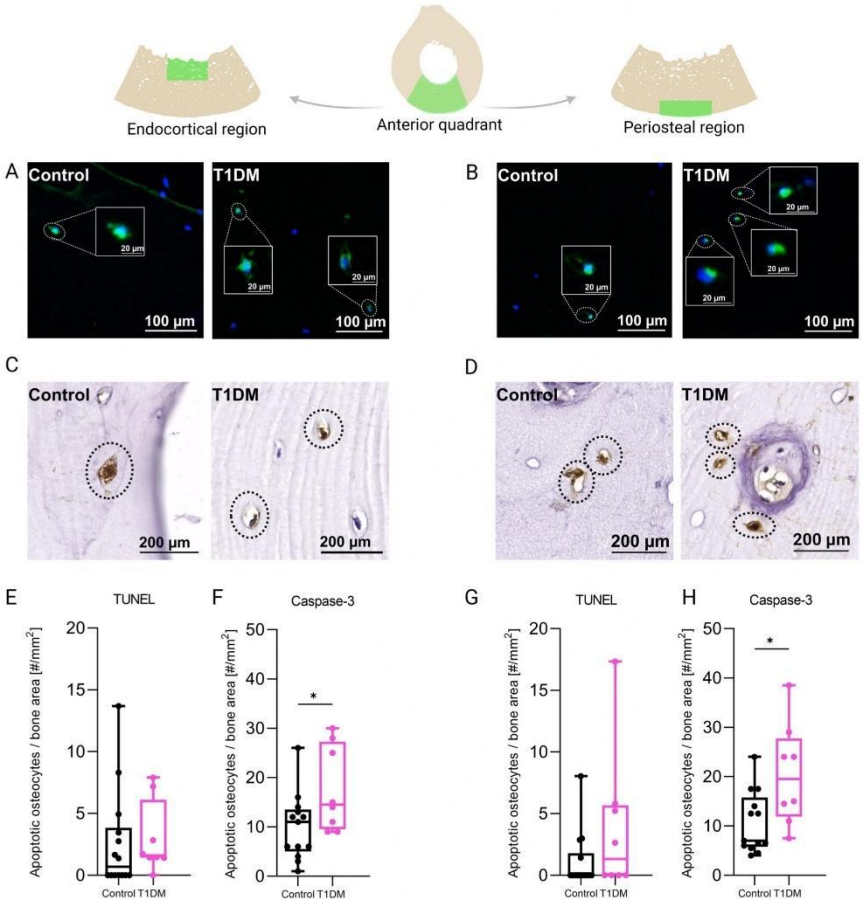

Fig. 1. T1DM promotes osteocyte apoptosis in cortical bone of the femoral mid-diaphysis. Representative images of apoptotic osteocytes stained with TUNEL (A) endocortical and (B) periosteal regions of the control and T1DM groups. Representative images of caspase-3 IHC showing apoptotic osteocytes highlighted by black circles in (C) endocortical and (D) periosteal regions of the control and T1DM groups. (E, G) The results from osteocyte apoptosis detection using TUNEL labeling (endocortical: $p = 0.322$ and periosteal: $p = 0.239$). (F, H) Caspase-3 IHC staining results show a significantly higher number of apoptotic osteocytes in T1DM (endocortical: $p = 0.035$ and periosteal: $p = 0.013$). Boxplots represent the minimum, 25th percentile, median, 75th percentile, and maximum. A t test was applied for normally distributed data to determine p values, and the Mann–Whitney test was used for nonnormally distributed data. $^{*}p < 0.05$.

cleotidyl transferase dUTP nick-end labeling (TUNEL) assay, DNA fragmentation (one hallmark of apoptosis) was labeled, thereby identifying apoptotic osteocytes in human cortical bone. The number of apoptotic osteocytes was normalized to the analyzed cortical bone area for the evaluation. The results showed a comparable number of TUNEL-positive lacunae per bone area between the control and T1DM groups in the endocortical ($p = 0.322$; Fig. 1C) and periosteal regions ($p = 0.239$; Fig. 1E). However, we also employed caspase-3 staining—a more sensitive technique that also detects earlier stages of apoptosis [37]. Caspase-3 IHC staining showed a higher occurrence of apoptotic osteocytes per bone area in then T1DM group than for the control group for both the endocortical region ($p = 0.035$; Fig. 1D) and the periosteal region ($p = 0.013$; Fig. 1F).

3.2. Increased abundance of fully mineralized osteocyte lacunae in the periosteal cortex of T1DM individuals

Mineralization of the osteocyte lacunae (micropetrosis) is the final morphological state of osteocytes undergoing cell death. We visualized osteocyte lacunae undergoing mineralization with high-resolution quantitative backscattered electron imaging (Fig. 2A, B) and determined the number of partially and fully mineralized lacunae per bone area to demonstrate the longitudinal process of micropetrosis (Fig. 2C-F). To evaluate lacunar mineralization, a deep learning model specifically trained on this data set was used to distinguish and count empty, partially mineralized, and fully mineralized lacunae. The custom-made deep learning algorithm achieved $mAP = 0.77 \pm 0.07$. Empty lacunae, partially mineralized lacunae and fully mineralized lacunae were correctly classified in 95.7%,

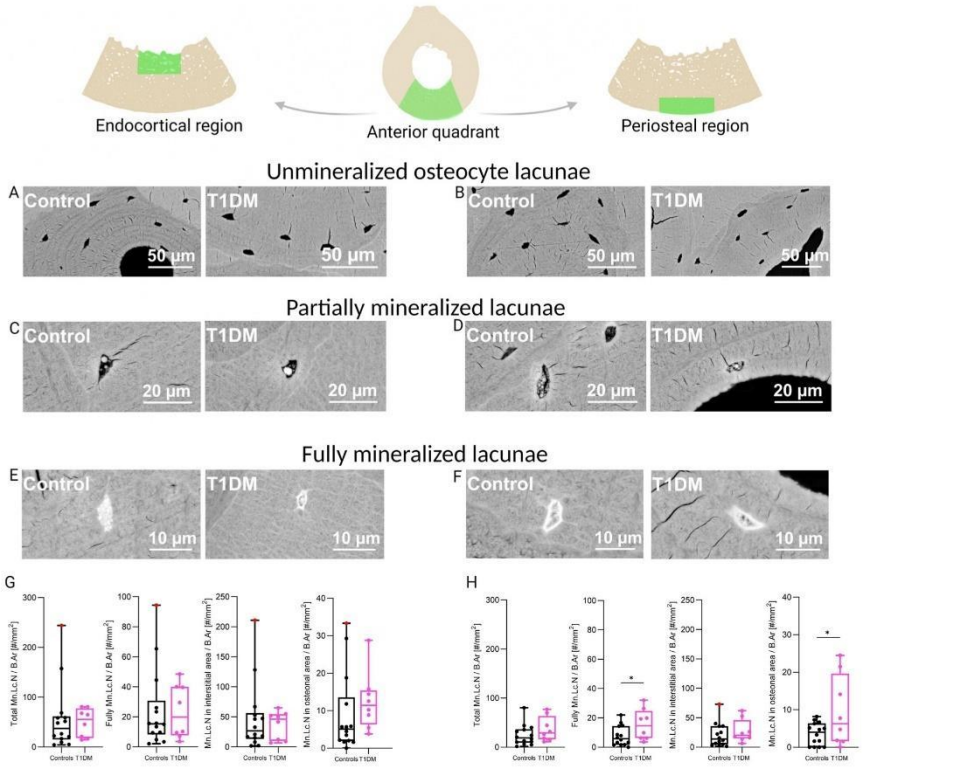

Fig. 2. Osteocyte viability is altered in the periosteal region in the T1DM group. High-resolution backscattered scanning electron microscopy allows the detection of osteocyte lacunae undergoing the mineralization process (micropetrosis), which reflects the viability of osteocytes in cortical bone. Representative images of typical osteocyte lacunae in the (A) endocortical and (B) periosteal regions of the control and T1DM groups. After osteocyte cell death, the lacuna gradually fills with mineral occlusions. Partially filled lacunae are identified by clearly visible calcified nanospherites or by a white halo on the lacunar edges and reflect an intermediate step toward fully mineralized lacunae. Partially filled lacunae are visible in images from the (C) endocortical and (D) periosteal regions for the control and T1DM groups. The last stage of micropetrosis is complete filling of lacunae with calcified nanospherites. Fully mineralized lacunae are shown from the (E) endocortical and (F) periosteal regions for the control and T1DM groups. (G) The analysis of mineralized lacunae in the endocortical region showed comparable values between control and T1DM group in following parameters: total number of mineralized lacunae per bone area (Total Mn.Lc.N/B.At; partially and fully mineralized lacunae; $p = 0.570$); number of fully mineralized lacunae per bone area (Fully Mn.Lc.N/B.At; $p = 0.868$); number of mineralized lacunae per interstitial bone area (Mn.Lc.N/B.At in interstitial area; $p = 0.920$); number of mineralized lacunae per osteonal bone area (Mn.Lc.N/B.At in osteonal area; $p = 0.145$). (H) The analysis of mineralized lacunae in the periosteal region revealed a significantly higher number of Fully Mn.Lc.N/B.At ($p = 0.046$) and Mn.Lc.N/B.At in osteonal area ($p = 0.041$) in T1DM group compared to control specimens. Total Mn.Lc.N/B.At ($p = 0.212$) and Mn.Lc.N/B.At in interstitial area ($p = 0.297$) was unchanged in control and T1DM groups. For abbreviations see G. Boxplots represent the minimum, 25th percentile, median, 75th percentile, and maximum. Red circles denote identified potential outliers using the ROUT method with Q = 1%. A t test was applied for normally distributed data to determine p values, and the Mann–Whitney test was used for nonnormally distributed data. $^{*}p < 0.05$.

70.2%, and 78.2% of cases, respectively. The confusion matrix and example predictions with the confidence score for the endocortical region and periosteal region are shown in Supplemental Fig. 3.

The total number of micropetrotic lacunae per bone area did not differ significantly between the control and T1DM groups in either the endocortical ($p = 0.570$, Fig. 2G) or the periosteal region ($p = 0.212$, Fig. 2H). The number of fully mineralized lacunae, however, was significantly higher in the T1DM group than in the control group in the periosteal region ($p = 0.046$; Fig. 2G), while no such difference was evident in the endocortical region ($p = 0.868$, Fig. 2H). Furthermore, only in the osteonal area did the number of micropetrotic osteocytes per bone area show intergroup differences in the periosteal region, with more micropetrotic osteocytes in T1DM than in the control group ($p= 0.041$; Fig. 2G); the numbers were similar in the endocortical region ($P = 0.145$; Fig. 2H). This difference between the control and T1DM groups was not evident in the interstitial area in either the endocortical ($p = 0.920$, Fig. 2G) or the periosteal region ($p = 0.297$; Fig. 2H).

3.3. Cortical bone calcium density distinguishes younger osteonal bone and older interstitial bone in both the T1DM and control groups

Calcium is the most abundant inorganic element in the mineralized bone matrix. Its amount and distribution affect tissue hardness and therefore the local mechanical properties of the bone tissue. The mean calcium weight percentage did not differ between the control and T1DM groups in either the endocortical region ($p = 0.412$) or the periosteal region ($p = 0.551$). Subdivision into the osteonal and interstitial areas did not reveal differences in calcium content between the control and T1DM groups in either the endocortical ($F(1,13) = 0.494$; $p = 0.495$, Fig. 3C) or the periosteal region ($F(1,13) = 0.099$; $p = 0.757$, Fig. 3D). However, in both study

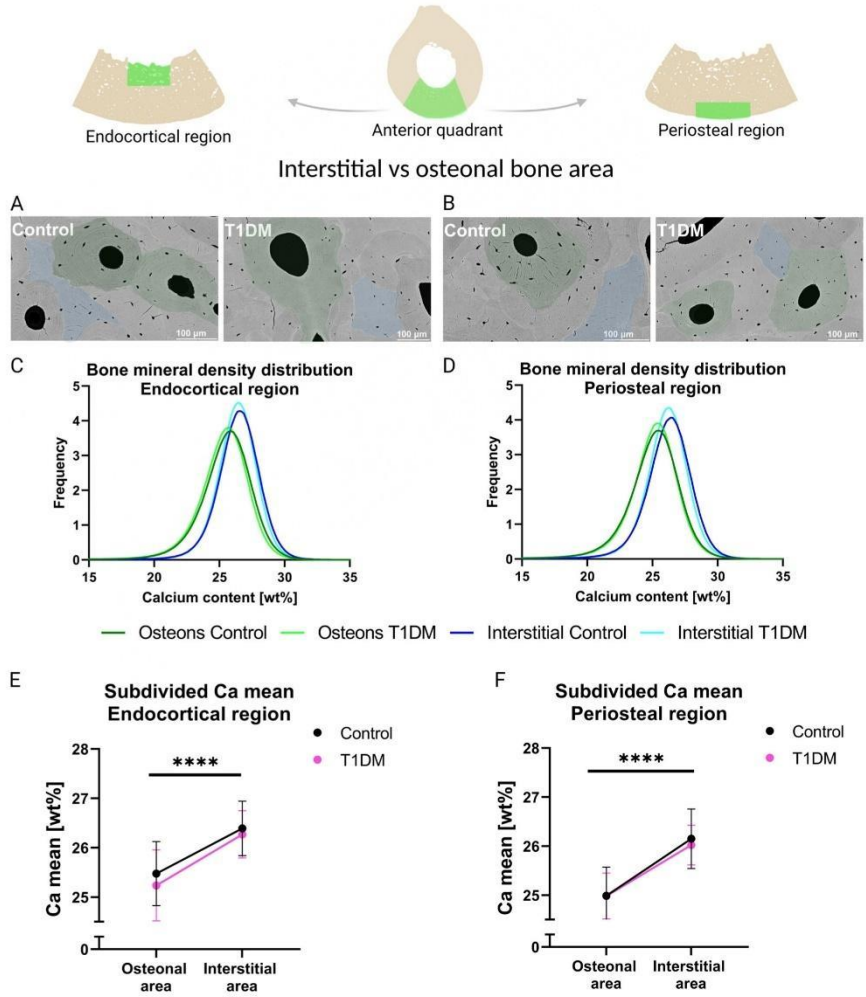

Fig. 3. Bone mineral density distribution is not altered in T1DM. The grayscale level in the images is quantitatively related to the mineral content. Therefore, regions with higher mineral content appear brighter (interstitial areas), while those with lower mineral content appear darker (osteonal areas). A highly mineralized cement line visible as a white contour in the images creates an interface between the osteonal and interstitial areas. High-resolution quantitative backscattered electron images from the control and T1DM groups in the (A) endocortical and (B) periosteal regions, with highlighted examples of the osteonal area in blue and the interstitial area in green. Graphs of the frequency distribution illustrate the distribution of minerals, showing a higher calcium content in the interstitial area than in the osteonal area in both the control and T1DM groups in the (C) endocortical and (D) periosteal regions. The mean calcium weight percentage (Ca mean, wt%) is derived from the grayscale images. The osteonal area consistently showed a significantly lower Ca mean than the interstitial area in both the (E) endocortical and (F) periosteal regions in the control and T1DM groups. Comparison of bone areas (osteonal vs. interstitial) by repeated-measures ANOVA. $^{****}p < 0.001$.

groups, we observed a consistently lower degree of mineralization in the osteonal bone area than in the interstitial area for both the endocortical ($F(1,13) = 159.3$; $p = <0.0001$, Fig. 3E) and periosteal ($F(1,13) = 65,24$; $p = <0.0001$, Fig. 3F) regions, indicating that the tissue age of the osteonal area was younger than that of the interstitial area in both groups.

3.4. Greater microcrack accumulation and microcrack length in the periosteal femoral cortex in the T1DM group

Rhodamine-6G-infiltrated bone specimens were visualized using confocal microscopy to determine microcrack occurrence in the endocortical (Fig. 4A) and periosteal regions (Fig. 4B). To evalu-

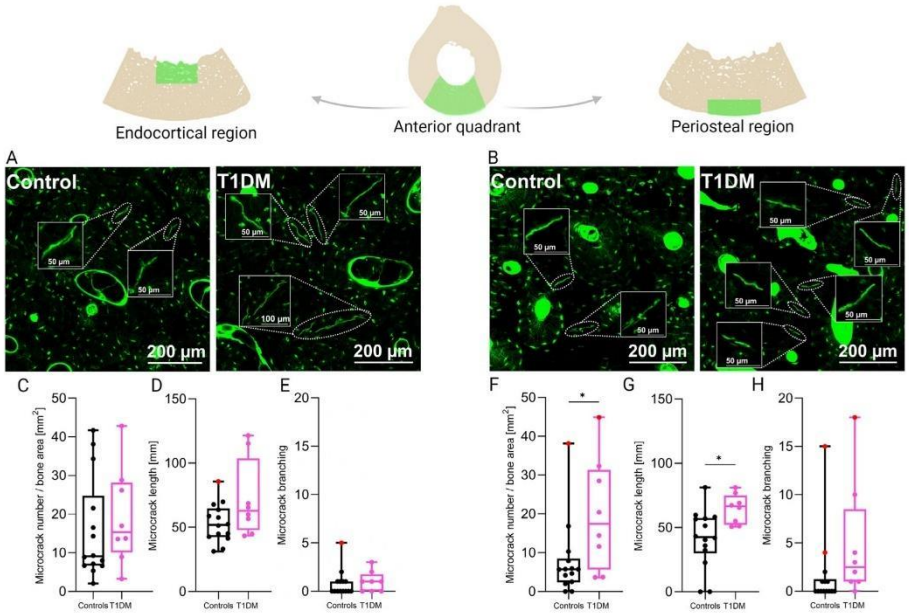

Fig. 4. Microcrack accumulation and total microcrack length in the periosteal region are higher in the T1DM group than in the control group. Rhodamine-6G-infiltrated bone specimens were visualized using confocal laser scanning microscopy. Representative images of linear microcracking in (A) endocortical and (B) periosteal regions of the control and T1DM groups. Confocal imaging results, including the (C, F) number of linear microcracks per bone area (endocortical: $p = 0.365$ and periosteal: $p = 0.048$), (D, G) microcrack length per bone area (endocortical: $p = 0.165$ and periosteal: 0.015), and (E, H) microcrack branching as microcracks derived from the main branch (endocortical: $p = 0.720$ and periosteal: $p = 0.059$). Boxplots represent the minimum, 25th percentile, median, 75th percentile, and maximum. Red circles denote identified potential outliers using the ROUT method with Q = 1%. A t test was applied for normally distributed data to determine p values, and the Mann–Whitney test was used for nonnormally distributed data. $^{*}p < 0.05$.

ate microdamage accumulation, the number of microcracks and microcrack length were normalized to the mineralized bone area. Confocal imaging results showed no effect of T1DM on the number, length or branching of microcracks in the endocortical region (Fig. 4C-E). In contrast, a higher number of linear microcracks per unit bone area in the T1DM group than in the control group was seen in the periosteal region ($p = 0.048$; Fig. 4F). Additionally, the difference in total microcrack length between the T1DM and control groups in the periosteal region was statistically significant ($p = 0.015$; Fig. 4G). Microcracks derived from the main branch were counted as branching. We noted prominent branching in the periosteal region; the degree of branching tended to be greater in the T1DM group than in the control group, but this difference was not statistically significant ($p = 0.059$; Fig. 4H).

4. Discussion

Patients with T1DM have a six-fold higher risk of hip fracture [39] than patients without T1DM; this difference cannot be explained solely by the lower BMD of the former group, as current fracture predictors based on BMD underestimate the burden of fractures in individuals with T1DM. We have utilized multiscale imaging approaches in our previous studies and determined a cohort of elevated cortical porosity as well as higher advanced glycation endproducts to contribute to bone disease with type two diabetes mellitus (T2DM) [40,41]. Here, combining high-resolution microcomputed tomography, quantitative backscattered electron imaging, confocal laser scanning microscopy with immunohistochemistry (IHC) and static bone histomorphometry, we evaluated cortical bone quality in T1DM with a focus on osteocyte viability, mineralization, and microdamage accumulation in human samples from the midshaft femur. We analyzed bone samples from eight individuals diagnosed with T1DM and 14 age-matched control individuals. Using this multiscale characterization approach, we found signs of an elevated level of osteocyte apoptosis associated with T1DM. In the periosteal region of the T1DM group, we found a higher accumulation of linear microcracks accompanied by a greater occurrence of fully mineralized osteocyte lacunae. Furthermore, lacunar mineralization was more prominent within the younger osteonal bone of the periosteal region (Fig. 5).

Although low bone turnover is expected in T1DM [14], the rate of bone turnover and the number of bone cells are already low in the cortical bone compared with the trabecular bone compartment [42], which hinders the identification of intergroup differences between the T1DM and control groups. Moreover, clinical studies have pointed to reduced BMD in T1DM; however, we did not find differences in vertebral BMD on *ex vivo* DXA scans or in the femoral cortical geometric indices, which is consistent with a previous study [43]. Microarchitectural changes in T1DM bone are more apparent in individuals with diabetic complications, as suggested by Shanbhogue and colleagues, which might explain these discrepancies [44].

To better capture remodeling activity, we investigated osteocyte viability parameters in the cortical bone rather than the metabolically active trabecular bone. Osteocyte apoptosis with fatigue microcracking induces targeted activation of new resorption centers in bone tissue, as first demonstrated by Cordoso et al. [45]. *In vitro* studies and animal studies [46,47] have shown that high glucose

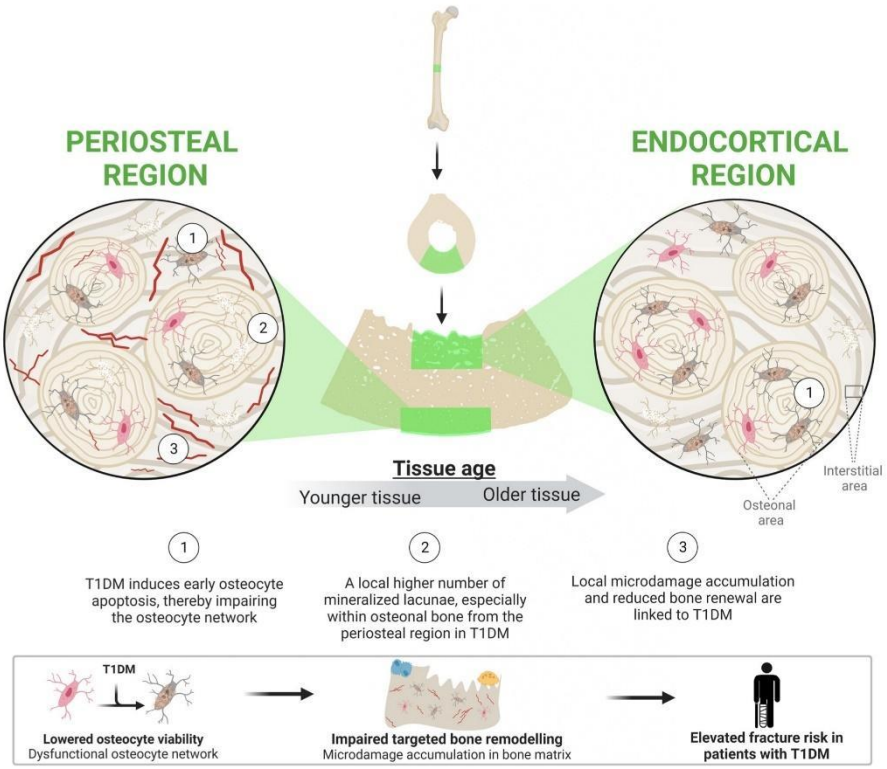

Fig. 5. The effects of T1DM on bone fragility. Increased osteocyte death accompanied by a higher level of mineralized lacunar occlusion contributes to a decreased ability to detect and repair microdamage, leading to a failure and delay or prevention of the remodeling process in the diabetic cortical bone remodeling process.

or diabetes can increase osteocyte apoptosis. Although the TUNEL data did not reveal statistically significant intergroup differences, they indicated a potential trend of elevated osteocyte apoptosis in the T1DM group. Therefore, it was necessary to pair the TUNEL assay with a more sensitive approach to quantify apoptosis. The DNA fragmentation detected by the TUNEL assay might also be found in nonapoptotic cells, i.e., cells undergoing DNA repair [48]; the caspase-3 assay has superior sensitivity [37]. The sensitivity advantage of the caspase-3 assay might also be due to DAB detection, which provides signal amplification. With caspase-3 IHC, we showed that apoptosis of osteocytes in human cortical bone was significantly higher in T1DM patients than in healthy controls.

In our previous work, we showed that occlusion of osteocyte lacunae with mineral aggregates, a phenomenon termed micropetrosis, is pronounced in aged human bone and could therefore be associated with increased fracture risk [17,25]. In the current study, we distinguished between partially and fully mineralized osteocyte lacunae, as partially mineralized lacunae are considered a preliminary step toward fully mineralized lacunae. In addition, partially mineralized lacunae may not necessarily reach the complete mineralization stage (full mineralization of the lacunae) because they can still be removed during remodeling. In contrast, fully mineralized osteocyte lacunes are recognized as the endpoint of micropetrotic events. With aging, the accumulation of mineralized lacunae preferentially occurs in the endocortical region compared with the periosteal region, as we showed in our previous study [17]. The younger tissue age of the entire periosteal region is due to the apposition of new bone matrix in this region during aging [49]. Geometric cross-section indices were not lower in the T1DM group than in the age-matched control group, meaning that the process of periosteal apposition appears not to be affected by T1DM. In the current study, we observed an elevated number of micropetrotic lacunae in the osteonal bone at the periosteal region of the T1DM group compared with the healthy control group, which is counterintuitive in light of the younger bone tissue. Increased osteocyte apoptosis, leading to reduced numbers of viable osteocytes and increased micropetrosis, negatively affects the mechanical properties of bone. Specifically, a higher number of micropetrotic lacunae leads to a more brittle bone matrix [50,51], which is more prone to microcracking. Our results indeed show an increased number and length of linear microcracks per bone area in the periosteal region in the T1DM group compared to the control group. Therefore, we hypothesize that T1DM induces early osteocyte cell death, causing dysfunction of the osteocyte network, which may impair targeted bone remodeling and result in lower microcrack removal and therefore elevated microcrack accumulation in the cortical bone of T1DM.

Finally, we used high-resolution imaging of the cortical bone to compare the osteonal and interstitial areas of both the periosteal and endosteal regions. Osteonal areas consist of 'younger' bone,

whereas interstitial areas consist of 'older' bone. Older interstitial bone tends to have a more mineralized matrix than younger osteonal bone [52,53]. A novel finding from our BMDD analysis was that T1DM patients and controls had similar differences in mineralization levels between younger osteonal bone and older interstitial bone. Furthermore, we found differences between T1DM patients and healthy controls in these osteonal and interstitial areas within the periosteal region: the number of micropetrotic lacunae in the osteonal bone area was higher in T1DM patients than in controls. With aging, the older interstitial bone areas show a higher degree of bone mineralization, and these highly mineralized bone packets are characterized by a limited supply of nutrients, which allows increased accumulation of micropetrotic lacunae compared with younger bone within osteons [17,18]. Interestingly, we observed an increased number of micropetrotic lacunae within the osteonal, younger areas in the periosteal region of T1DM group. Therefore, we hypothesize that T1DM might accelerate the cellular aging processes and lead to the premature death of osteocytes, thereby causing prominent lacunar mineralization, as shown in the osteonal bone of the periosteal region in the T1DM group.

Our study has a few limitations. As human bone material was collected during autopsy, the bone was not labeled with fluorescent markers to enable the assessment of dynamic bone formation indices. However, all specimens were obtained during autopsy exclusively for the purpose of multiscale bone quality assessment. Therefore, anatomical orientation and positioning of the regions of interest could be controlled, facilitating normalizing procedures and high data reproducibility. Deidentified data of the donors did not contain information about diabetes disease onset or duration because of the postmortem origin of the specimens. However, due to the known course of T1DM, we assume an early onset of the disease in childhood or young adulthood with insulin supplementation in donors with T1DM. We collected rare femoral cross-sections during autopsy, allowing us to use an exceptionally large region of interest for the quantitative bone quality assessment. Here, we focused on the anterior quadrant to provide data at a high spatial resolution. Additionally, the anterior quadrant ensures no influence of muscle and tendon attachments on the bone microstructure. The alterations in LCN were deduced based on direct morphological changes in the bone matrix caused by mineralization of lacunae, apoptosis of osteocytes, and linear microcracks. While the predictions of our deep learning model for mineralized lacunae detection are not perfect, the results are generally promising and have practical value within the context of the work. The difficulty in clearly identifying partially mineralized lacunae is reflected in the relatively low accuracy for this class. However, it must be noted that the same difficulty affects human experts, i.e., the labels may be less reliable than those of fully mineralized or nonmineralized lacunae. In fact, the deterministic nature of the learned model presents an advantage in our setting, where the distinction between the three classes is made in the same way for all lacunae. Despite these potential limitations, our study provides new and critical insight into how T1DM affects bone quality and offers evidence for the underlying mechanism of diabetic bone disease in human cortical bone.

5. Conclusion

In summary, the current study highlights osteocyte apoptosis as a potential determinant of cortical T1DM pathology. Osteocyte apoptosis was more frequent in both endocortical and periosteal regions in our T1DM cohort. In addition, we found increased mineralized lacunae in the osteonal area of the periosteal region, signifying that the osteocyte network was disrupted by hypermineralized calcified matter. The accompanying elevated microcrack accumulation in the periosteal region further highlights impaired bone quality in T1DM. Although the periosteal region is considered to consist of younger bone than the endocortical region, we determined that the periosteal region in T1DM is the preferential site for fully mineralized lacunar spaces and microdamage accumulation, which would be more expected in the endocortical region of older bone. In addition, T1DM led to preferential micropetrosis in osteonal areas of the periosteal region, pointing toward osteocyte pathology within newly formed bone. These findings suggest that T1DM accelerates the aging effects in the bone matrix and leads to the premature death of osteocytes.

Data availability statement

The data that support the findings of this study are available upon reasonable request from the corresponding author BB. The data are not publicly available due to privacy concerns or ethical restrictions.

Funding

This project has received funding from the European Union's Horizon 2020 research and innovation program under the Marie Skłodowska-Curie grant agreement no. 860898 to LCH, MR, BB, and KJR. BB receives funding from the German Research Foundation (DFG) under BU2562/10-1. KJR receives funding from German Cancer Aid (Deutsche Krebshilfe) under MSNZ Hamburg HaTRiCS4. LH received funding from the Elsbeth-Bonhoff-Foundation. PM received funding from the Ministry of Science of the Republic of Serbia and from the Science Fund of the Republic of Serbia.

Author contributions

SDK, KJ-R, and BB designed the study. BW, HM, KP and BO carried out autopsies and evaluated patient data. SDK and EMW prepared the specimens for ex vivo analysis. SDK, EMW and KJ-R designed and performed experiments and analyzed the data. MN performed experiments. AVF processed the imaging data. SDK performed the statistical analysis. SDK, EMW, HH, PM, LCH, MR, AV, AS, BB and KJ-R interpreted the data. SDK, KJ-R and BB wrote the manuscript. All authors approved the final version of the manuscript.

Disclosure

The authors have no conflicts of interest to declare. All coauthors have seen and agree with the contents of the manuscript, and there is no financial interest to report. We certify that the submission is original work and is not under review at any other publication.

Declaration of Competing Interest

The authors declare that they have no known competing financial interests or personal relationships that could have appeared to influence the work reported in this paper.

The authors declare the following financial interests/personal relationships which may be considered as potential competing interests:

CRediT authorship contribution statement

Sofie Dragoun Kolibová: Conceptualization, Methodology, Investigation, Formal analysis, Writing – original draft, Writing – review & editing. **Eva Maria Wölfel:** Conceptualization, Investigation, Writing – review & editing. **Haniyeh Hemmatian:** Investigation, Writing – review & editing. **Petar Milovanovic:** Investigation,

Writing – review & editing. **Herbert Mushumba:** Investigation. **Birgit Wulff:** Investigation. **Maximilian Neidhardt:** Investigation. **Klaus Püschel:** Investigation. **Antonio Virgilio Failla:** Investigation. **Annegreet Vlug:** Investigation. **Alexander Schlaefer:** Investigation. **Benjamin Ondruschka:** Investigation. **Michael Amling:** Investigation. **Lorenz C. Hofbauer:** Investigation, Writing – review & editing. **Martina Rauner:** Investigation, Writing – review & editing. **Björn Busse:** Conceptualization, Methodology, Investigation, Writing – review & editing. **Katharina Jähn-Rickert:** Conceptualization, Methodology, Investigation, Writing – review & editing.

Acknowledgments

The authors thank Sandra Perkovic and Dr. Imke Fiedler (Department of Osteology and Biomechanics, University Medical Center Hamburg-Eppendorf) and Dr. Bernd Zobiak (UKE Microscopy Imaging Facility, University Medical Center Hamburg-Eppendorf) for their technical and scientific support.

Supplementary materials

Supplementary material associated with this article can be found, in the online version, at doi:10.1016/j.actbio.2023.02.037.

References

[1] , in: International Diabetes Federation. IDF Diabetes Atlas, 10th ed., International Diabetes Federation, Brussels, Belgium, 2021, p. 2021.
[2] L.A. DiMeglio, C. Evans-Molina, R.A. Oram, Type 1 diabetes, Lancet 391 (2018) 2449–2462, doi:10.1016/S0140-6736(18)31320-5.
[3] M. Mobasseri, M. Shirmohammadi, T. Amiri, N. Vahed, H. Hosseini Fard, M. Ghojazadeh, Prevalence and incidence of type 1 diabetes in the world: a systematic review and meta-analysis, Health Promot. Perspect. 10 (2020) 98–115, doi:10.34172/hpp.2020.18.
[4] V.N. Shah, C.S. Shah, J.K. Snell-Bergeon, Type 1 diabetes and risk of fracture: meta-analysis and review of the literature, Diabet. Med. 32 (2015) 1134–1142, doi:10.1111/dme.12734.
[5] T. Vilaca, M. Paggiosi, J.S. Walsh, D. Selvarajah, R. Eastell, The effects of Type 1 diabetes and diabetic peripheral neuropathy on the musculoskeletal system: a case-control study, J. Bone Miner. Res. (2021), doi:10.1002/jbmr.4271.
[6] T. Vilaca, M. Schini, S. Harnan, A. Sutton, E. Poku, I.E. Allen, S.R. Cummings, R. Eastell, The risk of hip and non-vertebral fractures in type 1 and type 2 diabetes: A systematic review and meta-analysis update, Bone 137 (2020) 115457, doi:10.1016/j.bone.2020.115457.
[7] M. Janghorbani, R.M. van Dam, W.C. Willett, F.B. Hu, Systematic review of type 1 and type 2 diabetes mellitus and risk of fracture, 166 (2007) 495–505. doi: 10.1093/aje/kwm106.
[8] H. Fang, L. Huang, I. Welch, C. Norley, D.W. Holdsworth, F. Beier, D. Cai, Early changes of articular cartilage and subchondral bone in the DMM mouse model of osteoarthritis, Sci. Rep. (2018), doi:10.1038/s41598-018-21184-5.
[9] P.J. Lopez-Ibarra, M.M. Pastor, F. Escobar-Jimenez, M.D. Pardo, A.G. Gonzalez, J.D. Luna, M.E. Requena, M.A. Diosdado, Bone mineral density at time of clinical diagnosis of adult-onset type 1 diabetes mellitus, Endocr. Pract. 7 (2001) 346–351, doi:10.4158/EP.7.5.346.
[10] C. Eller-Vainicher, V. v Zhukouskaya, Y. v Tolkachev, S.S. Koritko, E. Cairoli, E. Grossi, P. Beck-Peccoz, I. Chiodini, A.P. Shepelkevich, Low bone mineral density and its predictors in type 1 diabetic patients evaluated by the classic statistics and artificial neural network analysis, Diabetes Care. 34 (2011) 2186–2191, doi:10.2337/dc11-0764.
[11] A. Joshi, P. Varthakavi, M. Chadha, N. Bhagwat, A study of bone mineral density and its determinants in type 1 diabetes mellitus, J. Osteoporos. 2013 (2013) 397814, doi:10.1155/2013/397814.
[12] N. Soto, R. Pruzzo, F. Eyzaguirre, G. Iniguez, P. Lopez, J. Mohr, F. Perez-Bravo, F. Cassorla, E. Codner, Bone mass and sex steroids in postmenarcheal adolescents and adult women with Type 1 diabetes mellitus, J. Diabetes Complicat. 25 (2011) 19–24, doi:10.1016/j.jdiacomp.2009.10.002.
[13] K. Hygum, J. Starup-Linde, T. Harsløf, P. Vestergaard, B.L. Langdahl, Mechanisms in Endocrinology: diabetes mellitus, a state of low bone turnover – a systematic review and meta-analysis, Eur. J. Endocrinol. 176 (2017) R137–R157, doi:10.1530/eje-16-0652.
[14] L.J. Raggatt, N.C. Partridge, Cellular and molecular mechanisms of bone remodeling, J. Biol. Chem. 285 (2010) 25103–25108, doi:10.1074/jbc.r109.041087.
[15] L.F. Bonewald, The amazing osteocyte, J. Bone Miner. Res. 26 (2011) 229–238, doi:10.1002/jbmr.320.
[16] P.R. Buenzli, N.A. Sims, Quantifying the osteocyte network in the human skeleton, Bone 75 (2015) 144–150, doi:10.1016/J.BONE.2015.02.016.
[17] B. Busse, D. Djonic, P. Milovanovic, M. Hahn, K. Püschel, R.O. Ritchie, M. Djuric, M. Amling, Decrease in the osteocyte lacunar density accompanied by hypermineralized lacunar occlusion reveals failure and delay of remodeling in aged human bone, Aging Cell 9 (2010) 1065–1075, doi:10.1111/j.1474-9726.2010.00633.x.
[18] P. Milovanovic, E.A. Zimmermann, C. Riedel, A. vom Scheidt, L. Herzog, M. Krause, D. Djonic, M. Djuric, K. Püschel, M. Amling, R.O. Ritchie, B. Busse, Multi-level characterization of human femoral cortices and their underlying osteocyte network reveal trends in quality of young, aged, osteoporotic and antiresorptive-treated bone, Biomaterials (2015), doi:10.1016/j.biomaterials.2014.12.024.
[19] R.S. Weinstein, R.W. Nicholas, S.C. Manolagas, Apoptosis of osteocytes in glucocorticoid-induced osteonecrosis of the Hip 1, J. Clin. Endocrinol. Metab. 85 (2000), doi:10.1210/jcem.85.8.6714.
[20] C.C. Kennedy, A. Papaioannou, J.D. Adachi, A. for correspondence, Glucocorticoid-induced osteoporosis, Women's Health. 2 (2006) 65–74. doi: 10.2217/17455057.2.1.65.
[21] T. Rolvien, P. Milovanovic, † Felix, N. Schmidt, S. von Kroge, E.M. Wölfel, M. Krause, B. Wulff, K. Püschel, R.O. Ritchie, M. Amling, B. Busse, Long-term immobilization in elderly females causes a specific pattern of cortical bone and osteocyte deterioration different from postmenopausal osteoporosis, (2020). doi: 10.1002/jbmr.3970.
[22] L.I. Plotkin, SKELETAL BIOLOGY AND REGULATION (MR FORWOOD AND A ROBLING, SECTION EDITORS) Apoptotic osteocytes and the control of targeted bone resorption, (n.d.). doi: 10.1007/s11914-014-0194-3.
[23] J.Y. Ru, Y.F. Wang, Osteocyte apoptosis: the roles and key molecular mechanisms in resorption-related bone diseases, (n.d.). doi: 10.1038/s41419-020-03059-8.
[24] H.M. Frost, *In vivo* osteocyte death, J. Bone Jt. Surg. Am. (1960) 42 A, doi:10.2106/00004623-196042010-00011.
[25] H.M. Frost, Micropetrosis, J. Bone Jt. Surg. Am. (1960) 144–150 42-A https://www.ncbi.nlm.nih.gov/pubmed/13849862 .
[26] P. Milovanovic, E.A. Zimmermann, A. vom Scheidt, B. Hoffmann, G. Sarau, T. Yorgan, M. Schweizer, M. Amling, S. Christiansen, B. Busse, The formation of calcified nanospherites during micropetrosis represents a unique mineralization mechanism in aged human bone, Small 13 (2017) 1602215, doi:10.1002/smll.201602215.
[27] P. Milovanovic, B. Busse, Phenomenon of osteocyte lacunar mineralization: indicator of former osteocyte death and a novel marker of impaired bone quality? Endocr. Connect. 9 (2020) R70–R80, doi:10.1530/ec-19-0531.
[28] S. Qiu, D.S. Rao, D.P. Fyhrie, S. Palnitkar, A.M. Parfitt, The morphological association between microcracks and osteocyte lacunae in human cortical bone, Bone 37 (2005) 10–15, doi:10.1016/J.BONE.2005.01.023.
[29] O.D. Kennedy, D.M. Laudier, R.J. Majeska, H.B. Sun, M.B. Schaffler, Osteocyte apoptosis is required for production of osteoclastogenic signals following bone fatigue *in vivo*, Bone 64 (2014) 132–137, doi:10.1016/j.bone.2014.03.049.
[30] O. Verborgt, G.J. Gibson, M.B. Schaffler, Loss of osteocyte integrity in association with microdamage and bone remodeling after fatigue *in vivo*, J. Bone Miner. Res. 15 (2000) 60–67, doi:10.1359/jbmr.2000.15.1.60.
[31] D. Vashishth, O. Verborgt, G. Divine, M.B. Schaffler, D.P. Fyhrie, Decline in osteocyte lacunar density in human cortical bone is associated with accumulation of microcracks with age, Bone 26 (2000) 375–380 https://www.ncbi.nlm.nih.gov/pubmed/10719281.
[32] X. Liu, W. Li, J. Cai, Z. Yan, X. Shao, K. Xie, X.E. Guo, E. Luo, D. Jing, Spatiotemporal characterization of microdamage accumulation and its targeted remodeling mechanisms in diabetic fatigued bone, FASEB J. 34 (2020) 2579–2594, doi:10.1096/fj.201902011rr.
[33] V. Sládek, V. Sabolová, O. Šebesta, T. Zikmund, J. Kaiser, S. Čerevková, Effect of deriving periosteal and endosteal contours from microCT scans on computation of cross-sectional properties in non-adults: the femur, J. Anat. 233 (2018) 381–393, doi:10.1111/joa.12835.
[34] D.W. Dempster, J.E. Compston, M.K. Drezner, F.H. Glorieux, J.A. Kanis, H. Malluche, P.J. Meunier, S.M. Ott, R.R. Recker, A.M. Parfitt, Standardized nomenclature, symbols, and units for bone histomorphometry: A 2012 update of the report of the ASBMR Histomorphometry Nomenclature Committee, J. Bone Miner. Res. 28 (2013) 2–17, doi:10.1002/jbmr.1805.
[35] G. Jocher, A. Stoken, J. Borovec, NanoCode012, ChristopherSTAN, L. Changyu, Laughing, tkianai, yxNONG, A. Hogan, lorenzomammana, AlexWang1900, A. Chaurasia, L. Diaconu, Marc, wanghaoyang0106, ml5ah, Doug, Durgesh, F. 0Ingham, Frederik, Guilhen, A. Colmagro, H. Ye, Jacobsolawetz, J. Poznanski, J. Fang, J. Kim, K. Doan, 十力军 L.Y., ultralytics/yolov5: v4.0 - nn.SiLU activations, Weights & Biases logging, PyTorch Hub integration, (2021). doi: 10.5281/ZENODO.4418161.
[36] A. Bressenot, S. Marchal, L. Bezdetnaya, J. Garrier, F. Guillemin, F. Plénat, Assessment of apoptosis by immunohistochemistry to active caspase-3, active caspase-7, or cleaved PARP in monolayer cells and spheroid and subcutaneous xenografts of human carcinoma, J. Histochem. Cytochem. 57 (2009) 289–300, doi:10.1369/jhc.2008.952044.
[37] W.R. Duan, D.S. Garner, S.D. Williams, C.L. Funckes-Shippy, I.S. Spath, E.A. Blomme, R. Duan, D.S. Garner, S.D. Williams, C.L. Funckes-Shippy, I.S. Spath, E.A. Blomme, Comparison of immunohistochemistry for activated caspase-3 and cleaved cytokeratin 18 with the TUNEL method for quantification of apoptosis in histological sections of PC-3 subcutaneous xenografts, 199 (2003) 221–228. doi: 10.1002/path.1289.
[38] M. Kerschnitzki, W. Wagermaier, P. Roschger, J. Seto, R. Shahar, G.N. Duda, S. Mundlos, P. Fratzl, The organization of the osteocyte network mirrors the extracellular matrix orientation in bone, J. Struct. Biol. 173 (2) (2011) 303–311, doi:10.1016/j.jsb.2010.11.014.
[39] P. Vestergaard, Discrepancies in bone mineral density and fracture risk in pa-

tients with type 1 and type 2 diabetes–a meta-analysis, Osteoporos. Int. 18 (2007) 427–444, doi:10.1007/s00198-006-0253-4.
[40] E.M. Wölfel, K. Jähn, A.K. Siebels, L.-Y. Ma, G.E. Sroga, A. vom Scheidt, F.N. Schmidt, B. Wulff, H. Mushumba, K. Püschel, M. Amling, D. Vashishth, E. Schaible, P. Milovanovic, E. Zimmermann, B. Busse, In type 2 diabetes mellitus collagen fibril plasticity is altered along with higher glyco-oxydative damage and non-osteoporotic bone mineral density, Bone Rep. 13 (2020), doi:10.1016/j.bonr.2020.100694.
[41] E.M. Wölfel, I.A.K. Fiedler, S. Dragoun Kolibova, J. Krug, M.C. Lin, B. Yazigi, A.K. Siebels, H. Mushumba, B. Wulff, B. Ondruschka, K. Püschel, C.C. Glüer, K. Jähn-Rickert, B. Busse, Human tibial cortical bone with high porosity in type 2 diabetes mellitus is accompanied by distinctive bone material properties, Bone 165 (2022) 116546, doi:10.1016/J.BONE.2022.116546.
[42] J. Compston, L. Skingle, D.W. Dempster, Bone histomorphometry, vitamin D: fourth edition, 1 (2018) 959–973,doi: 10.1016/B978-0-12-809965-0.00053-7.
[43] T. Miazgowski, S. Pynka, M. Noworyta-Zietara, B. Kryzanowska-Świniarska, R. Pikul, Bone mineral density and hip structural analysis in type 1 diabetic men, Eur. J. Endocrinol. (2007) 156, doi:10.1530/eje.1.02309.
[44] V. Shanbhogue, S. Hansen, M. Frost, N.R. Jørgensen, A.P. Hermann, J.E. Henriksen, K. Brixen, Bone Geometry, Volumetric density, microarchitecture, and estimated bone strength assessed by HR-pQCT in adult patients with Type 1 diabetes mellitus, J. Bone Miner. Res. 30 (2015), doi:10.1002/jbmr.2573.
[45] L. Cardoso, B.C. Herman, O. Verborgt, D. Laudier, R.J. Majeska, M.B. Schaffler, Osteocyte apoptosis controls activation of intracortical resorption in response to bone fatigue, J. Bone Miner. Res. 24 (2009) 597–605, doi:10.1359/JBMR.081210.
[46] M. Maycas, K.A. McAndrews, A.Y. Sato, G.G. Pellegrini, D.M. Brown, M.R. Allen, L.I. Plotkin, A.R. Gortazar, P. Esbrit, T. Bellido, PTHrP-derived peptides restore bone mass and strength in diabetic mice: additive effect of mechanical loading, J. Bone Miner. Res. 32 (2017) 486–497, doi:10.1002/jbmr.3007.
[47] S. Portal-Núñez, D. Lozano, L. Fernández De Castro, A.R. de Gortázar, X. Nogués, P. Esbrit, Alterations of the Wnt/b-catenin pathway and its target genesfor the N- and C-terminal domains of parathyroid hormone-related proteinin bone from diabetic mice, FEBS Lett. 584 (2010) 3095–3100, doi:10.1016/j.febslet.2010.05.047.
[48] D.T. Loo, *In situ* detection of apoptosis by the TUNEL assay: an overview of techniques, in: 2011: pp. 3–13. doi: 10.1007/978-1-60327-409-8_1.
[49] E. Seeman, P.D. Delmas, Bone quality — The material and structural basis of bone strength and fragility, N. Engl. J. Med. 354 (2006), doi:10.1056/nejmra053077.
[50] W.S.S. Jee, Integrated Bone Tissue Physiology: Anatomy and Physiology, Bone Mechanics Handbook, 2001 Second Edition.
[51] T.M. Boyce, R.D. Bloebaum, Cortical aging differences and fracture implications for the human femoral neck, Bone (1993) 14, doi:10.1016/8756-3282(93)90209-S.
[52] C. Bergot, Y. Wu, E. Jolivet, L.Q. Zhou, J.D. Laredo, V. Bousson, The degree and distribution of cortical bone mineralization in the human femoral shaft change with age and sex in a microradiographic study, Bone (2009) 45, doi:10.1016/j.bone.2009.05.025.
[53] Y. Wu, C. Bergot, E. Jolivet, L.Q. Zhou, J.D. Laredo, V. Bousson, Cortical bone mineralization differences between hip-fractured females and controls. A microradiographic study, Bone (2009) 45, doi:10.1016/j.bone.2009.04.202.

Review

Thieme

Micropetrosis – Occlusion of Osteocyte Lacunae

Mikropetrosis – Okklusion der Osteozytenlakunen

Authors
Sofie Dragoun Kolibová[1], Björn Busse[1,2], Katharina Jähn-Rickert[1,3]

Affiliations
1 Institut für Osteologie und Biomechanik, Universitätsklinikum Hamburg-Eppendorf, Hamburg, Germany
2 Interdisciplinary Competence Center for Interface Research, Universitätsklinikum Hamburg-Eppendorf, Hamburg, Germany
3 Mildred Scheel Nachwuchszentrum, Universitäres Cancer Center Hamburg, Universitätsklinikum Hamburg-Eppendorf, Hamburg, Germany

Keywords
micropetrosis, osteocyte lacunar mineralization, osteocytes, diabetes mellitus, osteoporosis

Schlüsselwörter
Mikropetrose, Osteozytenlakunen Mineralisierung, Osteozyten, Diabetes mellitus, Osteoporose

received 18.08.2022
accepted 09.10.2022

Bibliography
Osteologie 2022; 31: 280–288
DOI 10.1055/a-1958-3727
ISSN 1019-1291

Georg Thieme Verlag, Rüdigerstraße 14,
70469 Stuttgart, Germany

Correspondence
Dr. Katharina Jähn-Rickert
Universitätsklinikum Hamburg-Eppendorf
Institut für Osteologie und Biomechanik,
Lottestr. 55a,
22529 Hamburg
Germany
Tel.: +49407410-26301
k.jaehn@uke.de

ABSTRACT

This article summarizes the current knowledge on micropetrosis – osteocyte lacunar occlusion, while focusing on the latest data on osteocyte viability and diabetic bone disease. The lacunae are fluid-filled ellipsoid spaces where osteocytes reside within the mineralized matrix. During osteocyte lifetime, the lacunar space is kept in a non-mineralized state. However, a dying osteocyte appears to enable the initiation of lacunar mineralization – creating a fossil within the living tissue. Elevated frequencies of micropetrosis are observed with advanced age, but also type 1 diabetes mellitus. The latter is a common health threat to our society with rising numbers of patients suffering from the disease associated symptoms including a secondary type of osteoporosis with an elevated risk of fragility fractures. While the underlying mechanism of diabetic bone disease is not entirely understood, more evidence is pointing towards a combinatory effect of loss of bone mass and an impaired overall bone quality. The high number of micropetrotic osteocyte lacunae leads to a more brittle bone tissue prone to microcracking. Further investigations are required to determine the implications of elevated micropetrosis as a reliable target of bone fragility.

ZUSAMMENFASSUNG

Mikropetrose, die Okklusion der Osteozytenlakunen, stellt eine besondere Art der Mineralisation innerhalb des Knochens dar. In ihrem Verlauf werden Osteozyten-behauste Lakunen stufenweise komplett ausmineralisiert. Somit entstehen lokale Unterbrechungen des mechanoregulatorischen Osteozyten Netzwerkes, welches Knochenumbauprozesse im Knochen steuert. Die Sprödigkeit der Knochenmatrix wird durch die lokale Anhäufung der mineralisierten Lakunen erhöht, Stressdissipationsmechanismen fehlen, und es kann zur Anhäufung von Mikrocracks kommen. Die beiden letzteren Faktoren können zu einer erhöhten Brüchigkeit der Knochenmatrix beitragen. Mikropetrose wurde zuerst in Knochenproben alternder Individuen detektiert. Ein erhöhtes Vorkommen mikropetrotischer Lakunen findet sich in osteoporotischen Patienten, sowohl mit altersbedingter, als auch mit sekundärer Diabetes Mellitus-bedingter Osteoporose. Diabetes mellitus geht mit einem erhöhten Frakturrisiko einher, wobei bei Typ 1 Diabetes Mellitus das Frakturrisiko um das 7-fache erhöht sein kann. Mechanistische Untersuchungen, welche die ursächlichen Zusammenhänge der brüchigen Knochenmatrix mit Typ 1 Diabetes Mellitus erklären sind noch rar, weisen jedoch auf eine Kombination aus Knochenmasseverlust und beeinträchtigter Knochenqualität hin. Unsere Untersuchungen an Typ 1 Diabetes Mellitus korti-

9.2. Publication 2: Micropetrosis – Occlusion of Osteocyte Lacunae

kalen Knochenproben konnten zeigen, dass es lokal zu einer erhöhten Bildung mikropetrotischer Osteozytenlakunen kommt. Diese lokalen Okklusionen befinden sich in der relativ jüngeren Knochenmatrix – dem periostalen Bereich, spezifischer in den osteonalen Knochenumbaueinheiten dieses Bereiches und nicht in der lokal älteren interstitialen Knochenmatrix. Daraus ergibt sich unsere Arbeitshypothese, dass Typ 1 Diabetes Mellitus zu einer pathologischen Knochenalterung einhergehend mit gehäuftem Osteozyten-Zelltod, Mikropetrose und Mikrocrack-Ansammlung führt. Die Bedeutung des lebenden Osteozytennetzwerkes für den Erhalt der physiologischen Knochenmatrixqualität sollte durch die spezifische Charakterisierung der Mikropetrose, dem fossilen Osteozytennetzwerk, erweitert werden. Zukünftige Studien zur Verbesserung der pharmakologischen Behandlung von Knochenpathologien sollten Osteozytenparameter miteinbeziehen.

Introduction

Osteoporosis is a systemic disease characterized by a loss of bone mass, and the subsequent decrease in bone density and an elevated susceptibility to fractures. There is a distinction between primary osteoporosis present in postmenopausal women and the older population in general, and secondary osteoporosis, with underlying conditions e. g., diabetes mellitus, medication, or even immobilization resulting in fragility fractures [1, 2]. The global health data confirms a higher incidence of osteoporosis in diabetes mellitus type 1 (T1DM) and type 2 (T2DM) patients [3]. Both types of diabetes mellitus are associated with an increased risk of osteoporotic fractures. However, the relative fracture risk is more prominent in T1DM [4], mainly due to the lack of insulin and its anabolic impact on the bone [5]. Bone mineral density (BMD) in T2DM remains unchanged or even elevated, however, it does not protect against osteoporotic fractures. Therefore, the increased fracture risk cannot be solely explained by reduced bone mass but rather points toward additional causes impairing bone quality rather than quantity.

Osteocytes are the most abundant cells in bone tissue and serve to sense and translate the mechanical information during locomotion to primarily control bone turnover mediated via bone remodeling [6, 7] enabling the adaptation of the skeleton to the current needs of the organism while at the same time removing old and damaged parts of the bone to preserve its integrity [8]. During aging and bone pathologies, bone matrix renewal is severely disturbed, hampering the capability of bone tissue to withstand mechanical loads. It is believed that osteocyte viability plays a crucial role in bone maintenance. One confounding factor of osteoporotic bone loss and decreased bone turnover in diabetic bone disease is an elevated osteocyte cell death [9, 10]. Osteocyte death is also seen with postmenopausal and glucocorticoid-induced osteoporosis [11, 12]. Furthermore, diabetic hyperglycemia can directly cause osteocyte death [13–15]. With osteocytes beings entrapped inside lacunae within the mineralized bone matrix, their cell death can lead to a unique micro-mineralization process of lacunar space – micropetrosis. Therefore, a micropetrotic lacuna is a long-lasting evidence of the osteocyte death buildup within the bone tissue. A higher level of osteocyte cell death leads to more extensive lacunar mineralization, seen in aged, osteoporotic, and diabetic bone specimens [14, 16]. Accumulation of mineralized lacunae could negatively affect bone mechanosensitivity and mechanical competence [16–18]. Hence here we present the increased occurrence of micropetrosis in metabolic bone diseases as a potential novel biomarker of altered bone quality. A detailed investigation of lacunar mineralization under pathological conditions and their manifestations could provide a better understanding of where bone fragility originates, which is a crucial step in targeting preventive and therapeutic strategies to overcome complications associated with high bone fragility.

Bone mineralization and its distribution

Bone matrix mineralization or biomineralization is an essential factor in the mechanical competence of the skeleton[19]. During a highly ordered mineralization process, the organic bone matrix is filled with hydroxyapatite nanocrystals [20, 21]. Composition and the distribution of the bone minerals affect material properties such as strength and stiffness of the bone. Biomineralization starts with osteoblasts lining the osteoid, a newly formed bone [22]. Osteoblasts secrete organic components of the extracellular matrix, mainly type I collagen, and are also responsible for hydroxyapatite formation via the expression of tissue-non-specific alkaline phosphatase [23]. Mineralization could be described in two steps. The first one is the formation of the hydroxyapatite crystal inside matrix vesicles, and the second step of hydroxyapatite crystal propagation through the membrane into the extracellular matrix, where it fills the space between collagen fibrils [22]. We can measure bone mineralization with dual-energy X-ray absorptiometry (DXA) and obtain bone mineral density (BMD), a clinical parameter for diagnosing osteoporosis [24]. BMD measured by DXA gives a density measure depending on the amount of bone mass and its mineralization. However, it does not provide any information about the mineralization at the tissue level. Bone mineral density distribution (BMDD) provides information about the degree and heterogeneity of mineralization, which is independent of the input bone mass. Therefore, it provides a specific measure of the mineralization at the tissue level in high spatial resolution [25].

Human bone matrix is structurally arranged in dense cortical bone, providing bone strength, and the spongy trabecular bone, serving as metabolically more active compartment. The hierarchical structure of human bone matrix is composed of bone-specific building elements. On the microscale, the osteon is the basic structural unit of cortical bone. Osteon formation occurs at different time points during the remodeling/modeling events. Therefore, each osteon has a unique arrangement of collagen fibrils and mineralization degree, as the mineral content highly depends on the deposition time [26]. Osteonal bone units are considered younger

tissue compared to the older interstitial regions, which consist of old osteonal fragments and are located between newer osteons. We determined the local BMDD of osteonal and interstitial bone regions and showed significant differences in the mineralization level between younger osteonal and older interstitial tissue. The older interstitial bone presents with a relatively higher mineralized bone matrix than the osteonal bone [27, 28].

Osteocytes as the regulatory cells of bone adaptation

To ensure bone strength and fracture resistance during adulthood, bone matrix must be maintained by continuously removing old and damaged regions via bone resorbing osteoclasts and replacing them with newly formed bone tissue by the action of osteoblasts [8]. During this process of bone remodeling, some osteoblasts will be buried in the bone matrix during bone formation and start their transformation into young osteocytes [29]. The young osteocytes are located close to the bone surface within the osteoid. Osteocytes reside inside enclosed spaces within a bone matrix called lacunae surrounded by a perilacunar matrix. The mineralization of the perilacunar bone matrix gives rise to the mature osteocyte, located more distant from the bone surface and with a reduced number of cytoplasmic organelles [30, 31]. Mature osteocytes are the most abundant bone cells and the master orchestrators of bone remodeling [32].

Osteocyte mechanoregulation involves the sensation and translation of mechanobiological stimuli e. g. from locomotion into biochemical signals to modulate osteoclast and osteoblast activities during bone re/modeling processes [6]. Communication between osteocytes is mediated by the lacuno-canalicular network (LCN). This global network within the mineralized bone matrix is composed of the osteocyte lacunae and nano-canals (canaliculi) through which the osteocytes are interconnected by long cytoplasmic extensions [33]. Through LCN currents, extracellular fluid flow boosting the molecular transport of nutrients, signal molecules, and waste products to keep osteocytes healthy. Osteocyte viability and integrity of its entire LCN are fundamental factors of bone homeostasis and bone quality [7, 34].

The lifespan of osteocytes is proposed to vary from 1 to 50 years, and it can end in one of the cell death mechanisms. There are several mechanisms of cell death possible, those have been reviewed elsewhere. Most frequently, necrotic cell death may occur as an uncontrolled cellular burst, while apoptosis is a programmed mechanism of cell death [35, 36]. Osteocyte apoptosis is essential for initiating bone repair via bone remodeling. Apoptosis of osteocytes can occur at the site of microtrauma where the LCN gets locally disrupted by microdamage/microcracks. Apoptotic osteocytes release RANKL (receptor activator of nuclear factor-kappa B ligand), resulting in osteoclastogenesis and initiation of bone resorption at the damage region [37, 38]. Thereby osteocyte apoptosis is a vital process to maintain normal mineralization levels and to prevent microdamage accumulation within the bone matrix.

Generally, removing cellular debris is necessary to maintain immunological tolerance. If osteoclasts will not resorb the osteocyte cell death affected bone area and macrophages cannot reach the fading osteocytes, the dying cell stays buried inside its lacuna within the mineralized bone tissue. This makes cellular organelle removal difficult, and some parts could remain inside the osteocye lacuna. So far only described in human bone, this process appears to end in the osteocyte lacuna being filled with mineral substance, a unique local mineralization termed micropetrosis [39].

Phenomenon of osteocyte lacunar mineralization

Micropetrosis is a process where the osteocyte lacuna is gradually filled with bone minerals until the lacuna is completely sealed with the mineral content. Frost first described this in 1960 when he identified unstained lacunae in the basic fuchsin bone section, proposed their mineralization, and termed the process "micropetrosis" [16, 17, 39] However, histological staining is not optimal to study lacunar mineralization. Using backscattered electron microscopy, which distinguishes between bone matrix and lacunar mineralization, we presented in 2010 that in the aged skeleton low bone remodeling and micropetrosis coincide [16].

A systematic understanding if osteocyte lacunar mineralization is an active or passive mineralization process is still lacking. However, osteocytes produce crystallization inhibitors (e. g., pyrophosphates or osteopontin) to maintain an unmineralized lacunar cavity[41, 42]. Therefore, it is generally accepted that osteocyte death precedes the lacunar mineralization events. Micropetrotic lacunae have been called "living fossilization" in human bone, and they are observed the presence of apoptotic cellular remnants and globular elements inside mineralized lacunae [43]. These cellular elements could serve as nuclei for spontaneous mineralization processes. Another line of evidence pointing in the same direction is an increased magnesium content within the mineralized lacuna compared to the surrounding mineralized matrix, as magnesium is an essential intracellular ion accumulating during the induction of apoptosis [44], and is also present within the apoptotic bodies and matrix vesicles [45]. Increased magnesium content but also phosphorus and oxygen inside the mineralized lacuna than in the surrounding matrix were confirmed with energy dispersive x-ray spectroscopy (EDX) [18, 40].

Backscatter electron microscopy provides high precision data on mineralization, showing a significantly higher mineral content of the micropetrotic lacuna compared to the adjacent bone matrix [18, 40]. Further investigation of the molecular composition indicates a higher mineral-to-matrix and carbonate-to-phosphate ratios. Mineral-to-matrix ratio characterizes the normalized mineral content to the amount of present collagen [46]. The increased mineral-to-matrix ratio further confirms higher mineral content and a lack of collagen within the mineralized lacunae [18, 40]. The carbonate-to-phosphate represents the amount of carbonate substitution for hydroxyapatite, thus providing information on bone maturation or tissue age. The minerals inside the lacuna are formed earlier than the minerals in the surrounding bone matrix, which under normal mineralization, leads to a lower carbonate-to-phosphate ratio. Therefore, an increased carbonate-to-phosphate ratio suggests different lacunar mineralization from the bone matrix mineralization [18, 40].

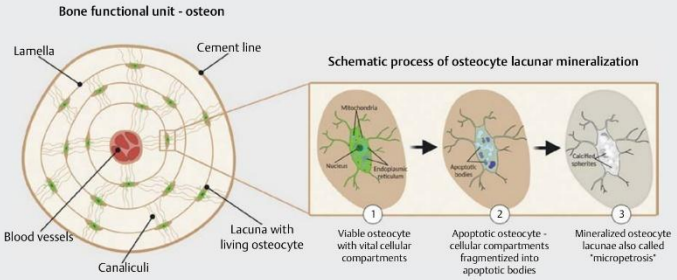

▶ **Fig. 1** Osteocyte cell death preceding osteocyte-lacunar mineralization. The osteon is the basic structural unit of the compact human bone, consisting of individual lamellae and a central Haversian canal with blood vessels. Osteocytes reside within the mineralized bone matrix and maintain bone homeostasis and biomechanical quality. Osteocyte communication is mediated by the lacuno-canalicular network (LCN), an extensive network of nano-canals called canaliculi through which cytoplasmic extensions interconnect individual osteocytes. With aging or bone pathologies (osteoporosis or diabetes mellitus), we observe a higher rate of osteocyte cell death leading to increased osteocyte lacunar mineralization (micropetrosis). 1) Viable osteocytes produce crystallization inhibitors (pyrophosphates) to maintain the lacunar cavity unmineralized. 2) The lacunar mineralization begins with the dying osteocyte as it starts to fragmentize its cellular compartments and releases matrix vesicles and apoptotic bodies. These cellular elements could serve as nuclei for spontaneous mineralization processes and turn into calcified spherites. 3) Finally, lacunar mineralization reaches the stage where the individual mineral spherites fuse and thus completely seal the cavity with mineral.

▶ **Abb. 1** Mikropetrose von Osteozytenlakunen nach dem Zelltod von Osteozyten. Osteone bilden die mikroskopischen Grundstrukturen des kortikalen Knochens. Sie bestehen aus einzelnen Lamellen, die konzentrisch um einen von Blutgefäßen durchzogenen Havers-Kanal angeordnet sind. Osteozyten sind in der mineralisierten Knochenmatrix eingeschlossen und erhalten die Knochenhomöostase und biomechanische Knochenqualität. Die Kommunikation der Osteozyten wird durch das umfassende lakunäre-kanalikuläre Netzwerk ermöglicht. Innerhalb von Nano-Kanälen – den Kanalikuli – befinden sich die zytoplasmatischen Fortsätze der Osteozyten, welche einzelne Zellen miteinander verbinden. Mit fortschreitendem Alter oder Knochenpathologien (Osteoporose oder Diabetes mellitus), kommt es zu einem gehäuften Auftreten von Osteozytenzelltod, welcher die Mineralisierung der Osteozytenlakunen nach sich zieht (Mikropetrose). 1) Vitale Osteozyten produzieren Mineralisationsinhibitoren (Pyrophosphate), um die Mineralisation der Lakunen zu verhindern. 2) Mit dem Zelltod der Osteozyten beginnt auch der Prozess der Mikropetrose und zelluläre Fragmente können als Kristallisationskeime dienen. 3) Zuletzt kommt es zur Fusion einzelner Kristallisationskeime und der Mineralisation von kompletten Osteozytenlakunen.

Detailed morphological analysis of mineralized lacunae revealed two types of calcified nanospherite morphologies that are generally about 120 % harder and 50 % stiffer than the standard bone matrix [40]. With scanning (SEM) and transmission (TEM) electron microscopy, we distinguished two nanospherite shapes i) homogeneous with smooth outlines and ii) nanospherites with protruding needle-like agglomerates [18]. Different morphological characteristics could indicate two different origins for nanospherite formation, possibly from the cellular material (matrix vesicles, organelles, or apoptotic bodies) ▶ **Fig. 1–3** [18].

Micropetrosis is more prominent with increasing age or during pathological conditions like osteoporosis or diabetes mellitus. A higher density of mineralized lacunae within the bone matrix leads to the accumulation of mineral-rich spots making bone more brittle and reducing bone biomechanical competence [16–18]. Furthermore, micropetrotic lacunae create plugs and block bone cell signaling, thereby preventing proper bone maintenance and contributing to impaired bone quality in aged or diseased individuals [47–49].

Mineralization of osteocyte lacunae under pathological conditions

The aging skeleton undergoes pathological changes affecting osteocyte viability. Our previous work showed a decline in osteocyte lacunar density and increasing micropetrosis accumulation in aged human bone [16–18]. Such changes in the functional osteocyte network cause an alteration in osteocyte communication. Functional osteocyte signaling is essential to maintain bone remodeling and its integrity. Moreover, osteocyte lacunae are involved in bone toughening mechanisms. The elliptical lacunae can attract or deflect cracks and therefore allow a stress redistribution which prevents crack propagation and dissipate energy [50, 51]. With increased mineralization of lacunar spaces, the bone protective mechanisms are weakened. Thus, the augmented level of osteocyte cell death with subsequent micropetrosis threatens bone quality and increases its susceptibility to fracture [52–55].

Tissue age plays a role in the localization of mineralized lacunae. When we look at a femoral cross-section, we can distinguish two regions with different tissue ages. The tissue i) lining around the inner surface of the marrow cavity is the endocortical region, and tissue covering ii) the outer bone surfaces is a periosteal region. With aging, the accumulation of mineralized lacunae preferentially occurs in the endocortical region compared to the periosteal region, as we showed in our previous study [16]. The younger tissue age of the entire periosteal region is reasoned due to the apposition of new bone matrix occurring here during aging [56]. Furthermore, the older interstitial bone area is highly mineralized and has a limited supply of nutrients allowing a more frequent formation

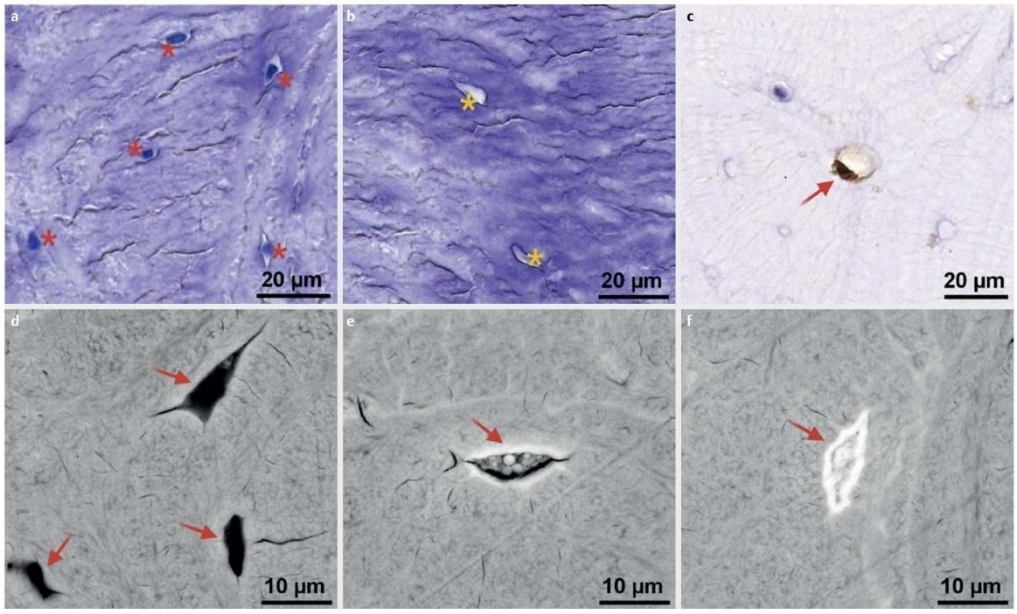

▸ **Fig. 2** Osteocyte lifetime: From a living cell to a fossilized osteocyte. (A) The histological image of toluidine blue stained human cortical bone with viable osteocytes marked by red asterisks. (B) Toluidine blue stained human cortical bone demonstrating empty osteocyte lacune marked by yellow asterisks. (C) Immunohistochemistry of caspase-3 staining showing an osteocyte undergoing apoptosis highlighted by the red arrow. After osteocyte cell death, its lacuna gradually fills with mineral in several stages detectable by electron microscopy. (D) Normally appearing osteocyte lacunas are highlighted by red arrows. (E) Red arrows mark the partially mineralized lacuna with visible individual calcified spherites inside of it. (F) The last stage of micropetrosis is a complete occlusion of lacunae with mineral. The red arrow highlights a fully mineralized lacuna.

▸ **Abb. 2** Der Lebenszyklus von Osteozyten: von der lebenden Zelle zum Fossil. (A) Histologisches Bild von Toluidin Blau gefärbtem kortikalem humanen Knochen mit vitalen Osteozyten (markiert mit roten Sternchen). (B) Toluidin Blau gefärbter humaner kortikaler Knochen mit leeren Osteozyten Lakunen (markiert mit gelben Sternchen). (C) Immunhistochemische Anfärbung von Caspase-3 zur Darstellung von apoptotischen Osteozyten (markiert mit rotem Pfeil). Nach Osteozytenzelltod kommt es zur schrittweisen Mineralisation der Lakune. (D) Rückstreu-Elektronenmikroskopie von humanem kortikalem Knochen mit normalen Osteozytenlakunen (markiert mit roten Pfeilen). (E) Rote Pfeile markieren partiell mineralisierte Lakune in der elektronenmikroskopischen Aufnahme. (F) Die Endstufe der Mikropetrose ist das komplette Ausfüllen der Osteozytenlakunen mit Mineral (markiert mit rotem Pfeil).

of mineralized lacunae here than in the younger osteonal bone area [16, 52]. Understanding the lacunar fate after osteocyte death is particularly interesting because mineralized lacunae could negatively affect bone mechanical properties. Specifically, micropetrotic lacunae create hypermineralized spots within the bone matrix which do not contribute toward toughening mechanisms and increase the bone brittleness [47]. The thereby impaired bone mechanical competence makes bone more vulnerable to low-energy fractures [48].

Some studies showed the increase of mineralized osteocyte lacunae in aged bone [16, 39]. However, only a few studies pay attention to the possible modifications of this phenomenon under pathological conditions like osteoporosis or metabolic diseases. A higher number of micropetrotic osteocyte lacunae in trabecular bone biopsies from osteoporotic (OP) and osteoarthritic (OA) patients was determined compared to numbers in specimens obtained from healthy individuals [57]. The increase in lacunar mineralization was independent of the overall calcium content of the bone specimens as no difference in mineralization level between the OP, OA, and control groups were reported [57]. The higher incidence of micropetrosis in OP and OA patients highlights lacunar mineralization as a novel valuable feature of pathological changes in osteoporotic bone. Denosumab is a commonly used treatment for osteoporotic bone loss. As a monoclonal antibody to the RANKL protein, it prevents the activation of its receptor (RANK) on the surface of osteoclasts and their precursors, inhibiting osteoclasts formation and lowering bone remodeling by reducing bone resorption [58]. We have previously analyzed bone biopsies of patients on denosumab treatment, patients who had discontinued their denosumab treatment without further osteoporosis treatment, and a treatment-naive group [59]. Our results showed a persistently lower osteocyte viability without elevated osteocyte apoptosis level extending into treatment discontinuation if no follow-up osteoporosis drug was given. In addition, we determined higher levels of micropetrosis in the cortical bone of denosumab treated patients, demonstrating the importance of bone remodeling status

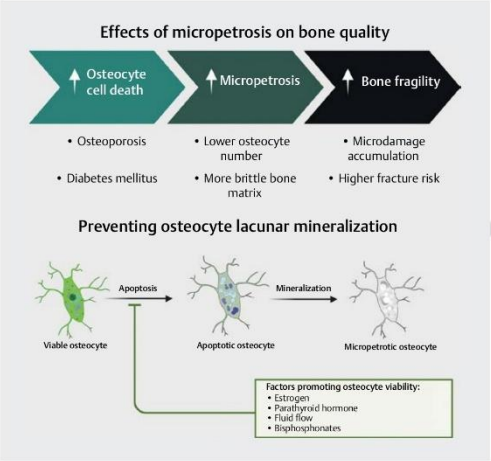

▶ **Fig. 3** Summary of the observed effects of osteocyte death and micropetrosis on bone quality. Metabolic diseases like osteoporosis and diabetes mellitus contribute to increased osteocyte cell death, leading to increased micropetrosis within the bone tissue. Consequently, we observe a decline in osteocyte number and a more brittle bone matrix. These morphological changes in the bone matrix lead to an increased microdamage accumulation and impaired bone quality and contribute to higher bone fragility. Healthy and viable osteocytes are essential for proper bone functionality, and factors like estrogen, parathyroid hormone, or bisphosphonates can prevent osteocyte apoptosis and preserve osteocyte viability.

▶ **Abb. 3** Zusammenfassende Darstellung der Beobachtungen von Osteozytenzelltod und Mikropetrose und deren Einfluss auf die Knochenqualität. Metabolische Erkrankungen wie Osteoporose und Diabetes mellitus tragen zum vermehrten Auftreten von Osteozytenzelltod bei, welcher auch zu Mikropetrose führen kann. Demzufolge beobachteten wir einen Rückgang an vitalen Osteozyten, sowie eine brüchigere Knochenmatrix. Die morphologischen Veränderungen können die Akkumulation von Mikrorissen zur Folge haben. Die dadurch verminderte Knochenqualität kann zu einer erhöhten Knochenfragilität beitragen. Vitale Osteozyten sind für die Funktionalität des Knochens von Bedeutung. Osteozytenzelltod kann durch Faktoren wie Östrogen, Parathormon oder Bisphosphonate verhindert werden.

and more precisely the removal of old bone matrix to maintain bone matrix with viable osteocytes. While bisphosphonates also inhibit osteoclast bone resorption, they simultaneously prevent osteocyte apoptosis and enhance their viability. At the same time, bisphosphonates are analogs to pyrophosphates (mineralization inhibitors) which help to overcome excessive lacunar mineralization and help maintain the fluid flow within the osteocyte network, which has a beneficial effect on bone turnover regulation [60].

Hormonal balance also significantly affects osteocyte viability and, consequently, micropetrotic events. A decrease in parathyroid hormone (PTH) and estrogen levels is connected to a higher presence of mineralized lacunae [61–63]. Moreover, metabolic diseases like diabetes mellitus also burden osteocyte vitality [14, 64, 65]. Insulin is necessary for healthy bone mineralization and development. The increased insulin levels or hyperinsulinemia occur naturally during life periods like puberty or pregnancy as it enables mineral accretion [66, 67] Both type 1 diabetes mellitus (T1DM) and type 2 diabetes mellitus (T2DM) cause chronic hyperglycemia and osteocyte dysfunction [68, 69]. Hyperglycemia harms bone quality directly via the formation of advanced glycation endproducts (AGE) and their receptor RAGE, leading to increased oxidative stress. These matrix changes boost cytokine production and negatively affect the viability of osteoblasts and osteocytes [69–71]. In T2DM, hyperglycemia, together with hyperinsulinemia, could lead to more excessive lacunar mineralization in bone tissue[69]. Furthermore, T2DM is linked to decreased remodeling rate [72, 73], which may contribute to the accumulation of micropetrosis. Both T1M and T2DM are associated with a higher risk of fractures, although for T1DM patients the fracture risk more elevated than in T2DM [4, 68]. The impact of long-term glycemic control on fracture risk differs between patients with T1DM and T2DM as well [74]. While in patients with T1DM is, poor glycemic control identified as a risk factor for fractures, the evidence for T2DM is less convincing [74–76]. Glycemia, or blood sugar level, is a primary indicator of a healthy metabolism, and glucose level directly affects osteocyte functionality. Therefore fluctuations in blood glucose have detrimental effects on osteocytes and reduce their viability [13, 77, 78]. Lower osteocyte viability can lead to higher lacunar mineralization and possibly contribute to the accumulation of micropetrosis. As glycemic control influences more T1DM patients [76], we can assume that poor glycemic control will have a more pronounced impact on micropetrotic events in T1DM than with T2DM. Our latest study on T1DM affected human cortical bone describes an elevated number of mineralized osteocyte lacunae in the T1DM bone specimens solely at the periosteal bone site. Surprisingly we observed an increased number of micropetrotic lacunae within the periosteal osteons in T1DM, which is counter-intuitive with the younger bone tissue being present in osteonal bone. Therefore, we hypothesize that T1DM accelerates cellular aging and leads to the premature death of osteocytes, resulting in a prominent mineralization of osteocyte lacunae, as shown in the periosteal region of T1DM [14]. The cortical BMDD analysis shows comparable values in T1DM and healthy control specimens, as seen in OP and OA [57], where the matrix mineralization was also unchanged between healthy and diseased groups. These data suggest that lacunar mineralization is indeed independent of normal matrix mineralization and could potentially serve as a novel biomarker of altered bone quality in osteoporosis and hormonal/metabolic disorders.

Conclusion

Micropetrosis is a unique process of osteocyte lacunar mineralization that significantly differs from normal bone matrix mineralization in terms of composition and mechanical properties. Since the lacunar occlusion with mineral spherites is incompatible with osteocyte survival, it is considered that osteocyte cell death precedes osteocyte lacunar mineralization. Osteocytes create an extensive communication network through the bone tissue functioning as a backbone of skeletal health because osteocytes oversee the bone tissues adaptive response to mechanical loading. Micropetrosis influences the overall bone quality as the calcified spherites inside

the lacuna create hypermineralized plugs within the osteocyte network, which hamper the fluid flow through the lacuno-canalicular system. The resulting output is altered bone mechanosensitive function, which has been demonstrated to be increased with aging or under pathological conditions. Chronic bone-related diseases such as osteoporosis or diabetic bone disease affect millions of people and represent substantial economic costs for health and social care. The widely used treatments for bone loss predominantly focus on regulating the actions of osteoblasts or osteoclasts and underestimate the potential benefit of focusing pharmacological targets on osteocytes. Further basic and clinical research on the micropetrotic structural consequences is needed to better understand the processes after osteocyte apoptosis in disease conditions to provide novel therapeutic opportunities.

Funding Information

H2020 Marie Skłodowska-Curie Actions – ITN - "FIDELIO"
Deutsche Forschungsgemeinschaft – BU2562/10-1
Deutsche Krebshilfe – HaTRiCs4

Conflict of Interest

The authors declare that they have no conflict of interest.

References

[1] Harvey NC, Curtis EM, Dennison EM et al. The epidemiology of osteoporotic fractures. In: Primer on the Metabolic Bone Diseases and Disorders of Mineral Metabolism. 2018

[2] Cole ZA, Dennison EM, Cooper C. Osteoporosis epidemiology update. Curr Rheumatol Rep 2008; 10: 92–96. doi: 10.1007/s11926-008-0017-6

[3] Hamann C, Kirschner S, Günther KP et al. Bone, sweet bone – Osteoporotic fractures in diabetes mellitus 2012

[4] Vestergaard P. Discrepancies in bone mineral density and fracture risk in patients with type 1 and type 2 diabetes – a meta-analysis. Osteoporos Int 2007; 18: 427–444. doi:10.1007/s00198-006-0253-4

[5] Thrailkill KM, Lumpkin CK, Bunn RC et al. Is insulin an anabolic agent in bone? Dissecting the diabetic bone for clues 2005

[6] Li MCM, Chow SKH, Wong RMY et al. The role of osteocytes-specific molecular mechanism in regulation of mechanotransduction – A systematic review. J Orthop Translat 2021; 29: 1–9. doi:10.1016/J.JOT.2021.04.005

[7] Knothe Tate ML. "Whither flows the fluid in bone?" An osteocyte's perspective. J Biomech 2003; 36: 1409–1424. doi:10.1016/S0021-9290(03)00123-4

[8] Raggatt LJ, Partridge NC. Cellular and Molecular Mechanisms of Bone Remodeling. Journal of Biological Chemistry 2010; 285: 25103–25108. doi:10.1074/jbc.r109.041087

[9] Hygum K, Starup-Linde J, Harsløf T et al. MECHANISMS IN ENDOCRINOLOGY: Diabetes mellitus, a state of low bone turnover – a systematic review and meta-analysis. Eur J Endocrinol 2017; 176: R137–R157. doi:10.1530/eje-16-0652

[10] Bonewald LF. Osteocyte biology: Its implications for osteoporosis. Journal of Musculoskeletal Neuronal Interactions 2004; 4: 101–104

[11] Weinstein RS, Nicholas RW, Manolagas SC. Apoptosis of Osteocytes in Glucocorticoid-Induced Osteonecrosis of the Hip 1. J Clin Endocrinol Metab 2000; 85: doi:10.1210/jcem.85.8.6714

[12] Kennedy CC, Papaioannou A, Adachi JD et al. Glucocorticoid-induced osteoporosis. Women's Health 2006; 2: 65–74. doi:10.2217/17455057.2.1.65

[13] Tanaka KI, Yamaguchi T, Kanazawa I et al. Effects of high glucose and advanced glycation end products on the expressions of sclerostin and RANKL as well as apoptosis in osteocyte-like MLO-Y4-A2 cells. Biochem Biophys Res Commun 2015; 461: 193–199. doi:10.1016/J.BBRC.2015.02.091

[14] Kolibova S, Wölfel EM, Hemmatian H et al. Local microdamage accumulation and impaired osteocyte viability in human cortical bone is linked to type 1 diabetes mellitus. Bone Rep 2022; 16: 101253. doi:10.1016/J.BONR.2022.101253

[15] Parajuli A, Liu C, Li W et al. Bone's responses to mechanical loading are impaired in type 1 diabetes. Bone 2015; 81: 152–160. doi:10.1016/j.bone.2015.07.012

[16] Busse B, Djonic D, Milovanovic P et al. Decrease in the osteocyte lacunar density accompanied by hypermineralized lacunar occlusion reveals failure and delay of remodeling in aged human bone. Aging Cell 2010; 9: 1065–1075. doi:10.1111/j.1474-9726.2010.00633.x

[17] Milovanovic P, Busse B. Phenomenon of osteocyte lacunar mineralization: Indicator of former osteocyte death and a novel marker of impaired bone quality? BioScientifica 2020

[18] Milovanovic P, Zimmermann EA, vom Scheidt A et al. The Formation of Calcified Nanospherites during Micropetrosis Represents a Unique Mineralization Mechanism in Aged Human Bone. Small 2017; 13: 1602215. doi:10.1002/smll.201602215

[19] Currey JD. The relationship between the stiffness and the mineral content of bone. J Biomech 1969; 2: doi:10.1016/0021-9290(69)90023-2

[20] Orimo H. The mechanism of mineralization and the role of alkaline phosphatase in health and disease. Journal of Nippon Medical School 2010; 77: 4–12. doi: 10.1272/jnms.77.4

[21] Murshed M. Mechanism of Bone Mineralization. Cold Spring Harb Perspect Med 2018; 8: a031229. doi:10.1101/cshperspect.a031229

[22] Clarke Anderson H. Matrix Vesicles and Calcification. Curr Rheumatol Rep 2003; 5: 222–226

[23] Blair HC, Larrouture QC, Li Y et al. Osteoblast Differentiation and Bone Matrix Formation In Vivo and In Vitro. doi:10.1089/ten.teb.2016.0454

[24] Blake GM, Fogelman I. The role of DXA bone density scans in the diagnosis and treatment of osteoporosis. Postgrad Med J 2007; 83:

[25] Roschger P, Fratzl P, Eschberger J et al. Validation of quantitative backscattered electron imaging for the measurement of mineral density distribution in human bone biopsies. Bone 1998. doi:10.1016/S8756-3282(98)00112-4

[26] Jäger I, Fratzl P. Mineralized Collagen Fibrils: A Mechanical Model with a Staggered Arrangement of Mineral Particles. Biophys J 2000; 79: 1737–1746. doi:10.1016/S0006-3495(00)76426-5

[27] Bergot C, Wu Y, Jolivet E et al. The degree and distribution of cortical bone mineralization in the human femoral shaft change with age and sex in a microradiographic study. Bone 2009; 45: doi:10.1016/j.bone.2009.05.025

[28] Wu Y, Bergot C, Jolivet E et al. Cortical bone mineralization differences between hip-fractured females and controls. A microradiographic study. Bone 2009; 45: doi:10.1016/j.bone.2009.04.202

[29] Dallas SL, Bonewald LF. Dynamics of the transition from osteoblast to osteocyte. In: Annals of the New York Academy of Sciences. 2010

[30] Jande SS, Belanger LF. The life cycle of the osteocyte. CLINORTHOP 1973; no.94: doi:10.1097/00003086-197307000-00035

[31] Irie K, Ejiri S, Sakakura Y et al. Matrix mineralization as a trigger for osteocyte maturation. Journal of Histochemistry and Cytochemistry 2008; 56: doi:10.1369/jhc.2008.950527

[32] Bonewald LF. The amazing osteocyte. Journal of Bone and Mineral Research 2011; 26: 229–238. doi:10.1002/jbmr.320

[33] Buenzli PR, Sims NA. Quantifying the osteocyte network in the human skeleton. Bone 2015; 75: 144–150. doi:10.1016/J.BONE.2015.02.016

[34] vom Scheidt A, Busse B. Characteristics of the osteocyte network in healthy and diseased human bone. Osteologie 2016; 25: doi:10.1055/s-0037-1619006

[35] Fink SL, Cookson BT. Apoptosis, pyroptosis, and necrosis: Mechanistic description of dead and dying eukaryotic cells. Infect Immun 2005; 73:

[36] Farber E. Programmed cell death: necrosis versus apoptosis. Mod Pathol 1994; 7: 605–609

[37] Plotkin LI. SKELETAL BIOLOGY AND REGULATION (MR FORWOOD AND A ROBLING, SECTION EDITORS) Apoptotic Osteocytes and the Control of Targeted Bone Resorption. doi:10.1007/s11914-014-0194-3

[38] Ru J-Y, Wang Y-F. Osteocyte apoptosis: the roles and key molecular mechanisms in resorption-related bone diseases. doi:10.1038/s41419-020-03059-8

[39] FROST HM. In vivo osteocyte death. J Bone Joint Surg Am 1960; 42 A: doi:10.2106/00004623-196042010-00011

[40] You L-D, Weinbaum S, Cowin SC et al. Ultrastructure of the Osteocyte Process and its Pericellular Matrix 2004. doi:10.1002/ar.a.20050

[41] Thompson WR, Modla S, Grindel BJ et al. Perlecan/Hspg2 Deficiency Alters the Pericellular Space of the Lacunocanalicular System Surrounding Osteocytic Processes in Cortical Bone. doi:10.1002/jbmr.236

[42] Bell LS, Kayser M, Jones C. The mineralized osteocyte: A living fossil. Am J Phys Anthropol 2008; 137: doi:10.1002/ajpa.20886

[43] Trapani V, Mastrototaro L, Wolf FI. Magnesium and the yin-yang interplay in apoptosis. In: Magnesium in the Central Nervous System. 2011

[44] Reynolds JL, Joannides AJ, Skepper JN et al. Human Vascular Smooth Muscle Cells Undergo Vesicle-Mediated Calcification in Response to Changes in Extracellular Calcium and Phosphate Concentrations: A Potential Mechanism for Accelerated Vascular Calcification in ESRD 2004. doi:10.1097/01.ASN.0000141960.01035.28

[45] Shah FA, Lee BEJ, Tedesco J et al. Micrometer-Sized Magnesium Whitlockite Crystals in Micropetrosis of Bisphosphonate-Exposed Human Alveolar Bone. Nano Lett 2017; 17: doi:10.1021/acs.nanolett.7b02888

[46] Paschalis EP, Dicarlo E, Betts F et al. Calcified FTIR Microspectroscopic Analysis of Human Osteonal. Bone 1996

[47] Jee WSS. Integrated bone tissue physiology: Anatomy and physiology. In: Bone Mechanics Handbook, Second Edition. 2001

[48] Boyce TM, Bloebaum RD. Cortical aging differences and fracture implications for the human femoral neck. Bone 1993; 14: doi:10.1016/8756-3282(93)90209-S

[49] Zimmermann EA, Busse B, Ritchie RO. The fracture mechanics of human bone: influence of disease and treatment. Bonekey Rep 2015; 4: doi:10.1038/bonekey.2015.112

[50] Zimmermann EA, Schaible E, Bale H et al. Age-related changes in the plasticity and toughness of human cortical bone at multiple length scales. Proc Natl Acad Sci U S A 2011; 108: doi:10.1073/pnas.1107966108

[51] Yin D, Chen B, Lin S. Finite element analysis on multi-toughening mechanism of microstructure of osteon. J Mech Behav Biomed Mater 2021; 117: doi:10.1016/j.jmbbm.2021.104408

[52] Milovanovic P, Zimmermann EA, Riedel C et al. Multi-level characterization of human femoral cortices and their underlying osteocyte network reveal trends in quality of young, aged, osteoporotic and antiresorptive-treated bone. Biomaterials 2015. doi:10.1016/j.biomaterials.2014.12.024

[53] Busse B, Bale HA, Zimmermann EA et al. Vitamin D deficiency induces early signs of aging in human bone, increasing the risk of fracture. Sci Transl Med 2013; 5: doi:10.1126/scitranslmed.3006286

[54] Rolvien T, Milovanovic P, Schmidt FN et al. Long-Term Immobilization in Elderly Females Causes a Specific Pattern of Cortical Bone and Osteocyte Deterioration Different From Postmenopausal Osteoporosis 2020. doi:10.1002/jbmr.3970

[55] Milovanovic P, Zimmermann EA, Hahn M et al. Osteocytic Canalicular Networks: Morphological Implications for Altered Mechanosensitivity. ACS Nano 2013; 7: 7542–7551. doi:10.1021/nn401360u

[56] Seeman E, Delmas PD. Bone Quality – The Material and Structural Basis of Bone Strength and Fragility. New England Journal of Medicine 2006; 354: doi:10.1056/nejmra053077

[57] Carpentier VT, Wong J, Yeap Y et al. Increased proportion of hypermineralized osteocyte lacunae in osteoporotic and osteoarthritic human trabecular bone: Implications for bone remodeling. Bone 2012; 50: doi:10.1016/j.bone.2011.11.021

[58] Reid IR, Miller PD, Brown JP et al. Effects of denosumab on bone histomorphometry: The FREEDOM and STAND studies. Journal of Bone and Mineral Research 2010; 25: doi:10.1002/jbmr.149

[59] Jahn-Rickert K, Wolfel EM, Jobke B et al. Elevated Bone Hardness Under Denosumab Treatment, With Persisting Lower Osteocyte Viability During Discontinuation. Front Endocrinol (Lausanne) 2020; 11: 250. doi:10.3389/fendo.2020.00250

[60] Bellido T, Plotkin LI. Novel actions of bisphosphonates in bone: Preservation of osteoblast and osteocyte viability. Bone 2011; 49: 50–55. doi:10.1016/j.bone.2010.08.008

[61] Yajima A, Inaba M, Tominaga Y et al. Increased osteocyte death and mineralization inside bone after parathyroidectomy in patients with secondary hyperparathyroidism. Journal of Bone and Mineral Research 2010; 25: doi:10.1002/jbmr.126

[62] Yajima A, Tsuchiya K, Burr DB et al. Micropetrosis in hemodialysis patients. Bone Rep 2021; 15: doi:10.1016/j.bonr.2021.101150

[63] Tomkinson A, Reeve J, Shaw RW et al. The Death of Osteocytes via Apoptosis Accompanies Estrogen Withdrawal in Human Bone * . J Clin Endocrinol Metab 1997; 82: doi:10.1210/jcem.82.9.4200

[64] Maycas M, McAndrews KA, Sato AY et al. PTHrP-Derived Peptides Restore Bone Mass and Strength in Diabetic Mice: Additive Effect of Mechanical Loading. J Bone Miner Res 2017; 32: 486–497. doi:10.1002/jbmr.3007

[65] Portal-Núñez S, Lozano D, Fernández De Castro L et al. Alterations of the Wnt/b-catenin pathway and its target genesfor the N- and C-terminal domains of parathyroid hormone-related proteinin bone from diabetic mice. FEBS Lett 2010; 584: 3095–3100. doi:10.1016/j.febslet.2010.05.047

[66] Sonagra AD. Normal Pregnancy- A State of Insulin Resistance. JOURNAL OF CLINICAL AND DIAGNOSTIC RESEARCH 2014. doi:10.7860/jcdr/2014/10068.5081

[67] Goran MI, Gower BA. Longitudinal Study on Pubertal Insulin Resistance. Diabetes 2001; 50: doi:10.2337/diabetes.50.11.2444

[68] Napoli N, Chandran M, Pierroz DD et al. Mechanisms of diabetes mellitus-induced bone fragility 2017

[69] Cooper ID, Brookler KH, Crofts CAP. Rethinking fragility fractures in type 2 diabetes: The link between hyperinsulinaemia and osteofragilitas. Biomedicines 2021; 9: 1165. doi: 10.3390/biomedicines9091165

[70] King GL, Loeken MR. Hyperglycemia-induced oxidative stress in diabetic complications. Histochem Cell Biol 2004; 122: 333–338. doi:10.1007/s00418-004-0678-9

[71] Giacco F, Brownlee M. Oxidative Stress and Diabetic Complications. Circ Res 2010; 107: 1058–1070. doi:10.1161/CIRCRESAHA.110.223545

[72] Gaudio A, Privitera F, Battaglia K et al. Sclerostin levels associated with inhibition of the Wnt/β-catenin signaling and reduced bone turnover in type 2 diabetes mellitus. Journal of Clinical Endocrinology and Metabolism 2012; 97: doi:10.1210/jc.2012-1901

[73] Sassi F, Buondonno I, Luppi C et al. Type 2 diabetes affects bone cells precursors and bone turnover. BMC Endocr Disord 2018; 18: doi:10.1186/s12902-018-0283-x

[74] Vavanikunnel J, Charlier S, Becker C et al. Association between glycemic control and risk of fracture in diabetic patients: A nested case-control study. Journal of Clinical Endocrinology and Metabolism 2019; 104: doi:10.1210/jc.2018-01879

[75] Charlier S, Vavanikunnel J, Becker C et al. Antidiabetic Treatment, Level of Glycemic Control, and Risk of Fracture in Type 2 Diabetes: a Nested, Case-Control Study. J Clin Endocrinol Metab 2021; 106: 554–566. doi:10.1210/clinem/dgaa796

[76] Leanza G, Maddaloni E, Pitocco D et al. Risk factors for fragility fractures in type 1 diabetes. Bone 2019; 125: 194–199. doi:10.1016/j.bone.2019.04.017

[77] Wang Y, Han B, Ding J et al. Endoplasmic reticulum stress mediates osteocyte death under oxygen-glucose deprivation in vitro. Acta Histochem 2020; 122: doi:10.1016/j.acthis.2020.151577

[78] Pacicca DM, Brown T, Watkins D et al. Elevated glucose acts directly on osteocytes to increase sclerostin expression in diabetes. Sci Rep 2019; 9: doi:10.1038/s41598-019-52224-3

Bone 165 (2022) 116546

Contents lists available at ScienceDirect

Bone

journal homepage: www.elsevier.com/locate/bone

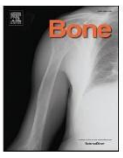

Full Length Article

Human tibial cortical bone with high porosity in type 2 diabetes mellitus is accompanied by distinctive bone material properties

Eva M. Wölfel [a], Imke A.K. Fiedler [a,b], Sofie Dragoun Kolibova [a], Johannes Krug [a], Mei-Chun Lin [a], Bashar Yazigi [a], Anna K. Siebels [a], Herbert Mushumba [c], Birgit Wulff [c], Benjamin Ondruschka [c], Klaus Püschel [c], Claus C. Glüer [d], Katharina Jähn-Rickert [a,e], Björn Busse [a,b,*]

[a] Department of Osteology and Biomechanics, University Medical Center Hamburg-Eppendorf, 22529 Hamburg, Germany
[b] Interdisciplinary Competence Center for Interface Research (ICCIR), University Medical Center Hamburg-Eppendorf, 22529 Hamburg, Germany
[c] Institute of Legal Medicine, University Medical Center Hamburg-Eppendorf, 22529 Hamburg, Germany
[d] Sektion Biomedizinische Bildgebung, Klinik für Radiologie und Neuroradiologie, Universitätsklinikum Schleswig-Holstein, Campus Kiel, Christian-Albrechts-Universitat zu Kiel, MOIN CC, 24118 Kiel, Germany
[e] Mildred Scheel Cancer Career Center Hamburg, University Cancer Center Hamburg, University Medical Center Hamburg Eppendorf, 20251 Hamburg, Germany

ARTICLE INFO

Keywords:
Diabetic bone disease
Cortical bone
Tibia
Impact indentation
Advanced glycation end products

ABSTRACT

Diabetes mellitus is a metabolic disease affecting bone tissue at different length-scales. Higher fracture risk in diabetic patients is difficult to detect with common clinical fracture risk assessment due to normal or high bone mineral density in diabetic patients. The observed higher fracture risk despite normal to high areal bone mineral density in diabetic patients points towards impaired bone material quality. Here, we analyze tibial bone from individuals with type 2 diabetes mellitus using a multiscale-approach, which includes clinical and laboratory-based bone quality measures.

Tibial cortical bone tissue from individuals with type 2 diabetes mellitus (T2DM) and age-matched healthy controls (n = 15 each) was analyzed with *in situ* impact indentation, dual energy X-ray absorptiometry (DXA), high resolution peripheral microcomputed tomography (HR-pQCT), micro-computed tomography (microCT), cyclic indentation, quantitative backscattered electron microscopy (qBEI), vibrational spectroscopy (Raman), nanoindentation, and fluorescence spectroscopy. With this approach, a high cortical porosity subgroup of individuals with T2DM was discriminated from two study groups: individuals with T2DM and individuals without T2DM, while both groups were associated with similar cortical porosity quantified by means of microCT.

The high porosity T2DM group, but not the T2DM group, showed compromised bone quality expressed by altered cyclic indentation properties (transversal direction) in combination with a higher carbonate-to-amide I ratio in endocortical bone. In addition, in the T2DM group with high cortical porosity group, greater cortical pore diameter was identified with HR-pQCT and lower tissue mineral density using microCT, both compared to T2DM group. Micromechanical analyses of cross-sectioned osteons (longitudinal direction) with cyclic indentation, qBEI, and nanoindentation showed no differences between the three groups.

High tibial cortical porosity in T2DM can be linked to locally altered bone material composition. As the tibia is an accessible skeletal site for fracture risk assessment in the clinics (CT, indentation), our findings may contribute to further understanding the site-specific structural and compositional factors forming the basis of bone quality in diabetes mellitus. Refined diagnostic strategies are needed for a comprehensive fracture risk assessment in diabetic bone disease.

1. Introduction

Diabetes mellitus is a metabolic disease occurring in about 19.3 % of the adult population (prevalence of diabetes, 65–99 years) with increasing prevalence leading to major health and economic burdens worldwide [1,2]. Despite presenting with normal to high areal bone

* Corresponding author at: Lottestr. 55A, 22529 Hamburg, Germany.
E-mail address: b.busse@uke.uni-hamburg.de (B. Busse).

https://doi.org/10.1016/j.bone.2022.116546
Received 1 May 2022; Received in revised form 9 September 2022; Accepted 11 September 2022
Available online 14 September 2022

9.3. Publication 3: Human tibial cortical bone with high porosity in type 2 diabetes mellitus is accompanied by distinctive bone material properties

mineral density (aBMD), diabetic patients experience an increased fracture risk [3]. As such detecting diabetes patients at increased fracture risk is challenging with common clinical tools, such as dual energy X-Ray absorptiometry (DXA) and high resolution peripheral quantitative computed tomography (HR-pQCT). In addition to the geometry, microstructure, and mineralization further bone quality factors are likely to contribute to the underlying mechanisms impairing diabetic bone [4,5].

The tibia is one preferred peripheral skeletal site for clinical assessment of fracture risk when using HR-pQCT in combination with areal bone mineral density (aBMD) measurements in the spine or hip using DXA. Additionally, the bone material strength index (BMSi) can be assessed by impact indentation of the tibial mid-diaphysis *in vivo* to explore if compositional matrix changes occur in diabetes mellitus [6]. Therefore, we set out to investigate how diabetes mellitus influences tibial bone properties by combining clinical imaging modalities available for fracture risk assessments (HR-pQCT, *in situ* impact indentation) with a multiscale characterization including structural and compositional properties in a laboratory setting [4]. The experimental assessment of bone quality factors in different skeletal sites is important as loading conditions differ in the skeleton, polyostotic heterogeneity exists across the human skeleton [7], and most importantly not all skeletal sites can be accessed *in vivo* with clinical imaging modalities. However, impact indentation has been developed to be used in a clinical setting to assess biomechanical properties of bone tissue with a hand-held device on the patients' tibial bone surface. With a single-use tip the tibial cortical bone surface in the anterior-medial quadrant of the mid-diaphysis is indented and provides the bone material strength index (BMSi) as output parameter [8,9]. The technique is based on the reference point indentation technology, where a reference probe surrounds the test probe and is used to mechanically characterize bone tissue [10].

The tibial bone microstructure in patients with type 2 diabetes mellitus (T2DM) has been shown to consist of a preserved trabecular microstructure. However, subgroups with exceptionally high cortical porosity in T2DM have been reported and high cortical porosity in T2DM may form the basis for increased bone fragility with T2DM [11–13]. Patsch et al., reported higher cortical porosity in T2DM patients with fractures compared to T2DM patients without fractures, while the porosity was not significantly different compared to non-diabetic patients with and without fractures [11]. Another study reported higher cortical porosity in the femoral subtrochanteric region in T2DM patients with fractures in comparison to T2DM patients without fractures, while the cortical porosity in the T2DM patients without fractures was lower compared to non-diabetic patients with fracture [14]. These studies support the notion that a specific sub-group of diabetes patients exhibits higher cortical porosity. This high-porosity subgroup in T2DM is challenging to identify with special regard to the discrimination from non-diabetic patients with porosity. Thus, questions about the cause of fracture susceptibility remain unanswered, as higher fracture risk has been reported for diabetes patients in comparison to healthy individuals with similar T-scores [15].

While impact indentation may reflect a combination of structural and compositional changes, BMSi values were reported to be lower in patients with fractures in comparison to patients without fractures – these findings were independent from aBMD [16]. However, studies on patients with T2DM have resulted in inconsistent data, varying from lower to unchanged BMSi in patients with T2DM compared to non-diabetics [6,17,19]. Thus, we hypothesize that higher fracture risk in T2DM patients cannot be solely explained by higher cortical porosity, but that other factors may play a role, which can't be directly assessed with clinical imaging and impact indentation [5,20].

In lab-based experiments, samples from patients with T2DM showed a changed mineralization pattern. Here, a higher average calcium content with lower mineral heterogeneity [21] and a higher mineral-to-matrix ratio along with unchanged collagen maturity was shown [22]. In both studies, samples from patients undergoing total hip replacement arthroplasty were analyzed suggesting osteoarthritis as comorbidity potentially affecting bone quality. Higher advanced glycation end-product (AGEs) accumulation has been suggested to impair bone material properties through their formation by glycation of proteins [5,22–24].

Pentosidine, a fluorescent AGE that may form cross-links between two collagen fibrils and thereby links neighboring fibrils, has been described as a potential contributor to bone fragility [25]. Further on, the non-crosslinking AGE carboxymethyl-lysine (CML) has been shown to be associated with increased fracture risk in diabetic patients [26] and its higher accumulation has been presented in femoral cortical bone from individuals with T2DM independent of the level of porosity in the cortex [24]. A tendency towards higher fAGE accumulation in cortical bone from the femoral neck [23] and significantly higher fAGE content in trabecular bone from the femoral head [27] were reported in individuals with T2DM.

Currently, data on the diabetic bone disease is based on both the clinical and the basic research perspective, while the translation and correlation of both is still incomplete and requires further analysis of skeletal sites that are accessible *in vivo*. Therefore, our study aimed to analyze tibial bone from the mid-diaphysis in order to combine clinical techniques in an *ex vivo* setup with a thorough investigation of bone material quality parameters in a lab setting. In this context, high-resolution imaging, spectroscopic, and biomechanical testing are carried out to elucidate bone matrix properties in tibial type 2 diabetes mellitus bone tissue. With this translational approach, we access the hierarchical structure of bone from the macroscopic to the microscopic level, while the correlation to clinical accessible data will allow us to deconstruct to what extent orientation-dependent changes at the tissue level are adequately reflected at the clinical accessible level. We hypothesize that both experimental and clinical testing set-ups result in material properties that do not only reflect bone quality indices in relation to disease conditions but also reflect site-specific orientation characteristics (*i.e.*, in clinical impact indentation the outer surface of the bone perpendicular to longitudinal osteons are tested (transversal direction), whereas in laboratory settings oftentimes cross-sectioned bone specimen are tested (longitudinal direction)). Our secondary hypothesis is that diabetes-specific tissue properties affect tibial biomechanical properties in T2DM, which are caused by locally altered matrix composition and pronounced cortical porosity in T2DM.

2. Materials and methods

2.1. Study design

During autopsy at the Institute of Legal Medicine (University Medical Center Hamburg-Eppendorf), 30 tibial samples of the mid-diaphysis as well as the 12th thoracic and adjacent vertebrae were obtained (WT037/15). Approximately 10 cm from the tibia were extracted from 15 healthy control cases without diabetes mellitus (3 females, 12 males; 73.67 ± 6.84 years) which were selected based on the absence of any bone-related diseases such as Paget's disease, renal or hepatic disorders, hyperparathyroidism, and bedrest. The same sample length was obtained from 15 individuals with diagnosed type 2 diabetes mellitus (T2DM; 6 females, 9 males; 76.8 ± 6.45 years). Samples were selected to be age-matched. Using micro-computed tomography (microCT) on the anterior-medial quadrant with a resolution of 10 μm, five T2DM cases were identified as high cortical porosity cases shown by a cortical porosity of above 20 % [24]. As such the T2DM group was sub-divided into a T2DM with similar porosity to the control group (4 females, 6 males; 77.2 ± 5.5 years) and a high cortical porosity subgroup named T2DMwHP based on a cortical porosity of above 20 % measured with micro-computed tomography (2 females, 3 males; 76 ± 8.7 years).

2.2. *In situ* impact indentation

In situ impact indentation was performed using the OsteoProbe® device (Active Life Scientific, Inc. USA). *Via* the hand-held indentation device, the mid-diaphysis of the tibia was indented according to the described protocol [9,28], prior to sample extraction (Fig. 1). Therefore, the leg was rotated slightly to the lateral side so that the anterior-medial side of the tibia was superior. By this approach, the tibia was indented in a transversal direction (perpendicular indentation to osteons aligned from proximal to distal). When the probe of the device penetrated the soft tissue, the probe was directed perpendicular on the tibial bone. A minimum of 10 indentations were performed, each with approximately 1 mm distance to the other. Following indentation of the tibia, the system was calibrated by 10 indentations on a polymethylmethacrylate block. Based on the software provided by the manufacturer, the bone material strength index (BMSi) was calculated.

2.3. Dual-energy X-ray absorptiometry

Following extraction, the samples were wrapped in phosphate-buffered saline (PBS) soaked gauze and stored at −20 °C until further analysis. De-identified data of the individuals were collected and included age, sex, weight, height, diabetes mellitus status, and if available diabetes mellitus treatment. Dual energy X-ray absorptiometry (GE Healthcare, GER) was applied on the frozen 12th thoracic vertebra to determine aBMD of each donor using an *ex vivo* protocol. Generally, DXA is applied to calculate the T-score according to the World Health Organization based on the lumbar spine. To compensate for missing soft tissue, a water phantom provided by the manufacturer was used producing a water column of 15 cm simulating the thickness of soft tissue of a person with body weight of 70 kg and height of 170 cm. The vertebrae were positioned in a plastic container filled with water and the water phantom was placed on top as reported previously [29]. With the software provided by the manufacturer, aBMD values from anterior-posterior (AP) and lateral (LAT) scan directions were obtained.

2.4. High-resolution peripheral quantitative computed tomography

The extracted, frozen mid-diaphyseal tibia samples were scanned in a HR-pQCT system (Xtreme CT I, Scanco, Medical AG, Switzerland; Fig. 1). Soft tissue was removed from the bone tissue and individual samples were placed in the sample holder and inserted into the gantry of

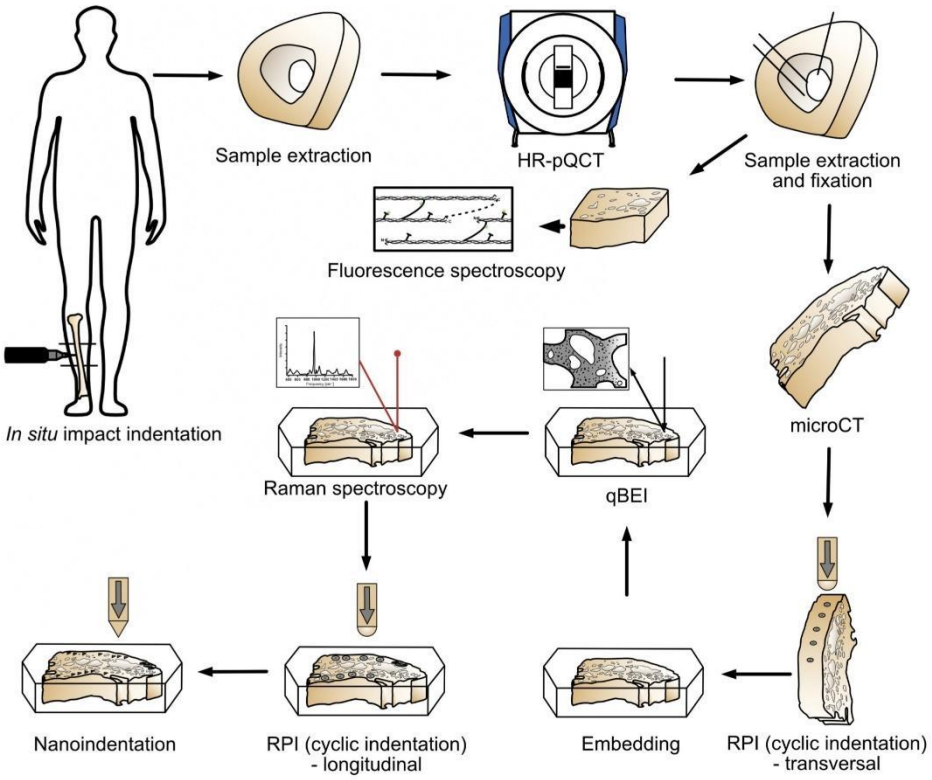

Fig. 1. Schematic overview of the experimental procedures testing tibial cortical bone tissue. Prior to extraction, *in situ* impact indentation was performed on the mid-diaphysis of the tibia. Approximately 10 cm of the mid-diaphysis of the tibia was extracted and scanned using HR-pQCT. Following scanning, a part of the anterior-medial quadrant was extracted, fixated, and scanned using microCT imaging. Next to the anterior-medial quadrant a smaller bone cube was removed for fAGE analysis using fluorescence spectroscopy. The anterior-medial quadrant was indented using RPI (cyclic indentation) in transversal direction and subsequently embedded. Following embedding, qBEI and Raman spectroscopy were performed on the cross-section in longitudinal direction for compositional analysis, while RPI (cyclic indentation) in longitudinal direction as well as nanoindentation was performed to assess biomechanical properties.

the system. Weekly and monthly calibration was performed using the manufacturer's calibration phantoms for quality control. The frozen tibial samples were placed into an *ex vivo* sample holder provided by the manufacturer and 12 mm of the middle were scanned to avoid inclusion of regions with extraction artefacts. A resolution of 82 μm was applied with 750 projections over 180° and an integration time of 100 ms at each angular position.

Following reconstruction, images were analyzed with the software provided by the manufacturer according to previously published protocols by Burghardt and colleagues [30] where a fixed global threshold was applied (40 % of the maximum possible greyscale value). In detail, the peripheral cortical bone structure was contoured, followed by analysis with the standard evaluation routine provided by the manufacturer. Then, the endocortical contour (automatically drawn with the standard evaluation routine) was inspected visually. If required, the endocortical contour was manually corrected and the standard evaluation routine was re-run. The final evaluation program calculated the following cortical parameters; cortical volumetric bone mineral density (Ct.vBMD, mg HA/cm^3), cortical porosity (Ct.Po, %), cortical thickness (Ct.Th, mm), cortical pore diameter (Ct.Po.Dm, mm), cortical perimeter (Ct.Pm, mm), cortical area (Ct.Ar, mm^2), and total area (Tt.Ar, mm^2).

2.5. Micro-computed tomography

Following HR-pQCT analysis, the anterior-medial quadrant of the tibial cross-section was extracted using a diamond belt saw (EXAKT Advanced Technologies GmbH, Germany) and fixated in 4 % buffered paraformaldehyde for a week. After fixation the bone quadrants were washed with PBS and transferred into 70 % ethanol. For microstructural analysis, the quadrants were scanned using a desktop micro-computed tomography (microCT) system (μCT40, SCANCO, Medical AG, Switzerland; Fig. 1). Therefore, the samples were placed in a sample holder and fixed with sponges to avoid movement during scanning. The bone quadrants were scanned with 10 μm isometric voxel size resolution, 55 kV, 145 μA, and 200 ms integration time. For each bone sample 400 slices were scanned, and the central 300 slices were evaluated.

Following reconstruction of the images, the region of interest was selected by excluding the sawing region of the samples to avoid inclusion of sawing artefacts in the analysis. The evaluation was performed by applying a threshold of 550 mg HA/cm^3 using the evaluation program provided by the manufacturer. Based on this cortical porosity (Ct. Po, %) and tissue mineral density (TMD, mg HA/cm^3) were determined. Cortical pore diameter (Ct.Po.Dm) was evaluated per slice in 2D using XamFlow software (Lucid Concept AG, Zurich, Switzerland) applying the model-independent sphere fitting method [31].

2.6. Reference point indentation

Following micro-CT analysis, the fixed bone quadrant was indented in transversal direction (Fig. 1) using the reference point indentation system BioDent™ (Active Life Scientific, Inc. USA). A semi-sharp reference probe (BP2) was used. The bone sample was fixed in a sample holder, so that the indentation was performed in transversal direction of the bone quadrant (Fig. 1). For each bone sample, seven randomly chosen indents were performed with 10 indentation cycles, an indentation frequency of 2 Hz and an applied force of 6 N. Prior to every indentation the system was calibrated on polymethylmethacrylate blocks. The force-displacement curves of each indent were visualized and based on these the following parameters were determined; first cycle indentation distance (ID 1st, μm), total indentation distance (TID, μm), first cycle creep indentation distance (CID, μm), indentation distance increase (IDI, μm), average creep indentation distance (AvgCID, μm), and average loading slope (AvgLS, N/μm).

For subsequent analysis, the bone quadrants were dehydrated and embedded in methylmethacrylate (Fig. 1). Following embedding the samples were indented again in longitudinal direction of the cortical bone sample (Fig. 1) as typically performed in a lab-based setup to allow for comparison of the different sample conditions. Here, two regions of interest were differentiated: (i) the endocortical region close to the bone marrow and (ii) the periosteal region close to the periost. In each region at least three indentations were performed.

2.7. Quantitative backscattered electron imaging

Quantitative backscattered electron imaging (qBEI) was performed on embedded, co-planar, and polished bone quadrants (Fig. 1). The samples were sputtered with carbon and imaging was performed in a scanning electron microscope (Zeiss crossbeam 340, Carl Zeiss AG, Germany) using a backscattered electron detector. By applying a constant working distance of 20 mm, a voltage of 20 kV, a constant beam current which is checked using a Faraday cup, and calibration with aluminum and carbon standard, grey scale images are obtained. For each region, endocortical and periosteal regions, five images were acquired and analyzed using a custom-made Matlab script routine (MATLAB, R2019b, MathWorks Inc.). Based on the obtained bone mineral density distribution the following parameter were determined; the average calcium concentration (CaMean, wt%), the most frequent calcium concentration (CaPeak, wt%), the mineralization heterogeneity which is based on the standard deviation of the bone mineral density distribution curve (CaWidth, wt%), and the percentage of bone area with low (CaLow, % bone area) and high (CaHigh, % bone area) mineralized bone packets.

2.8. Raman spectroscopy

To decipher changes in the matrix composition of bone obtained from individuals with diabetes mellitus, Raman spectroscopy was performed (Fig. 1) using a Raman spectrometer (Renishaw inVia, Renishaw, UK) and the provided software WiRE (WiRE 4.1, Renishaw, UK). Embedded, co-planar and polished samples were used to obtain one spectral map of 500 μm × 200 μm in each region (endocortical and periosteal) with a step size of 50 μm, 5 ms acquisition time, and 10 acquisitions. Following the measurements, data was post-processed with baselined correction using a polynomial intelligent fitting tool. By determining integrated peak areas and calculating ratios of the respective peaks, the mineral-to-matrix ratio (phosphate peak divided by the amide I peak), the carbonate-to-phosphate ratio (carbonate peak divided by the phosphate peak), the carbonate-to-amide I ratio (carbonate peak divided by the amide I peak), and the crystallinity (the reciprocal of the full width at half maximum of the phosphate band according to previously established protocols [32–34]) were calculated for each spectrum and averaged for each sample.

2.9. Nanoindentation

Nanoindentation was performed in longitudinal osteonal direction in endocortical and periosteal region (Fig. 1). Therefore, the embedded bone sample was polished using 3 μm and 1 μm diamond suspension, and 0.5 μm aluminum oxide suspension followed by ultrasonically cleaning in distilled water. Using a Berkovich diamond tip in an iMicro nanoindenter (KLA instruments, CA, USA), 30 indentations per region with 30 μm distance between each indent were obtained using depth-sensing continuous stiffness mode and a final depth of 2000 nm. Based on the method by Oliver and Pharr [35] and by applying a Poison's ratio of 0.3, the hardness and the Young's modulus were determined for 8 controls, 8 T2DM, and 5 T2DMwHP samples. Prior and following each measurement calibration of the tip was performed on fused silica.

2.10. Fluorescence spectroscopy and colorimetric assay

Total fluorescent AGEs (fAGEs) were quantified using fluorescence spectroscopy and normalized to collagen content assessed by

colorimetric assay (Fig. 1) [36]. Unfixed frozen tibial bone samples next to the anterior-medial quadrant of the mid-diaphyseal tibia cross-section were defatted by alternate soaking for 15 min in either 70 % ethanol or saline. After 18 h of lyophilization, the bone samples were hydrolyzed in 6 M HCl (10 µl of HCl per mg of bone) at 110 °C for 16 h. Bone hydrolysates were diluted in deionized water to a final concentration of 0.5 mg bone/ml and centrifuged at 13,000 rpm at 4 °C. The collected supernatant was used for the rest of the assay. To determine the total collagen content of bone, a colorimetric assay of hydroxyproline was performed using hydroxyproline standards (stock solution 2 mg/ml hydroxyproline in 0.001 N HCl). First, chloramine-T (0,06 M chloramine-T in a solution of deionized water, 2-metoxyethanol and hydroxyproline buffer in 2:3:5, respectively) was added to the bone hydrolysates and standards in a 1:2 ratio following incubation in the dark at room temperature (RT) for 20 min to oxidize hydroxyproline. The reaction was stopped by adding 4,5 M perchloric acid for 5 min at room temperature in the dark. Finally, *p*-dimethylaminobenzaldehyde (200 mg/ml in 2-metoxyethanol) was added, and the samples and standards were incubated at 60 °C for 20 min to produce a chromophore.

After cooling down for 5 min at room temperature, the absorbance of bone hydrolysates and hydroxyproline standards was measured at a wavelength of 570 nm in a 96-well plate using a multi-mode microplate reader (Inifinite® 200, Tecan Group Ltd., Männedorf, CH). For the fluorescence assay, serially diluted quinine standards (stock solution 10 µg quinine per ml of 0.1 N H_2SO_4) and hydrolysates of bone were measured in a 96-well plate using the multi-mode microplate reader at excitation of 360 nm and emission of 460 nm. All experiments were performed in darkness at room temperature. The collagen content is derived from prior knowledge that collagen consists of 14 % hydroxyproline [37]. The total fAGEs are presented in ng quinine fluorescence/mg collagen content.

2.11. Statistical analysis

Statistical analysis was performed using GraphPad Prism (Version 9, GraphPad Software, LLC, USA). Data was analyzed for normality using Kolmogorov-Smirnov test. Normally distributed data was tested using ANOVA with Tukey post-hoc test while not normally distributed data was analyzed using Kruskal Wallis test. Regional differences were determined using paired *t*-test following Bonferroni correction to account for multiple testing. An alpha level below 0.5 was regarded as statistically significant.

3. Results

3.1. Sample characteristics

Characteristics of the groups and results for DXA measurement on the 12th thoracic vertebrae are presented in Table 1. The high cortical porosity subgroup was determined using microCT, exceeding a cortical porosity of 20 %. The groups are age-matched and therefore present with similar age distributions. Interestingly, the T2DMwHP group presents with a significantly higher BMI compared to the control group ($p = 0.0438$) while the T2DM group shows a similar BMI as the control group. Assessment of aBMD at the vertebrae revealed lowest values in both scan directions in the T2DM group and the highest aBMD value in anterior-posterior direction in the T2DMwHP group, but no significant differences were observed between the groups. Due to the postmortem nature of the study, information on medication was limited; in the T2DM group two individuals received metformin and one individual insulin treatment, whereas in the T2DMwHP group one individual received metformin and another received insulin treatment.

Table 1
Sample characteristics of the control, T2DM, and T2DMwHP group including number of samples, sex, age, body mass index, aBMD in AP and LAT direction measured with DXA, and cortical porosity determined by microCT. Data is presented as mean ± standard deviation. T2DM: type 2 diabetes mellitus; T2DMwHP: type 2 diabetes mellitus with high porosity; aBMD: areal bone mineral density; AP: anterior-posterior; LAT: lateral.

Parameters	Control	T2DM	T2DMwHP
Sample number	15	10	5
Sex [female/male]	3/12	4/6	2/3
Age [years]	72.7 ± 6.8	77.2 ± 5.5	76 ± 8.7
Body mass index [kg/m^2]	26.73 ± 4.9	27.95 ± 6.4	34.07 ± 3.4
aBMD AP [mg HA/cm^2]	0.824 ± 0.272	0.689 ± 0.202	0.911 ± 0.218
aBMD LAT [mg HA/cm^2]	0.672 ± 0.247	0.501 ± 0.155	0.666 ± 0.249
Cortical porosity [%]	12.42 ± 4.26	12.05 ± 4.28	27.21 ± 5.84

3.2. Higher cortical porosity emphasized by HR-pQCT in the T2DM subgroup along with unchanged bone material strength index

Following indentation and extraction of the tibia mid-diaphysis (Fig. 2A), we have analyzed the tibial cross-section (Fig. 2B) using HR-pQCT before extracting the anterior-medial quadrant (Fig. 2C) for further analysis. Bone material strength index (Fig. 2D) did not show any differences between the three groups. Based on the definition of the reference range provided by the manufacturer, in 3 control and 3 T2DM samples showed decreased BMSi being below 79, whereas 2 control samples and 1 T2DMwHP sample presented with low values being defined as below 73. Three control samples and 1 T2DM sample presented with BMSi values above the average defined as higher than 91. HR-pQCT revealed similar cortical vBMD, area and thickness in all three groups (Fig. 2E–G), while cortical porosity was significantly higher in the T2DMwHP group compared to the control ($p = 0.0134$) and to the T2DM group ($p = 0.0312$). The higher cortical porosity was accompanied by a significantly higher cortical pore diameter in the T2DMwHP group compared to the T2DM group ($p = 0.03$).

3.3. High cortical porosity T2DM subgroup based on microCT analyses of the anterior-medial quadrant exhibits lower tissue mineral density compared to T2DM group

For subsequent analysis, the anterior-medial quadrant was extracted as the quadrant was indented using *in situ* impact indentation. Following microCT scanning, images were reconstructed in 3D (Fig. 3A) and a high cortical porosity was discriminated. Cortical pore diameter analysis using microCT revealed a similar data distribution in comparison to cortical pore diameter analyzed with HR-pQCT. However, using microCT cortical pore diameter did not differ between the groups (Fig. 3B). The high cortical porosity subgroup showed a significantly lower tissue mineral density compared to T2DM group ($p = 0.018$; Fig. 3C).

3.4. Higher transversal indentation distance increase in the high cortical porosity T2DM subgroup measured using reference point indentation

To verify our BMSi results, reference point indentation was performed in transversal direction. The first cycle indentation distance (meaning the distance that the probe penetrates the bone tissue) was significantly higher in the T2DMwHP group compared to the control ($p = 0.0257$) and the T2DM ($p = 0.0169$) group (Fig. 4A) after removal of one outlier from the control and one outlier from the T2DM group. The first cycle creep indentation distance (the distance that the probe penetrates the tissue during the first holding phase) was significantly higher in the T2DMwHP group (Fig. 4B) compared to the control ($p = 0.0252$) and the T2DM group ($p = 0.022$). Similarly, the total indentation distance was significantly higher in the T2DMwHP group compared to the control and the T2DM group ($p = 0.0195$ and $p = 0.0168$, respectively; Fig. 4C) after removing one outlier in the control and one outlier in the T2DM group. The indentation distance increase was significantly higher in the T2DMwHP group compared to the control group ($p = 0.0252$;

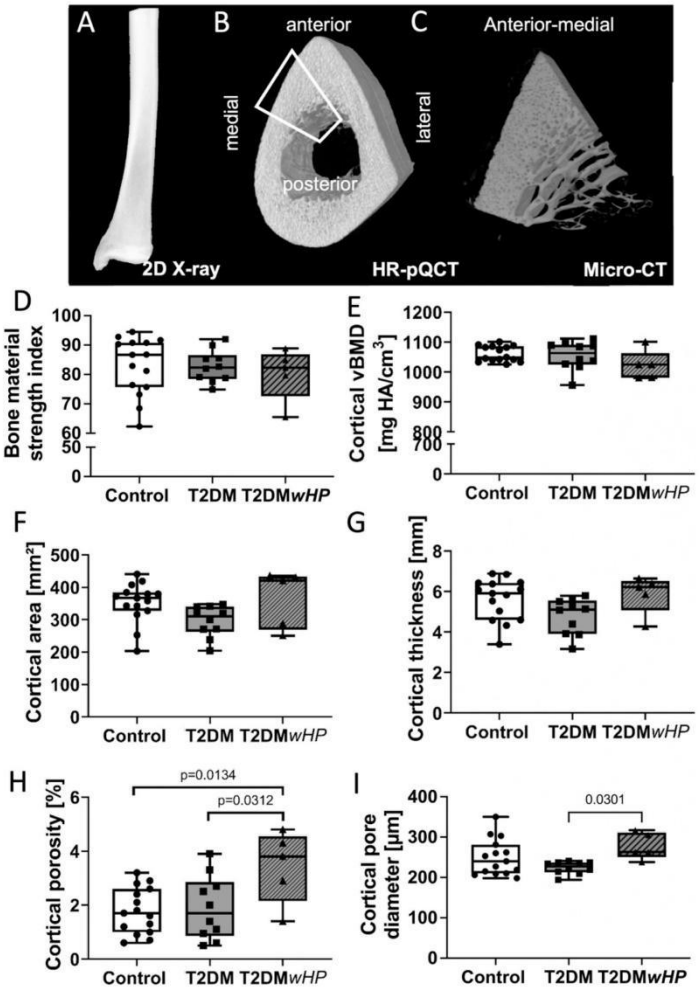

Fig. 2. Bone material strength index and high-resolution peripheral quantitative computed tomography indices in tibial cortical bone. (A) 2D X-ray radiography of the tibia. (B) 3D reconstruction of the mid-diaphysis of the tibia imaged using high-resolution peripheral quantitative computed tomography. (C) Extracted anterior-medial quadrant reconstructed after microCT scanning. (D) Clinically accessible bone material strength index shows similar results for all three groups. (E) Cortical vBMD did not differ between the groups. (F) Cortical area and (G) cortical thickness show similar results for all three groups, while (H) cortical porosity is higher in the T2DMwHP group compared to the T2DM and control group. Further, (I) cortical pore diameter was higher in the T2DMwHP group compared to the T2DM group. Data are presented in box plots with individual data points shown for each group. For all parameters one-way ANOVA was applied, except for differences in Ct.Po.Dm, where non-parametric Kruskal-Wallis test was performed. $p < 0.05$ is regarded as statistically significant. vBMD: volumetric bone mineral density; T2DM: type 2 diabetes mellitus; T2DMwHP: type 2 diabetes mellitus with high cortical porosity.

Fig. 4D), while the average creep indentation distance was similar (Fig. 4E). The average loading slope presented with a significantly lower value in the T2DMwHP group compared to the control group ($p = 0.0425$) and tended to be lower compared to the T2DM ($p = 0.0521$; Fig. 4F) after removing one outlier from the T2DM group.

3.5. Comparable degree of mineralization along mechanical properties in the longitudinal direction using qBEI and reference point indentation

Following reference point indentation in the transversal direction, the anterior-medial quadrant was embedded in MMA. To assess the degree of mineralization in the cortical bone tissue, we applied quantitative backscattered electron imaging (Fig. 5A). To take regional cross-sectional differences within the cortical bone into account, we differentiated the cortical bone tissue into endocortical and periosteal region. The endocortical region was defined as the region close to the bone marrow while the periosteal region was defined close to the periost.

Based on the bone mineral density distribution, we obtained the average and peak calcium weight content, as well as the mineralization heterogeneity. Additionally, the bone areas with high and low mineralized bone packages were determined. The obtained mineralization parameters were similar between all three groups and regions as presented in Table 2.

On the same samples, the effects of different testing directions were tested (*i.e.*, transversal direction *vs.* longitudinal direction). In the longitudinal osteonal direction, we performed reference point indentation to determine the cross-sectioned osteonal characteristics of the cortical bone tissue (Fig. 5B–C) and determined the same indices as in the transversal indentation direction. The results are shown in Fig. 6A–D.

Additionally, nanoindentation was performed to determine Young's modulus and hardness in the periosteal and endocortical region (Fig. 6E–F). Both, Young's modulus and hardness, presented with similar values between the T2DMwHP, T2DM, and control groups and for endocortical and periosteal regions.

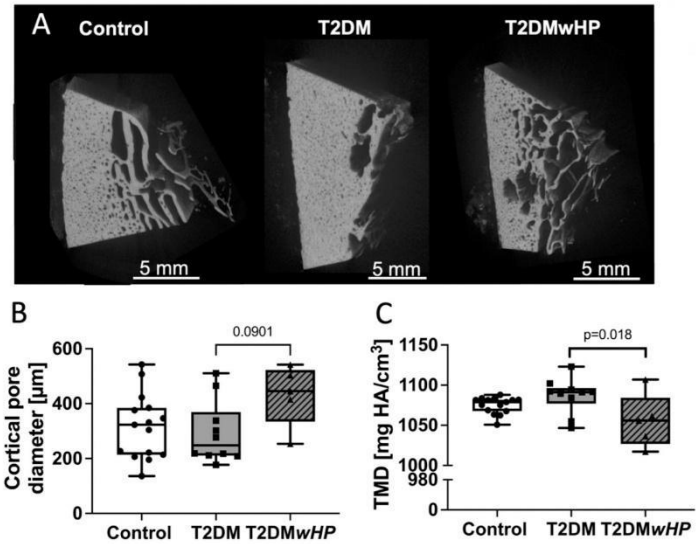

Fig. 3. High-porosity T2DM subgroup discriminated by microCT analysis of the anterior-lateral quadrant showed lower tissue mineral density compared to T2DM group. (A) 3D reconstructed microCT scans of the anterior-lateral quadrant of the control, T2DM, and T2DMwHP group. (B) Cortical pore diameter microCT results show a similar trend as Ct.Po.Dm measured with HR-pQCT but no significant differences. (C) TMD is lower in the T2DMwHP group compared to the T2DM group. Data are presented in box plots with individual data points shown for each group. One-way ANOVA was applied for statistical testing and $p < 0.05$ is regarded as statistically significant. T2DM: type 2 diabetes mellitus; T2DMwHP: type 2 diabetes mellitus with high cortical porosity.

3.6. Higher carbonate-to-amide I ratio in the endocortical region of the high porosity T2DM subgroup compared to the control and T2DM groups

The assessment of bone matrix composition was performed on the embedded bone samples for periosteal and endocortical cross-sectioned regions. Based on the obtained Raman spectra (Fig. 7A), different ratios describing the bone matrix composition were obtained. The mineral to matrix ratio (Fig. 7B) and the carbonate to phosphate ratio (Fig. 7C) were similar between all three groups and both regions. In the endocortical region, the carbonate-to-amide I ratio was significantly higher in the T2DMwHP group compared to both, the control ($p = 0.047$) and the T2DM group ($p = 0.029$), whereas no difference was observed in the periosteal region (Fig. 7D). The crystallinity was similar between all three groups but was shown to be significantly lower in the periosteal region compared to the endocortical region in the control group ($p = 0.005$) but not in the T2DM groups (Fig. 7E).

3.7. Advanced glycation end-products in tibial diabetic bone tissue

To assess AGE accumulation in diabetic bone, a fluorescent and colorimetric assay was performed. While we could not show any differences between the groups, the T2DMwHP presented with the highest mean value of 402.2 ± 149.6 ng quinine/mg collagen compared to the control group with 321.9 ± 121.2 ng quinine/mg collagen (Fig. 7F). Interestingly, the T2DM group presented with the lowest mean value of 305.7 ± 89.28 ng quinine/mg collagen.

4. Discussion

Bone quality analyses of different skeletal sites were carried out to unravel how structural and compositional factors in the mid-diaphysis of the tibia determine mechanical behavior in health and diabetes mellitus. Specifically, we combined *ex vivo* clinical imaging and *in situ* impact indentation with high-resolution imaging, bone matrix composition assessment, and biomechanical properties to study the effects of T2DM on bone quality. Here, we discriminated a high cortical porosity subgroup in a T2DM cohort, which was identified by microCT. This subgroup was also previously reported when the femoral cortex of T2DM individuals were analyzed [24]. The T2DM high cortical porosity subgroup also presented with a higher cortical pore diameter measured with HR-pQCT using a resolution of 82 µm in comparison to the T2DM group. Although HR-pQCT is the clinically available method to determine cortical porosity in patients, it did not detect the high cortical porosity cases in our previous study [24], nor did it show a significant difference when compared to the non-diabetic group in a clinical study [11]. Therefore, we identified the high cortical porosity cases using microCT instead of HR-pQCT.

Higher cortical porosity in T2DM has also been reported by other groups studying T2DM [11,12], however, cortical porosity alone cannot explain the increased fracture risk observed in diabetic patients [5,15]. Also, why T2DM patients with similar T-scores to non-diabetics present with higher fracture risk [38] remains unanswered. Here, analysis of cortical pore diameter using microCT showed a similar trend as in data that was obtained with HR-pQCT. Of note, the trend was not statistically significant. This might be due to the differences in resolution (82 µm *vs.* 10 µm) which allows inclusion of pores with lower diameter in the microCT measurement, and the different scanned bone regions (whole cross-sections *vs.* anterior-medial quadrants). Recently, it has been suggested that major cortical porosity develops at the early course of type 2 diabetes mellitus disease and is followed by a smaller steady and annually increase in cortical porosity [39]. While the origin of cortical porosity cannot be deconstructed within this study, both groups have been described in diabetic patients before and thus require further studying as bone fragility in diabetic patients seems to originate from both, cortical porosity and impaired bone material quality.

Mechanical behavior tested *via in situ* impact indentation (*i.e.*, BMSi) was similar between all three groups. Furst et al. showed a 9.2 % lower BMSi in postmenopausal women with T2DM compared to healthy controls, which was negatively correlated with disease duration and was accompanied by higher femoral neck and total hip aBMD but unchanged cortical bone microstructure [6]. Of note, in our study, only three cases presented with a BMSi below 73 while in the study by Furst et al., the mean BMSi of the control group was 70.12 [6], which points towards an overall higher BMSi in our study. Other studies reported no significant differences in BMSi in Caucasian patients [40] along with a higher aBMD at all skeletal sites and a trend of higher cortical porosity in the tibia

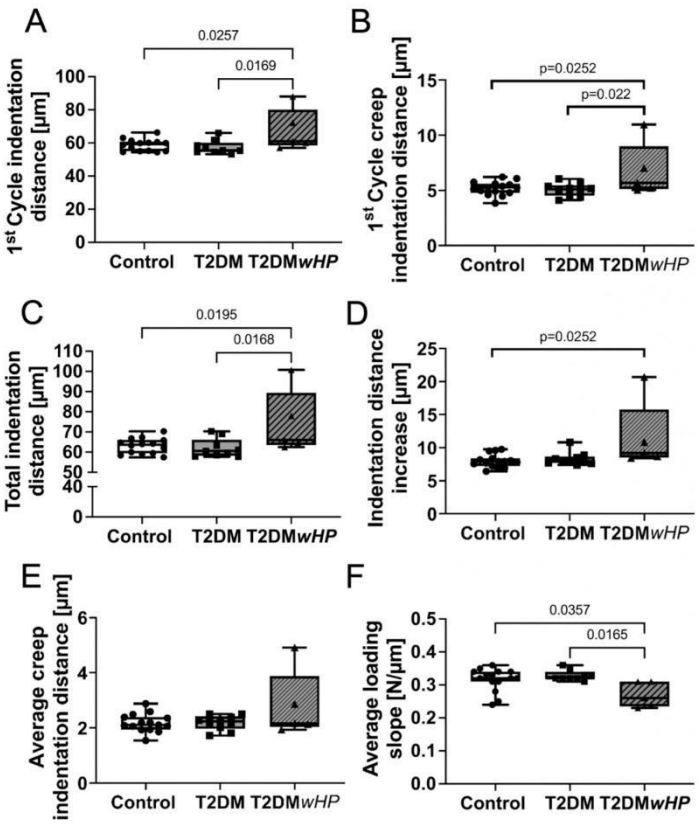

Fig. 4. Cyclic indentation reveals altered biomechanical properties in the transversal direction (*i.e.*, perpendicular to osteons aligned from proximal to distal) in the T2DMwHP group. (A) 1st Cycle indentation distance is similar between all three groups, while (B) 1st cycle creep indentation distance was significantly higher in the T2DMwHP group compared to the T2DM and control group. (C) The total indentation distance was significantly higher in the T2DMwHP group compared to control and T2DM group. (D) The indentation distance increase was significantly higher in T2DMwHP compared to control group. (E) The average creep indentation distance measured over all cycles shows similar values for all three groups, whereas (F) the average loading slope is significantly lower in the T2DMwHP group compared to the control and T2DM group. Data are presented in box plots with individual data points shown for each group. One-way ANOVA was performed for analysis of 1st cycle indentation distance after removal of one outlier in control and one outlier in T2DM group (values higher than mean ± 2 SD), creep indentation distance, total indentation distance after removal of the same outliers as for 1st cycle indentation distance, and average creep indentation distance. The other parameters were analyzed using Kruskal-Wallis test with removal of one outlier in the T2DM group for average loading slope (value lower than mean ± 2 SD). $p < 0.05$ is regarded as statistically significant. T2DM: type 2 diabetes mellitus; T2DMwHP: type 2 diabetes mellitus with high cortical porosity.

[19]. The variable results of the studies point towards a T2DM-independent change in BMSi.

With our integrated approach, involving experimental analyses (*i.e.*, cyclic indentation of bone tissue in transversal direction) in combination with clinical BMSi testing in transversal direction, we found higher 1st cycle indentation distance, 1st creep indentation distance, and total indentation distance in the T2DMwHP group compared to control and T2DM groups. All parameters are indications of the depth that the probe travels into the tissue. The 1st cycle indentation distance indicates the depth that the probe penetrates into the tissue in the first cycle, while the 1st cycle creep indentation distance indicates how deep the probe penetrates into the bone tissue during the holding phase of the first cycle and the total indentation distance is the distance traveled during the entire cycle. As all values are higher, it indicates that the probe penetrates deeper and therefore easier into the tissue, suggesting a lower tissue hardness [41], in T2DMwHP compared to control and T2DM groups. This result was further supported by a lower average loading slope, the latter being calculated based on the averaged loading slope between 50 and 100 % of the maximum force for all cycles, which can be linked to stiffness of the bone tissue suggesting a lower stiffness [42].

Additionally, a higher indentation distance increase in the T2DMwHP group was observed. It indicates that between the last and the first cycle the distance of the probe penetrates deeper into the tissue in the T2DMwHP group compared to the control and T2DM groups. The values reported for both *in situ* impact indentation and cyclic indentation are in line with previously reported data, where the authors found no correlation between BMSi parameters and cyclic indentation parameters [43]. Karim et al., who performed indentations in the longitudinal direction of femoral neck samples from T2DM patients undergoing total hip replacement surgery, showed higher 1st cycle creep indentation distance and indentation distance increase in individuals afflicted with T2DM [23]. Indentation distance increase has been shown to be higher in a diabetic ZDSD rat model and negatively correlated with bone's toughness assessed with 3-point bending in rat femurs, lumbar vertebrae, and dog ribs [41] suggesting lower bone toughness in the T2DMwHP group but not in the T2DM group.

In contrast to the data obtained from tests in the transversal direction, we were not able to show similar results when testing in the longitudinal direction. When comparing the cyclic indentation data in both directions, the parameters regarding indentation depth were all lower in the longitudinal measurement direction compared to the transversal measurement direction, while the average loading slope was higher in the longitudinal measurement direction. This was also reported by another study showing higher indentation depth in the transversal direction (indicated by average creep indentation distance), while stiffness expressed by the average loading slope was higher in the longitudinal direction in unfixed femoral bone of the mid-diaphysis [42].

Fixation of bone tissue as well as embedding influences bone tissue and therefore the biomechanical properties. However, we could show similar differences between both measurement directions as reported on

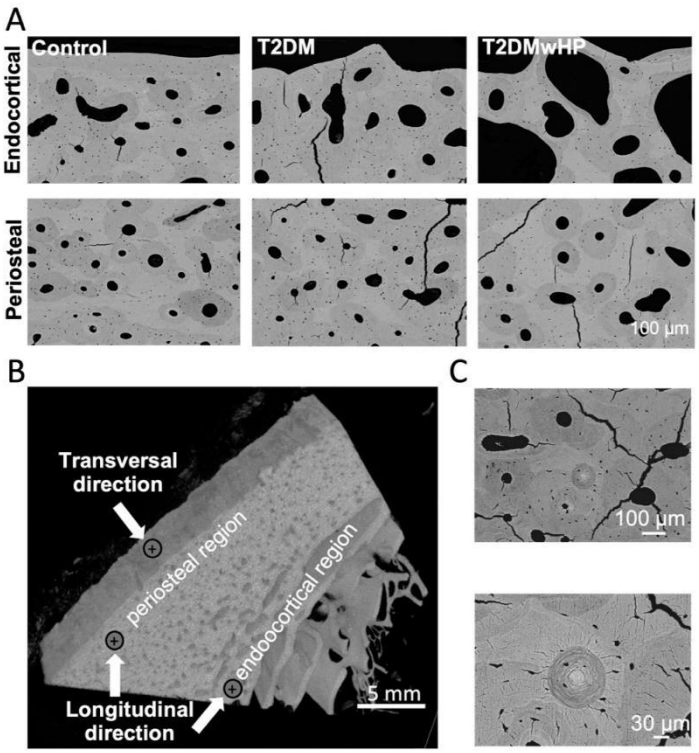

Fig. 5. Bone mineral density distribution in the cross-sectional osteons and cyclic indentation in longitudinal direction revealed no differences between the groups and regions. (A) Grey-scale images obtained with qBEI for control, T2DM, and T2DMwHP groups in endocortical and periosteal cross-sectioned bone region. (B) 3D microCT image of an anterior-lateral quadrant provides an impression of the transversal indentation direction and the longitudinal indentation direction (cross-sectioned osteons) used for cyclic indentation as well as periosteal and endocortical evaluation. (C) Cyclic indentation in longitudinal direction was performed in the interstitial bone packets between osteons. Only indentations that did not include voids or cracks were included into the analysis. T2DM: type 2 diabetes mellitus; T2DMwHP: type 2 diabetes mellitus with high cortical porosity.

Table 2
Mineralization parameters obtained with qBEI for control, T2DM, T2DMwHP groups in endocortical and periosteal region. Data is shown as mean ± standard deviation. Statistical analysis of all parameters was performed using one-way ANOVA. qBEI: quantitative backscattered electron imaging; T2DM: type 2 diabetes mellitus; T2DMwHP: type 2 diabetes mellitus with high cortical porosity, wt% weight percentage.

Parameters	Endocortical region			Periosteal region		
	Control	T2DM	T2DMwHP	Control	T2DM	T2DMwHP
Ca mean [wt%]	25.39 ± 0.29	25.29 ± 0.44	25.34 ± 0.66	25.31 ± 0.35	25.42 ± 0.44	25.25 ± 0.41
Ca peak [wt%]	25.83 ± 0.3	25.76 ± 0.39	25.66 ± 0.57	25.81 ± 0.36	25.82 ± 0.37	25.63 ± 0.31
Ca width [wt%]	2.28 ± 0.16	2.26 ± 0.16	2.18 ± 0.07	2.33 ± 0.14	2.27 ± 0.12	2.24 ± 0.05
Ca high [% bone area]	4.4 ± 1.03	4.77 ± 1.81	3.93 ± 1.71	4.99 ± 1.41	4.41 ± 1.62	4.54 ± 1.19
Ca low [% bone area]	5.1 ± 1.69	4.88 ± 2.85	5.61 ± 4.3	4.95 ± 1.96	5.81 ± 3.11	4.42 ± 2.81

unfixed bone samples. Indeed, it has been shown, that the organic bone matrix is irreversibly affected by formaldehyde fixation [44] resulting in a small effect on the Young's modulus determined by bending [45]. As RPI is a cyclic measurement technique assessing the material's behavior during several loading cycles but also during a holding time, effects on the organic matrix through fixation may also influence the bone's response to RPI. We used fixation to avoid natural degeneration during sample handling and to preserve the ultrastructure of the bone tissue. Furthermore, it is common practice to fix and embed the bone samples following extraction also in a clinical setup and we aimed to compare clinical data with lab-based settings. Due to the fixation a potential effect on the results cannot be ruled out. However, all samples have been treated identically, which allows the comparison between the different groups.

In a study with focus on cortical bone tissue from aged, osteoporotic, and bisphosphate treated individuals compared to a young control group, 1st cycle indentation distance was higher, which was accompanied by higher calcium peak and calcium mean values [46]. As we found no changes in tibial tissue mineralization in the groups (*i.e.*, based on calcium weight percentages), the absence of significant differences in biomechanical properties in the longitudinal direction may be a consequence of similar mineralization profiles.

In femoral cortical bone from T2DM individuals, we observed a higher percentage of low mineralized bone packets in the endocortical region of the T2DMwHP group compared to the control group along with a more heterogeneous mineralization [24]. Higher mean calcium content and a more homogeneous mineralization in the femoral neck of T2DM patients with osteoarthritis were shown in a previous study [21]. These results differ from the presented data in the present study, in which we could not determine any differences of calcium weight

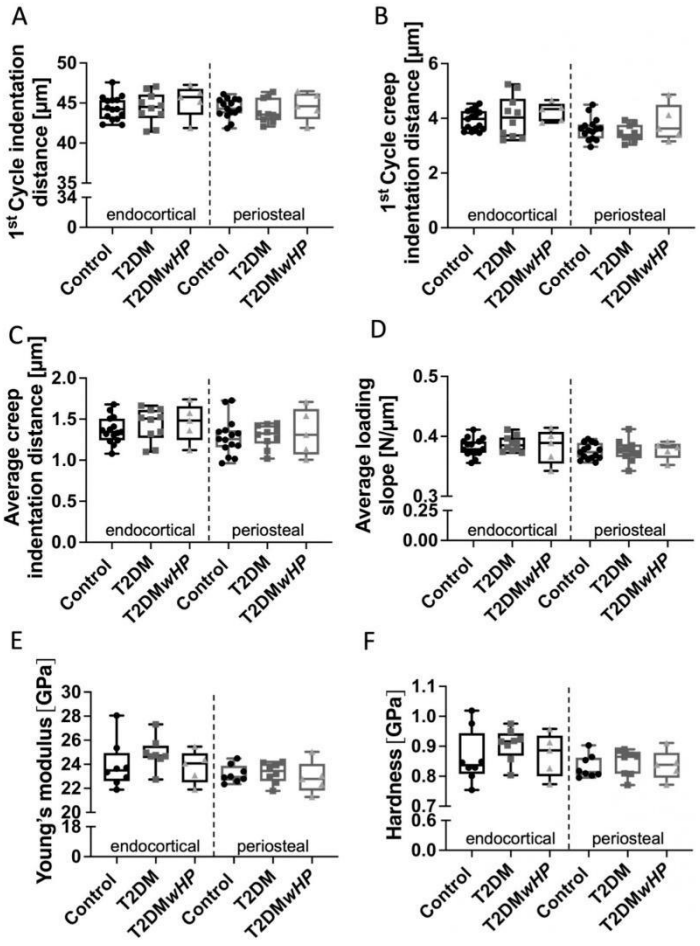

Fig. 6. Similar indentation indices across groups in longitudinal direction of cross-sectioned osteons using reference point indentation as well as similar Young's modulus and hardness assessed with nanoindentation. (A) 1st Cycle indentation distance, (B) 1st cycle creep indentation distance, (C) total indentation distance, and (D) average creep indentation distance were similar between all three groups and both regions. (E) Young's modulus and (F) hardness assessed at the nano-length scale did not differ between the groups and regions. Data are presented in box plots with individual data points shown for each group. Kruskal-Wallis was performed for analysis of 1st cycle indentation distance, Young's modulus, and hardness. One-way ANOVA was performed for analysis of 1st cycle creep indentation distance, total indentation distance, and average creep indentation distance. $p < 0.05$ is regarded as statistically significant. T2DM: type 2 diabetes mellitus; T2DMwHP: type 2 diabetes mellitus with high cortical porosity.

percentages based on qBEI. While the three studies used the same technique, our previous study looked at purely cortical bone from the femur [24] in contrast to the study of Pritchard et al., who analyzed femoral neck tissue including cortical and trabecular bone [21]. This indicates skeletal site-dependent differences in cortical bone mineral density distribution which has also been suggested by other groups [47].

To determine whether changes in bone stiffness and hardness were apparent in the T2DMwHP group, as suggested by the results of transversal RPI analysis, we performed nanoindentation of the embedded bone tissue in longitudinal direction and showed similar hardness and stiffness in endocortical and periosteal region and between the groups. In our previous study, we could also not see differences in nanoindentation despite a distinct mineralization pattern [24]. As nanoindentation assesses properties at the nano-scale rather than the micro-scale, this might indicate that tissue properties at a larger length scale might be affected that are not apparent at the nano-level when indenting individual lamellae, while it reflects the absent differences in mineralization degree and cyclic indentation parameters in the longitudinal direction.

Raman spectroscopic analyses determined a significantly higher carbonate-to-amide I ratio in the T2DMwHP group compared to control and T2DM groups. The higher ratio can either be explained by a higher carbonate content or a lower amide I content. Carbonate becomes substituted into hydroxyapatites over tissue maturation time [48]. As the carbonate to phosphate ratio was similar between all groups (Fig. 7C) and our mineralization analysis showed a similar mineralization degree between all groups and regions, it could be suggested that carbonate content is not affected. Consequently, a lower amide I content is postulated. Although fixation-related changes in collagen can be detected with Raman spectroscopy [49], the equal treatment for all bone samples within this study assures that the differences between the groups observed here are independent of fixation-related effects.

Fluorescent AGE content normalized to hydroxyproline content showed a tendency of 25 % higher fAGE values for T2DMwHP group compared to the control group, however, without reaching statistical significance. Other studies confirmed our results in cortical bone from the mid-diaphysis [24] and in trabecular tissue from the femoral head tissue of patients undergoing total hip arthroplasty [22]. A trend

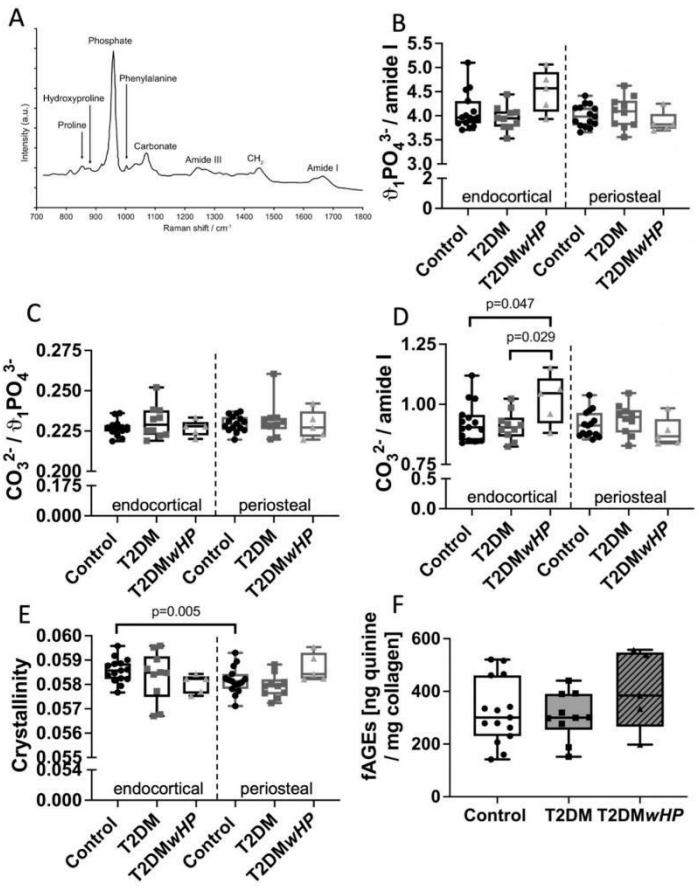

Fig. 7. Raman spectroscopy revealed higher carbonate-to-amide I ratio in the T2DMwHP group in the endocortical region. (A) Representative Raman spectrum of bone indicating the individual peaks. (B) Phosphate over amide I peak analysis showed similar values for all three groups and both cross-sectioned regions. (C) Carbonate-to-phosphate ratio presented with absent differences between the groups and regions. (D) Carbonate over amide I peak revealed a significantly higher value in the endocortical region in the T2DMwHP compared to the control and the T2DM groups, while in the periosteal region no differences were apparent. (E) Crystallinity was similar between the three groups but was significantly lower in the periosteal cross-sectioned region compared to the endocortical region in the control group. (F) fAGE analysis showed similar values for all three group despite highest fAGE levels in the T2DMwHP group. Data are presented in box plots with individual data points shown for each group. Phosphate-to-amide I ratio as well as carbonate-to-phosphate ratio were analyzed using Kruskal-Wallis test. Statistical analyses of all other parameters were performed using one-way ANOVA. $p < 0.05$ is regarded as statistically significant. T2DM: type 2 diabetes mellitus; T2DMwHP: type 2 diabetes mellitus with high cortical porosity.

towards higher fAGE accumulation was reported in cortical bone from the femoral neck [23], while two studies reported fAGE levels in trabecular bone. One study showed 1.5-fold higher fAGE level in trabecular bone from T2DM postmenopausal women with osteoarthritis undergoing total hip replacement using similar group sizes (n = 15 for control and n = 5 for T2DM group) [50] while another study presented significantly higher fAGE levels in trabecular bone from femoral heads of diabetes patients [27]. Possibly, the high standard deviation observed in our study, which is twice has high as in the cited studies, might contribute to the absence of statistical difference. Further, specific AGEs might be affected, that cannot be detected by fluorescent AGE assessment, for example CML, which could contribute to the observed changes in biomechanical properties [51]. Based on our previous study, we can only speculate [24], that CML might be higher in T2DM bone tissue, but further studies are needed to verify this assumption.

Overall, we observed peculiarities in bone material quality in individuals with T2DM expressed by higher cortical porosity using high-resolution lab-based techniques (*e.g.*, microCT, cyclic indentation, Raman spectroscopy), which were not apparent in clinically available modalities for fracture risk assessment due to limited resolution (*e.g.*, DXA, HR-pQCT, impact indentation). This suggests that ultrastructural material level changes in the diabetic bone disease may occur prior to manifestation of clinically identifiable impairments. While others have suggested that cortical porosity may develop early in the course of the disease [39], the exact evolution of the diabetic bone disease is still unknown and further studies are needed to determine the progression of diabetes induced alterations in bone tissue to allow for refined diagnosis strategies.

This study has a few limitations: Due to the *postmortem* study design, medical records including the diabetes duration, severity, medication, and blood glucose levels are not available for all included individuals. However, only the *postmortem* study design allows us to perform bone material quality analyses on the mid-diaphysis, which is an accessible site for clinical fracture risk assessment using impact indentation. Furthermore, the study groups have limited sizes and are accompanied by a certain degree of variability due to the heterogeneity in human samples and the multi-factorial disease diabetes mellitus. However, similar small sample sizes were used in other studies, where significant changes in diabetic bone quality could be reported [52–54]. Bone tissue was analyzed at just one specific time point, which we were using to characterize diabetic bone tissue with comparable or higher cortical porosity to healthy controls. The application of *ex vivo* imaging techniques implies differences compared to application *in vivo*; (i) HR-pQCT was performed on the mid-diaphysis of the tibia with soft tissue removed

prior to imaging instead of the peripheral site imaging of an intact tibia, and (ii) for DXA analysis of the vertebrae a water phantom was used to simulate the missing soft tissue. Lab-based experiments are usually performed on fixed and/or embedded bone tissue which influence bone tissue characteristics compared to native tissue *in vivo*. However, *in situ* impact indentation in this study has been performed postmortem on the intact leg of the individuals. With our combination of *in vivo* and lab-based techniques we provide further insight to translate experimental results into clinically applicable information.

In conclusion, our study reveals new data on bone material quality parameters in the tibial mid-diaphysis, which stems from clinical as well as experimental testing. By combining these data sets, we showed that the T2DM high cortical porosity subgroup showed higher cortical pore diameter compared to T2DM group measured with HR-pQCT. While we could not identify differences in clinical *in situ* impact indentation testing (BMSi), changed cyclic indentation properties indicative of softer bone tissue in the T2DMwHP group were observed in the experimental approach (RPI). Changed cyclic indentation properties were accompanied by a higher carbonate to amide I ratio in the cross-sectioned endocortical region, which seems to originate from a changed collagen structure. Although fluorescent AGEs were similar between the groups, a potential effect of AGE accumulation of the bone tissue cannot be excluded, as analysis were limited to fluorescent AGEs. We also provide new insight into altered cortical bone material quality in the tibial mid-diaphysis indicated by easier indenter penetration in bone tissue when carried out in the transversal direction which is accompanied by higher carbonate to amide I ratio in the cross-sectioned bone area in the endocortical region of the T2DM subgroup with high cortical porosity.

CRediT authorship contribution statement

EMW: Conceptualization, methodology, formal analysis, visualization, funding acquisition, writing – original draft; **IAKF:** Methodology, software, writing – review & editing; **SK:** Methodology, writing – review & editing; **JK:** Methodology, writing – review & editing; **ML:** Methodology, writing – review & editing; **BY:** Methodology, writing – review & editing; **AKS:** Methodology, writing – review & editing; **HM:** Resources, writing – review & editing; **BW:** Resources, writing – review & editing; **KP:** Resources, writing – review & editing; **BO:** Resources, writing – review & editing; **CG:** Validation, writing – review & editing; **KJR:** Project administration, supervision, writing – review & editing; **BB:** Conceptualization, methodology, funding acquisition, supervision, project administration, writing - review & editing.

Declaration of competing interest

The authors declare no conflict of interest.

Data availability

All data needed to evaluate the conclusion in the paper are presented in the paper. The datasets generated during and/or analyzed during the current study are not publicly available but are available from the corresponding author on reasonable request.

Acknowledgments

We would like to thank Laura E. Harder, Sandra Perkovic, and Andrea Thieke (Department for Osteology and Biomechanics) for excellent technical support.

Funding

Funding was received from the Faculty of Medicine, Post-Doc Fellowship (EMW), University Medical Center Hamburg-Eppendorf (UKE); European Union's Horizon 2020 - Research and Innovation Framework Programme H2020 Marie Skłodowska-Curie Actions grant 860898 (KJR, BB); Deutsche Forschungsgemeinschaft (German Research Foundation) grant JA2654/1-1 (KJR) and grant BU2562-10/1 (BB).

Appendix A. Supplementary data

Supplementary data to this article can be found online at https://doi.org/10.1016/j.bone.2022.116546.

References

[1] X. Lin, Y. Xu, X. Pan, J. Xu, Y. Ding, X. Sun, X. Song, Global, regional, and national burden and trend of diabetes in 195 countries and territories: an analysis from 1990 to 2025, Sci. Rep. 10 (2020) 1–11, https://doi.org/10.1038/s41598-020-71908-9.

[2] A. Alzaid, P.L. de Guevara, M. Beillat, V. Lehner, P. Atanasov, Burden of disease and costs associated with type 2 diabetes in emerging and established markets : systematic review analyses, Expert Rev. Pharmacoecon. Outcomes Res. 00 (2020) 1–14, https://doi.org/10.1080/14737167.2020.1782748.

[3] G.T. Russo, A. Giandalia, E.L. Romeo, M. Nunziata, M. Muscianisi, M.C. Ruffo, A. Catalano, D. Cucinotta, Fracture risk in type 2 diabetes: current perspectives and gender differences, Int. J. Endocrinol. 2016 (2016), https://doi.org/10.1155/2016/1615735.

[4] E.A. Zimmermann, I.A.K. Fiedler, B. Busse, Breaking new ground in mineralized tissue: assessing tissue quality in clinical and laboratory studies, J. Mech. Behav. Biomed. Mater. 113 (2021), https://doi.org/10.1016/j.jmbbm.2020.104138.

[5] L.C. Hofbauer, B. Busse, R. Eastell, S. Ferrari, M. Frost, R. Müller, A.M. Burden, F. Rivadeneira, N. Napoli, M. Rauner, Bone fragility in diabetes: novel concepts and clinical implications, Lancet Diabetes Endocrinol. 10 (2022) 207–220, https://doi.org/10.1016/S2213-8587(21)00347-8.

[6] J.R. Furst, L.C. Bandeira, W.W. Fan, S. Agarwal, K.K. Nishiyama, D.J. Mcmahon, E. Dworakowski, H. Jiang, S.J. Silverberg, M.R. Rubin, Advanced glycation endproducts and bone material strength in type 2 diabetes, J. Clin. Endocrinol. Metab. 101 (2016) 2502–2510, https://doi.org/10.1210/jc.2016-1437.

[7] V.J. Kingsmill, C.M. Gray, D.R. Moles, A. Boyde, Cortical vascular canals in human mandible and other bones, J. Dent. Res. 86 (2007) 368–372, https://doi.org/10.1177/154405910708600413.

[8] M. Schoeb, N.A.T. Hamdy, F. Malgo, E.M. Winter, N.M. Appelman Dijkstra, Added value of impact microindentation in the evaluation of bone fragility: a systematic review of the literature, Front. Endocrinol. (Lausanne) 11 (2020), https://doi.org/10.3389/fendo.2020.00015.

[9] D. Bridges, C. Randall, P.K. Hansma, A new device for performing reference point indentation without a reference probe, Rev. Sci. Instrum. 83 (2012), https://doi.org/10.1063/1.3693085.

[10] M.R. Allen, E.M.B. McNerny, J.M. Organ, J.M. Wallace, True gold or pyrite: a review of reference point indentation for assessing bone mechanical properties in vivo, J. Bone Miner. Res. 30 (2015) 1539–1550, https://doi.org/10.1002/jbmr.2603.

[11] J.M. Patsch, A.J. Burghardt, S.P. Yap, T. Baum, A.V. Schwartz, G.B. Joseph, T. M. Link, Increased cortical porosity in type 2 diabetic postmenopausal women with fragility fractures, J. Bone Miner. Res. 28 (2013) 313–324, https://doi.org/10.1002/jbmr.1763.

[12] A.J. Burghardt, A.S. Issever, A.V. Schwartz, K.A. Davis, U. Masharani, S. Majumdar, T.M. Link, High-resolution peripheral quantitative computed tomographic imaging of cortical and trabecular bone microarchitecture in patients with type 2 diabetes mellitus, J. Clin. Endocrinol. Metab. 95 (2010) 5045–5055, https://doi.org/10.1210/jc.2010-0226.

[13] E.J. Samelson, S. Demissie, L.A. Cupples, X. Zhang, H. Xu, C.T. Liu, S.K. Boyd, R. R. McLean, K.E. Broe, D.P. Kiel, M.L. Bouxsein, Diabetes and deficits in cortical bone density, microarchitecture, and bone size: Framingham HR-pQCT Study, J. Bone Miner. Res. 33 (2018) 54–62, https://doi.org/10.1002/jbmr.3240.

[14] M. Osima, R. Kral, T.T. Borgen, I.K. Høgestøl, R.M. Joakimsen, E.F. Eriksen, Å. Bjørnerem, Women with type 2 diabetes mellitus have lower cortical porosity of the proximal femoral shaft using low-resolution CT than nondiabetic women, and increasing glucose is associated with reduced cortical porosity, Bone 97 (2017) 252–260, https://doi.org/10.1016/j.bone.2017.01.037.

[15] P. Vestergaard, Discrepancies in bone mineral density and fracture risk in patients with type 1 and type 2 diabetes – a meta-analysis, Osteoporos. Int. 18 (2007) 427–444, https://doi.org/10.1007/s00198-006-0253-4.

[16] F. Malgo, N.A.T. Hamdy, S.E. Papapoulos, N.M. Appelman-Dijkstra, Bone material strength index as measured by impact microindentation is low in patients with fractures irrespective of fracture site, Osteoporos. Int. 28 (2017) 2433–2437, https://doi.org/10.1007/s00198-017-4054-8.

[17] J.N. Farr, M.T. Drake, S. Amin, L.J.M. Iii, L.K. Mccready, In vivo assessment of bone quality in postmenopausal women with type 2 diabetes, J. Bone Miner. Res. 29 (2014) 787–795, https://doi.org/10.1002/jbmr.2189.

[19] P. Samakkarnthai, J.G. Sfeir, E.J. Atkinson, S.J. Achenbach, P.W. Wennberg, P. J. Dyck, A.J. Tweed, T.L. Volkman, S. Amin, J.N. Farr, A. Vella, M.T. Drake, Determinants of bone material strength and cortical porosity in patients with type 2 diabetes mellitus, J. Clin. Endocrinol. Metab. 105 (2020) 3718–3729, https://doi.org/10.1210/clinem/dgaa388.

[20] M.R. Rubin, J.M. Patsch, Assessment of bone turnover and bone quality in type 2 diabetic bone disease: current concepts and future directions, Bone Res. 4 (2016) 1–9, https://doi.org/10.1038/boneres.2016.1.
[21] J.M. Pritchard, A. Papaioannou, C. Tomowich, L.M. Giangregorio, S.A. Atkinson, K. A. Beattie, J.D. Adachi, J. DeBeer, M. Winemaker, V. Avram, H.P. Schwarcz, Bone mineralization is elevated and less heterogeneous in adults with type 2 diabetes and osteoarthritis compared to controls with osteoarthritis alone, Bone 54 (2013) 76–82, https://doi.org/10.1016/j.bone.2013.01.032.
[22] H.B. Hunt, A.M. Torres, P.M. Palomino, E. Marty, R. Saiyed, M. Cohn, J. Jo, S. Warner, G.E. Sroga, K.B. King, J.M. Lane, D. Vashishth, C.J. Hernandez, E. Donnelly, Altered tissue composition, microarchitecture, and mechanical performance in cancellous bone from men with type 2 diabetes mellitus, J. Bone Miner. Res. 34 (2019) 1191–1206, https://doi.org/10.1002/jbmr.3711.
[23] L. Karim, J. Moulton, M. van Vliet, K. Velie, A. Robbins, F. Malekipour, A. Abdeen, D. Ayres, M.L. Bouxsein, Bone microarchitecture, biomechanical properties, and advanced glycation end products in the proximal femur of adults with type 2 diabetes, Bone 114 (2018) 32–39, https://doi.org/10.1016/j.bone.2018.05.030.
[24] E.M. Wölfel, K. Jähn-Rickert, F.N. Schmidt, B. Wulff, H. Mushumba, G.E. Sroga, K. Püschel, P. Milovanovic, M. Amling, G.M. Campbell, D. Vashishth, B. Busse, Individuals with type 2 diabetes mellitus show dimorphic and heterogeneous patterns of loss in femoral bone quality, Bone 140 (2020), 115556, https://doi.org/10.1016/j.bone.2020.115556.
[25] A.V. Schwartz, P. Garnero, T.A. Hillier, D.E. Sellmeyer, E.S. Strotmeyer, K. R. Feingold, H.E. Resnick, F.A. Tylavsky, D.M. Black, S.R. Cummings, T.B. Harris, D.C. Bauer, Pentosidine and increased fracture risk in older adults with type 2 diabetes, J. Clin. Endocrinol. Metab. 94 (2009) 2380–2386, https://doi.org/10.1210/jc.2008-2498.
[26] R. Dhaliwal, S.K. Ewing, D. Vashishth, R.D. Semba, A.V. Schwartz, Greater carboxy-methyl-lysine is associated with increased fracture risk in type 2 diabetes, J. Bone Miner. Res. 37 (2022) 265–272, https://doi.org/10.1002/jbmr.4466.
[27] P. Sihota, R.N. Yadav, R. Dhaliwal, J.C. Bose, V. Dhiman, D. Neradi, S. Karn, S. Sharma, S. Aggarwal, V.G. Goni, V. Mehandia, D. Vashishth, S.K. Bhadada, Investigation of mechanical, material, and compositional determinants of human trabecular bone quality in type 2 diabetes, J. Clin. Endocrinol. Metab. 106 (2021) e2271–e2289, https://doi.org/10.1210/clinem/dgab027.
[28] C. Randall, D. Bridges, R. Guerri, X. Nogues, L. Puig, E. Torres, L. Mellibovsky, K. Hoffseth, T. Stalbaum, A. Srikanth, J.C. Weaver, S. Rosen, H. Barnard, D. Brimer, A. Proctor, J. Candy, C. Saldana, S. Chandrasekar, T. Lescun, C.M. Nielson, E. Orwoll, D. Herthel, H. Kopeikin, H.T.Y. Yang, J.N. Farr, L. McCready, S. Khosla, A. Diez-Perez, P.K. Hansma, Applications of a new handheld reference point indentation instrument measuring bone material strength, journal of medical devices, Trans. ASME 7 (2013), https://doi.org/10.1115/1.4024829.
[29] A.M. Briggs, J.D. Wark, S. Kantor, N.L. Fazzalari, A.M. Greig, K.L. Bennell, Bone mineral density distribution in thoracic and lumbar vertebrae: an ex vivo study using dual energy X-ray absorptiometry, Bone 38 (2006) 286–288, https://doi.org/10.1016/j.bone.2005.07.018.
[30] A.J. Burghardt, H.R. Buie, A. Laib, S. Majumdar, S.K. Boyd, Reproducibility of direct quantitative measures of cortical bone microarchitecture of the distal radius and tibia by HR pQCT, Bone 47 (2010) 519–528, https://doi.org/10.1016/j.bone.2010.05.034.
[31] T. Hildebrand, P. Ruegsegger, A New Method for the Model-independent Assessment of Thickness in Three-dimensional Images, 1995.
[32] X. Yuan, R.A. Mayanovic, An empirical study on raman peak fitting and its application to raman quantitative research, Appl. Spectrosc. 71 (2017) 2325–2338, https://doi.org/10.1177/0003702817721527.
[33] M.D. Morris, G.S. Mandair, Raman assessment of bone quality, in: Clin Orthop Relat Res, Springer, New York LLC, 2011, pp. 2160–2169, https://doi.org/10.1007/s11999-010-1692-y.
[34] T. Rodic, E.M. Wölfel, P. Milovanovic, I.A.K. Fiedler, D. Cvetkovic, K. Jälin, M. Amling, J. Sopta, S. Nikolic, V. Zivkovic, B. Busse, M. Djuric, Bone quality analysis of jaw bones in individuals with type 2 diabetes mellitus—post mortem anatomical and microstructural evaluation, Clin. Oral Investig. 25 (2021) 4377–4400, https://doi.org/10.1007/s00784-020-03751-1.
[35] W.C. Oliver, G.M. Pharr, An improved technique for determining hardness and elastic modulus using load and displacement sensing indentation experiments, J. Mater. Res. 7 (1992).
[36] G.E. Sroga, A. Siddula, D. Vashishth, Glycation of human cortical and cancellous bone captures differences in the formation of maillard reaction products between glucose and ribose, PLoS One 10 (2015), https://doi.org/10.1371/journal.pone.0117240.
[37] J.E. Eastoe, The amino acid composition of mammalian collagen and gelatin, Biochem. J. (1955) 589–600, https://doi.org/10.1042/bj0610589.
[38] A.V. Schwartz, E. Vittinghoff, D.C. Bauer, T.A. Hillier, E.S. Strotmeyer, K.E. Ensrud, M.G. Donaldson, J.A. Cauley, T.B. Harris, A. Koster, C.R. Womack, L. Palermo, D. M. Black, Association of BMD and FRAX score with risk of fracture in older adults with type 2 diabetes, JAMA 305 (2011) 2184–2192, https://doi.org/10.1001/jama.2011.715.
[39] U. Heilmeier, G.B. Joseph, C. Pasco, N. Dinh, S. Torabi, K. Darakananda, J. Youm, J. Carballido-Gamio, A.J. Burghardt, T.M. Link, G.J. Kazakia, Longitudinal evolution of bone microarchitecture and bone strength in type 2 diabetic postmenopausal women with and without history of fragility fractures—a 5-year follow-up study using high resolution peripheral quantitative computed tomography, Front. Endocrinol. (Lausanne) 12 (2021), https://doi.org/10.3389/fendo.2021.599316.
[40] B. Dawson-Hughes, M. Bouxsein, K. Shea, Bone material strength in normoglycemic and hyperglycemic black and white older adults, Osteoporos. Int. 30 (2019) 2429–2435, https://doi.org/10.1007/s00198-019-05140-1.
[41] M.A. Gallant, D.M. Brown, J.M. Organ, M.R. Allen, D.B. Burr, Reference-point indentation correlates with bone toughness assessed using whole-bone traditional mechanical testing, Bone 53 (2013) 301–305, https://doi.org/10.1016/j.bone.2012.12.015.
[42] M. Granke, A. Coulmier, S. Uppuganti, J.A. Gaddy, M.D. Does, J.S. Nyman, Insights into reference point indentation involving human cortical bone: sensitivity to tissue anisotropy and mechanical behavior, J. Mech. Behav. Biomed. Mater. 37 (2014) 174–185, https://doi.org/10.1016/j.jmbbm.2014.05.016.
[43] L. Karim, M. van Vliet, M.L. Bouxsein, Comparison of cyclic and impact based reference point indentation measurements in human cadaveric tibia, Bone 106 (2018) 90–95, https://doi.org/10.1016/j.bone.2015.03.021.
[44] N. Hammer, C. Voigt, M. Werner, F. Hoffmann, K. Bente, H. Kunze, R. Scholz, H. Steinke, Ethanol and formaldehyde fixation irreversibly alter bones' organic matrix, J. Mech. Behav. Biomed. Mater. 29 (2014) 252–258, https://doi.org/10.1016/j.jmbbm.2013.09.008.
[45] J.D. Currey, K. Brear, P. Zioupos, G.C. Reilly, Effect of Formaldehyde Fixation on Some Mechanical Properties of Bovine Bone, 1995.
[46] P. Milovanovic, E.A. Zimmermann, C. Riedel, A. vom Scheidt, L. Herzog, M. Krause, D. Djonic, M. Djuric, K. Püschel, M. Amling, R.O. Ritchie, B. Busse, Multi-level characterization of human femoral cortices and their underlying osteocyte network reveal trends in quality of young, aged, osteoporotic and antiresorptive-treated bone, Biomaterials 45 (2015) 46–55, https://doi.org/10.1016/j.biomaterials.2014.12.024.
[47] P. Roschger, H.S. Gupta, A. Berzlanovich, G. Ittner, D.W. Dempster, P. Fratzl, F. Cosman, M. Parisien, R. Lindsay, J.W. Nieves, K. Klaushofer, Constant mineralization density distribution in cancellous human bone, Bone 32 (2003) 316–323, https://doi.org/10.1016/S8756-3282(02)00973-0.
[48] E.P. Paschalis, S. Gamsjaeger, K. Klaushofer, Vibrational spectroscopic techniques to assess bone quality, Osteoporos. Int. 28 (2017) 2275–2291, https://doi.org/10.1007/s00198-017-4019-y.
[49] I.A.K. Fiedler, M. Casanova, T. Keplinger, B. Busse, R. Müller, Effect of short-term formaldehyde fixation on raman spectral parameters of bone quality, J. Biomed. Opt. 23 (2018) 1, https://doi.org/10.1117/1.jbo.23.11.116504.
[50] A. Piccoli, F. Cannata, R. Strollo, C. Pedone, G. Leanza, F. Russo, V. Greto, C. Isgrò, C.C. Quattrocchi, C. Massaroni, S. Silvestri, G. Vadalà, T. Bisogno, V. Denaro, P. Pozzilli, S.Y. Tang, M.J. Silva, C. Conte, R. Papalia, M. Maccarrone, N. Napoli, Sclerostin regulation, microarchitecture, and advanced glycation end-products in the bone of elderly women with type 2 diabetes, J. Bone Miner. Res. 35 (2020) 2415–2422, https://doi.org/10.1002/jbmr.4153.
[51] M.J.L. Tice, S. Bailey, G.E. Sroga, E.J. Gallagher, D. Vashishth, Non-obese MKR mouse model of type 2 diabetes reveals skeletal alterations in mineralization and material properties, JBMR Plus. 6 (2022), https://doi.org/10.1002/jbm4.10583.
[52] D. Farlay, L.A.G. Armas, E. Gineyts, M.P. Akhter, R.R. Recker, G. Boivin, Nonenzymatic glycation and degree of mineralization are higher in bone from fractured patients with type 1 diabetes mellitus, J. Bone Miner. Res. 31 (2016) 190–195, https://doi.org/10.1002/jbmr.2607.
[53] J.C. Krakauer, M.J. McKenna, N.F. Buderer, D. Sudhaker Rao, F.W. Whitehouse, A. Michael Parfitt, Bone loss and bone turnover in diabetes, Diabetes 44 (1995) 775–782, https://doi.org/10.2337/diab.44.7.775.
[54] J.S. Manavalan, S. Cremers, D.W. Dempster, H. Zhou, E. Dworakowski, A. Kode, S. Kousteni, M.R. Rubin, Circulating osteogenic precursor cells in type 2 diabetes mellitus, J. Clin. Endocrinol. Metab. 97 (2012) 3240–3250, https://doi.org/10.1210/jc.2012-1546.

9.4. Publication 4: When Cortical Bone Matrix Properties Are Indiscernible between Elderly Men with and without Type 2 Diabetes, Fracture Resistance Follows Suit

RESEARCH ARTICLE

JBMR PLUS Open Access ASBMR

When Cortical Bone Matrix Properties Are Indiscernible between Elderly Men with and without Type 2 Diabetes, Fracture Resistance Follows Suit

Eva M. Wölfel,[1] Benjamin Bartsch,[1] Jasmin Koldehoff,[2,3] Imke A. K. Fiedler,[1,3] Sofie Dragoun-Kolibova,[1] Felix N. Schmidt,[1,3] Johannes Krug,[1] Mei-Chun Lin,[1] Klaus Püschel,[4] Benjamin Ondruschka,[4] Elizabeth A. Zimmermann,[5] Hans Jelitto,[2] Gerold Schneider,[2] Bernd Gludovatz,[6] and Björn Busse[1,3]

[1]Department of Osteology and Biomechanics, University Medical Center Hamburg-Eppendorf, Hamburg, Germany
[2]Institute of Advanced Ceramics, Hamburg University of Technology, Hamburg, Germany
[3]Interdisciplinary Competence Center for Interface Research (ICCIR), University Medical Center Hamburg-Eppendorf, Hamburg, Germany
[4]Institute of Legal Medicine, University Medical Center Hamburg-Eppendorf, Hamburg, Germany
[5]Faculty of Dental Medicine and Oral Health Sciences, McGill University, Montreal, Canada
[6]School of Mechanical and Manufacturing Engineering, University of New South Wales, Sydney (UNSW Sydney), Sydney, Australia

ABSTRACT

Type 2 diabetes mellitus (T2DM) is a metabolic disease affecting bone tissue and leading to increased fracture risk in men and women, independent of bone mineral density (BMD). Thus, bone material quality (i.e., properties that contribute to bone toughness but are not attributed to bone mass or quantity) is suggested to contribute to higher fracture risk in diabetic patients and has been shown to be altered. Fracture toughness properties are assumed to decline with aging and age-related disease, while toughness of human T2DM bone is mostly determined from compression testing of trabecular bone. In this case-control study, we determined fracture resistance in T2DM cortical bone tissue from male individuals in combination with a multiscale approach to assess bone material quality indices. All cortical bone samples stem from male nonosteoporotic individuals and show no significant differences in microstructure in both groups, control and T2DM. Bone material quality analyses reveal that both control and T2DM groups exhibit no significant differences in bone matrix composition assessed with Raman spectroscopy, in BMD distribution determined with quantitative back-scattered electron imaging, and in nanoscale local biomechanical properties assessed via nanoindentation. Finally, notched three-point bending tests revealed that the fracture resistance (measured from the total, elastic, and plastic J-integral) does not significantly differ in T2DM and control group, when both groups exhibit no significant differences in bone microstructure and material quality. This supports recent studies suggesting that not all T2DM patients are affected by a higher fracture risk but that individual risk profiles contribute to fracture susceptibility, which should spur further research on improving bone material quality assessment in vivo and identifying risk factors that increase bone fragility in T2DM. © 2023 The Authors. *JBMR Plus* published by Wiley Periodicals LLC on behalf of American Society for Bone and Mineral Research.

KEY WORDS: BONE MATERIAL QUALITY; CORTICAL BONE; FRACTURE TOUGHNESS; MECHANICAL TESTING; T2DM

Introduction

Type 2 diabetes mellitus (T2DM), a metabolic disease with increasing prevalence expected to affect an estimated 578 million adults worldwide by 2030, leads to various complications, including bone fragility, indicated by a relative risk of 1.2 for hip and 1.17 for any fracture.[1] The increased fracture risk is not directly linked to bone mineral density (BMD), so BMD fails to predict diabetic patients at increased risk of fracture.[2] Currently, clinical in vivo bone diagnostic tools, such as dual energy X-ray absorptiometry (DXA), high-resolution peripheral quantitative computed tomography (HR-pQCT), and impact indentation, are not sufficiently sensitive to identify and predict T2DM patients at increased fracture risk, whereas impaired bone

Received in original form September 3, 2023; revised form October 6, 2023; accepted October 19, 2023.
Address correspondence to: Björn Busse, PhD, Department of Osteology and Biomechanics, University Medical Center Hamburg-Eppendorf, Lottestr 55a, 22529, Hamburg, Germany. E-mail: b.busse@uke.de
Additional supporting information may be found online in the Supporting Information section.
JBMR® Plus (WOA), Vol. 7, No. 12, December 2023, e10839.
DOI: 10.1002/jbm4.10839

material quality, i.e., bone material properties affecting bone toughness without attribution to bone mass or quantity, has been proposed to contribute to higher fracture risk in T2DM.[3]

A higher cortical porosity subgroup measured with micro–CT (μCT) was identified ex vivo and associated with higher mineralization heterogeneity in human femoral cortical bone,[4] as well as higher lab-based cyclic indentation depth but unchanged in vivo impact indentation properties in the tibia.[5] A higher cortical porosity subgroup measured with HR-pQCT in vivo was also associated with fragility fractures.[6, 7] Independent of microstructural differences, higher accumulation of advanced glycation end products (AGEs), such as carboxymethyl-lysine, and lower collagen fibril deformation were measured in human T2DM cortical bone compared to nondiabetic bone.[4, 8] Higher cyclic indentation depth was also observed in femoral neck cortical bone from T2DM patients, with a trend toward higher AGE accumulation but no differences in compressive biomechanical properties in trabecular bone.[9] Studies on trabecular bone cores from the femoral head of T2DM patients showed lower bone volume and trabecular thickness, lower mineral content, and lower mineral-to-matrix ratio in combination with lower toughness measured with compression testing,[10] while others found higher pentosidine content and higher mineral-to-matrix ratio, in combination with a higher modulus but no difference in toughness, determined using compression testing of trabecular bone from T2DM male patients.[11] Individual tissue-level changes at different length scales, such as microstructural changes or changes in bone matrix composition, contribute to bone overall fracture susceptibility. The aforementioned studies are indicative for altered bone material quality in patients with T2DM that can partly be linked to changes in toughness at the tissue level in trabecular bone. However, data on the fracture behavior in human diabetic cortical bone tissue are currently limited.

Three-point bending tests of notched bone samples enable characterization of the fracture properties of bone tissue and allow for the analysis of bone resistance to the initiation and propagation of cracks. Furthermore, the combination of such testing with imaging techniques, such as optical or electron microscopy, enables the visualization of crack growth and the assessment of relevant bone toughening mechanisms.[12] However, this requires relatively large sample dimensions, which is often a limitation of bone research. Furthermore, different three-point bending setups, such as under vacuum using a scanning electron microscope for crack visualization or in a normal environment using an optical microscope along with different sample sizes and testing properties, have been applied, making comparisons across studies difficult.[13] While standardizations of three-point bending of nonbiological materials exist and are documented, for example, in ASTM International's Standard Test Method for Measurement of Fracture Toughness E 1820, no standardization for human bone as biomaterial is available across laboratories or countries. Nevertheless, using three-point bending tests, a significant reduction in fracture toughness in human cortical bone with age compared to young and middle-aged individuals has been shown,[14, 15] suggesting changes in fracture toughness in aging and possibly age-related diseases such as diabetes mellitus. All fracture toughness properties measured in cadaveric human cortical bone were shown to decrease with age, although age explains only 13% to 23% of the variance, while other parameters, such as bound and pore water, as well as indentation resistance properties, best explain fracture toughness variance, suggesting a multimodal assessment of fracture toughness in bone.[16] Using the same heterogeneous sample cohort, including three individuals with diabetes mellitus, two with osteoporosis, and six with cancer, a strong relationship was found between fracture toughness and collagen network connectivity.[17] While these studies include a large sample set (62 donors in total), only three donors were diabetic, and thus no firm conclusion can be drawn on diabetes-induced impacts on fracture toughness.

Differences in bone material quality in T2DM have been shown for cortical and trabecular bone, and they have been linked to partially altered mechanical properties in trabecular bone. Yet reports on cortical bone toughness in T2DM are lacking in the literature. In this case-controlled study, we therefore aimed to determine fracture toughness in T2DM cortical bone tissue in combination with a multiscale approach to assess the microstructure and bone material quality indices of the same bone tissue.

Materials and Methods

Study design

Femoral samples ($n = 29$) from the mid-diaphysis as well as the 12th thoracic and adjacent vertebrae were obtained from male individuals during autopsy (Ethical Approval WT037/15). Approximately 1.5-cm-thick femoral cross-sections (Fig. 1) were extracted from 18 healthy individuals (74.22 ± 6.67 years [range 61 to 89 years]) and 11 individuals diagnosed with T2DM (76.18 ± 6.62 years [range 69 to 89 years]). Following extraction, all samples were wrapped in phosphate-buffered saline (PBS)-soaked gauze and stored at −20°C until further analysis.

In both groups, inclusion criteria such as the absence of any bone-related diseases, e.g., Paget's disease of bone, osteogenesis imperfecta, fibrous dysplasia or malignancy, were applied. Additionally, individuals with renal or hepatic disorders, hyperparathyroidism, as well as bedrest, and those with bone metabolism affecting medications such as thiazolidinediones, glucocorticoids, or bisphosphonates were strictly excluded. De-identified data of all individuals were collected and included age, sex, weight, height, diabetes mellitus status, and, if available, antidiabetic treatment, which ranged from oral antidiabetics such as metformin to insulin treatment. Diabetes mellitus status was based on available medical and autopsy records but was limited to the presence of T2DM and, in some cases, diabetes medication.

Dual energy X-ray absorptiometry

Following an ex vivo protocol,[18] the 12th thoracic vertebra was scanned with DXA (GE Healthcare, GER) to determine the osteoporotic status based on vertebral areal (aBMD) (Fig. 1). Compensation for missing soft tissue due to dissection was done by a water phantom provided by the manufacturer producing a water column of 15 cm simulating the thickness of soft tissue of a person with a body weight of 70 kg and height of 170 cm. The vertebrae were positioned in a plastic container filled with water, and the water phantom was placed on top. The values of aBMD for anterior–posterior (AP) and lateral (LAT) scan directions were obtained using the manufacturer's software. In one control sample and one T2DM sample, no 12th thoracic vertebra was available for logistical reasons.

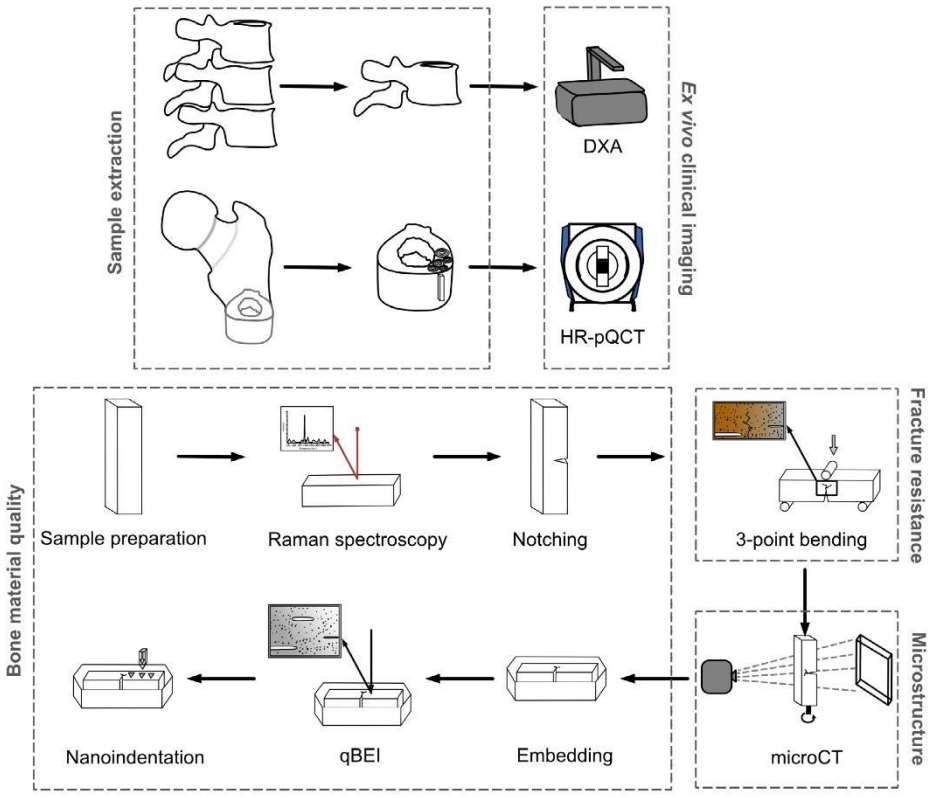

Fig. 1. Study design. The 12th thoracic vertebra with adjacent vertebrae and the mid-diaphysis of the femur were extracted from T2DM individuals and age-matched healthy controls (sample extraction). The 12th thoracic vertebra was scanned using DXA, and the femoral cross-sections were scanned with HR-pQCT to apply ex vivo clinical imaging. Bending beam samples were prepared and scanned with Raman spectroscopy to assess bone material quality indices in terms of bone matrix composition. Samples were notched and fracture resistance was assessed using three-point bending tests. Microstructure was analyzed using micro–CT, while further bone material quality indices were determined using quantitative back-scattered electron microscopy and nanoindentation on embedded bone samples.

High-resolution peripheral quantitative computed tomography

The extracted, frozen, mid-diaphyseal femur samples were scanned in a HR-pQCT system (Xtreme CT I, Scanco, Medical AG, Switzerland) following the removal of soft tissue (Fig. 1). Weekly and monthly calibration was performed using the manufacturer's calibration phantoms for quality control. Per sample, 12 mm of the mid region were scanned to avoid inclusion of regions with extraction artifacts. The scan was performed with 750 projections, a voxel size of 82 µm, and an integration time of 100 ms at each angular position over 180°. Following reconstruction, images were analyzed with the software provided by the manufacturer according to protocols previously published by Burghardt and colleagues[19] and as described in our previous publication.[5] The following cortical parameters were evaluated: cortical volumetric bone mineral density (Ct.vBMD, mg HA/cm^3), cortical porosity (Ct.Po, %), cortical thickness (Ct.Th, mm), cortical pore diameter (Ct.Po.Dm, mm), cortical perimeter (Ct.Pm, mm), cortical area (Ct.Ar, mm^2), and total area (Tt.Ar, mm^2). However, three samples in the control group were incomplete and could therefore not be analyzed using HR-pQCT.

Sample preparation

The frozen femoral mid-diaphyseal samples were sawed with a diamond band saw (EXAKT Technologies, Inc., USA) to extract smaller, rectangular bone samples of at least 12 mm in length from the lateral region of the femoral quadrant (Fig. 1). The smaller bone samples were further sawed using a low-speed saw (Buehler Ltd., Germany) with a 300-µm-thick diamond blade to obtain bending beams of 2 mm thickness (B) × 3 mm height

(W) × 12 mm length (L). The bone samples were then polished using 1-μm diamond suspension to provide a final surface finish for imaging of the crack propagation during three-point bending testing on one surface of the bending beam dedicated to crack imaging. All procedures were performed while keeping the bone samples hydrated in PBS.

Raman spectroscopy

Raman micro-spectroscopy was performed on moist and unfixed bone specimens (inVia, Renishaw, United Kingdom; Fig. 1). Samples were positioned on a microscope slide, and a 63× immersion objective was used to allow spectral acquisition while keeping samples hydrated in PBS, as previously performed,[20] and to determine the region of interest in the middle of the bone sample. For each sample, spectral maps of 200 × 30 μm were acquired at a 5-μm step size (287 spectra per sample) using the streamline mode with an integration time of 8 ms, a grating of 1200 lines per mm, a 785-nm laser wavelength, and a spectral range of ~800 to 1800 cm^{-1}. During the whole scan time, the bone samples were kept humid in PBS. Spectra processing was done using the WiRE software provided by the manufacturer and a custom-made MATLAB code (MATLAB, R2019b, MathWorks Inc., USA) and included removal of cosmic rays, averaging of all spectra per sample, and linear baseline removal under the peaks of interest. The following previously established parameters were obtained[21–23]: mineral-to-matrix ratios (phosphate ν_1 peak at 962 cm^{-1}/amide I peak envelope between 1600 and 1720 cm^{-1}; phosphate ν_1 peak at 962 cm^{-1}/amide III envelope between 1215 and 1365 cm^{-1}), carbonate-to-phosphate ratio (carbonate peak at 1070 cm^{-1}/ν_1 phosphate peak), carbonate-to-amide I peak (carbonate peak/amide I envelope), crystallinity calculated with the reciprocal of the full width at half maximum (FWHM) of the ν_1 phosphate peak, and amide I subpeak ratio 1666/1685 cm^{-1} based on the fitting of amide I subpeaks.

Sample notching

Following Raman spectroscopy, the cortical bone tissue was notched according to previously described protocols[14] (Fig. 1). In brief, the first part of the notch was induced using a low-speed saw with 300-μm blade thickness. A razor blade was inserted into the notch and the final notch length of approximately half the sample height W was prepared with 1-μm diamond suspension. Using an optical microscope, the notch length for every sample was measured and recorded on the surface selected for crack imaging.

Three-point bending

The prepared bone samples were incubated in PBS overnight to avoid an additional freeze–thaw cycle and sufficiently hydrate the bone tissue. Three-point bending tests (Fig. 1) were performed at room temperature in ambient air using a custom-made three-point bending machine[24] with 10 mm support span and round contact points of 1-mm radius. During testing, images of the bone surface were taken using a 400× optical microscope objective to record crack propagation. Furthermore, the samples were continuously moistened with PBS. The samples were preloaded to 2 N at a displacement rate of 2 μm/s. Testing was conducted at an initial displacement rate of 1 μm/s to a load of 15 N. Subsequently, the displacement rate was reduced to 0.15 μm/s. During the entire measurement, force and displacement were continuously recorded using a custom-made software interface in LabView collecting one data point per second. To enable stable crack growth, the testing machine used an automatic control system, which sensed the beginning of crack growth by a decrease in the slope of the recorded force–displacement curve; a slope of −0.45 N/μm over the last 15 data points resulted in a partial unloading of the sample followed by manual restart of the loading. Each test was terminated after a crack length of approximately 700 μm (i.e., ~47% of the remaining ligament b) was observed.

Data analysis

The recorded images were analyzed using ImageJ to determine the crack length for each increment of crack growth. Load–displacement curves were exported from LabView. Determination of the area under the load–displacement curve, curve fitting, and determination of the 95% confidence interval were performed using a custom-made MATLAB script (MATLAB, R2023a, MathWorks Inc., USA).

Bone shows not only elastic but also plastic deformation during mechanical loading. To account for both elastic and plastic deformation, the nonlinear elastic J-integral was measured. The total J-integral was computed as the sum of elastic and plastic components. In this way the J-integral at any point of the load–displacement curve can be determined according to ASTM E1820-01. The elastic J-integral (J_{el}, J/m^2) is calculated as

$$J_{el} = \frac{K_I^2(1-\nu^2)}{E}.$$

with the stress intensity factor (K_I) calculated according to ASTM E1820-01 using a Poisson ratio of $\nu = 0.3$[25] and an E-modulus of E = 19.5 GPa, based on our nanoindentation results.

$$K_I = \frac{PS}{BW^{\frac{3}{2}}} f\left(\frac{a}{W}\right),$$

K_I is calculated based on the measured load P, the support span $S = 10$ mm, the sample thickness B, the sample height W, and the geometric factor $f\left(\frac{a}{W}\right)$ according to ASTM E1820-01.

$$f\left(\frac{a}{W}\right) = \frac{3\left(\frac{a}{W}\right)^{\frac{1}{2}}\left[1.99 - \left(\frac{a}{W}\right)\left(1-\frac{a}{W}\right) \times \left(2.15 - 3.93\left(\frac{a}{W}\right) + 2.7\left(\frac{a^2}{W^2}\right)\right)\right]}{2\left(1+2\frac{a}{W}\right)\left(1-\frac{a}{W}\right)^{\frac{3}{2}}}.$$

The plastic J-integral (J_{pl}, J/m^2) was calculated by dividing the plastic area underneath the load–displacement curve by the uncracked ligament width multiplied by the width of the sample based on the following formula:

$$J_{pl} = \frac{2A_{pl}}{B(W-a)},$$

with A_{pl} being the area under the load–displacement curve between two crack growth events enclosed by parallel lines with an identical slope to the loading slope prior to the first crack extension.

Finally, the total J-integral (J_{tot}, J/m^2) was determined:

$$J_{tot} = J_{el} + J_{pl}.$$

Micro–CT

Directly after fracture toughness testing, the cortical bone samples were fixed in 4% buffered paraformaldehyde for 1 week followed by storage in PBS. To determine cortical porosity (Ct.Po, %) and tissue mineral density (TMD, mg HA/cm^3), the bone samples were scanned using a desktop μCT system (μCT 40, Scanco) using 6 μm resolution, 300 ms integration time, 55 kV X-ray tube voltage, and 145 mA X-ray tube current (Fig. 1). The image data were analyzed, and three-dimensional (3D) renderings were obtained using Xamflow (version 1.8.09, Lucid Concepts AG, Switzerland). Additionally, canal parameters such as canal diameter and canal separation were evaluated based on the sphere fitting method.[26]

Quantitative back-scattered electron imaging

Following μCT imaging, the cortical bone samples were embedded in polymethyl methacrylate, grinded to a coplanar state, and polished to provide a smooth surface of the bone tissue. Quantitative back-scattered electron imaging (qBEI) was performed using a scanning electron microscope (Zeiss crossbeam 340, Carl Zeiss AG, Germany) with a back-scattered electron detector (Fig. 1). Prior to scanning, the embedded bone samples were sputtered with carbon. Gray scale images were obtained through a constant beam current determined using a Faraday cup and calibration standard with aluminum and carbon (MAC Consultants Ltd., England), in combination with a constant working distance of 20 mm and a voltage of 20 kV. In total, five images per sample around the crack were acquired and analyzed using a custom-made MATLAB script routine (MATLAB, R2019b, MathWorks Inc., USA). Based on the BMD distribution the following parameters were determined: average calcium concentration (CaMean, wt%), most frequent calcium concentration (CaPeak, wt%), and mineralization heterogeneity, which is based on the standard deviation of the BMDdistribution curve (CaWidth, wt%).

Nanoindentation

To determine the material properties of the bone tissue, nanoindentation was performed close to the crack surface (Fig. 1). The embedded bone sample surface was further polished using 3-μm and 1-μm diamond suspension and 0.5-μm aluminum oxide suspension, followed by ultrasonic cleaning in distilled water. Using a Berkovich diamond tip in an iMicro nanoindenter (KLA instruments, CA, USA), 30 indentations in close vicinity to the crack path were obtained using depth-sensing continuous stiffness mode and a final depth of 2000 nm. Prior to and following each measurement calibration of the tip was performed on fused silica. Based on the method by Oliver and Pharr[27] and by applying a Poison's ratio of 0.3, hardness and Young's modulus were determined for eight control and five T2DM samples.

Statistical analysis

GraphPad Prism (version 9, GraphPad Software, LLC, USA) was used for statistical analysis. The normal distribution of the data was verified using a Kolmogorov–Smirnov test. Normally distributed data were tested using a Student's *t* test, while nonnormally distributed data were analyzed using a Mann–Whitney U test. An alpha level below 0.05 was regarded as statistically significant.

Results

Using a multiscale approach, we determined bone material quality indices in combination with fracture toughness in cortical bone samples from male individuals with T2DM ($n = 11$) and healthy age-matched controls ($n = 18$). All individuals were male, ruling out any sex-related differences. Sample characteristics are described in Table 1. Both groups did not differ significantly in age, BMI, and aBMD of the 12th thoracic vertebra measured with DXA assuring an absence of osteoporosis.

Additionally, cortical bone microstructure was assessed as in a clinical setup using HR-pQCT showing no significant differences in microstructure determined at a resolution of 82 μm; specifically, cortical vBMD was 1063 ± 43.58 and 1048 ± 27.7 mg HA/cm^3, while cortical porosity was 2 ± 1.6 and 2 ± 1% for the control and T2DM groups, respectively. The cortical perimeter was 104.2 ± 4.04 and 103.7 ± 10.35 μm, and the cortical thickness was 6.76 ± 1.07 and 6.49 ± 0.99 mm for the control and T2DM groups, respectively.

Bone microstructure was further analyzed using μCT. Fig. 2*A* shows the reconstructed 3D image of a representative cortical bone sample after three-point bend testing scanned at a resolution of 6 μm. Cortical porosity and tissue mineral density did not differ significantly between both groups (Fig. 2*B,C*). This was further confirmed by the analysis of canal parameters (Fig. 2*D*), showing no significant differences in canal diameter (Fig. 2*E*) but a tendency ($p = 0.0667$) to lower canal separation in the T2DM group (Fig. 2*F*).

To determine bone material quality, we combined several approaches. First, we performed Raman spectroscopy on the unembedded hydrated bone sample (Fig. 3*A*), indicating no significant differences in bone matrix composition in both groups, shown by a carbonate-to-phosphate ratio of 0.1173 ± 0.0097 in the control group and 0.1184 ± 0.0067 in the T2DM group and no significant differences in collagen quality of 1.137 ± 0.163 and 1.149 ± 0.194 in the control and T2DM groups, respectively. Similarly, other parameters showed no significant differences (Table S1). For a detailed look at the mineralization degree of the bone tissue around the crack path, we applied qBEI, which is based on calcium weight percentages. The average calcium content was 25.54 ± 0.45 and 25.79 ± 0.57 calcium weight percentage, while the most frequent calcium weight percentage measured was

Table 1. Sample Characteristics of 18 Control and 11 T2DM Cases

	Control	T2DM
Number of samples	18	11
Age (years)	74.22 ± 6.67	76.18 ± 6.62
BMI (kg/m^2)	25.63 ± 2.84	25.81 ± 3.3
Ex vivo aBMD of 12th thoracic vertebra (g/cm^2)	AP: 0.908 ± 0.279 LAT: 0.681 ± 0.225	AP: 0.856 ± 0.163 LAT: 0.657 ± 0.125
Diabetes medication		
Oral antidiabetics	-	5 (45.5%)
Insulin	-	1 (9%)
No information available	-	5 (45.5%)

Neither group showed significant differences in age and BMI. Areal BMD was not significantly different between the groups in both scanning directions.

AP = anterior posterior; LAT = lateral.

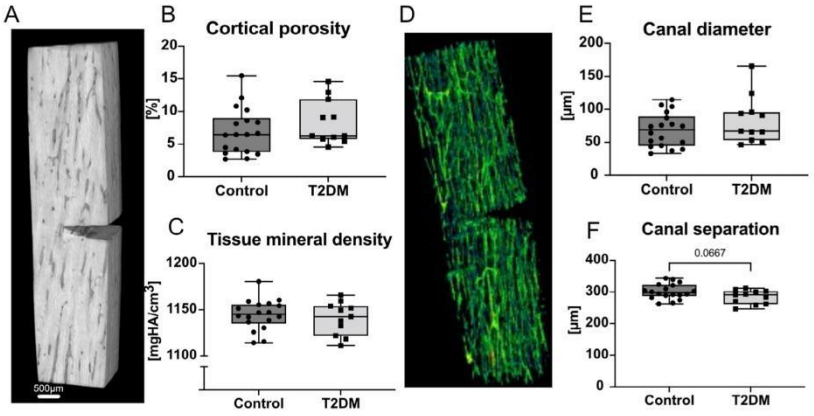

Fig. 2. Bone sample microstructural analysis of control and T2DM cases. (*A*) 3D reconstruction of micro–CT scanned bone sample. (*B*) Cortical porosity and (*C*) tissue mineral density do not significantly differ between both groups. (*D*) 3D reconstruction of canal structure and canal indices, (*E*) canal diameter, and (*F*) canal separation.

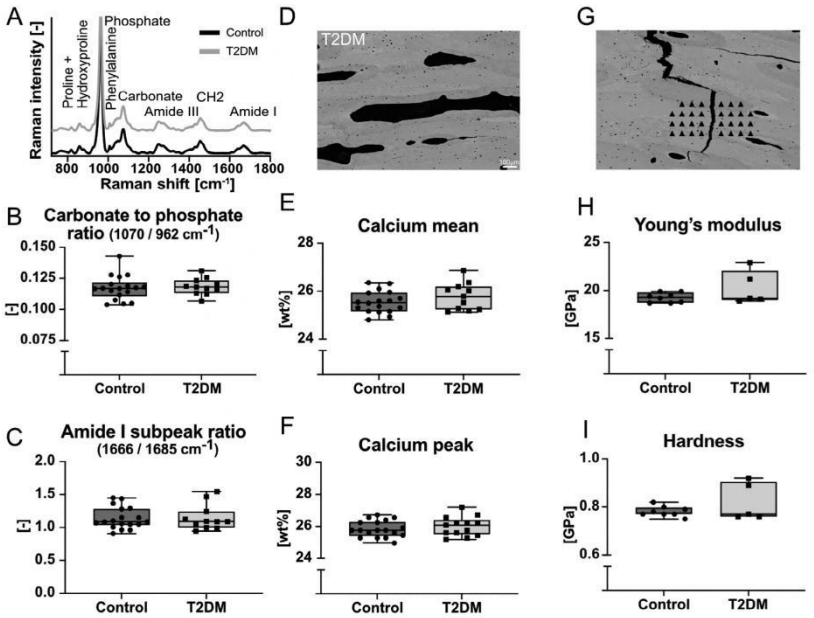

Fig. 3. Bone quality analyses of control and T2DM cases combining Raman spectroscopy, quantitative back-scattered electron imaging (qBEI), and nanoindentation. (*A*) Averaged Raman spectra of both groups. (*B*) Carbonate-to-phosphate ratio and (*C*) collagen subpeak ratios indicate no significant differences in bone matrix composition. (*D*) Representative image obtained with qBEI, (*E*) average calcium weight percentage, and (*F*) highest calcium weight percentage show no significant differences in mineralization profiles around crack path. (*G*) Nanoindentation was performed in vicinity of crack path. (*H*) Young's modulus and (*I*) hardness show no significantly different values for a subset of samples from both groups.

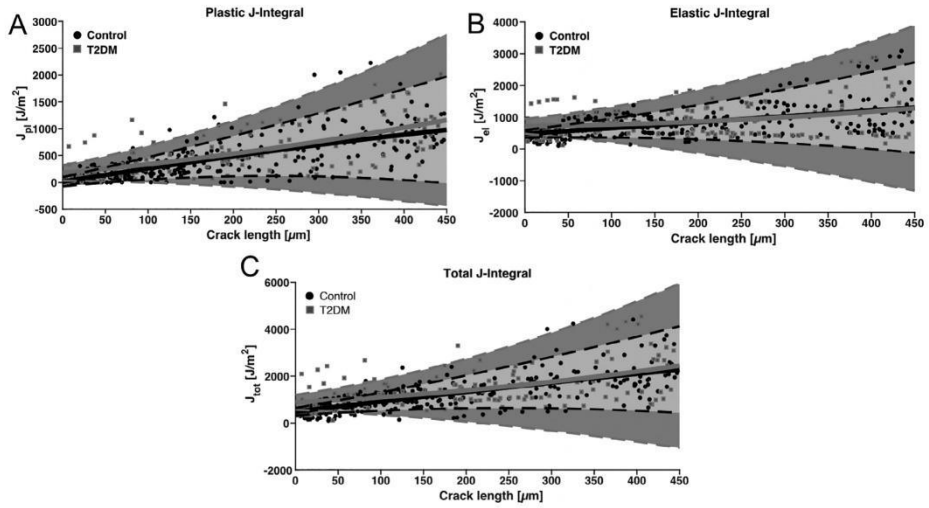

Fig. 4. Three-point bending tests of cortical bone samples from T2DM and healthy controls. (*A*) Plastic J-integral curves, (*B*) elastic J-integral curves, and (*C*) total J-integral curves, all showing individual points of each sample and second-order fitted curves for control (black) and T2DM (gray) groups including 95% confidence interval.

25.84 ± 0.51 and 26.01 ± 0.6 calcium weight percentage for control and T2DM groups, respectively. Data on the mineralization heterogeneity showed no significant differences and can be seen in Table S1. On a smaller sample set, nanoindentation was performed in the vicinity of the crack path. This reflected the results seen in the mineralization parameters, where there were no significant differences in Young's modulus (control: 19.26 ± 0.5 GPa and T2DM: 20.26 ± 1.74 GPa) and hardness (control: 0.78 ± 0.02 GPa and T2DM: 0.82 ± 0.08 GPa).

Using a three-point bending test, the bone samples were loaded, and crack propagation was visualized with a brightfield microscope. Based on the load–displacement curves and crack propagation measurements, the plastic, elastic, and total J-integrals were determined. Fig. 4 displays the individual data points of all samples and second-order fitting lines for control and T2DM samples. While the T2DM fitting line is slightly above the control line, no difference is observed for plastic J-integral (Fig. 4*A*), elastic J-integral (Fig. 4*B*), and total J-integral (Fig. 4*C*).

Discussion

In this study, we analyzed human cortical bone from male individuals with T2DM compared to age-matched healthy controls in a case-controlled post mortem study to assess bone material quality in combination with fracture toughness. While compression testing of trabecular bone from T2DM patients was previously performed,[9–11] the toughness properties of cortical diabetic bone have rarely been studied. In our cohort of bone samples with a nonsignificantly different microstructure, shown by the analysis of bone and canal structures using μCT, we saw no significant differences in bone matrix composition, mineralization profile around the crack path, and biomechanical properties at the nanolength scale. These similarities were also apparent in fracture toughness behavior and failure characteristics, which did not significantly differ between the groups.

While we could not identify differences in bone material quality indices in this cohort, we and others showed differences in the mineral and collagen properties of bone tissue from individuals with T2DM. Previous studies were performed on a variety of different tissues, such as femoral head, femoral neck, or cortical bone from mid-diaphyseal femur and tibia, with a focus on different compartments, i.e., trabecular and cortical bone. When studying human bone tissue, high variation is often observed, which can be augmented through the complexity of T2DM, which poses an additional challenge in the identification of a clear underlying mechanism contributing to the pathophysiology of diabetic bone fragility at the tissue level. One phenomenon seen in some but not all T2DM postmenopausal women is the presence of high cortical porosity,[6, 7] which was shown to be accompanied by compositional changes, as studied previously by our group in a cohort of both male and female individuals.[4, 5] In our previous study of male individuals with no significant difference in cortical porosity, we identified differences in collagen fibril deformation in T2DM individuals[8] by tensile testing with simultaneous synchrotron X-ray diffraction to measure the deformation of collagen fibrils, i.e., a structure at the nanolength scale of bone tissue. It is possible that changes at this length scale are compensated at larger length scales, which can lead to the results presented here.

Furthermore, sex-specific differences should be taken into account when assessing and discussing fracture risk and bone material quality indices in T2DM individuals. Currently, more men live with diabetes mellitus than women,[28] and men are

younger and have a lower BMI when diagnosed.[29] Nonetheless, at the time of diagnosis, women bear a greater burden of risk factors and face a higher relative risk of cardiovascular disease. Conversely, in men, a higher absolute risk exists, where cardiovascular events remain more prevalent.[29] Hormone levels play a significant role in the risk of developing T2DM, with women having a higher risk when they have elevated testosterone levels, while men face an increased risk when their testosterone levels are low.[29] Postmenopausal women are at a higher risk of osteoporosis and fragility fractures than men due to the decline in estrogen levels. Additionally, individuals with T2DM who have microvascular disease exhibit cortical bone deficits.[30] Hence, to specifically investigate bone material changes in T2DM and account for sex-related influences on our outcomes, we have chosen to exclusively study male individuals, as we did in our previous study[8] and was done by others.[11] Further research is warranted to elucidate the sex-specific variations in the pathophysiology of bone fragility associated with T2DM to support the development of tailored diagnostic and treatment approaches for both men and women.

Previous post mortem analysis of human cortical bone tissue of different aged donors using three-point bending test showed lower crack initiation toughness and crack growth toughness with age, including one aged sample with diabetes mellitus, which presented with lower growth toughness and initiation toughness compared to bone from young donors, not to bone tissue from healthy aged donors.[31] Lower fracture toughness with age in human cortical bone has also been shown by others.[14, 15] Additionally, lower fracture toughness properties with age were confirmed, while collagen network integrity best explained variances in fracture toughness.[16, 17] While these two studies included three individuals with diabetes mellitus, the former study did not aim at determining fracture toughness in diabetic individuals, and the low number of diabetic cases did not allow for drawing conclusions on fracture toughness behavior within the cohort.

Ribosylation is often performed on animal or cadaveric human bone tissue as an artificially induced glycosylation of the bone matrix to simulate diabetes-related bone matrix changes and subsequent study bone fracture toughness. Ribosylation of bovine bone for 40 days resulted in improved fracture toughness properties such as higher critical fracture toughness and higher J_{el}, while J_{pl} did not significantly differ compared to control samples.[32] Incubation of bovine tibial bone for 15 days resulted in lower J_{pl} when tested in quasi-static condition (10^{-3} mm/s) but no differences in J-integral, either elastic or plastic, were observed when tested in fall-like conditions (10 mm/s).[33] These data indicate that incubation time and testing strain rate significantly influence the results obtained using ex vivo ribosylation. This points to a major influence of disease duration on bone fracture susceptibility. Due to the post mortem nature of our study, diabetes duration was not accessible in the autopsy protocols. A Swedish cohort study suggested that T2DM may not per se induce an increased fracture risk but that specific risk factors, such as diabetes disease duration, tremendously increase fracture risk in the T2DM population.[34] While this might not affect every T2DM patient, the authors postulate that 21 million individuals are affected by a risk factor profile contributing to increased fracture risk.[34] A longer diabetes duration signifies prolonged high glucose condition within the body, which affects osseos cellular activity, leading to low bone turnover in T2D, which can result in more highly mineralized bone tissue and absence of microcrack removal. Additionally, the longer the high glucose condition continues, the more AGEs can be formed and, thus, impair collagen properties within the bone tissue. Unknown disease duration and differences between individuals may explain why no statistically significant differences were found in this study. However, the presented study design allowed us to obtain sufficiently large bone samples for three-point bending tests and to control for the orientation of microstructural features that can impact the mechanical properties of bone tissue.

Another approach to determining fracture toughness in diabetes conditions are diabetic small animal models. In Zucker Diabetic-Sprague Dawley rats, a higher resistance to crack initiation was observed at 16 and 22 weeks of age compared to control rats, with a decline in toughness with aging and, thus, no difference at 29 weeks of age.[35] In diabetic TallyHo mice, a lower toughness was observed at 16 and 34 weeks of age, which did not become worse with age/disease duration, while initiation toughness and cracking toughness were the same compared to control mice.[36] In a high-fat-diet-induced obesity mouse model, whole femoral fracture toughness was reduced along with larger bone size but less ordered osteocytes and lamellar structure and poorer mineral organization, suggesting that bone material properties may influence size-independent mechanical properties.[37] Lower initiation toughness and lower maximum toughness in combination with higher AGE accumulation was seen in high-fat-diet mice compared to low-fat-diet mice at 32 weeks of age.[38] These data suggest an overall lower fracture toughness in bone from small diabetic animals. However, these models are often not representative of diabetic bone changes seen in humans, where either none or cortical rather than trabecular bone microstructural changes are observed. Furthermore, the bone specimens tested are very different, as human cortical bone is prepared in rectangle-shaped samples, while in small-animal studies whole femora are notched and tested, resulting in a cylindrical sample geometry.

This study has a few limitations. We used a three-point bending setup under environmental conditions, capturing changes in crack propagation at the surface of the bone samples using an optical microscope, while keeping the bone sample hydrated with PBS droplets. While this approach avoided the dehydration of the samples and, as such, a reduction in crack initiation toughness and crack growth resistance, as shown by others,[39] visualization of crack propagation in our study was limited to the bone surface and captured manually at varying time points. Continuous automatic recording of the bone surface rather than manual capture would improve crack propagation measurement. Furthermore, the used machine was generated to control for stable crack growth in less heterogeneous material than bone tissue. Therefore, temporary partial deloading occurred when the slope of the force–displacement curve was below a certain threshold. These unloading phases were not always synchronized with crack growth at the bone surface. This can be understood because crack growth can also happen only in the inner part of the sample and, thus, is not visible on the surface. However, this is a principal limitation of optical crack length determination. With a larger support span of 40 mm and two position encoders at the specimen, the average crack length can be precisely determined with the compliance method. Unfortunately, up to now this has not been possible with a support distance of 10 mm due to technical reasons. We agree with others researchers[13] that more standardized procedures for cortical bone crack growth determination are needed to improve fracture toughness testing and comparison between individual studies. Here,

we applied a variety of techniques (ex vivo clinical imaging, μCT, spectroscopy, electron microscopy, and nanoindentation) to characterize bone material quality. While this allowed us to assess bone material quality at several length scales and different properties, additional indices, such as water content or individual advanced glycation end products (e.g., carboxymethyl-lysine or pentosidine), have not been addressed in this study but can influence the fracture properties of diabetic bone and need to be taken into consideration in future work.

In conclusion, our study showed that cortical bone from T2DM individuals with no significant differences in microstructure and bone material quality as compared to age-matched healthy individuals also showed no significant differences in fracture toughness. These data support recent studies demonstrating that not all T2DM patients but measurable subgroups of patients experience an increased fracture risk potentially due to a specific risk profile. To what extent bone matrix and fracture toughness properties within these patient subgroups differ remains to be elucidated in the future.

Acknowledgments

The authors would like to thank Sandra Perkovic, Julius Fröhlich, Liang-Yu Ma, Anna K. Siebels, and Eric Grisolia Seifert (Department for Osteology and Biomechanics, University Medical Center Hamburg-Eppendorf) for their excellent technical support. Bernd Gludovatz acknowledged support from the UNSW Scientia Fellowship scheme. This project received funding from the European Union's Horizon 2020 research and innovation program under the Marie Skłodowska-Curie Grant Agreement 860898. Further funding was received from the DFG (Deutsche Forschungsgemeinschaft/German Research Foundation) under Grant BU2562-5/1/BU2562-12/1 to BB and from the Forum Medical Technology & Health Hamburg (FMTHH) (EMW, JK). Open Access funding enabled and organized by Projekt DEAL.

Author Contributions

Eva M. Wölfel: Conceptualization; data curation; formal analysis; funding acquisition; investigation; methodology; supervision; visualization; writing – original draft; writing – review and editing. **Benjamin Bartsch:** Data curation; formal analysis; investigation. **Jasmin Koldehoff:** Conceptualization; data curation; funding acquisition; investigation; methodology. **Imke A. K. Fiedler:** Formal analysis; investigation; methodology; resources; supervision; writing – original draft; writing – review and editing. **Sofie Dragoun-Kolibova:** Investigation; methodology. **Felix N. Schmidt:** Formal analysis; investigation; methodology. **Johannes Krug:** Formal analysis; investigation; methodology; software; visualization; writing – original draft; writing – review and editing. **Mei-Chun Lin:** Conceptualization; data curation; formal analysis; investigation; visualization; writing – original draft; writing – review and editing. **Klaus Püschel:** Investigation; resources. **Benjamin Ondruschka:** Investigation; resources; writing – review and editing. **Elizabeth A. Zimmermann:** Formal analysis; resources; validation. **Hans Jelitto:** Formal analysis; investigation; methodology; resources. **Gerold Schneider:** Investigation; methodology; resources; validation. **Bernd Gludovatz:** Formal analysis; investigation; methodology; validation; writing – review and editing. **Björn Busse:** Conceptualization; formal analysis; funding acquisition; methodology; project administration; resources; writing – original draft; writing – review and editing.

Disclosures

No authors have conflicts of interest to disclose.

Peer Review

The peer review history for this article is available at https://www.webofscience.com/api/gateway/wos/peer-review/10.1002/jbm4.10839.

Data Availability Statement

The datasets generated and/or analyzed for this study are not publicly available but can be obtained from the corresponding author on reasonable request. All data needed to evaluate the conclusion in the paper are presented in the paper.

References

1. Moayeri A, Mohamadpour M, Mousavi SF, Shirzadpour E, Mohamadpour S, Amraei M. Fracture risk in patients with type 2 diabetes mellitus and possible risk factors: a systematic review and meta-analysis. *Ther Clin Risk Manage*. 2017;13:455–468.
2. Vestergaard P. Discrepancies in bone mineral density and fracture risk in patients with type 1 and type 2 diabetes—a meta-analysis. *Osteoporos Int*. 2007;18(4):427–444.
3. Hofbauer LC, Busse B, Eastell R, et al. Bone fragility in diabetes: novel concepts and clinical implications. *Lancet Diabetes Endocrinol*. 2022;10(3):207–220.
4. Wölfel EM, Jähn-Rickert K, Schmidt FN, et al. Individuals with type 2 diabetes mellitus show dimorphic and heterogeneous patterns of loss in femoral bone quality. *Bone*. 2020;140:115556.
5. Wölfel EM, Fiedler IAK, Dragoun Kolibova S, et al. Human tibial cortical bone with high porosity in type 2 diabetes mellitus is accompanied by distinctive bone material properties. *Bone*. 2022;165:116546.
6. Burghardt AJ, Issever AS, Schwartz AV, et al. High-resolution peripheral quantitative computed tomographic imaging of cortical and trabecular bone microarchitecture in patients with type 2 diabetes mellitus. *J Clin Endocrinol Metabol*. 2010;95(11):5045–5055.
7. Patsch JM, Burghardt AJ, Yap SP, et al. Increased cortical porosity in type 2 diabetic postmenopausal women with fragility fractures. *J Bone Miner Res*. 2013;28(2):313–324.
8. Wölfel EM, Schmidt FN, vom Scheidt A, et al. Dimorphic mechanisms of fragility in diabetes mellitus: the role of reduced collagen fibril deformation. *J Bone Miner Res*. 2022;37(11):2259–2276.
9. Karim L, Moulton J, Van Vliet M, et al. Bone microarchitecture, biomechanical properties, and advanced glycation end-products in the proximal femur of adults with type 2 diabetes. *Bone*. 2018;114:32–39.
10. Sihota P, Yadav RN, Dhaliwal R, et al. Investigation of mechanical, material, and compositional determinants of human trabecular bone quality in type 2 diabetes. *J Clin Endocrinol Metab*. 2021;106(5):e2271–e2289.
11. Hunt HB, Torres AM, Palomino PM, et al. Altered tissue composition, microarchitecture, and mechanical performance in cancellous bone from men with type 2 diabetes mellitus. *J Bone Miner Res*. 2019;34(7):1191–1206.
12. Nalla RK, Kruzic JJ, Kinney JH, Ritchie RO. Mechanistic aspects of fracture and R-curve behavior in human cortical bone. *Biomaterials*. 2005;26(2):217–231.
13. Dapaah D, Martel DR, Iranmanesh F, Seelemann C, Laing AC, Willett T. Fracture toughness: bridging the gap between hip fracture and fracture risk assessment. *Curr Osteoporos Rep*. 2023;21(3):253–265.

14. Zimmermann EA, Schaible E, Bale H, et al. Age-related changes in the plasticity and toughness of human cortical bone at multiple length scales. *Proc Natl Acad Sci U S A*. 2011;108(35):14416–14421.
15. Wang X, Shen X, Li X, Mauli AC. Age-related changes in the collagen network and toughness of bone. *Bone*. 2002;31(1):1–7.
16. Granke M, Makowski AJ, Uppuganti S, Does MD, Nyman JS. Identifying novel clinical surrogates to assess human bone fracture toughness. *J Bone Miner Res*. 2015;30(7):1290–1300.
17. Willett TL, Dapaah DY, Uppuganti S, Granke M, Nyman JS. Bone collagen network integrity and transverse fracture toughness of human cortical bone. *Bone*. 2019;120:187–193.
18. Briggs AM, Wark JD, Kantor S, Fazzalari NL, Greig AM, Bennell KL. Bone mineral density distribution in thoracic and lumbar vertebrae: an ex vivo study using dual energy X-ray absorptiometry. *Bone*. 2006;38(2):286–288.
19. Burghardt AJ, Buie HR, Laib A, Majumdar S, Boyd SK. Reproducibility of direct quantitative measures of cortical bone microarchitecture of the distal radius and tibia by HR-pQCT. *Bone*. 2010;47(3):519–528.
20. Fiedler IAK, Casanova M, Keplinger T, Busse B, Müller R. Effect of short-term formaldehyde fixation on Raman spectral parameters of bone quality. *J Biomed Opt*. 2018;23(11):116504.
21. Morris MD, Mandair GS. Raman assessment of bone quality. *Clin Orthop Relat Res*. 2011;469(8):2160–2169.
22. Unal M, Uppuganti S, Timur S, Mahadevan-Jansen A, Akkus O, Nyman JS. Assessing matrix quality by Raman spectroscopy helps predict fracture toughness of human cortical bone. *Sci Rep*. 2019;9(1):7195.
23. Paschalis EP, Gamsjaeger S, Klaushofer K. Vibrational spectroscopic techniques to assess bone quality. *Osteoporos Int*. 2017;28(8):2275–2291.
24. Jelitto H, Hackbarth F, Özcoban H, Schneider GA. Automated control of stable crack growth for R-curve measurements in brittle materials. *Exp Mech*. 2013;53(2):163–170.
25. Zysset PK, Edward Guo X, Edward Hoffler C, Moore KE, Goldstein SA. Elastic modulus and hardness of cortical and trabecular bone lamellae measured by nanoindentation in the human femur. *J Biomech*. 1999;32(10):1005–1012.
26. Hildebrand T, Rüegsegger P. A new method for the model-independent assessment of thickness in three-dimensional images. *J Microsc*. 1997;185(1):67–75.
27. Oliver WC, Pharr GM. An improved technique for determining hardness and elastic modulus using load and displacement sensing indentation experiments. *J Mater Res*. 1992 Jun;7(6):1564–1583.
28. *IDF Diabetes Atlas*. 10th ed. Brussels: International Diabetes Federation; 2021.
29. Kautzky-Willer A, Leutner M, Harreiter J. Sex differences in type 2 diabetes. *Diabetologia*. 2023;66(6):986–1002.
30. Shanbhogue VV, Hansen S, Frost M, et al. Compromised cortical bone compartment in type 2 diabetes mellitus patients with microvascular disease. *Eur J Endocrinol*. 2016;174(2):115–124.
31. Koester KJ, Barth HD, Ritchie RO. Effect of aging on the transverse toughness of human cortical bone: evaluation by R-curves. *J Mech Behav Biomed Mater*. 2011;4(7):1504–1513.
32. Britton M, Parle E, Vaughan TJ. An investigation on the effects of in vitro induced advanced glycation end-products on cortical bone fracture mechanics at fall-related loading rates. *J Mech Behav Biomed Mater*. 2023;138:105619.
33. Jia S, Gong H, Cen H, et al. Influence of non-enzymatic glycation on the mechanical properties of cortical bone. *J Mech Behav Biomed Mater*. 2021;119:104553.
34. Axelsson KF, Litsne H, Kousoula K, Franzén S, Eliasson B, Lorentzon M. Risk of fracture in adults with type 2 diabetes in Sweden: a national cohort study. *PLoS Med*. 2023;20(1):e1004172.
35. Creecy A, Uppuganti S, Merkel AR, et al. Changes in the fracture resistance of bone with the progression of type 2 diabetes in the ZDSD rat. *Calcif Tissue Int*. 2016;99(3):289–301.
36. Creecy A, Uppuganti S, Unal M, Clay Bunn R, Voziyan P, Nyman JS. Low bone toughness in the TallyHO model of juvenile type 2 diabetes does not worsen with age. *Bone*. 2018;110:204–214.
37. Ionova-Martin SS, Do SH, Barth HD, et al. Reduced size-independent mechanical properties of cortical bone in high-fat diet-induced obesity. *Bone*. 2010;46:217–225.
38. LLabre JE, Sroga GE, Tice MJL, Vashishth D. Induction and rescue of skeletal fragility in a high-fat diet mouse model of type 2 diabetes: an in vivo and in vitro approach. *Bone*. 2022;156:116302.
39. Shin M, Zhang M, vom Scheidt A, et al. Impact of test environment on the fracture resistance of cortical bone. *J Mech Behav Biomed Mater*. 2022;129:105155.

10 Abstract

Diabetes mellitus (DM) is a chronic metabolic condition resulting in high blood glucose levels. Recent studies have shown that both type 1 diabetes (T1DM) and type 2 diabetes (T2DM) patients experience a higher rate of fragility fractures. The causes of poor bone health in T1DM and T2DM are complex, multifactorial, and not completely understood. The presented work aims to deliver novel insights into the multiscale characteristics of the human bone matrix, which is affected by diabetic bone disease. The goal is to identify potential biomarkers that can be used to detect impaired bone matrix in individuals with DM.

The influence of hyperglycemia on bone quality was studied in T1DM cortical bone compared to age-matched healthy individuals. T1DM bone exhibits increased osteocyte apoptosis and excessive osteocyte-lacunar mineralization, which impairs the biomechanical competence of the bone tissue. The impairment of the osteocyte network leads to compromised bone repair mechanisms, resulting in microdamage accumulation in diabetic bone. Further investigation was focused on the frequency and implications of osteocyte-lacunar mineralization, also known as micropetrosis, in metabolic disorders such as osteoporosis and DM. The data revealed that micropetrosis is more prevalent in individuals with these conditions and has a detrimental effect on bone mechanical properties. This underscores the significance of maintaining a balanced bone turnover to ensure an adequate pool of osteocytes for optimal bone mechanosensitive function.

Bone quality parameters in T2DM were evaluated using high-resolution imaging and diverse laboratory techniques. In the T2DM group, we identified a subgroup of individuals with high cortical porosity (T2DMwHP). The T2DMwHP subgroup was also presented with a higher cortical pore diameter measured with high-resolution peripheral quantitative computed tomography (HR-pQCT) compared to the T2DM group. In addition, we observed a rise of 25% in fAGEs in this particular group compared to the T2DM and control groups. Biomechanical properties from clinical in situ impact indentation (BMSi) and reference point indentation (RPI) found no significant difference. However, the RPI measurement revealed altered cyclic indentation properties in the T2DMwHP group, suggesting lower bone toughness in the T2DMwHP group but not in the T2DM group.

Further investigation of cortical bone in male individuals with T2DM found no significant differences in microstructure and fracture toughness when compared to healthy individuals. The evaluation of tissue mineralization using qBEI indicates that the calcium density distribution remained constant in the T2DM group. The fracture toughness remains consistent among this particular cohort, indicating that only certain subgroups of patients with T2DM may be at a greater risk of fractures. This implies that not all patients with T2DM share this risk profile.

In conclusion, the results presented in this thesis provide a novel insight into the osteocyte pathology in T1DM, suggesting accelerated aging effects in the diabetic bone matrix. Additionally, it suggests lacunar mineralization as a potential novel biomarker of altered bone quality, highlighting the importance of removing old bone matrix and underlining the significance of bone remodeling status. This work not only improves our comprehension of diabetic bone disease but also highlights the differences in bone matrix characteristics across T1DM and T2DM, which can help to develop tailored strategies for assessing and treating fracture risk in people with diabetes mellitus.

11 Zusammenfassung

Diabetes mellitus (DM) ist eine chronische Stoffwechselerkrankung, die zu einem hohen Blutzuckerspiegel führt. Aktuelle Studien haben gezeigt, dass sowohl Patienten mit Typ-1-Diabetes (T1DM) als auch Typ-2-Diabetes (T2DM) ein erhöhtes Risiko für Fragilitätsfrakturen haben. Die Ursachen für die schlechte Knochengesundheit bei T1DM und T2DM sind komplex, multifaktoriell und nicht vollständig geklärt. Ziel der vorgestellten Arbeit ist es, neue Einblicke in die multiskaligen Eigenschaften der menschlichen Knochenmatrix zu liefern, die von diabetischen Knochenerkrankungen betroffen sind. Hierbei sollen neue Biomarker identifiziert werden, mit denen sich eine beeinträchtigte Knochenmatrix bei Personen mit DM erkennen lässt.

Der Einfluss von Hyperglykämie auf die Knochenqualität wurde an kortikalen Proben aus dem Femurschaft von Individuen mit T1DM, im Vergleich zu knochengesunden Proben von gleichaltrigen Personen, untersucht. T1DM-Knochen wiesen eine erhöhte Osteozyten-Apoptose und eine übermäßige Osteozyt-Lakunen Mineralisierung auf. Die Veränderung des Osteozyten-Netzwerks führt zu einer Beeinträchtigung der Knochenreparaturmechanismen, was zu einer Anhäufung von Mikroschäden im diabetischen Knochen führt und somit die biomechanische Kompetenz des Knochengewebes kumulativ beeinflusst. Weitere Untersuchungen konzentrierten sich auf die Häufigkeit und Auswirkungen der Osteozyt-Lakunen Mineralisierung, auch bekannt als Mikropetrose, bei Stoffwechselstörungen wie Osteoporose und DM. Die Daten zeigten, dass Mikropetrose bei Personen mit diesen Erkrankungen häufiger auftritt und sich nachteilig auf die mechanischen Eigenschaften der Knochen auswirkt. Dies unterstreicht die Bedeutung der Aufrechterhaltung eines ausgewogenen Knochenumsatzes, um einen ausreichenden Osteozyten-Zellpool für eine optimale mechanosensitive Knochenfunktion sicherzustellen.

Knochenqualitätsparameter bei T2DM wurden mithilfe von hochauflösender Bildgebung und verschiedensten Labortechniken bewertet. In der T2DM-Gruppe identifizierten wir eine Untergruppe von Personen mit hoher kortikaler Porosität (T2DMwHP). Die Menge an fAGEs zeigte in Knochenproben von T2DMwHP einen Anstieg um 25 %. In dieser Gruppe fanden wir im Vergleich zur T2DM-Gruppe auch einen höheren kortikalen Porendurchmesser, gemessen mit hochauflösender peripherer quantitativer Computertomographie (HR-pQCT). Bei den biomechanischen Eigenschaften der klinischen In-situ-Indentation (BMSi) und der Referenzpunkt-Indentation (RPI) wurde kein signifikanter Unterschied festgestellt. Die RPI-Messung ergab jedoch veränderte zyklische Indentationseigenschaften in der T2DMwHP-Gruppe, was auf eine geringere Knochenfestigkeit in der T2DMwHP-Gruppe, nicht jedoch in der T2DM-Gruppe, schließen lässt.

Weitere Untersuchungen in kortikalen Knochenproben von männlichen Individuen mit T2DM konnten in Bezug auf Mikrostruktur keine Unterschiede zu gesunden Kontrollproben zeigen. In dem T2DM Proben gab es zudem keine Änderung der Bruchzähigkeit im Vergleich zu den knochengesunden Proben, was darauf hindeutet, dass möglicherweise nur eine bestimmte Untergruppe von Personen mit T2DM einem höheren Fraktur Risiko ausgesetzt ist.

Zusammenfassend liefern die in dieser Arbeit präsentierten Ergebnisse einen neuen Einblick in die Osteozyten-Pathologie bei T1DM, und lassen auf beschleunigte Alterungseffekte in der diabetischen Knochenmatrix schließen. Darüber hinaus stellt die lakunäre Mineralisierung einen neuen potenziellen Biomarker für eine veränderte Knochenqualität dar, was die Bedeutung der Entfernung geschädigter Knochenmatrix hervorhebt. Diese Arbeit verbessert damit unser Verständnis diabetischer Knochenerkrankungen, und verdeutlicht auch die Unterschiede in den Knochenmatrixeigenschaften zwischen T1DM und T2DM. Die dargelegten Ergebnisse könnten dazu beitragen maßgeschneiderte Strategien zur Beurteilung des Frakturrisikos von Personen mit Diabetes Mellitus zu entwickeln.

12 Declaration of contribution to publications

Publication 1: ***Osteocyte apoptosis and cellular micropetrosis signify skeletal aging in type 1 diabetes.***
Acta Biomaterialia 2023, doi: org/10.1016/j.actbio.2023.02.037
S. Dragoun Kolibová, *E.M. Wölfel, H. Hemmatian, P. Milovanovic, H. Mushumba, B. Wulff, M. Neidhardt, K. Püschel, A.V. Failla, A. Vlug, A. Schlaefer, B. Ondruschka, M. Amling, L.C. Hofbauer, M. Rauner, B. Busse, K. Jähn-Rickert*

Author role: First author
Contributions: SDK, KJ-R, and BB designed the study. BW, HM, KP, and BO carried out autopsies and evaluated patient data. SDK and EMW prepared the specimens for ex vivo analysis. SDK, EMW, and KJ-R designed and performed experiments and analyzed the data. MN performed experiments. AVF processed the imaging data. SDK performed the statistical analysis. SDK, EMW, HH, PM, LCH, MR, AV, AS, BB, and KJ-R interpreted the data. SDK, KJ-R, and BB wrote the manuscript. All authors approved the final version of the manuscript.

Publication 2: ***Micropetrosis - Occlusion of Osteocyte Lacunae***
Osteologie 2022, doi: 10.1055/a-1958-3727
S. Dragoun Kolibová, *K. Jähn-Rickert****,*** *B. Busse*

Author role: First author
Contributions: SDK: Data acquisition, visualization, writing-original draft; writing-review and editing. KJE: Writing-original draft; writing-review and editing. BB writing-review and editing. All authors approved the final version of the manuscript.

Publication 3: ***Human tibial cortical bone with high porosity in type 2 diabetes mellitus is accompanied by distinctive bone material properties***

Bone 2022, doi:org/10.1016/j.bone.2022.116546
E.M. Wölfel, I.A.K. Fiedler, ***S. Dragoun Kolibová****, J. Krug, M.C. Lin, B. Yazigi, A.K. Siebels, H. Mushumba, B. Wulff, B. Ondruschka, K. Püschel, C.C. Glüer, K. Jähn-Rickert, B.*

Author role: Co-author
Contributions: EMW: Conceptualization, methodology, formal analysis, visualization, funding acquisition, writing – original draft; IAKF: Methodology, software, writing – review & editing; SK: Methodology, writing – review & editing; JK: Methodology, writing – review & editing; ML: Methodology, writing – review & editing; BY: Methodology, writing – review & editing; AKS: Methodology, writing – review & editing; HM: Resources, writing – review & editing; BW: Resources, writing – review & editing; KP: Resources, writing – review & editing; BO: Resources, writing – review & editing; CG: Validation, writing – review & editing; KJR: Project administration, supervision, writing – review & editing; BB: Conceptualization, methodology, funding acquisition, supervision, project administration, writing - review & editing.

Publication 4: ***When Cortical Bone Matrix Properties Are Indiscernible between Elderly Men with and without Type 2 Diabetes, Fracture Resistance Follows Suit***

JBMR Plus 2023, doi: 10.1002/jbm4.10839

Wölfel, E. M., Bartsch, B., Koldehoff, J., Fiedler, I. A. K., ***Dragoun Kolibová, S.****, Schmidt, F. N., Krug, J., Lin, M.-C., Püschel, K., Ondruschka, B., Zimmermann, E. A., Jelitto, H., Schneider, G., Gludovatz, B., & Busse, B*

Author role: Co-author

Contributions: EMW: Conceptualization; data curation; formal analysis; funding acquisition; investigation; methodology; supervision; visualization; writing – original draft; writing – review and editing. BB: Data curation; formal analysis; investigation. JK: Conceptualization; data curation; funding acquisition; investigation; methodology. IAKF: Formal analysis; investigation; methodology; resources; supervision; writing – original draft; writing – review and editing. SDK: Investigation; methodology. FNS: Formal analysis; investigation; methodology. JK: Formal analysis; investigation; methodology; software; visualization; writing – original draft;writing – review and editing. MCL: Conceptualization; data curation; formal analysis; investigation; visualization;writing – original draft; writing – review and editing. KP: Investigation; resources. BO:Investigation; resources; writing – review and editing. EAZ: Formal analysis; resources; validation. HJ: Formal analysis; investigation; methodology; resources. GS: Investigation; methodology;resources; validation. BG: Formal analysis; investigation; methodology; validation; writing – review and editing. BB: Conceptualization; formal analysis; funding acquisition; methodology; project administration; resources; writing – original draft; writing – review and editing.

13 Publication record

1. **S. Dragoun Kolibová**, E.M. Wölfel, H. Hemmatian, P. Milovanovic, H. Mushumba, B. Wulff, M. Neidhardt, K. Püschel, A.V. Failla, A. Vlug, A. Schlaefer, B. Ondruschka, M. Amling, L.C. Hofbauer, M. Rauner, B. Busse, K. Jähn-Rickert, Osteocyte apoptosis and cellular micropetrosis signify skeletal aging in type 1 diabetes, Acta Biomater 162 (2023) 254–265.

2. **S.Dragoun Kolibová**, B. Busse, K. Jähn-Rickert, Micropetrosis - Occlusion of Osteocyte Lacunae, Osteologie 31 (2022).

3. E.M. Wölfel, I.A.K. Fiedler, **S. Dragoun Kolibová**, J. Krug, M.C. Lin, B. Yazigi, A.K. Siebels, H. Mushumba, B. Wulff, B. Ondruschka, K. Püschel, C.C. Glüer, K. Jähn-Rickert, B. Busse, Human tibial cortical bone with high porosity in type 2 diabetes mellitus is accompanied by distinctive bone material properties, Bone 165 (2022) 116546.

4. E.M. Wölfel, B. Bartsch, J. Koldehoff, I.A.K. Fiedler, **S. Dragoun Kolibová**, F.N. Schmidt, J. Krug, M.-C. Lin, K. Püschel, B. Ondruschka, E.A. Zimmermann, H. Jelitto, G. Schneider, B. Gludovatz, B. Busse, When Cortical Bone Matrix Properties Are Indiscernible between Elderly Men with and without Type 2 Diabetes, Fracture Resistance Follows Suit., JBMR Plus 7 (2023) e10839.

14 Conference contributions

Invited presentations

1. **Dragoun Kolibová S**, K. Jähn-Rickert, B. Busse. Micropetrosis – mineralization of osteocyte lacunae, Oral presentation (10 min). *Kongress OSTEOLOGIE 06/2023.*

Oral presentations

1. **Dragoun Kolibová S**, Bone matrix characterization and analysis of AGE accumulation/oxidative stress in diabetic bone, Oral presentation (10 min). *European Calcified Tissue Society (ECTS), Annual Meeting 04/2023*

2. **S. Kolibová,** E.M. Wölfel, H. Hemmatian, H. Mushumba, B. Wulff, K. Püschel, B. Busse, K. Jähn-Rickert. Cortical Bone Quality in Type 1 Diabetes Mellitus, Oral presentation (10 min). *MusculoSkeletal Interdisciplinary Translational Young Researchers(MuSkITYR), Annual Meeting 11/2021*

Oral poster presentations

1. **S. Kolibová**, E.M. Wölfel, H. Hemmatian, H. Mushumba, B. Wulff, K. Püschel, B. Ondruschka, B. Busse, K. Jähn-Rickert, Local microdamage accumulation and impaired osteocyte viability in human cortical bone is linked to type 1 diabetes mellitus. Oral Poster. *European Calcified Tissue Society (ECTS), Annual Meeting 05/2022*

Poster presentations

1. **S. Kolibová,** E.M. Wölfel, H. Hemmatian, H. Mushumba, B. Wulff, K. Püschel, B. Busse, K. Jähn-Rickert, Femur specimens from type 1 diabetes mellitus individuals presented with unaffected cortical bone matrix quality, but altered cellular histomorphometry. Poster. *European Calcified Tissue Society (ECTS), Annual Meeting 05/2021,* Virtual event

2. **S. Kolibová,** E.M. Wölfel, H. Hemmatian, H. Mushumba, B. Wulff, K. Püschel, B. Ondruschka, B. Busse , K. Jähn-Rickert. Femoral Cortical Bone from Type 1 Diabetes Mellitus Individuals Exhibit Impaired Osteocyte Viability in the Periosteal Region. Poster. *American Society for Bone and Mineral Research (ASBMR), Annual Meeting 10/2021,* Virtual event

15 Curriculum Vitae

CV is omitted for data protection reasons.

Lebenslauf entfällt aus datenschutzrechtlichen Gründen.

16 Affidavit / Eidesstattliche Erklärung

I hereby certify that the work submitted is my own and has been undertaken independently, without any external assistance. I confirm that I have not consulted any sources or aids other than those explicitly indicated and that any material used verbatim or in substance from any other works has been appropriately referenced, including the edition and year of publication.
Furthermore, I confirm that I have not submitted this dissertation to any other educational institution for review and have not applied for admission to a doctorate elsewhere.
I agree that the Faculty of Medicine Dean's Office may use plagiarism detection software to verify the authenticity of my dissertation.

Ich versichere ausdrücklich, dass ich die Arbeit selbständig und ohne fremde Hilfe
verfasst, andere als die von mir angegebenen Quellen und Hilfsmittel nicht benutzt und die aus den benutzten Werken wörtlich oder inhaltlich entnommenen Stellen einzeln nach Ausgabe (Auflage und Jahr des Erscheinens), Band und Seite des benutzten Werkes kenntlich gemacht habe.
Ferner versichere ich, dass ich die Dissertation bisher nicht einem Fachvertreter
an einer anderen Hochschule zur Überprüfung vorgelegt oder mich anderweitig um
Zulassung zur Promotion beworben habe.
Ich erkläre mich einverstanden, dass meine Dissertation vom Dekanat der Medizinischen Fakultät mit einer gängigen Software zur Erkennung von Plagiaten überprüft werden kann.

Signature / Unterschrift: .....